

Fall 2006

Investigation of ethanol dehydration in a microscale pervaporation process

Sudhir Ramprasad
Louisiana Tech University

Follow this and additional works at: <https://digitalcommons.latech.edu/dissertations>



Part of the [Chemical Engineering Commons](#)

Recommended Citation

Ramprasad, Sudhir, "" (2006). *Dissertation*. 543.
<https://digitalcommons.latech.edu/dissertations/543>

This Dissertation is brought to you for free and open access by the Graduate School at Louisiana Tech Digital Commons. It has been accepted for inclusion in Doctoral Dissertations by an authorized administrator of Louisiana Tech Digital Commons. For more information, please contact digitalcommons@latech.edu.

**INVESTIGATION OF ETHANOL DEHYDRATION IN A
MICROSCALE PERVAPORATION PROCESS**

by

Sudhir Ramprasad, B.E.

A Dissertation Presented in Partial Fulfillment
of the Requirements for the Degree
Doctor of Philosophy in Engineering

COLLEGE OF ENGINEERING
LOUISIANA TECH UNIVERSITY

November 2006

UMI Number: 3261294

INFORMATION TO USERS

The quality of this reproduction is dependent upon the quality of the copy submitted. Broken or indistinct print, colored or poor quality illustrations and photographs, print bleed-through, substandard margins, and improper alignment can adversely affect reproduction.

In the unlikely event that the author did not send a complete manuscript and there are missing pages, these will be noted. Also, if unauthorized copyright material had to be removed, a note will indicate the deletion.

UMI[®]

UMI Microform 3261294

Copyright 2007 by ProQuest Information and Learning Company.

All rights reserved. This microform edition is protected against unauthorized copying under Title 17, United States Code.

ProQuest Information and Learning Company
300 North Zeeb Road
P.O. Box 1346
Ann Arbor, MI 48106-1346

LOUISIANA TECH UNIVERSITY


THE GRADUATE SCHOOL


+ 10/19/06
Date

We hereby recommend that the dissertation prepared under our supervision
by SUDHIR RAMPRASAD

entitled INVESTIGATION OF ETHANOL DEHYDRATION IN A MICROSCALE
PERVAPORATION PROCESS

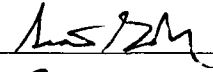
be accepted in partial fulfillment of the requirements for the Degree of
DOCTOR OF PHILOSOPHY

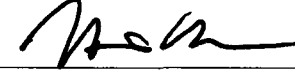


Supervisor of Dissertation Research


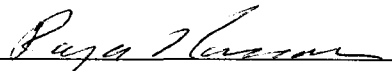
Head of Department
CHEMICAL ENGINEERING
Department

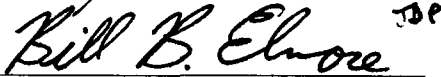
Recommendation concurred in:

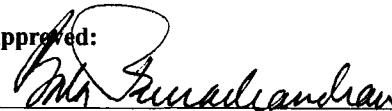




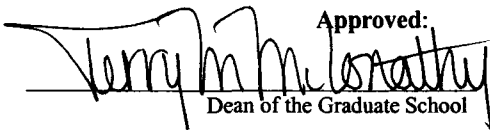
Advisory Committee



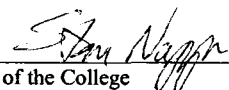


Approved: 

Director of Graduate Studies

Approved: 

Dean of the Graduate School



Dean of the College

ABSTRACT

Challenges due to surface tension effects for vaporization in microchannels have restricted the implementation of conventional separation processes that involve liquid boiling in a micro-chemical system. However, membrane separations offer a feasible alternative for exploring the advantages of liquid phase separation in micro-chemical systems. The main objective of this research was to evaluate the process intensification effects in a microscale pervaporation process with experiments involving the separation of ethanol/water using a commercially available polymer dehydration membrane.

The microchannels in the microseparator were fabricated by the dry etch process at Louisiana Tech University. Microchannel depths of 20 to 120 μm , with hydraulic diameter in the range of 30 μm to 80 μm were studied. The feed ethanol solution was fed through the microchannels parallel to the direction of the membrane with an effective membrane area of 3 cm^2 . A novel membrane module with an *in-situ* heating unit was developed in order to achieve controlled isothermal conditions. An elevated operating temperature and high vacuum at the permeate region provided the driving force required for separation. A laminar liquid flow regime with Reynolds number in the range of 8 to 180 existed in all experiments. Changes in the feed concentration that occurred as a result of selective removal of water by the membrane were measured at regular intervals using an ABBE Mark II refractometer. The total flux and selectivity as a function of residence time and hydraulic diameter was studied. The resistance-in-series model and Sherwood

correlations were used for the prediction of mass transfer coefficients in the boundary layer. The overall mass transfer resistance and boundary layer mass transfer resistance were calculated. The experimental results indicated that the separation performance of the microseparator was independent of changes for the range of hydraulic diameter and residence time tested. The boundary layer resistance calculated was over three orders of magnitude lower than the overall mass transfer resistance, which corroborated that the membrane resistance was the dominant resistance for the transport process.

Key Words: Micro-chemical systems, Microfluidics, Pervaporation, Polymer membrane

APPROVAL FOR SCHOLARLY DISSEMINATION

The author grants to the Prescott Memorial Library of Louisiana Tech University the right to reproduce, by appropriate methods, upon request, any or all portions of this Dissertation. It is understood that "proper request" consists of the agreement, on the part of the requesting party, that said reproduction is for his personal use and that subsequent reproduction will not occur without written approval of the author of this Dissertation. Further, any portions of the Dissertation used in books, papers, and other works must be appropriately referenced to this Dissertation.

Finally, the author of this Dissertation reserves the right to publish freely, in the literature, at any time, any or all portions of this Dissertation.

Author *Bradley C. Brand*

Date 10/23/06

TABLE OF CONTENTS

ABSTRACT	iii
LIST OF TABLES	viii
LIST OF FIGURES	xiv
ACKNOWLEDGMENTS	xxii
CHAPTER 1 INTRODUCTION	1
1.1 Motivation.....	1
1.2 Objectives	3
1.3 Background	3
1.4 Membrane Separations.....	4
1.4.1 Membrane Process.....	5
1.4.2 Classification of Membranes and Membrane Processes.....	6
1.4.2.1 Microfiltration and ultrafiltration.....	7
1.4.2.2 Reverse osmosis.....	8
1.4.2.3 Electrodialysis.....	8
1.4.2.4 Facilitated transport	8
1.5 Pervaporation	9
1.5.1 Batch and Continuous Pervaporation Process	12
1.5.2 Solution-Diffusion Model.....	13
1.5.3 Characterization of Pervaporation Membranes	14
1.5.4 Membrane Material.....	15
1.5.5 Applications of Pervaporation	16
1.5.6 Concentration Polarization.....	17
1.6 Process Intensification Review	18
1.6.1 Definition of Process Intensification	19
1.6.2 Examples of Process Intensification	19
1.7 Micro-Chemical System	20
1.7.1 Advantages of Micro-Chemical System.....	21
1.7.2 Literature Review of Separation Processes in Micro-Chemical Systems.....	22
CHAPTER 2 METHODS AND MATERIALS	28

2.1 Pervaporation Experiments Based on Single Pass.....	28
2.2 Description of Membrane Module/ <i>In-situ</i> Heat Exchanger.....	32
2.3 Pervaporation Experimental Setup Based on Retentate Recycle.....	36
2.4 Design and Fabrication of the Microseparator.....	43
2.4.1 Background for Design of Microseparator	43
2.4.2 Characterization of Microseparator	47
2.5 Mathematical Treatment of Mass Data Obtained from Balance	50
2.6 Mathematical Model	53
 CHAPTER 3 RESULTS AND DISCUSSION.....	 55
3.1 Microseparator Geometry Justification.....	55
3.2 Results from Single Pass Pervaporation Experimental Setup.....	56
3.3 Pervaporation Experimental Setup with Retentate Recycle	64
3.3.1 Permeate Collection	65
3.3.2 Effect of Evaporation.....	73
3.3.3 Effect of Separation Factor with Varying Feed Ethanol Concentration.....	76
3.3.4 Effect of Total Flux with Varying Feed Ethanol Concentration.....	78
3.3.5 Effect of Operating Temperature	79
3.3.6 Effect of <i>In-situ</i> Heat Exchanger/ Direct Heating of Membrane.....	80
3.3.7 Effect of Permeate Pressure	84
3.3.8 Effect of Feed Flow Rate/Residence Time	85
3.3.9 Effect of Varying Hydraulic Diameter on Separation Performance.....	93
 CHAPTER 4 CONCLUSIONS AND FUTURE WORK.....	 97
4.1 Conclusions.....	97
4.2 Future Work	98
 APPENDIX A ETHANOL METHOD DEVELOPMENT IN A HP 5890 Series II GAS CHROMATOGRAPH	 101
 APPENDIX B ETHANOL METHOD DEVELOPMENT IN ABBE MARK II REFRACTOMETER	 112
 APPENDIX C FABRICATION OF SILICON MICROSEPARATOR.....	 119
 APPENDIX D EXPERIMENTAL DATA OF PERVAPORATION EXPERIMENTS WITH RETENTATE RECYCLE	 129
 APPENDIX E COOLER LENGTH CALCULATIONS.....	 205
 APPENDIX F VITON TUBING CALIBRATION FOR FEED PUMP	 208
 REFERENCES	 211

LIST OF TABLES

Table 2.1	Microseparator specifications.....	41
Table 3.1	ANOVA for mean flux from single pass pervaporation experiments.....	57
Table 3.2	ANOVA for mean separation factor from single pass pervaporation experiments.....	59
Table 3.3	Comparison of permeate and retentate flux.....	67
Table 3.4	Apparent water flux data from relative humidity calculations.....	72
Table 3.5	Index of flow rates used at varying depths of microseparator.....	86
Table 3.6	Coefficients for Sherwood correlations.....	88
Table 3.7	Exponents relating hydraulic diameter to boundary layer thickness and pressure drop.....	91
Table 3.8	Confidence interval for separation factor and flux data from retentate recycle experiments.....	95
Table A.1	GC ethanol method development data.....	109
Table A.2	GC ethanol method development chromatograph details -1.....	110
Table A.3	GC ethanol method development chromatograph details -2.....	111
Table B.1	Ethanol standard solution data for method development in refractometer...117	
Table B.2	Refractive index data from ethanol method development in refractometer.117	
Table C.1	Process parameters for Deep Reactive Ion Etching.....	125
Table C.2	Description of sequence in photolithography for silicon microseparator.....	127
Table D.1	Experiment-152 Operating parameters for 22 μm deep channel, 47 milliseconds, 2/19/06 to 2/20/06.....	130

Table D.2	Experiment - 152 Recorded data for 22 μm deep channel, 47 milliseconds, 2/19/06 to 2/20/06.....	131
Table D.3	Experiment - 153 Operating parameters for 22 μm deep channel, 117 milliseconds, 2/20/06 to 2/21/06.....	132
Table D.4	Experiment - 153 Recorded data for 22 μm deep channel, 117 milliseconds, 2/20/06 to 2/21/06.....	132
Table D.5	Experiment - 156 Operating parameters for 22 μm deep channel, 23 milliseconds, 2/23/06 to 2/24/06.....	134
Table D.6	Experiment - 156 Recorded data for 22 μm deep channel, 23 milliseconds, 2/23/06 to 2/24/06.....	135
Table D.7	Experiment - 157 Operating parameters for 22 μm deep channel, 235 milliseconds, 2/24/06 to 2/25/06.....	136
Table D.8	Experiment - 157 Recorded data for 22 μm deep channel, 235 milliseconds, 2/24/06 to 2/25/06.....	137
Table D.9	Experiment - 158 Operating parameters for 22 μm deep channel, 23 milliseconds, 2/26/06 to 2/27/06.....	139
Table D.10	Experiment - 158 Recorded data for 22 μm deep channel, 23 milliseconds, 2/26/06 to 2/27/06.....	140
Table D.11	Experiment - 176 Operating parameters for 22 μm deep channel, 23 milliseconds, 3/29/06 to 3/30/06.....	142
Table D.12	Experiment - 176 Recorded data for 22 μm deep channel, 23 milliseconds, 3/29/06 to 3/30/06.....	142
Table D.13	Experiment - 177 Operating parameters for 22 μm deep channel, 235 milliseconds, 3/30/06 to 3/31/06.....	144
Table D.14	Experiment - 177 Recorded data for 22 μm deep channel, 235 milliseconds, 3/30/06 to 3/31/06.....	144
Table D.15	Experiment - 180 Operating parameters for 22 μm deep channel, 47 milliseconds, 4/3/06 to 4/4/06.....	146
Table D.16	Experiment - 180 Recorded data for 22 μm deep channel, 47 milliseconds, 4/3/06 to 4/4/06.....	146

Table D.17	Experiment - 181 Operating parameters for 22 μm deep channel, 47 milliseconds, 4/4/06 to 4/6/06.....	148
Table D.18	Experiment - 181 Recorded data for 22 μm deep channel, 47 milliseconds, 4/4/06 to 4/6/06.....	148
Table D.19	Experiment - 182 Operating parameters for 22 μm deep channel, 47 milliseconds, 4/6/06 to 4/7/06.....	150
Table D.20	Experiment - 182 Recorded data for 22 μm deep channel, 47 milliseconds, 4/6/06 to 4/7/06.....	150
Table D.21	Experiment - 183 Operating parameters for 22 μm deep channel, 47 milliseconds, 4/7/06 to 4/8/06.....	152
Table D.22	Experiment - 183 Recorded data for 22 μm deep channel, 47 milliseconds, 4/7/06 to 4/8/06.....	153
Table D.23	Experiment - 184 Operating parameters for 22 μm deep channel, 47 milliseconds, 4/9/06 to 4/10/06.....	154
Table D.24	Experiment - 184 Recorded data for 22 μm deep channel, 47 milliseconds, 4/9/06 to 4/10/06.....	155
Table D.25	Experiment - 101 Operating parameters for 47 μm deep channel, 20 milliseconds, 12/17/05 to 12/18/05.....	156
Table D.26	Experiment - 101 Recorded data for 47 μm deep channel, 20 milliseconds, 12/17/05 to 12/18/05.....	157
Table D.27	Experiment - 109 Operating parameters data for 47 μm deep channel, 20 milliseconds, 12/31/05 to 1/1/06.....	158
Table D.28	Experiment - 109 Recorded data for 47 μm deep channel, 20 milliseconds, 12/31/05 to 1/1/06.....	158
Table D.29	Experiment - 129 Operating parameters for 47 μm deep channel, 10 milliseconds, 1/17/06 to 1/18/06.....	160
Table D.30	Experiment - 129 Recorded data for 47 μm deep channel, 10 milliseconds, 1/17/06 to 1/18/06.....	161
Table D.31	Experiment - 131 Operating parameters for 47 μm deep channel, 100 milliseconds, 1/19/06 to 1/20/06.....	162

Table D.32	Experiment - 131 Recorded data for 47 μm deep channel, 100 milliseconds, 1/19/06 to 1/20/06.....	163
Table D.33	Experiment - 132 Operating parameters for 47 μm deep channel, 502 milliseconds, 1/20/06 to 1/22/06.....	164
Table D.34	Experiment - 132 Recorded data for 47 μm deep channel, 502 milliseconds, 1/20/06 to 1/22/06.....	165
Table D.35	Experiment - 135 Operating parameters for 47 μm deep channel, 50 milliseconds, 1/24/06 to 1/25/06.....	167
Table D.36	Experiment - 135 Recorded data for 47 μm deep channel, 50 milliseconds, 1/24/06 to 1/25/06.....	168
Table D.37	Experiment - 136 Operating parameters for 47 μm deep channel, 100 milliseconds, 1/25/06 to 1/26/06.....	170
Table D.38	Experiment - 136 Recorded data for 47 μm deep channel, 100 milliseconds, 1/25/06 to 1/26/06.....	171
Table D.39	Experiment - 163 Operating parameters for 47 μm deep channel, 251 milliseconds, 3/9/06 to 3/10/06.....	172
Table D.40	Experiment - 163 Recorded data for 47 μm deep channel, 251 milliseconds, 3/9/06 to 3/10/06.....	172
Table D.41	Experiment - 169 Operating parameters for 47 μm deep channel, 251 milliseconds, 3/20/06 to 3/21/06.....	174
Table D.42	Experiment - 169 Recorded data for 47 μm deep channel, 251 milliseconds, 3/20/06 to 3/21/06.....	174
Table D.43	Experiment - 170 Operating parameters for 47 μm deep channel, 50 milliseconds, 3/21/06 to 3/22/06.....	176
Table D.44	Experiment - 170 Recorded data for 47 μm deep channel, 50 milliseconds, 3/21/06 to 3/22/06.....	176
Table D.45	Experiment - 171 Operating parameters for 47 μm deep channel, 50 milliseconds, 3/22/06 to 3/23/06.....	178
Table D.46	Experiment - 171 Recorded data for 47 μm deep channel, 50 milliseconds, 3/22/06 to 3/23/06.....	179

Table D.47	Experiment – 172a Operating parameters for 47 μm deep channel, 50 milliseconds, 3/23/06 to 3/24/06.....	180
Table D.48	Experiment – 172a Recorded data for 47 μm deep channel, 50 milliseconds, 3/23/06 to 3/24/06.....	180
Table D.49	Experiment – 138 Operating parameters for 120 μm deep channel, 25 milliseconds, 1/28/06 to 1/29/06.....	182
Table D.50	Experiment – 138 Recorded data for 120 μm deep channel, 25 milliseconds, 1/28/06 to 1/29/06.....	183
Table D.51	Experiment – 140 Operating parameters for 120 μm deep channel, 51 milliseconds, 1/30/06 to 2/1/06.....	185
Table D.52	Experiment – 140 Recorded data for 120 μm deep channel, 51 milliseconds, 1/30/06 to 2/1/06.....	186
Table D.53	Experiment – 143 Operating parameters for 120 μm deep channel, 51 milliseconds, 2/6/06 to 2/7/06.....	188
Table D.54	Experiment – 143 Recorded data for 120 μm deep channel, 51 milliseconds, 2/6/06 to 2/7/06.....	189
Table D.55	Experiment – 144 Operating parameters for 120 μm deep channel, 256 milliseconds, 2/7/06 to 2/8/06.....	190
Table D.56	Experiment – 144 Recorded data for 120 μm deep channel, 256 milliseconds, 2/7/06 to 2/8/06.....	191
Table D.57	Experiment – 145 Operating parameters for 120 μm deep channel, 25 milliseconds, 2/8/06 to 2/9/06.....	193
Table D.58	Experiment – 145 Recorded data for 120 μm deep channel, 25 milliseconds, 2/8/06 to 2/9/06.....	193
Table D.59	Experiment – 159 Operating parameters for 120 μm deep channel, 128 milliseconds, 3/3/06 to 3/5/06.....	195
Table D.60	Experiment – 159 Recorded data for 120 μm deep channel, 128 milliseconds, 3/3/06 to 3/5/06.....	195
Table D.61	Experiment – 160 Operating parameters for 120 μm deep channel, 256 milliseconds, 3/5/06 to 3/6/06.....	197

Table D.62	Experiment – 160 Recorded data for 120 μm deep channel, 256 milliseconds, 3/5/06 to 3/6/06.....	197
Table D.63	Experiment – 162 Operating parameters for 120 μm deep channel, 51 milliseconds, 3/6/06 to 3/8/06.....	199
Table D.64	Experiment – 162 Recorded data for 120 μm deep channel, 51 milliseconds, 3/6/06 to 3/8/06.....	199
Table D.65	Experiment – 173 Operating parameters for 120 μm deep channel, 25 milliseconds, 3/25/06 to 3/26/06.....	201
Table D.66	Experiment – 173 Recorded data for 120 μm deep channel, 25 milliseconds, 3/25/06 to 3/26/06.....	201
Table D.67	Experiment – 174 Operating parameters for 120 μm deep channel, 25 milliseconds, 3/26/06 to 3/27/06.....	203
Table D.68	Experiment – 174 Recorded data for 120 μm deep channel, 25 milliseconds, 3/26/06 to 3/27/06.....	203

LIST OF FIGURES

Figure 1.1	Effect of mass transfer coefficient on hydraulic diameter.....	2
Figure 1.2	Schematic representation of membrane process.....	5
Figure 1.3	Comparison of membrane processes in terms of pore diameter.....	7
Figure 1.4	Schematic of pervaporation process.....	10
Figure 1.5	Mechanism of liquid permeation through a membrane.....	13
Figure 1.6	Assembly of a counterflow microchannel chemical separation device.....	23
Figure 2.1	Schematic of experimental setup for batch pervaporation experiments.....	30
Figure 2.2	Schematic of the membrane module.....	32
Figure 2.3	A schematic of the brass manifold used for <i>in-situ</i> heat exchanger.....	33
Figure 2.4	Picture of top plate in the membrane module.....	34
Figure 2.5	Picture of bottom plate in the membrane module.....	35
Figure 2.6	Picture of holes for heat exchanger in the membrane module.....	35
Figure 2.7	Picture of porous membrane support.....	36
Figure 2.8	Picture of experimental setup for retentate recycle pervaporation process ...	38
Figure 2.9	Schematic of pervaporation experimental setup with retentate recycle.....	40
Figure 2.10	U-tube vacuum trap.....	43
Figure 2.11	Serrated vacuum trap.....	43
Figure 2.12	Mask layout of first-generation microseparator.....	44
Figure 2.13	Mask layout of second-generation microseparator.....	44

Figure 2.14	Schematic of a first-generation microseparator.....	45
Figure 2.15	Schematic of a second-generation microseparator.....	45
Figure 2.16	Geometry of second-generation microseparator.....	46
Figure 2.17	Picture of second-generation microseparator.....	47
Figure 2.18	SEM image of inlet/outlet, manifold and channels.....	48
Figure 2.19	SEM image of channel walls and surface of the chip.....	48
Figure 2.20	2-D image for measuring width and depth.....	49
Figure 2.21	3-D image for surface smoothness testing.....	50
Figure 2.22	Sample representation of untreated mass data obtained from the balance.....	51
Figure 2.23	Sample representation of mass data between a sampling interval.....	51
Figure 2.24	Sample representation of a treated mass data.....	52
Figure 2.25	Ethanol concentration analysis by Abbe Mark II refractometer.....	53
Figure 3.1	Comparison of inlet and channel pressure drop with hydraulic diameter..	56
Figure 3.2	Mean flux vs. flow rate for 22 μm deep channel in single pass pervaporation experiments.....	58
Figure 3.3	Mean flux vs. flow rate for 120 μm deep channel in single pass pervaporation experiments.....	58
Figure 3.4	Mean flux vs. depth of microchannel in single pass pervaporation experiments.....	59
Figure 3.5	Mean separation factor vs. temperature in single pass pervaporation experiments.....	60
Figure 3.6	Mean separation factor vs. flow rate for 22 μm deep channel in single pass pervaporation experiments.....	61
Figure 3.7	Mean separation factor vs. flow rate for 120 μm deep channel in single pass pervaporation experiments.....	61

Figure 3.8	Mean separation factor vs. depth of microchannel at different operating temperatures in single pass pervaporation experiments.....	62
Figure 3.9	Mean separation factor vs. flow rate for 22 μm deep channel at different operating temperatures in single pass pervaporation experiments.....	62
Figure 3.10	Mean separation factor vs. flow rate for 120 μm deep channel at different operating temperatures in single pass pervaporation experiments.....	63
Figure 3.11	Permeate mass recovery analysis.....	68
Figure 3.12	Total permeate flux vs. total retentate flux.....	69
Figure 3.13	Comparison of permeate and retentate total flux with residence time.....	70
Figure 3.14	Comparison of ethanol flux from permeate and retentate with residence time.....	70
Figure 3.15	Comparison of water flux from permeate and retentate with residence time.....	71
Figure 3.16	Permeate analysis of separation factor.....	73
Figure 3.17	Mass loss by evaporation vs. time.....	74
Figure 3.18	Ethanol-water evaporation effects with varying ethanol concentration.....	75
Figure 3.19	Changes in composition in ethanol feed by evaporation.....	76
Figure 3.20	Effect of separation factor by varying ethanol concentration in feed.....	77
Figure 3.21	Flux variations with ethanol concentration in feed.....	78
Figure 3.22	Calculation of overall mass transfer coefficient.....	79
Figure 3.23	Overall mass transfer coefficients vs. operating temperature.....	80
Figure 3.24	Acquired membrane module temperature data.....	81
Figure 3.25	Membrane module temperature stabilization data.....	82
Figure 3.26	Behavior of membrane module temperature during a pervaporation experiment.....	82

Figure 3.27	Membrane module temperature effects on residence time.....	83
Figure 3.28	Overall mass transfer coefficients vs. permeate pressure.....	84
Figure 3.29	Effect of different Sherwood correlations in 22 μm deep channel at 12.7 cm/s.....	89
Figure 3.30	Effect of different Sherwood correlations in 22 μm deep channel at 127 cm/s.....	89
Figure 3.31	Overall mass transfer coefficients vs. residence time.....	93
Figure 3.32	Overall mass transfer coefficients vs. hydraulic diameter.....	94
Figure 3.33	Mass transfer resistances vs. residence time.....	96
Figure A.1	Calibration chart for ethanol analysis by gas chromatography.....	103
Figure A.2	Picture of Hewlett-Packard gas chromatograph 5890 series II.....	107
Figure B.1	Calibration chart for ethanol analysis by refractometer.....	114
Figure B.2	X-Bar analysis for calibration chart.....	115
Figure B.3	Picture of shadow mark intersection with cross lines in refractometer....	116
Figure C.1	Spin curve for Shipley 1813 photoresist.....	122
Figure C.2	Spin curve for AZ9260 photoresist.....	126
Figure C.3	Schematic of photolithography process for silicon microseparator.....	128
Figure D.1	Experiment - 152 Untreated mass data for 22 μm deep channel, 47 milliseconds, 2/19/06 to 2/20/06.....	131
Figure D.2	Experiment - 152 Membrane module temperature profile for 22 μm deep channel, 47 milliseconds, 2/19/06 to 2/20/06.....	131
Figure D.3	Experiment - 153 Untreated mass data for 22 μm deep channel, 117 milliseconds, 2/20/06 to 2/21/06.....	133
Figure D.4	Experiment - 153 Membrane module temperature profile for 22 μm deep channel, 117 milliseconds, 2/20/06 to 2/21/06.....	133
Figure D.5	Experiment - 156 Untreated mass data for 22 μm deep channel, 23 milliseconds, 2/23/06 to 2/24/06.....	135

Figure D.6	Experiment - 156 Membrane module temperature profile for 22 μm deep channel, 23 milliseconds, 2/23/06 to 2/24/06.....	135
Figure D.7	Experiment - 157 Untreated mass data for 22 μm deep channel, 235 milliseconds, 2/24/06 to 2/25/06.....	137
Figure D.8	Experiment - 157 Membrane module temperature profile for 22 μm deep channel, 235 milliseconds, 2/24/06 to 2/25/06.....	138
Figure D.9	Experiment - 158 Untreated mass data for 22 μm deep channel, 23 milliseconds, 2/26/06 to 2/27/06.....	140
Figure D.10	Experiment - 158 Membrane module temperature profile for 22 μm deep channel, 23 milliseconds, 2/26/06 to 2/27/06.....	141
Figure D.11	Experiment - 176 Untreated mass data for 22 μm deep channel, 23 milliseconds, 3/29/06 to 3/30/06.....	143
Figure D.12	Experiment - 176 Membrane module temperature profile for 22 μm deep channel, 23 milliseconds, 3/29/06 to 3/30/06.....	143
Figure D.13	Experiment - 177 Untreated mass data for 22 μm deep channel, 235 milliseconds, 3/30/06 to 3/31/06.....	145
Figure D.14	Experiment - 177 Membrane module temperature profile for 22 μm deep channel, 235 milliseconds, 3/30/06 to 3/31/06.....	145
Figure D.15	Experiment - 180 Untreated mass data for 22 μm deep channel, 47 milliseconds, 4/3/06 to 4/4/06.....	147
Figure D.16	Experiment - 180 Membrane module temperature profile for 22 μm deep channel, 47 milliseconds, 4/3/06 to 4/4/06.....	147
Figure D.17	Experiment - 181 Untreated mass data for 22 μm deep channel, 47 milliseconds, 4/4/06 to 4/6/06.....	149
Figure D.18	Experiment - 181 Membrane module temperature profile for 22 μm deep channel, 47 milliseconds, 4/4/06 to 4/6/06.....	149
Figure D.19	Experiment - 182 Untreated mass data for 22 μm deep channel, 47 milliseconds, 4/6/06 to 4/7/06.....	151
Figure D.20	Experiment - 182 Membrane module temperature profile for 22 μm deep channel, 47 milliseconds, 4/6/06 to 4/7/06.....	151

Figure D.21 Experiment - 183 Untreated mass data for 22 μm deep channel, 47 milliseconds, 4/7/06 to 4/8/06.....	153
Figure D.22 Experiment - 183 Membrane module temperature profile for 22 μm deep channel, 47 milliseconds, 4/7/06 to 4/8/06.....	153
Figure D.23 Experiment - 184 Untreated mass data for 22 μm deep channel, 47 milliseconds, 4/9/06 to 4/10/06.....	155
Figure D.24 Experiment - 184 Membrane module temperature profile for 22 μm deep channel, 47 milliseconds, 4/9/06 to 4/10/06.....	156
Figure D.25 Experiment - 101 Untreated mass data for 47 μm deep channel, 20 milliseconds, 12/17/05 to 12/18/05.....	157
Figure D.26 Experiment - 109 Untreated mass data for 47 μm deep channel, 20 milliseconds, 12/31/05 to 1/1/06.....	159
Figure D.27 Experiment - 129 Untreated mass data for 47 μm deep channel, 10 milliseconds, 1/17/06 to 1/18/06.....	161
Figure D.28 Experiment - 131 Untreated mass data for 47 μm deep channel, 100 milliseconds, 1/19/06 to 1/20/06.....	163
Figure D.29 Experiment - 131 Membrane module temperature profile for 47 μm deep channel, 100 milliseconds, 1/19/06 to 1/20/06.....	163
Figure D.30 Experiment - 132 Untreated mass data for 47 μm deep channel, 502 milliseconds, 1/20/06 to 1/22/06.....	165
Figure D.31 Experiment - 132 Membrane module temperature profile for 47 μm deep channel, 502 milliseconds, 1/20/06 to 1/22/06.....	166
Figure D.32 Experiment - 135 Untreated mass data for 47 μm deep channel, 50 milliseconds, 1/24/06 to 1/25/06.....	168
Figure D.33 Experiment - 135 Membrane module temperature profile for 47 μm deep channel, 50 milliseconds, 1/24/06 to 1/25/06.....	169
Figure D.34 Experiment - 136 Untreated mass data for 47 μm deep channel, 100 milliseconds, 1/25/06 to 1/26/06.....	171
Figure D.35 Experiment - 136 Membrane module temperature profile for 47 μm deep channel, 100 milliseconds, 1/25/06 to 1/26/06.....	171

Figure D.36 Experiment - 163 Untreated mass data for 47 μm deep channel, 251 milliseconds, 3/9/06 to 3/10/06.....	173
Figure D.37 Experiment - 163 Membrane module temperature profile for 47 μm deep channel, 251 milliseconds, 3/9/06 to 3/10/06.....	173
Figure D.38 Experiment - 169 Untreated mass data for 47 μm deep channel, 251 milliseconds, 3/20/06 to 3/21/06.....	175
Figure D.39 Experiment - 169 Membrane module temperature profile for 47 μm deep channel, 251 milliseconds, 3/20/06 to 3/21/06.....	175
Figure D.40 Experiment - 170 Untreated mass data for 47 μm deep channel, 50 milliseconds, 3/21/06 to 3/22/06.....	177
Figure D.41 Experiment - 170 Membrane module temperature profile for 47 μm deep channel, 50 milliseconds, 3/21/06 to 3/22/06.....	177
Figure D.42 Experiment - 171 Untreated mass data for 47 μm deep channel, 50 milliseconds, 3/22/06 to 3/23/06.....	179
Figure D.43 Experiment - 171 Membrane module temperature profile for 47 μm deep channel, 50 milliseconds, 3/22/06 to 3/23/06.....	179
Figure D.44 Experiment - 172a Untreated mass data for 47 μm deep channel, 50 milliseconds, 3/23/06 to 3/24/06.....	181
Figure D.45 Experiment - 172a Membrane module temperature profile for 47 μm deep channel, 50 milliseconds, 3/23/06 to 3/24/06.....	181
Figure D.46 Experiment - 138 Untreated mass data 120 μm deep channel, 25 milliseconds, 1/28/06 to 1/29/06.....	183
Figure D.47 Experiment - 138 Membrane module temperature profile for 120 μm deep channel, 25 milliseconds, 1/28/06 to 1/29/06.....	184
Figure D.48 Experiment - 140 Untreated mass data for 120 μm deep channel, 51 milliseconds, 1/30/06 to 2/1/06.....	186
Figure D.49 Experiment - 140 Membrane module temperature profile for 120 μm deep channel, 51 milliseconds, 1/30/06 to 2/1/06.....	187
Figure D.50 Experiment - 143 Untreated mass data for 120 μm deep channel, 51 milliseconds, 2/6/06 to 2/7/06.....	189

Figure D.51 Experiment - 143 Membrane module temperature profile for 120 μm deep channel, 51 milliseconds, 2/6/06 to 2/7/06.....	190
Figure D.52 Experiment - 144 Untreated mass data for 120 μm deep channel, 256 milliseconds, 2/7/06 to 2/8/06.....	191
Figure D.53 Experiment - 144 Membrane module temperature profile for 120 μm deep channel, 256 milliseconds, 2/7/06 to 2/8/06.....	192
Figure D.54 Experiment - 145 Untreated mass data for 120 μm deep channel, 25 milliseconds, 2/8/06 to 2/9/06.....	194
Figure D.55 Experiment - 145 Membrane module temperature profile for 120 μm deep channel, 25 milliseconds, 2/8/06 to 2/9/06.....	194
Figure D.56 Experiment - 159 Untreated mass data for 120 μm deep channel, 128 milliseconds, 3/3/06 to 3/5/06.....	196
Figure D.57 Experiment - 159 Membrane module temperature profile for 120 μm deep channel, 128 milliseconds, 3/3/06 to 3/5/06.....	196
Figure D.58 Experiment - 160 Untreated mass data for 120 μm deep channel, 256 milliseconds, 3/5/06 to 3/6/06.....	198
Figure D.59 Experiment - 160 Membrane module temperature profile for 120 μm deep channel, 256 milliseconds, 3/5/06 to 3/6/06.....	198
Figure D.60 Experiment - 162 Untreated mass data for 120 μm deep channel, 51 milliseconds, 3/6/06 to 3/8/06.....	200
Figure D.61 Experiment - 162 Membrane module temperature profile for 120 μm deep channel, 51 milliseconds, 3/6/06 to 3/8/06.....	200
Figure D.62 Experiment - 173 Untreated mass data for 120 μm deep channel, 25 milliseconds, 3/25/06 to 3/26/06.....	202
Figure D.63 Experiment - 173 Membrane module temperature profile for 120 μm deep channel, 25 milliseconds, 3/25/06 to 3/26/06.....	202
Figure D.64 Experiment - 174 Untreated mass data for 120 μm deep channel, 25 milliseconds, 3/26/06 to 3/27/06.....	204
Figure F.1 Masterflex tubing calibration chart.....	209

ACKNOWLEDGMENTS

I express my sincere gratitude to my major professor Dr. James Palmer for his suggestions and advice all through the project. The 5 years that I spent working with Dr. Palmer, have been a great learning experience, and all through this journey he has not only guided me through my research project but also infused enough confidence in me to deal with the mundane challenges in life. I will always remain grateful to him.

I would like to thank Dr. Bill Elmore for helping me overcome many of the roadblocks I had to face with either administrative issues or those related to my research. I would also like to thank Dr. Hisham Hegab for being kind and always helpful in several ways. I am thankful to Dr. Raja Nassar for his guidance with the statistical analysis for my experimental data. I would like to thank Dr. Scott Gold for his time and interest in helping me with all my doubts whenever I approached him. I am thankful to all of my committee members for providing their suggestions and comments on my dissertation. I would also like to acknowledge the financial assistance from the National Science Foundation, Grant # 0407097.

During my initial stages of microfabrication, Mr. Ji Fang and his student Jackie Chen were of immense help. I am grateful to Mr. Ji Fang for his valuable suggestions all throughout my experience in the clean room. I would like thank Dr. Ramu Ramachandran for allowing me to use the refractometer for my analytical method. I am also thankful to

Dr. Dixie Griffin for lending his water circulator at the most important period of the project.

I would like to extend my special thanks to Mr. Jimmy Cook and Mr. Danny Eddy for their assistance in several ways while building my experimental set-up.

I am thankful to my loving family for their prayers all through the challenging times of my project. I am indebted to my mother Ms. Geetha Ramprasad and my father Mr. Rama Prasad who made it possible for me to pursue my graduate studies abroad. I would also like to express my profound gratitude to my brother Mr. Vijay Ramprasad and my sister Dr. Sushma Ramprasad for their constant encouragement and emotional support during my entire stay away from home.

Lastly, I thank God for providing me several opportunities to learn new exciting things here and in helping me cope with all the challenges.

I appreciate the assistance from all of them listed below and also others who have contributed to this project.

Staff

- Dr. Alfred Gunashekar (I/M)
- Mr. Murray Rasbury (Machine Shop)
- Mr. Bill Jones (Network Administrator)
- Mr. Scott Williams (I/M)
- Mr. Dee Tatum (I/M)
- Mr. Tom Emory (Electrical Engg)
- Mr. Gene Murphy (Chemical Engg)
- Mr. John McDonald (I/M)
- Dr. Karen Zhu (I/M)
- Ms. Regina Foster (Library)
- Mr. Ray Mckinney (Mechanical Engg)

Colleagues

- Amish Patel
- Anita Alfred
- Kalyani Vejella
- Lixiao Zheng
- Nitin Gupta
- Ravi Kumar Dokku
- Scott Forrest
- Shaila Rani Reddy
- Shihuai Zhao
- Xiaoshuo Wu
- Wen Jie
- Javeed S.M
- Keyur Shah
- Weisong Wang
- Woocheol Shin
- Yanjun David Tang

Friends

- Christopher Cicirello
- Jackie Chen
- Jason Bardis
- Zonghuan Lu

CHAPTER 1

INTRODUCTION

1.1 Motivation

The increasing pressure of the global economy necessitates investigation of avenues that offer potential competitive advantages. The utilization of microchannels in chemical processes has resulted in the process intensification of heat exchangers [1-2], reactors [3-5], etc., due to reductions in transport distances. Conventional separation processes which involve liquid boiling cannot be scaled effectively to a chemical microsystem due to the surface tension effects that suppress vaporization. Surface tension effects in microchannels produce challenges to the nucleation of vapor bubbles requiring temperatures approaching 90% of the components critical point. Rapid and complete phase changes are observed negating establishment of an equilibrium between the vapor and liquid phases [6-7]. Therefore, alternative separation techniques such as membrane processes provide a promising avenue for separation.

Liquid phase separations are the focus due to the lower diffusivities of a liquid when compared with a gas. Typical values of liquid and gas phase diffusivities are 10^{-1} cm^2/s and 10^{-5} cm^2/s respectively. Using Fick's law of diffusion, one predicts that 0.4 s is required for a liquid to diffuse 20 μm and 63 s to diffuse 250 μm . Similarly, a gas would

only require 4×10^{-5} and 6.3×10^{-3} s over the same respective distances. Therefore, liquid separations should benefit from smaller diffusion distances as the predicted timescales are of an order of magnitude as contact times of the liquid in the separator.

The choice of the channel depth can also be justified by examining the mass transfer coefficient as a function of hydraulic diameter. The Sherwood correlation for laminar flow in a rectangular channel used in this discussion was developed by Huang [8]. Figure 1.1 depicts the exponential decrease of mass transfer coefficient as the hydraulic diameter is increased to 100 μm . The width of the channel was held constant at 60 μm , while the depth was increased by increments of 5 μm from an initial value of 5 μm . The mass transfer coefficient of 20 μm deep channel is ~ 2 times more than the mass transfer coefficient for the 120 μm deep channel.

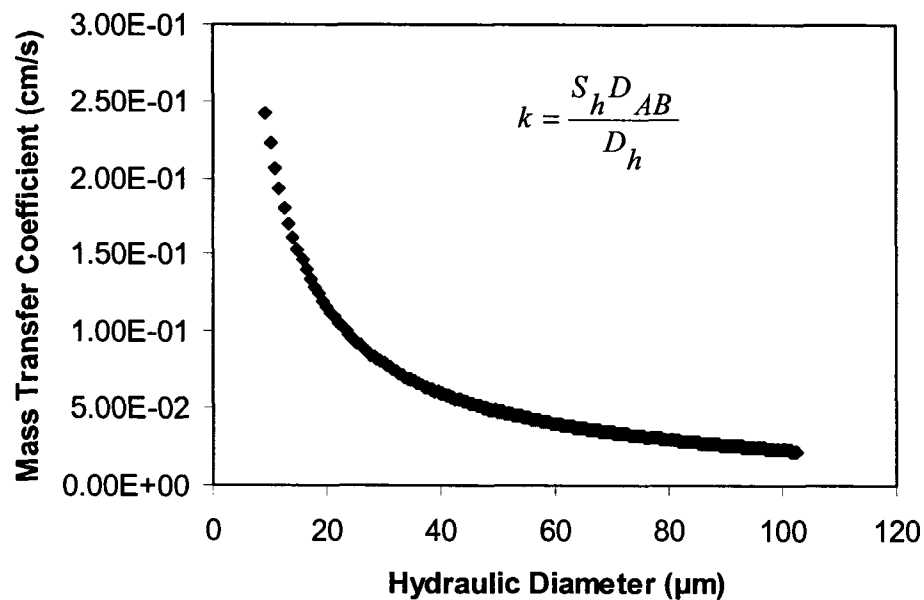


Figure 1.1 Effect of mass transfer coefficient on hydraulic diameter.

The membrane processes have the inherent problem of concentration polarization which occur in the boundary layer and consequently reduces the efficiency of the membrane performance. The concentration polarization can potentially be minimized by the utilization of microchannels with the hydraulic diameter smaller than the boundary layer thickness generally achievable through turbulent flow.

1.2 Objectives

The main focus of this project is to evaluate the process intensification effects for dehydration of ethanol by microscale pervaporation process.

- The microseparator with varying depths was designed and fabricated by conventional photolithography and etching techniques at the Institute of Micromanufacturing in Louisiana Tech University.
- A pervaporation process experimental setup was designed and developed to test the microseparator.
- Separation of ethanol/water mixture beyond the azeotropic concentration by pervaporation process was demonstrated.
- The permeation and selectivity of different depths in microchannels using a polymer dehydration membrane were reported.

1.3 Background

In the chemical industry, separation techniques play a key role for efficient operation. It has been reported that about 50-90% of the capital in a chemical plant is invested on equipment for separation processes [9]. In addition to the traditional separation techniques such as distillation, absorption, extraction, etc., advanced novel

separation techniques such as membrane separations, exsorption, field flow fractionation, magnetic separations, bio separations, etc., are being explored. There is a tradeoff by employing these classic separation processes because they present frequent process related problems such as weeping, entrainment, foaming, etc., and lack of flexibility (flooding, loading, etc.), slower rates, higher energy requirements, etc. [10] On the other hand, these advanced novel techniques have demonstrated promising solutions to the problems above.

1.4 Membrane Separations

Membrane separation is one of the novel techniques that has witnessed dramatic developments in the recent times. It has been reported that, biologists and colloid chemists were the pioneers of membrane phenomena. During the early stages of membrane research, investigators were experimenting on every type of membrane available to them; they used animal sacs such as pig, ox or fish bladders, animal intestines and others. Sausage casings of animal gut and of regenerated cellulose were used for routine dialysis. Membrane theory was developed as a consequence of attempting to explain phenomena of biological systems and, in particular, those involving selective concentration and transport and membrane electric potentials [11].

Many observations like dialysis by Graham, osmosis by Nollet, diffusion by Fick have led to the understanding of many complex membrane process of the present [12]. Although the early membrane processes date back to the middle of 18th century it was not until the 1950's the potential of applications of membrane technology in the chemical industries was realized [13]. The development of membrane technology until then was hindered by its low selectivity and expensive operations. The actual breakthrough that

brought about the much required revolutionary change for the future of membrane techniques was the invention of the high flux ultra-thin membranes by S. Loeb [14]. From this period membrane technology has witnessed significant advances in membrane development and module development in addition to paving the way for myriad applications in many industrial sectors.

1.4.1 Membrane Process

A membrane can be defined as a material between two phases through which selective separation of certain species in a fluid takes place under the action of a driving force. In the membrane system, the feed stream is divided into two streams, i.e., the retentate and the permeate streams. A schematic representation of membrane process is given in Figure 1.2. The retentate stream consists of components retained by the membrane while permeate stream consists of components that could pass through the membrane.

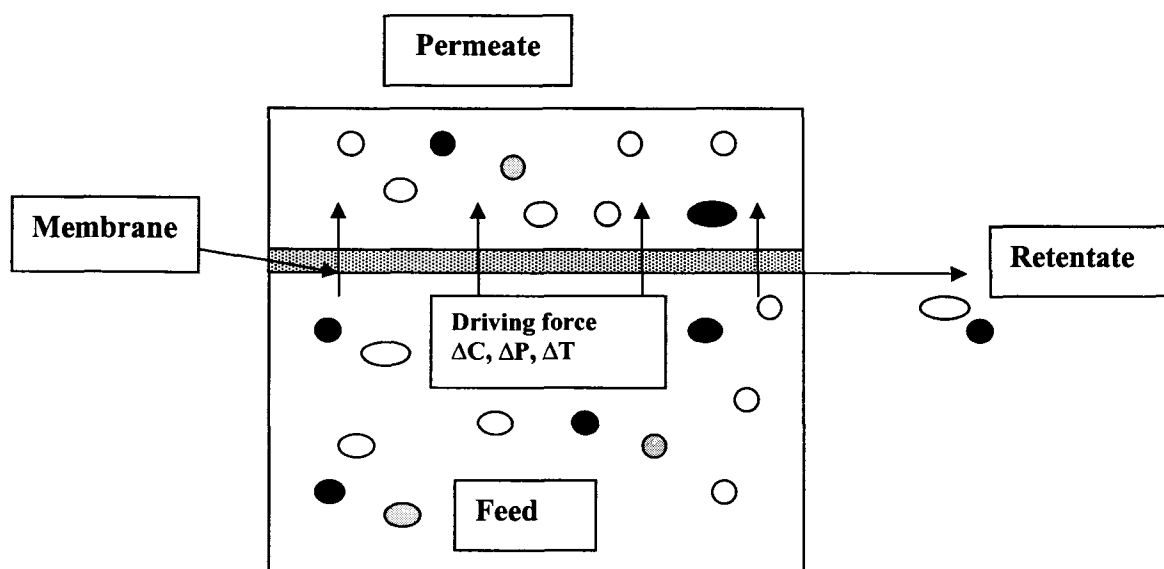


Figure 1.2 Schematic representation of membrane process.

The significant features of membrane techniques include low energy consumption and provision to develop hybrid separation processes. Membrane processes can be operated under mild conditions, as the membrane properties are variable and can be adjusted [13]. It has been reported by Strathmann [15] that the applications of membrane technology can be observed in four key industrial sectors, namely in the separation of molecular and particulate mixtures, in the controlled release of active agents, in membrane reactors and artificial organs, and in the energy storage and conservation systems.

1.4.2 Classification of Membranes and Membrane Processes

Baker et al. has classified the membrane processes into two broad categories: developed membrane technologies and developing and yet-to-be developed membrane technologies [11]. The developed industrial membrane separation processes include microfiltration, ultrafiltration, reverse osmosis, and electrodialysis. Gas separations involving polymer membranes and pervaporation fall into the category of developing processes while facilitated transport is a yet-to-be-developed technology.

The driving forces through the membrane in addition to the structure and material of the membranes are the controlling parameters in membranes. The driving forces used in membrane processes such as pressure, concentration, temperature difference and electric potential determine the selection of the membrane process that could be employed.

Typical pressure-driven processes are microfiltration, ultrafiltration, nanofiltration and reverse osmosis. The characteristic of such processes are bound by the solute's physical and chemical properties which dictate the type of membrane to be used. The

particle size of the solute is one of the parameters used to choose the membrane depending on its pore size and distribution. Figure 1.3 adapted from Baker et al. [9] depicts the classification of membrane processes in terms of pore size of the membrane.

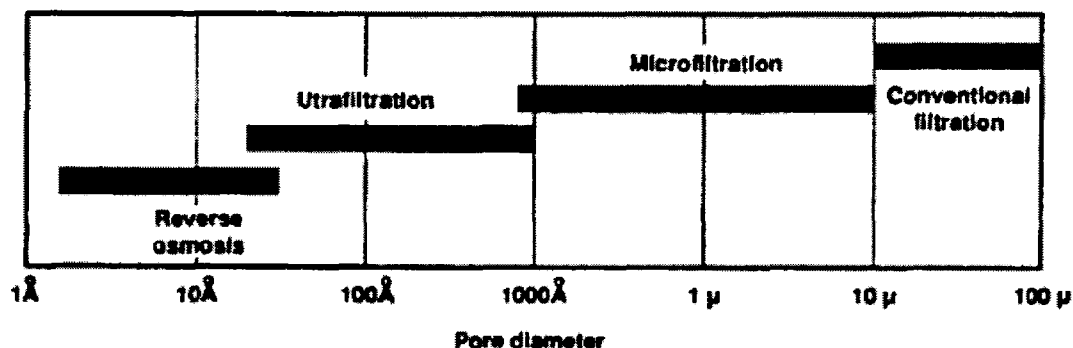


Figure 1.3 Comparison of membrane processes in terms of pore diameter.

1.4.2.1 Microfiltration and ultrafiltration

Microfiltration membranes have pore sizes with diameters from 0.1 to 10 μm while ultrafiltration membranes separates particle from 1 nm to 0.05 μm . Ultrafiltration membranes retain compounds of high molecular weight on one side of the membrane while allowing solvents to pass through. The main difference between the processes is in the pore size of the membrane. Porous membranes are normally used for these membrane processes with the separation based totally on the particle size. The membranes could be either polymeric or ceramic. Microfiltration is used for water treatment, i.e., removal of bacteria from water, removal of heavy metals from pre-treated waste streams, etc. Ultrafiltration is used mostly to concentrate or fractionate high molecular weight dissolved macromolecules, insoluble solids and emulsified organic molecules in water. It is also used in varied industries such as semiconductors, textiles, metallurgical, and dairy [16].

1.4.2.2 Reverse osmosis

Reverse osmosis (RO) utilizes a pressure greater than the osmotic pressure of the solute to separate the solvent by permeating the solvent through a semipermeable membrane. A typical membrane pore size is in the range of 5-20 Å in diameter. Dense polymer membranes are commonly used and the transport process in the membrane is based on the solution-diffusion model. RO is widely commercialized especially in potable water industries where it is used to separate salts from sea water. Reverse osmosis units are ubiquitous in purification of water, for food processing, for medical use, etc [17].

1.4.2.3 Electrodialysis

In electrodialysis, direct electric current is applied for transporting ions through the charged membranes. In this case electric potential is the driving force. The membranes used are an ion exchange membrane or cation exchange membrane and are generally non-porous. The membrane materials are usually cross-linked copolymers based on divinylbenzene with polystyrene copolymers of polytetrafluoroethylene (PTFE) and polysulfonfylfluoridevinylether. Electrodialysis is used in desalination of water, the removal of salts and acids from pharmaceutical solutions and in food processing, separation of amino acids, production of salt, etc. The other processes in which ionic membranes is used are membrane electrolysis, bipolar membranes and fuel cells [18].

1.4.2.4 Facilitated transport

Facilitated transport is driven by concentration difference. The separation principle for facilitated transport is based on the affinity of the carrier or rather the specific chemical reactions [11]. Unlike other membrane process that use a solid

membrane, facilitated transport requires membranes of different category; which can be classified as follows: supported liquid membranes, emulsion liquid membrane, and fixed carrier membranes. This separation process is mostly used in removal of specific ions, separation of organic liquids, removal of phenol, etc [13]. The in-depth discussion on this area is beyond the scope of this research, a detailed review of facilitated transport is covered by Baker et al. [11].

1.5 Pervaporation

Pervaporation is one of the developing techniques in the membrane industry. Kober concocted the name pervaporation in 1917 [19]. It has also been reported that since the permeate undergoes a phase change from liquid to vapor during its transport through the membrane, the process was named pervaporation. It can be observed from reviewing the literature that the development of the process was mostly dormant until 1970's, that is, with no significant breakthrough. It is only after this period, also the juncture at which the advantages of mass transfer through dense membranes were exploited, that the way was eventually paved for the pervaporation process to be economically feasible [11]. A complete review of the pervaporation process is given in Huang 1991 [20].

In pervaporation, the components of a liquid selectively diffuse through a membrane followed by vaporization on the permeate side of the membrane. Driving force for the transport through the membrane is achieved by difference in partial pressure across the membrane; i.e., the pressure on the vapors in the permeate side is lower than the pressure on the liquid side. The phase change occurs because the partial pressures of the permeating components are lower than the corresponding saturation pressures

[21]. This difference in partial pressure can be created by using vacuum or sweeping gases in the downstream or creating partial vacuum by cooling [20] and condensing the permeate vapor [22].

In a typical pervaporation process as shown in Figure 1.4 the feed liquid is initially preheated to an appropriate temperature so that it receives the required heat for vaporization. A feed pump circulates the feed solution through a pre-heater before it reaches the membrane. Generally, the membrane is placed in a specially constructed cell known as a membrane module separated by the membrane into two divisions such that the feed liquid comes in contact with the membrane in one of the divisions while the other division which is the downstream side of the membrane is generally kept under vacuum generated by a vacuum pump. The permeate is evaporated due to the applied vacuum and is condensed in a vacuum trap.

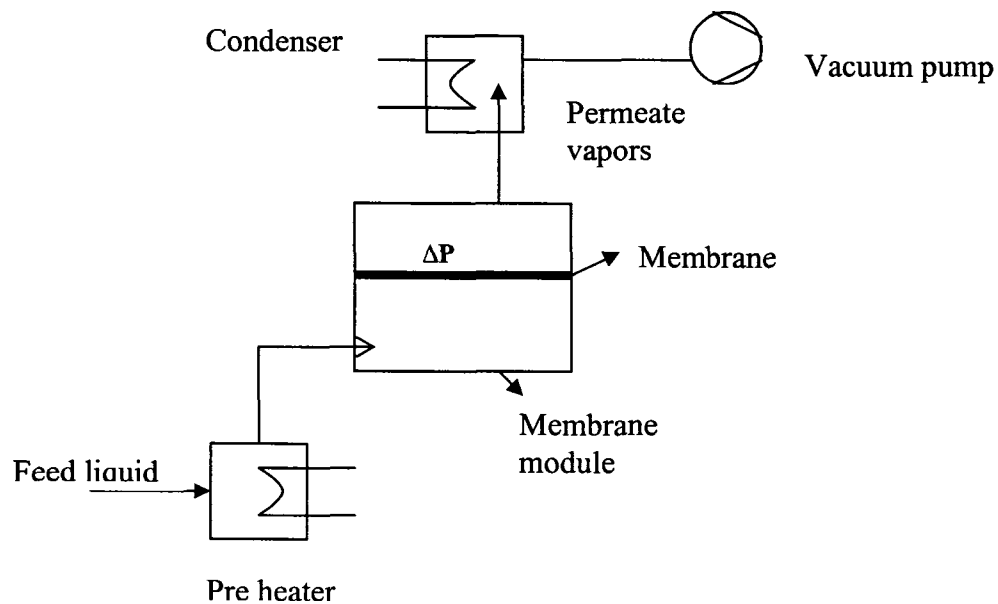


Figure 1.4 Schematic of pervaporation process.

During the pervaporation process, heat loss in the membrane module occurs because of vaporization of the permeate at the downstream surface of the membrane that causes localized cooling. Karlsson and Tragardh have reported in their study that heat transfer in pervaporation affects the mass transfer [24]. Wnuk and Chmiel [25] have suggested direct heating of membrane to supply the heat consumed during the pervaporation process. According to these authors, the direct heating of the membrane eliminates the need for interstage heating which is more commonly used in pervaporation experiments. In addition to these benefits it is also possible to maintain the membrane module at isothermal conditions with direct heating of the membrane.

In comparison with reverse osmosis, pervaporation is reported to offer certain specialized advantages in sectors where reverse osmosis cannot operate economically. In reverse osmosis the driving force is the hydrostatic pressure across the membrane, whereas for pervaporation it is the differential pressure created by vacuum on the downstream side of the membrane. Also, for certain applications RO is limited by osmotic pressure and in RO the separation is achieved by transport of solvent molecules in the membrane but in pervaporation the solute molecules are permeated and evaporated through the membrane, consequently reducing energy consumption [26].

A mixture is said to have a homogeneous azeotrope when in equilibrium, liquid and vapor phases exhibit similar composition. A complete understanding of vapor-liquid equilibrium effects and the formation of azeotrope is vital for efficient implementation of liquid phase separation process involving a vapor-liquid equilibrium. A common azeotrope is the ethanol-water system. A conventional distillation process cannot separate ethanol from water beyond the azeotropic concentration that is 95.6 % w/w without the

aid of a third component. At this composition the liquid and vapor phases in a distillation operation have the same composition so no further separation of water from ethanol can be accomplished. Distillation separates components based on relative volatility. If these volatility differences are insignificant, then it is uneconomical because the columns are expensive when the relative volatility is close to one (when the relative volatility is ~ 1 the reflux ratio is high, and also large amounts of energy is supplied to reboiler and removed from condenser, which makes the process expensive) [9].

Pervaporation, as described earlier, utilizes the interaction of the membrane material with the feed mixture to allow separation that would not otherwise be possible due to an azeotrope point. Pervaporation does not depend on phase equilibrium and can be used for separating azeotropic mixtures [27]. The ethanol-water system has been studied extensively and is considered a reference to assess pervaporation performance [20]. Ethanol/water separation is a low-energy and cost-effective process. It has also been observed that concentrated ethanol could be used as a potential energy resource by biomass [28].

1.5.1 Batch and Continuous Pervaporation Process

Pervaporation process can be operated in batch and continuous systems. It has been reported by Sulzer Chemtech, a pioneer in pervaporation process, that continuous pervaporation processes offers the lowest energy consumption. It is used mostly for continuous processing of solids-free feeds and is most economical process option for low water contents. Batch pervaporation is mostly ideal for multi-purpose plants, e.g., toll recycling, since it has simple equipment with very flexible operation [27]. It has been reported in the literature that the performance of the pervaporation process also depends

to a large extent on operating conditions such as feed/operating temperature, feed flow rate, feed concentration, and permeate pressure [20, 22, 29, and 30].

1.5.2 Solution-Diffusion Model

The solution-diffusion model is the most widely accepted model to describe the mass transfer in the pervaporation process, an extensive review on this model is published by Wijmans and Baker [31]. According to these authors the assumption in describing the model is that the pressure inside the membrane is constant and the difference in chemical gradient is a result of the concentration gradient. A schematic of the solution-diffusion model is shown in Figure 1.5 adapted from Feng et al. [33].

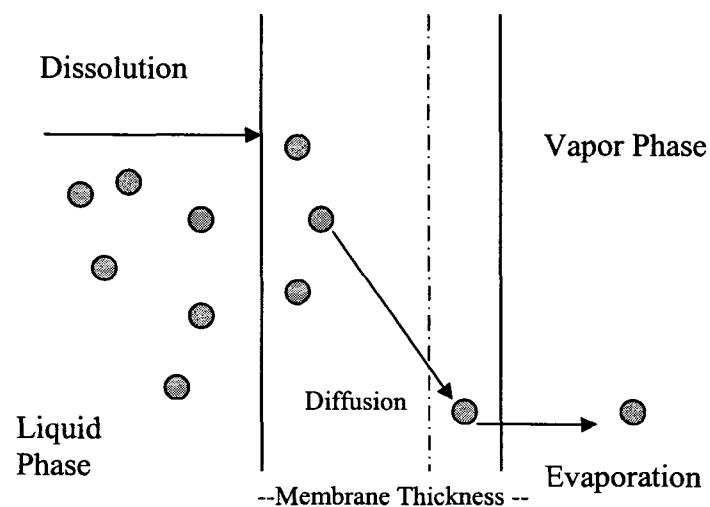


Figure 1.5 Mechanism of liquid permeation through a membrane.

The solution diffusion model describes the following three steps involved during the pervaporation process:

- (a) Sorption into the membrane at the upstream surface

- (b) Diffusion of the sorbed component through the membrane and
- (c) Evaporation of the diffused liquid into a vapor phase at the downstream side

1.5.3 Characterization of Pervaporation Membranes

The separation performance of the pervaporation membrane is characterized by two important parameters; the flux and the separation factor. The flux is usually defined as the mass permeating through 1 m² of the membrane per unit time. Pervaporation fluxes, J , are generally expressed in kg h⁻¹ m⁻² or l h⁻¹ m⁻² [32]. The flux depends on both the intrinsic permeability and the effective thickness of the membrane. It has been very widely reported that minimizing the thickness of the membrane results in higher flux. Membrane performance is characterized by the retention and the permeation rates. The flux of a component is given by Eq. (1).

$$J_i \equiv \frac{P_i(x_i\gamma_i p_i^\circ - y_i p_p)}{\ell} \quad (1)$$

J_i = permeation rate

P_i = permeability coefficient

γ_i = activity coefficient of component i

p_i° = saturation pressure of the pure component i at a given temperature

ℓ = membrane thickness

The selectivity of the membrane is estimated in terms of separation factor (α) and enrichment factor (β) a dimensionless number defined as follows:

$$\alpha = (c'_A/c'_B)/(c_A/c_B) \quad (2)$$

with c and c' being the weight concentrations of the faster permeant (A) in the feed (c) and in the permeate (c'), respectively.

$$\beta = c'/c$$

When the separation factor is unity, no separation occurs, but when it approaches unity, the membrane becomes semipermeable [33].

1.5.4 Membrane Material

In the earlier discussion it was mentioned that the type of membrane material is chosen based on the application. The polymers for the membrane can be broadly classified into two types namely glassy and rubbery polymers.

Glassy polymer or crystalline polymers

Glassy polymers exhibit a glass transition temperature greater than the room temperature. These polymers are observed to have a higher permeability when compared with the amorphous polymer due to the physical cross-links that prevent a high degree of swelling. The commercially available glassy polymers are water selective. Polyvinyl alcohol (PVA), cellulose acetate, and Poly(1-trimethylsilyl-1-propyne) (PTMSP) are the most commonly used in the industry. Glassy polymers such as cellulose acetate exhibit fewer solute/solvent interactions. Selectivity in a glassy polymer is predicted largely by the relative molecular size of the compounds. Cellulose acetate [34] and polyvinyl alcohol have been demonstrated in the literature to be selective to the smaller water molecules in an ethanol/water system. It has been reported that the limiting diffusivity D^* of water is approximately a hundred times higher than that of alcohol [32]

$$\text{Water: } D^* 10^{-8} \text{ cm}^2 \text{ sec}^{-1}$$

$$\text{Ethanol: } D^* 10^{-10} \text{ cm}^2 \text{ sec}^{-1} \text{ at } 25 \text{ }^\circ\text{C}$$

Rubbery Polymers

These polymers exhibit a glass transition temperature lower than that of the room temperature. It has been observed that due to higher chain mobility than the glassy polymers the fluxes in elastomers are higher preferentially absorb and permeate organic components. As such, they are an ideal choice for removal of organic compounds from water. Among the rubbery polymers, polydimethyl siloxane is very popular. Rubbery polymers such as polydimethyl siloxane (PDMS) exhibit a large degree of solute/solvent interactions. The hydrophobicity of PDMS will result in ethanol selectivity in an ethanol/water solution despite the smaller molecular size of water [35]. Sorption-diffusion mechanism is strongly dependent on solvent-polymer interactions. Therefore, the nature of the membrane material and the swelling capacity of the polymer have a direct impact on the separation [36]. The selectivity of the membrane utilized in the pervaporation process depends on the state of the polymer membrane at the temperature of operation.

Membranes typically used in industries can also be classified as homogeneous, asymmetric and composite membranes, while the different configurations that are employed are plate and frame membranes, spiral membranes, tubular membranes and hollow fiber membranes [13, 15].

1.5.5 Applications of Pervaporation

Pervaporization has been utilized for concentration of ethanol produced by fermentation of biomass [35]. The other commercial applications of pervaporization include dehydration of alcohol and other solvents [33, 35 - 46], removal of small amounts of organic compounds from contaminated waters [47 - 52], separation of close boiling

mixtures [13] and azeotropes [53 - 56] these applications are notable in water desalination, water purification and gas separation industries [56]. This process has emerged as an energy efficient alternative to conventional separation techniques such as distillation [20]. Pervaporation is also popular for its compactness, flexibility, simplicity and versatility. It has been reported that it is relatively easy to integrate pervaporation units with traditional separation techniques so that the advantages of a hybrid process can be exploited [13, 32].

To summarize the key applications of pervaporation, Feng's [33] classification for the applications of pervaporation into three categories can be considered:

- (a) Dehydration of organic solvents
- (b) Removal of organic compounds from aqueous solutions
- (c) Separation of anhydrous organic mixtures

1.5.6 Concentration Polarization

Membrane processes exhibit a decline in efficiency due to concentration polarization. The separation capabilities in membrane technology rely mostly on the functioning of the membrane. However, this separation performance of a membrane changes with time which can be observed by the decrease in flux through the membrane over time. This decline can be caused by several factors, such as concentration polarization, adsorption, gel layer formation and plugging of pores [15]. These factors induce additional resistances on the feed side to the transport across the membrane. The extent of these phenomena is strongly dependent on the types of membrane process and feed solution employed. Flux decline has a negative influence on the economics of a given membrane operation, therefore measures must be taken to reduce its incidence.

Concentration polarization is a phenomenon that takes place when mass transfer arises from a concentration gradient between the more concentrated boundary solution and the less concentrated bulk. It is known that concentration polarization can be a serious problem for these membrane processes, in general leading to a decrease in flux and separation characteristics. Huang et al. [57] have observed that the concentration polarization depends on the membrane selectivity in addition to the membrane permeability and system hydrodynamics. Their analysis have revealed that the effect of concentration polarization may be more pronounced in pervaporation of dilute solutions at lower concentration levels where the minor component is the preferential component for the membrane. However, when the feed concentration is relatively high the concentration polarization may not affect the separation performance. The problem of concentration polarization has not been widely reported in the literature for removal of water from ethanol mixtures using polymer dehydration membranes.

1.6 Process Intensification Review

The need for a new technology in the chemical industry is long overdue. The electronics industry has already passed through several phases that have brought about spectacular changes. The chemical industry has always been in the spotlight whenever environmental concerns have arisen. Researchers all over the world have been working on developing novel technologies that could make an impact to improve the quality of life universally and process intensification is one such technology currently gaining tremendous momentum. Vision 2020 is an industry led partnership of both private and public organizations involved in continuous collaboration to foster technology innovations. Their goal statement is “to provide chemical companies with options to

incorporate process intensification so that they can react to increasing market demand and environmental regulations.”

1.6.1 Definition of Process Intensification

Ramshaw, one of the pioneers in the process intensification field, defines “process intensification as a strategy for making dramatic reductions in the size of chemical plant so as to reach a given production objective” [58]. According to Moulijn et al., [58] process intensification consists of the development of novel apparatuses and techniques that, compared with those commonly used today, are expected to bring dramatic improvements in manufacturing and processing, substantially decreasing equipment size/production capacity ratio, energy consumption, or waste production, and ultimately resulting in cheaper, sustainable technologies. Charpentier defines process intensification as “complex technologies that replace large, expensive, energy-intensive equipment or processes with smaller, less costly, more efficient plants, or plants that combine multiple operations into a single apparatus or into fewer devices” [59].

1.6.2 Examples of Process Intensification

Imperial chemical industry’s quest for decreasing plant costs and increasing the production in a chemical plant led to the birth of “Higee” a liquid/vapor contacting mass transfer device. It was constructed on the postulations based on the Sherwood flooding correlation that provided framework to build a rotor with high specific surface area packing design. These rotors generate very high centrifugal forces, ‘g’, that eventually intensified the heat and mass transfer. On comparison with conventional columns “Higee” demonstrated 500-fold increase in performance. This device has successfully

been used for distillation, absorption and desorption. “Higee” exhibits the entire features essential in a process intensifying equipment; it is smaller, safer, and cheaper [60-61].

A similar principle was applied to develop a spinning disk reactor. In this process liquid solution is introduced into the center of the rotating disk. This liquid forms a thin film on the disk and extends into a waveform as it moves towards the edge. The centrifugal force causes interference of these waves that in turn facilitates very high heat and mass transfer rates. It has been reported by researchers at Newcastle University in London, who developed these reactors so that they exhibit very low residence times, and the liquid flowing is in plug flow due to absence of back mixing. They have been presently used on fast and very fast liquid-liquid reactions such as nitration, sulphonation and polymerization where heat management is critical. The researchers have demonstrated residence times in the magnitude of 0.1 s and heat transfer rates of 10,000 W/m²K. The industrial collaborators who have applied this technology have reported 99.9 % reduction in reaction time and inventory [62].

The reason the above examples have been cited is to illustrate the fact that from the earliest process-intensifying equipment such as “Higee” to the more recent spinning disk reactor, a common feature was adapted to obtain thin film for intensifying the heat and mass transfer. Micro-chemical systems can also achieve this thin layer by means of their miniaturized dimensions for process intensification of various chemical processes.

1.7 Micro-Chemical System

MEMS (Micro Electro Mechanical Systems) involve the miniaturization of electrical and mechanical processes. The mechanical and electrical components are fabricated on integrated circuits with dimensions ranging from microscale to milliscale.

The advancement in MEMS has facilitated significant progress in microfabrication techniques. The implementation of these techniques has created bridges and united multidisciplinary fields of chemical engineering, chemistry, biology, electronics and many more. As such, there is now in existence some novel areas such as μ -total analysis systems and lab-on-a chip that exhibits these varied technologies on a common platform.

Reactions or unit operations made possible in microstructured devices can be identified under the theme of microreaction technology. Microreaction technology is the sought pathway for process intensification in the recent times. It is evident from its increasing application in pharmaceuticals [63-66] and many other industries that the future of this innovative technology lies on a fertile ground. Micro-chemical systems are an emerging technology in chemical engineering; researchers in academia and industry are exploring this area to develop miniaturized unit operations so as to exploit the advantages presented by scaling down to the microscale. The dimensions of these microreactors are in the order of micrometers with structural components possibly at the nanoscale [67]. They are built using advanced fabrication techniques such as LIGA (lithography, galvanofornung, abformung), bulk micromachining (wet and dry etching), mechanical micromachining, electron discharge machining, laser ablation, hot embossing etc. The most common substrates for microreaction technology are glass, silicon, high-alloyed steel, titanium, polymers, and ceramics [68].

1.7.1 Advantages of Micro-Chemical System

Micro reactors offer certain inherent advantages such as short residence times, small hold up of liquid volume and enhanced safety due to their smaller dimensions. The higher heat and mass transfer rates in model gas, liquid reaction systems provide better

control of reactions with high selectivity, conversion rates, yield, and product quality. According to Wegeng et al. [3] it is because of the reduction in resistances that the heat and mass transfer rates are increased by orders of magnitude. Certain reactions difficult for macroscale reactors may potentially be produced in a microscale reactor easily. The specific surface of these microreactors is in the range from 10,000 - 50,000 m^2/m^3 in comparison with the conventional laboratory and production vessels which generally offer 100 and 1000 m^2/m^3 [66]. These high surfaces provide better temperature control during reactions. The short wall-to-wall distances accessible in the microreactors facilitate several diffusion-limited chemical processes [69] and also minimize concentration gradients [70]. The most unique advantage of microreactors is in the distributed point-of-use and on demand synthesis of hazardous chemicals [71]. These are being studied for potential use in chemical synthesis, and process development. [73]. More recently, microreactors are finding applications in small-scale processing, including fuel processing, and combinatorial or analytical methods [69]. Thus, microreactors are gaining more importance with high potential for further research and also commercial use.

1.7.2 Literature Review of Separation Processes in Micro-Chemical Systems

Most unit operations studied to date in micro-chemical system are primarily of gas phase catalytic reactors, heat exchangers, liquid phase mixers and extractors. For micro-chemical systems to provide a complete synthesis solution, chemical separation processes must be developed. The conventional separation process that has been miniaturized is the liquid-liquid contactor, as described below.

Martin et al. [71] from Pacific Northwest National Laboratory outline the intrinsic advantages of micro-chemical systems in their research on microchannel reactors and separation systems. They have used a diffusion bonded lamination method to construct solid metal microchannel devices since this method facilitates fabrication of smooth walls of any complex design or aspect ratio. Their microchannel device consisted of a series of microchannels separated by micromachined metal or polyimide membranes shown in Figure 1.6 adapted from Martin et al. [71].

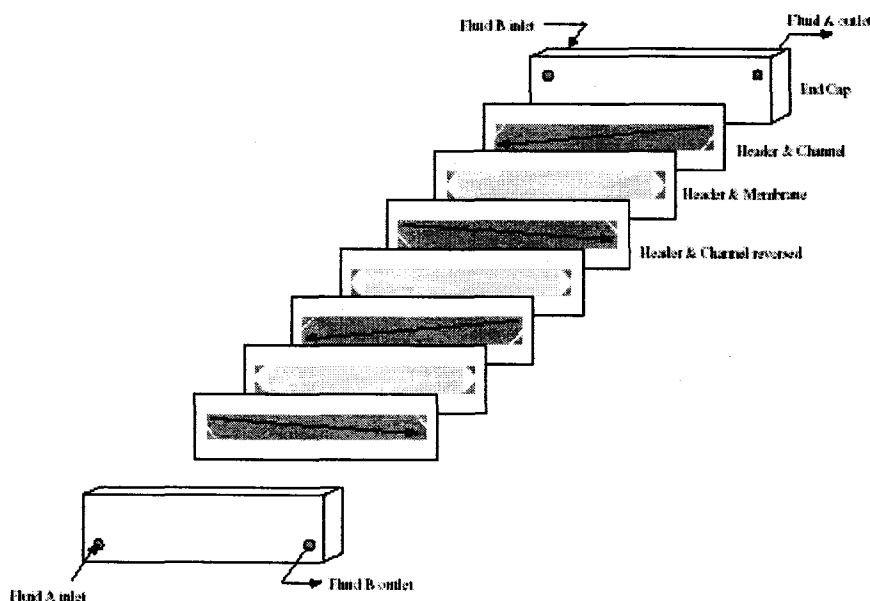


Figure 1.6 Assembly of a counterflow microchannel chemical separation device.

A type 304-stainless steel shim was used in the construction of channels and the membrane. The fabricated microchannels exhibited a high aspect ratio of 1000, the length of the microchannels was 8 cm, width 100 μm and height 1 cm. Laser micromachined technique was used to create an array of 5 μm to 30 μm diameter micropores on the polyimide separation membrane. This separation unit was used for extraction of solute

from a fluid waste stream. The researchers have reported that the separation unit demonstrated improved performance as a result of short liquid/liquid contact times in the device [71].

Micro-chemical systems integrated with membrane technology offer tremendous potential as an alternative avenue for separation processes. The short diffusion path inherent in a microchannel device should allow process intensification of a mass transfer limited unit operation such as membrane separation. The commonly involved membranes for gas separation such as palladium membranes have been used in microreactors for hydrogen separation. The following paragraphs outline the research with palladium membranes and also polymer membranes in microreactors.

Jones et al. [73] have fabricated a microreactor on silicon with 10 channels, 50 mm in length, 500 μm in width and 10 μm in depth. This reactor was developed to test the dehydrogenation reaction of cyclohexane to benzene using a palladium membrane. The palladium membrane was also fabricated on the channels, and the thickness was in the range of 3-6 μm . Simulations by a model developed by these authors predicted that the reaction performance could be improved by effectively controlling the thickness of the membrane, channel depth and operating pressures.

Schmidt et al. [74] in their research on palladium membrane microreactors have demonstrated a hydrogenation reaction in which selective hydrogen flux has been observed. A microreactor was designed with two flow channels separated by a thin palladium membrane. The membrane was deposited by e-beam and supported by silicon nitride and silicon oxide layers; its width was slightly less than 700 μm . A channel of 1.2 cm length was fabricated in the silicon wafer using conventional bulk micromachining

techniques. The other channel was formed by attaching an epoxy cap to the top of the device. The topside of the membrane was uncapped and exposed to air during the flow of hydrogen/nitrogen mixture. It was shown that hydrogen permeating through the membrane reacted with oxygen in the air, forming water. The reactor performance was characterized with respect to mechanical strength and hydrogen flux. According to the authors, this technology represents a novel application of MEMS in microfluidics and also microfabricated palladium membrane reactor is used due to their small size, fast thermal response times, and higher efficiencies.

Schiewe et al. [75-76] have developed a prototype membrane module in a microreactor. They have focused on developing a miniaturized separation module for online separation and enrichment of gaseous products from the ethylene oxide microreactor. It was observed that the gases to be separated were very similar in their molecular size and structure, which required efficient separation. Hence, dense polymer membranes such as polyimide used in other difficult separation processes were employed as starting materials. After detailed observations it was found that ethylene oxide reacted with these polymer membranes. It was later concluded that the membranes to be used for separation of ethylene oxide have to be cross-linked by physical or chemical methods. Schiewe et al. have reported that by introducing strong electronegative substituents or polar cross-linking agent's solubility for ethylene oxide / ethylene separation could be increased.

The synergy of membrane technology and microfluidics has provided a platform for several new applications and research in these areas have a wide array of focus. Lammertink et al. have outlined the scope and prospects of this confluence in their recent

review on membranes and microfluidics [77]. Researchers have miniaturized diffusion limited conventional membrane processes such as dialysis, pervaporation and reverse osmosis. The following paragraphs describe the pervaporation studies in microscale.

Yeung et al. [78-79] have developed a microreactor consisting of 35 channels of 300 μm in width, 600 μm in depth and 2.5 cm in length for the synthesis of fine chemicals. They have constructed the microchannels on a stainless steel plate using electro-discharge micromachining. The microreactor also functioned as a membrane microreactor. A hydrophilic ZSM-5 zeolite membrane selectively separated water from Knoevenagel condensation reaction of benzaldehyde and ethyl cyanoacetate solutions. They observed that the average permeation rate of pure water through the ZSM-5 membrane was 0.04 $\text{kg}/\text{m}^2\text{hr}$, and this rate improved to 0.15 $\text{kg}/\text{m}^2\text{hr}$ for a longer residence time of 0.8 h. Their work also highlights the increase in yield due to improved mass transfer rates at the microscale. They have used pervaporation process to selectively remove water that would otherwise have inhibited the conversion rate in the Knoevenagel condensation reaction. They have reported an increase in 25% conversion in addition to improved product quality made possible by the use of the membrane microreactor.

Eijkel et al. [80] have developed microfluidic channel structures for osmosis and pervaporation using polyimide. They used a combination of spinning of photopatternable polyimide and sacrificial-layer etching of aluminum to produce sub-micron channels. Their design consisted of polyimide walls of 4 μm long and 500nm high arranged in arrays of 16 parallel channels 2-30 μm width. They have reported a seven-fold increase in concentration of KNO_3 solution by dehydrating water using polyimide by pervaporation techniques. For the osmosis process, they used a branched nanochannel structure with the

channels 30 μm wide and 500 nm high. The length of these branched channel structure in the permeation area was 1mm.

Research involving pervaporation process in the microscale to study the effects of concentration polarization and process intensification effects in separation performance has not been reported to date. Ethanol/water separation in microscale pervaporation process delineates an attempt to approach to the prevailing problem of concentration polarization in pervaporation systems. Pervaporation process for separation of organics from water has been widely studied for concentration polarization effects, and it has been reported that the transport resistance through the boundary layer is dominating [81-91]. Many researchers have developed techniques to minimize the effect of concentration polarization by focusing their efforts in developing novel membrane modules such as vibrating module [92] or other techniques such as using turbulent promoters, pulsing feed flow over the membrane, etc. [93] The ultimate goal of these researchers was to increase the mass transfer coefficient in the boundary layer. In a conventional pervaporation process sensitive to concentration polarization, the boundary layer thickness is a function of the flow velocity. In the present study, a silicon microseparator was developed with the largest hydraulic diameter of 80 μm . This hydraulic diameter is smaller than the boundary layer thickness typically present in the conventional pervaporation systems for laminar flow. Incorporating microfluidic channels for fluid flow in the membrane module should therefore provide a potential solution for reducing the boundary layer resistance in systems the exhibit concentration polarization effects.

CHAPTER 2

METHODS AND MATERIALS

In this project, two different experimental setups were developed to study separation performance of a microchannel pervaporation process. In the preliminary experimental setup, the pervaporation process was based on a single pass of the retentate. This setup was later subjected to modifications such that the retentate was recycled back to the feed tank. The details of the setup and methodology involved are explained in the following sections.

2.1 Pervaporation Experiments Based on Single Pass

Pervaporation of ethanol/water mixture through a commercial polymer dehydration membrane was carried out by an ordinary pervaporation technique. The membrane used was a polymer dehydration membrane (PERVAP 2216) supplied by Sulzer Chemtech. This membrane was a composite membrane having three layers. The principal layer was a non-woven fabric to strengthen the membrane, support made of PAN (polyacrylonitrile), and the separation layer of cross-linked PVA (polyvinyl alcohol). The total thickness of the membrane was 200 microns while the thickness of the active separation layer was about 3 microns. The maximum long-term temperature for operation with this membrane was 100°C, and the maximum short term temperature was

105°C. The effective membrane surface area available during pervaporation experiments was 3 cm².

The feed solution used was 90 % v/v ethanol (Sigma Aldrich- Reagent Grade) and this was introduced into the microchannels and circulated at flow rates in the range of 0.4 ml/hr to 1 ml/hr (0.006 to 0.16 ml/min) from a syringe pump (model 74900 series, K.D. Scientific). The syringe pump had an accuracy of $\pm 0.5\%$, reproducibility of $\pm 0.2\%$, and maximum pressure of 40 psi. The range of flow rate that could be used by this pump was from 0.008 $\mu\text{l}/\text{min}$ to 147 ml/min. A glass syringe with luer lock (Hamilton) of 50 ml capacity was used in all the experiments.

The microchannel and the membrane are placed inside a module described in Section 2.2. The downstream pressure was maintained at 0.3 Torr. Experiments were conducted at operating temperatures of 40°C and 60°C. Vacuum was applied on the permeate side of the membrane using a Welch CHEMSTAR 1376N vacuum pump. The ultimate pressure that this vacuum pump could operate was 0.00013 Torr and this pump was equipped with gas ballast that facilitated in expelling the unwanted vapor from the pump.

Permeate vapors were trapped in a vacuum trap. Due to the short duration of each experiment resulting in only a small amount of material being transferred across the membrane, adequate quantity of permeate was not collected to calculate either the permeate flux or the selectivity. As such, the retentate was collected and weighed to report the flux and selectivity. The duration of the experiment for each trial at any flow rate was based on at least three residence times of that particular flow rate. The collected retentate was analyzed using a Hewlett-Packard 5890 Series II gas chromatograph

equipped with a Flame Ionization Detector (FID) in order to analyze the concentration of the organic contents. The ethanol concentration in the retentate was calculated by using a calibration curve as described in Appendix A. A schematic of the experimental setup is shown in Figure 2.1.

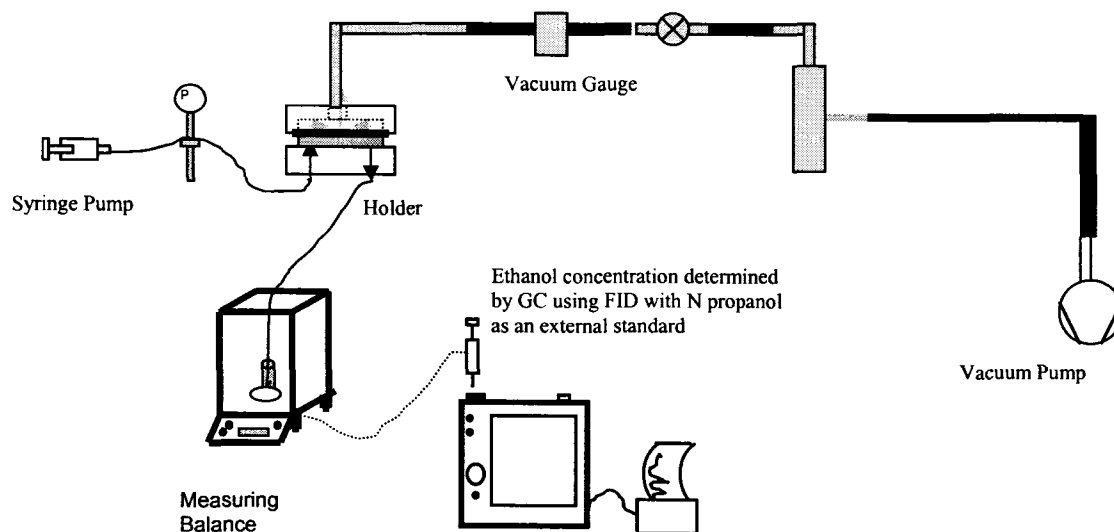


Figure 2.1 Schematic of experimental setup for batch pervaporation experiments.

The residence time in the microchannels was calculated as follows:

Total volume of channel zone, $V = n \times L \times W \times D$

Here, n = no. of channels

W = width of channel

L = length of channel

D = depth of channel

The residence time is calculated using the equations below:

$$\text{Residence time } t_r = \frac{V}{Q} \quad (Q - \text{volumetric flow rate})$$

The flux and separation factor were calculated using the following equations:

$$\text{Mass flux through membrane} = \left[\text{flowrate} \left(\frac{\text{ml}}{\text{hr}} \right) * \text{density} \left(\frac{\text{g}}{\text{cm}^3} \right) \right] - \frac{\text{SampleMass} \left(\frac{\text{g}}{\text{hr}} \right)}{\text{Time}}$$

$$\text{Flux} = \frac{\text{Mass flux through membrane} \left(\frac{\text{kg}}{\text{m}^2 \text{hr}} \right)}{(1000 * \text{MembraneArea})}$$

A mass balance was developed around the system to calculate the mass of permeate and consequently concentration of ethanol/water in permeate. The equations below were used in these calculations:

$$M_{\text{in}} = M_{\text{out-perm}} + M_{\text{out-ret}}$$

$$M_{\text{in}} * X_{\text{eth}} = M_{\text{out-perm}} * X_{\text{eth-perm}} + M_{\text{out-ret}} * X_{\text{eth-out ret}}$$

$$M_{\text{out-perm}} = M_{\text{in}} - M_{\text{ret}}$$

$$X_{\text{eth-perm}} = \frac{[M_{\text{in}} * X_{\text{eth-in}} - M_{\text{out-ret}} * X_{\text{eth-outret}}]}{(M_{\text{in}} - M_{\text{out-ret}})}$$

$$M_{\text{in}} = \text{Total mass of feed ethanol solution}$$

$$M_{\text{out-perm}} = \text{Mass of permeate}$$

$$M_{\text{out-ret}} = \text{Mass of retentate}$$

$$X_{\text{eth}} = \text{Concentration of ethanol in feed}$$

$$X_{\text{eth-perm}} = \text{Concentration of ethanol in permeate}$$

Similar equations were used to calculate the concentration of water in the permeate. The separation factor is calculated as follows:

$$\alpha = (c'_A / c'_B) / (c_A / c_B)$$

where c and c' being the weight concentrations of the faster permeant (A) in the feed (c) and in the permeate (c'), respectively.

2.2 Description of Membrane Module/*In-situ* Heat Exchanger

The holder/membrane module was machined from an aluminum block and the schematic is shown in Figure 2.2. The *in-situ* heat exchanger/membrane module was made up of bottom and top plates with an inlet and outlet port for fluidic connections provided on the bottom plate. The dimensions were 2.5 x 3.65 inches. Four through holes of 5/32 inches ID that were equally spaced were drilled through the surface of the 0.5 inch thick wall of the bottom plate. Similarly, two holes were drilled on the top plate that aligned with the holes on the edges of the bottom plate (refer Figures 2.6). These holes facilitated the circulation of heated ethylene glycol solution continuously circulated using a programmable digital circulator (Polyscience Model 9510). Polyscience Model 9510 circulator that was used had a temperature stability of $\pm 0.01^\circ\text{C}$ and a readout accuracy of $\pm 0.25^\circ\text{C}$. The temperature range (non-refrigerated) was ambient + 5°C to 200°C and the temperature range (refrigerated) was -45°C to 200°C .

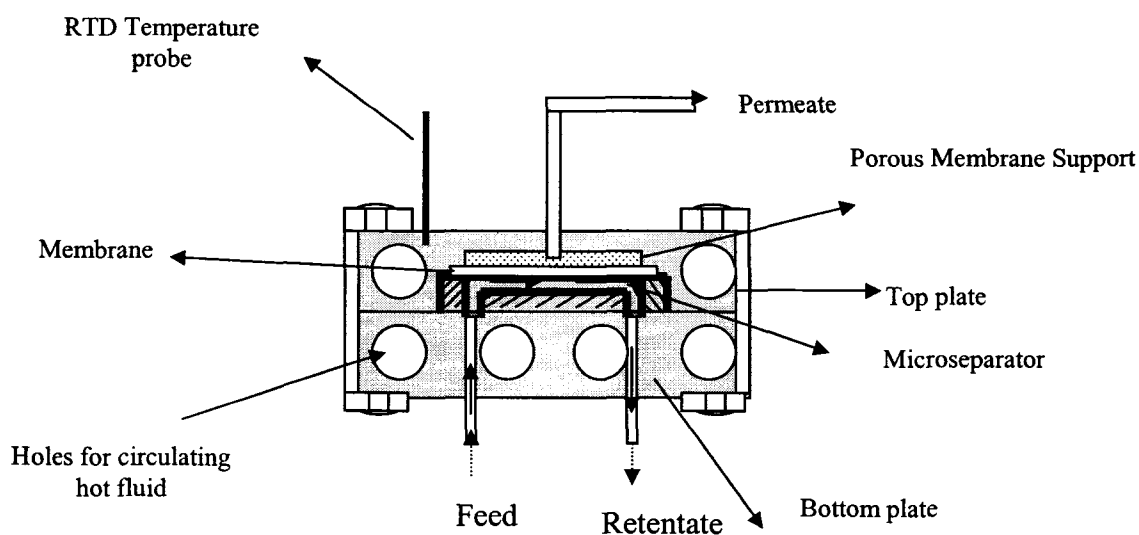


Figure 2.2 Schematic of the membrane module.

Polyscience Model 9510 also had the facility to use a remote probe. The pump flow rate (Pressure) @ 120V, 60 Hz was 11 to 24 liters/min. Ethylene glycol solution (100 %) was used as the internal fluid in this circulator because it offered a temperature range of 50-125°C that was well suited for our application.

Two brass manifolds (McMaster-Carr), as shown in Figure 2.3 (Adapted from www.mcmaster.com), were used for multiple point distribution from a common source so that the inlet and outlet tubing lines from the circulator were connected to one manifold on each side of the holder respectively. These manifolds had two inlets (one at each end). Brass manifolds were chosen because they have excellent strength/durability in addition to good chemical and corrosion resistance. The temperature range at which this brass manifold could be operated was – 53.8°C to 121°C. The six outlets of the manifold were 1/4" NPT Inlet X 1/8" NPT Outlet, and these were connected with appropriate hose fittings that enabled the use of high-temperature Viton tubing (McMaster-Carr). Viton tubing was chosen because it could be used for a wide temperature range (-26.1°C to + 200°C) and did not leach in the presence of ethanol.

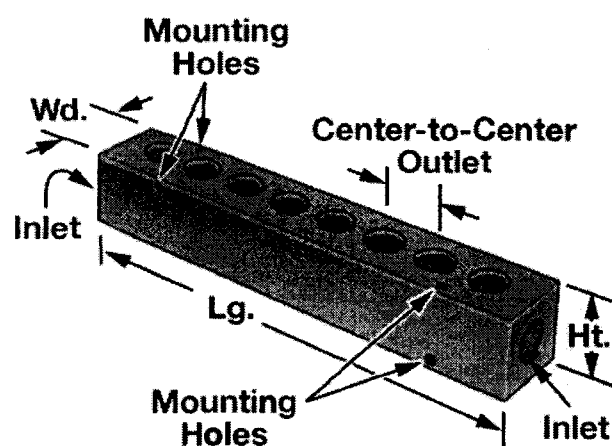


Figure 2.3 A schematic of the brass manifold used for *in-situ* heat exchanger.

The holder was designed such that five bolts on each side of the plates facilitated tight sealing. The holder served as the interface unit for the microchannel membrane module to the macro-scale laboratory environment. It also served as an *in-situ* heat exchanger to provide heat of vaporization required for the feed ethanol solution to achieve separation. The top plate of the membrane module as shown in Figure 2.4 consists of a receptacle for a porous support to the membrane. The receptacle was 1/8 inch deep, 3/8 inch wide and 1.25 inches long, with a 1/8 inch diameter through hole that extends outside to the vacuum line. The bottom plate in which the microseparator was aligned with the holes for the inlet and outlet is shown in Figure 2.5.

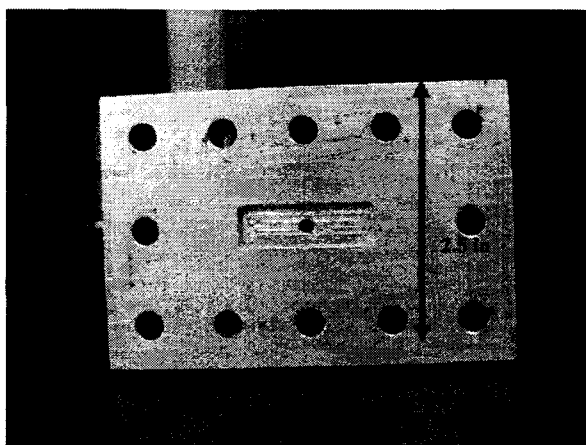


Figure 2.4 Picture of top plate in the membrane module.

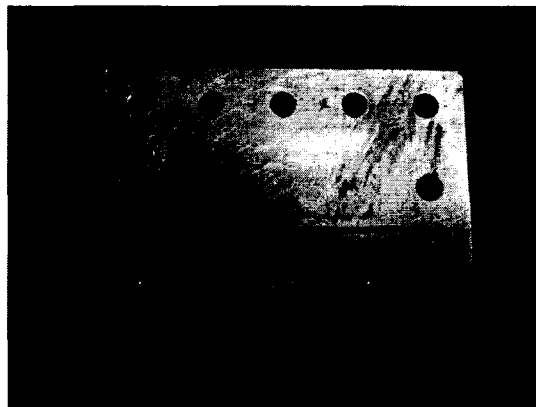


Figure 2.5 Picture of bottom plate in the membrane module.

The two holes in the top plate and the four holes in the bottom plate for circulating hot fluid are shown in Figure 2.6.

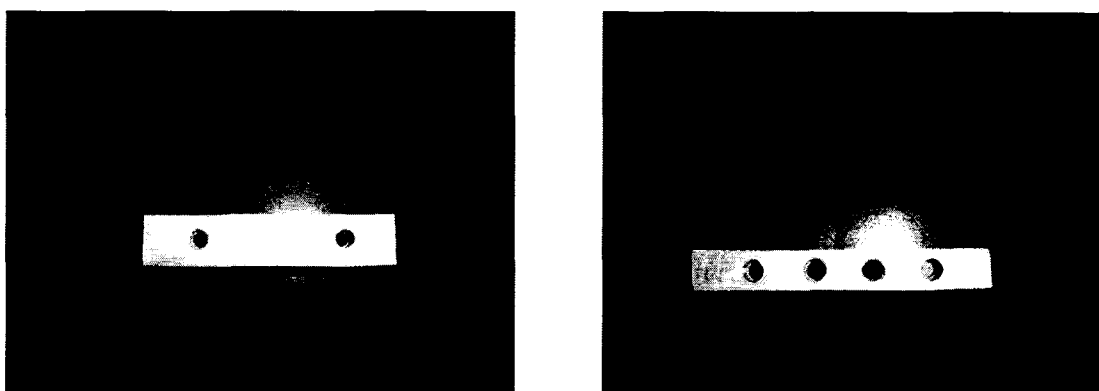


Figure 2.6 Picture of holes for heat exchanger in the membrane module.

The porous support used was a coarse polypropylene sheet (POREX Porous products Group) as shown in Figure 2.7. It had an average pore size of 125-175 μm and the thickness of the sheet was 1/8" inch. To prevent the flow of fluids outside the microchannels, a transparent silicone rubber plain back sheet (McMaster) of 1/32" thickness was used as a gasket for all the experiments.



Figure 2.7 Picture of porous membrane support.

2.3 Pervaporation Experimental Setup **Based on Retentate Recycle**

Description of experimental setup

Separation of ethanol-water mixtures through a commercially available polymer dehydration membrane was carried out by pervaporation technique. The membrane used was a flat sheet (PERVAP 2216) supplied by Sulzer Chemtech. The feed ethanol solution was circulated at varying flow rates [1 to 50 ml/min] by a Masterflex peristaltic pump. The Masterflex[®] L/S[®] pump was a computer-compatible/programmable drive, with 1.6-100 rpm range. This pump also had a LED display, remote inputs, and RS-232 port. The pump could be used for the flow range of 0.1 to 580 ml/min with a speed control of $\pm 0.25\%$ (1 rpm at 600 rpm; 0.1 rpm at 100 rpm).

Selecting an appropriate tubing material for the Masterflex feed pump was important. The feed solution used being ethanol, it was imperative to use tubing that exhibited high compatibility with this organic compound. From our earlier experience with Norprene tubing, we realized that on extended use of Norprene with ethanol solution results in leaching and subsequent discoloration of the feed solution. Since all analysis was subjected to the measurement of refractive index, it was critical to avoid such problems. Hence, Masteflex Viton tubing was chosen because this tubing was rated to have the best compatibility with ethanol in addition to its wide temperature range of -23

°C to + 205 °C. The size of the Viton tubing used was Size -16, with an ID-0.123 mm. The calibration for the tubing at the various flow rates is included in Appendix F.

Experiments were conducted at a constant feed temperature of 90°C controlled by a programmable circulator (Polyscience Model 9510) and a vacuum pressure range from 2 to 3 Torr measured by a Supco vacuum gauge (VG62). The vacuum gauge used had an analog meter of 5 inches display. The range of vacuum that could be measured was 50-5000 microns.

The feed solution of ethanol (Sigma Aldrich-Reagent Grade) was diluted to the desired concentration using de-ionized water. De-ionized water obtained from CORNING Mega Pure system, was the main constituent of all experimental fluids performed with the microseparator.

The feed ethanol solution was introduced into a 50 ml glass beaker previously set on an Ohaus explorer analytical balance. The Ohaus explorer balance used had a capacity to weigh 410 g with a readability of 0.001g, repeatability of 0.0015 g, linearity of ± 0.002 g. This balance was used in all the experiments because it could be interfaced with a computer to enable online monitoring of the balance readout. To ensure stable readings from the balance, the balance was placed on a hard top granite table as shown in Figure 2.8. It was also ensured that the portion of the inlet and outlet lines inside the balance were not in contact at any time with any physical part of the balance or the feed tank, to minimize external disturbances. The mass change in the feed was acquired at 10 second intervals for the entire duration of the experiment.

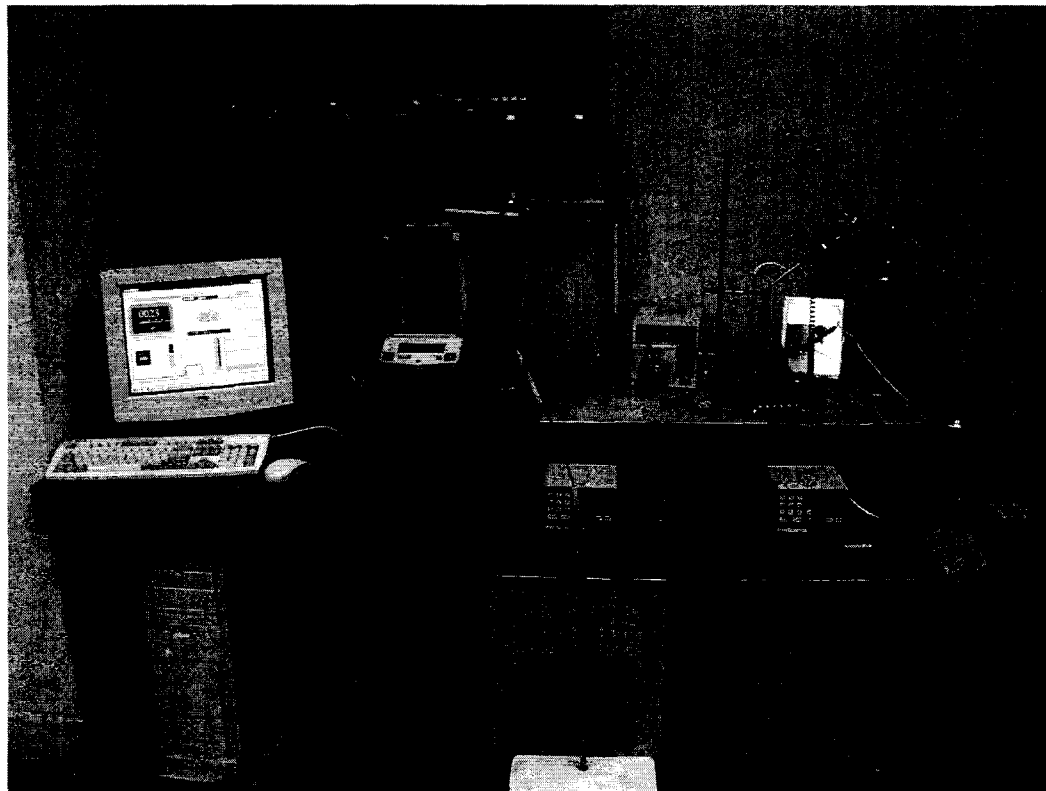


Figure 2.8 Picture of experimental setup for retentate recycle pervaporation process.

The initial feed ethanol solution used in all the experiments was 27.5 g corresponding to 33 ml. The initial feed mass was so chosen because about 50 % of the feed solution was required to fill up the inlet and outlet lines. The remaining feed ethanol solution was circulated through the microchannel membrane module, and the retentate/outlet was recycled back to the feed tank. A fraction of the retentate lines was immersed inside a chiller (Polyscience Model 9510) in order to ensure that the feed ethanol solution inside the feed tank is at room temperature. The temperature inside the feed tank was continuously acquired by a type K thermocouple probe connected to the digital multimeter (Extech-Model 382860) that was connected to a computer. Temperature measurements were recorded for every 30 seconds throughout the

experiment. This multimeter could be used to measure the temperature in the range from - 40 ° C to 200 ° C ($\pm 3 \% + 5$ digits). The resolution of this multimeter was 1 ° C.

Most of the experiments lasted between 24 to 36 hours. The experiments were terminated when the ethanol concentration in the feed tank had reached 98 % w/w or until the volume of feed solution in the feed tank reached a level within the range of measurability in the balance.

To minimize the fluid volume in the feed and retentate lines, small diameter tubing was used in most sections of the tubing lines. As such PEEK (polyetheretherketone) tubing (Upchurch Scientific) was chosen because it was inert and had a wide choice of inner diameters. The tubing size used in the experimental setup was 0.030 inch ID and 4 feet in length. A copper tubing of 1/16 inch diameter and ~ 3.5 feet length was used for the sections of the retentate line immersed inside the chiller. Copper tubing was used for its high thermal conductivity.

It is critical to use a filter during experiments to remove dust or any foreign particle in the microchannels. As such, an inline strainer and filter assembly obtained from Swagelok was used. The strainer contained pore size of 140 μm which removed larger sized particles and the filter contained pore size of 15 μm which trapped fine particles in a dense matrix.

As shown in the schematic (Figure 2.9) of the experimental setup, the feed ethanol solution was fed through microchannels parallel to the direction of the membrane. The microchannel and the membrane are housed inside a holder as described earlier.

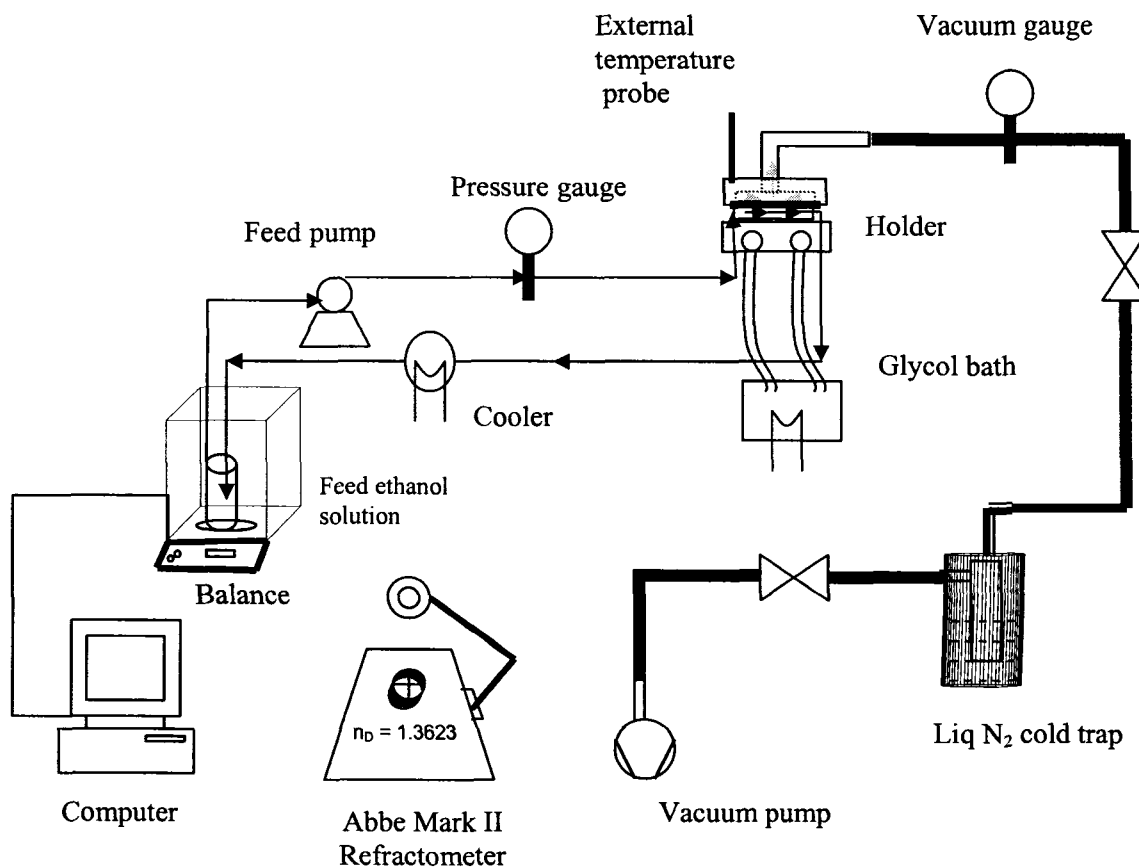


Figure 2.9 Schematic of pervaporation setup with retentate recycle.

The membrane was maintained at a lower pressure on the downstream side by the vacuum generated by a vacuum pump. A needle valve was used in the vacuum line to isolate and consequently protect the pressure gauge and the membrane module with the microseparator during start up and shut down procedures of the vacuum pump. This valve also regulated the flow and controlled the vacuum pressure on the downstream side of the membrane. Another needle valve which served as the pump valve was used as shown in the schematic. The water components that selectively permeate through the membrane were collected in a vacuum trap refrigerated with liquid nitrogen.

Changes in the feed concentration that occurred during the experiment as a result of selective removal of water by the membrane were measured periodically using a

Reichert ABBE Mark II refractometer. The details of the calibration for the refractometer are included in Appendix B. The total flux and selectivity as a function of microchannel depth and residence times was reported. Table 2.1 gives a brief summary of microseparator specifications.

Table 2.1 Microseparator specifications.

Membrane module material	aluminum
Membrane	PERVAP 2216 (Sulzer Chemtech)
Effective membrane area	3 cm ²
Preferential component	water
Starting volume of feed ethanol solution	33 ml
Initial feed ethanol concentration	90 wt %
Feed temperature	90°C
Vacuum pressure	2-3 Torr
Feed flow rate	1 – 50 ml/min

To facilitate precise temperature measurement of the membrane module throughout the pervaporation process, a small aperture of 0.125 inch deep was drilled on the top plate of the *in-situ* heat exchanger/membrane module. An external temperature probe (Resistance Temperature Detector probe from Weed Instruments) connected to the circulator was inserted into this aperture to maintain an efficient contact with the top plate to measure the temperature accurately. This RTD probe used was a straight sheath temperature sensor with a R_0 and temperature coefficient of 100 Ohm Platinum 0.00385055 TCR 100 Ohms @ 0° C. The maximum temperature limit that could be measured with this probe was 260 °C. This probe was specially designed to communicate with the Polyscience digital temperature controller (model 9510). The RTD temperature probe had 4 lead wires, and the sheath diameter was ¼ inch and length was 6 inches.

The temperature data of the membrane module were acquired for every 30 seconds using a commercial software Labworldsoft v 4.5 during the entire experimental time. This software enabled a computer to communicate with a Polyscience digital temperature controller. The external probe in contact with the membrane module was maintained at 90 °C, and the temperature data were acquired continuously through out the duration of the experiment. Glass wool was covered on the top of the holder and the external probe to minimize heat losses due to convection. Temperature shifts due to the localized cooling in addition to the heat loss along tubing lines were eliminated and efficient temperature management was obtained by using the *in-situ* heat exchanger.

Different designs of vacuum traps were tried, in order to condense all the permeate vapors. Figure 2.10 is a U-tube vacuum trap which was designed and custom made to suit our requirements by Allen Glass Company. Figure 2.11 is the vacuum trap with serrated connections (Chem glass). This vacuum trap was a two-piece construction for easy removal of condensate. The stopper had a standard taper inner joint and body had an outer joint. Body length was measured below the joint. Serrated hose connections had an O.D. of 13 mm at the smallest serration and 16 mm at the largest serration.

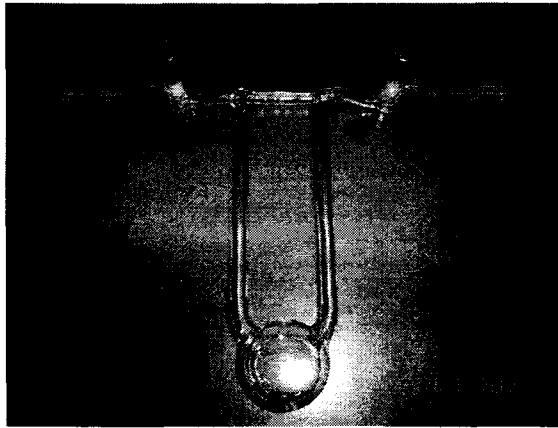


Figure 2.10 U-tube vacuum trap.

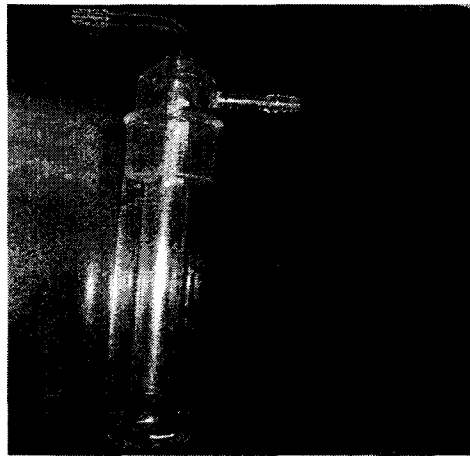


Figure 2.11 Serrated vacuum trap.

2.4 Design and Fabrication of the Microseparator

2.4.1 Background for Design of Microseparator

A design of the microseparator was created using AutoCAD 14. In one of our first designs of the microseparator an arrangement as shown in Figure 2.12 was made to utilize the maximum area available in the four-inch silicon wafer. The experiments with this first generation microseparator demonstrated that the arrangement of the

microseparators in the wafer decreased the effective dicing area around the microseparator and the manifold as shown in Figure 2.13.

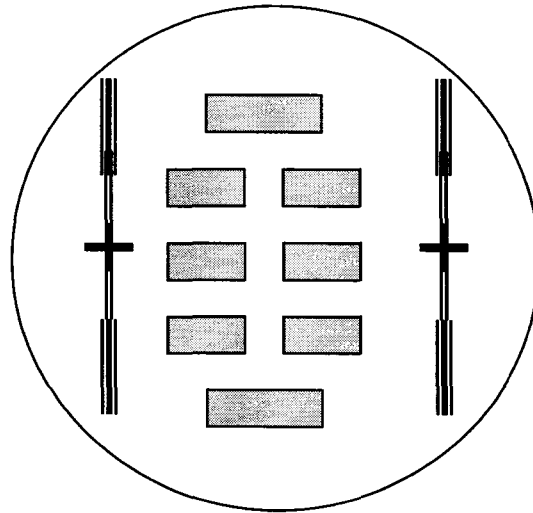


Figure 2.12 Mask layout of first-generation microseparator.

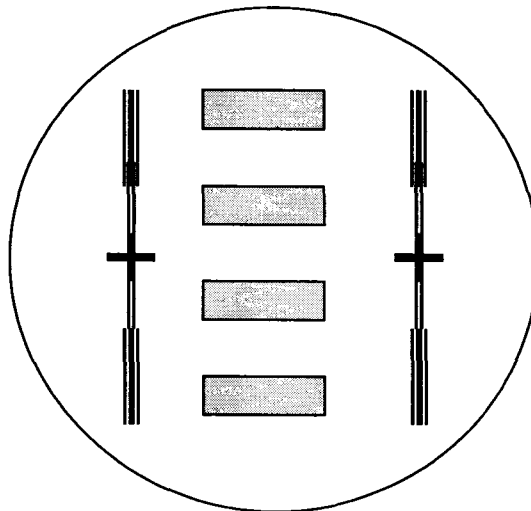


Figure 2.13 Mask layout of second-generation microseparator.

The small sealing area was one of the reasons that the microseparator would easily break on tightening the bolts of the holder that housed the microseparator assembly.

As such a new design was created with only four microseparators in a four-inch silicon wafer as shown in Figures 2.14 and 2.15. This new design ensured that the sealing area around each of the microseparator was adequate to provide sufficient width to the microseparator. The holder was also redesigned by providing additional bolts that helped to distribute the pressure evenly around the microseparator while tightening the bolts.

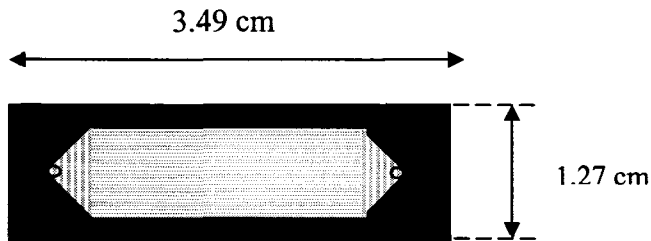


Figure 2.14 Schematic of a first-generation microseparator.

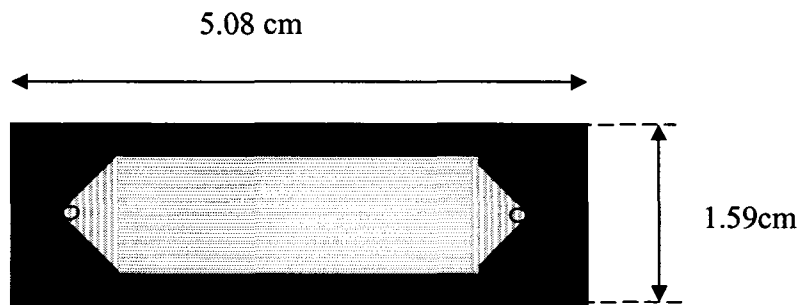


Figure 2.15 Schematic of a second-generation microseparator.

Alignment marks were designed on either side of the microseparator arrangement. Each of these marks had lines of two different widths as shown in Figures 2.12 and 2.13 that extended on the top and below the mark, which facilitated in finding the alignment mark easily during the alignment process. Two masks were generated for the fabrication of the microseparator. The frontside mask had the microchannels with the manifold while the backside mask had the inlet and outlet vias. Also, while designing the mask a 1cm

distance from the edge of the wafer diameter was maintained to facilitate easy handling during ICP etch process.

The detailed geometry of the microchannel separator used with the inlet, outlet and microchannels are shown in Figure 2.16. The three fabricated microseparators had 99 channels 60 μm wide, 30,000 μm long but varied with depths of 22, 47, and 120 μm . The fabrication procedure is included in Appendix C. On completion of fabricating the microseparator the wafer was sent to a commercial dicing company. The diced wafer enabled us to separate each of the microseparators easily.

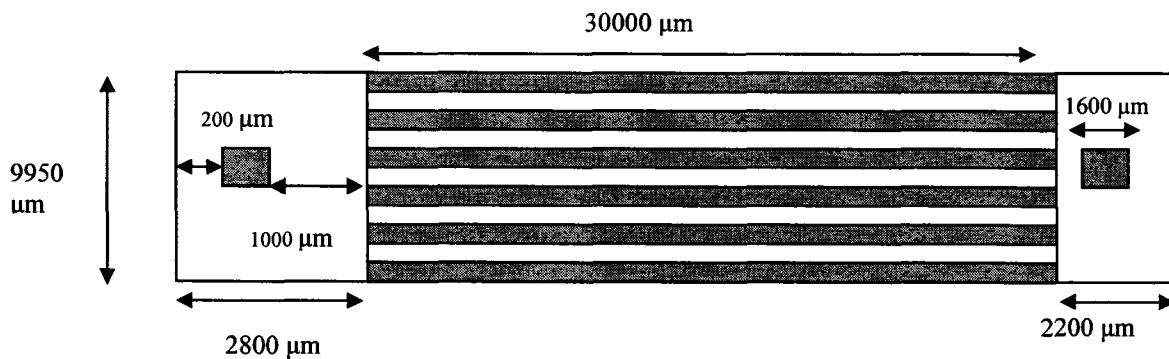


Figure 2.16 Geometry of second-generation microseparator.

A picture of the microseparator is shown in Figure 2.17.

Details of microseparator shown in Figure 2.17:

Number of channels: 99

Length of channel: 3 cm

Width of channel: 60 μm

Depth of channel: 47 μm

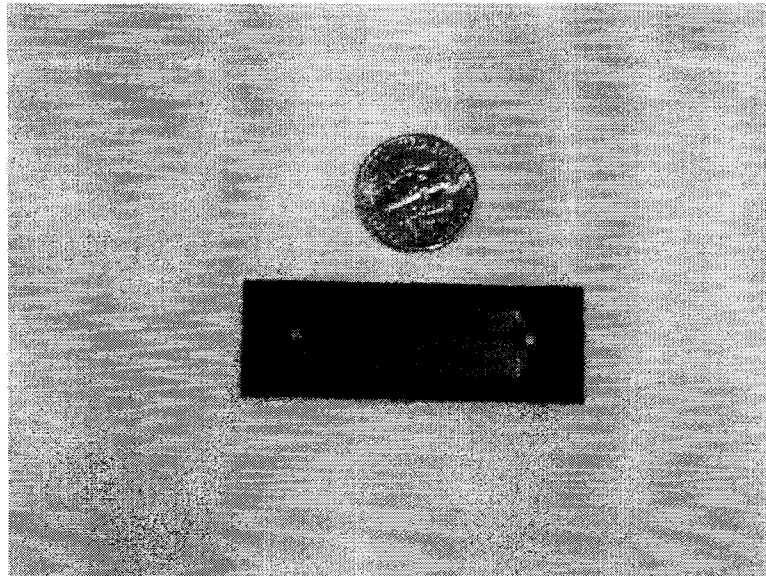


Figure 2.17 Picture of second-generation microseparator.

2.4.2 Characterization of Microseparator

Each of these microseparators was characterized by the following techniques:

- (a) Scanning Electron Microscope
- (b) Stylus Profilometer
- (c) WYKO Roughness/Step Tester

Scanning Electron Microscope (SEM) (Scanning electron microscope - 1830 Amray) images at different views of the microseparator such as microchannels, manifold, and the vias were taken. These images show the straight channels and manifold region. A few selected pictures are shown in Figures 2.18 and 2.19.

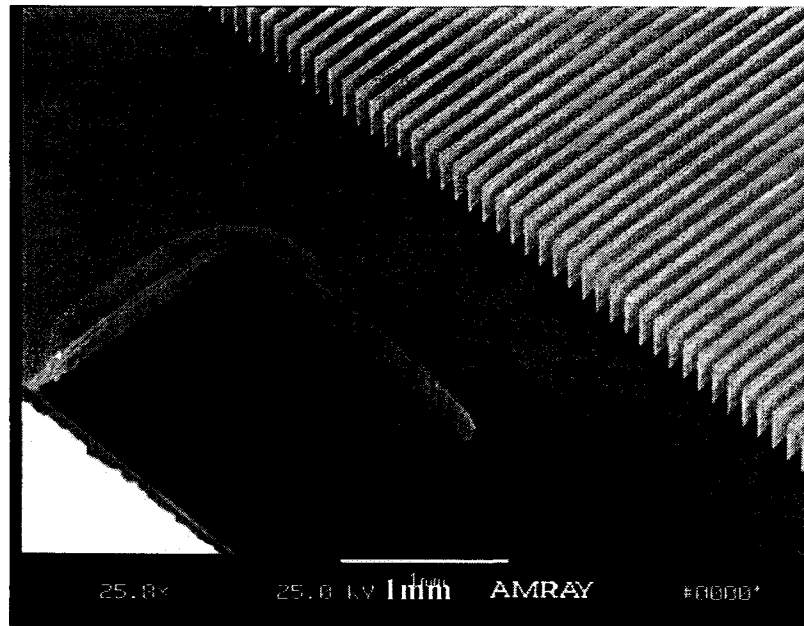


Figure 2.18 SEM image of inlet/outlet, manifold and channels.

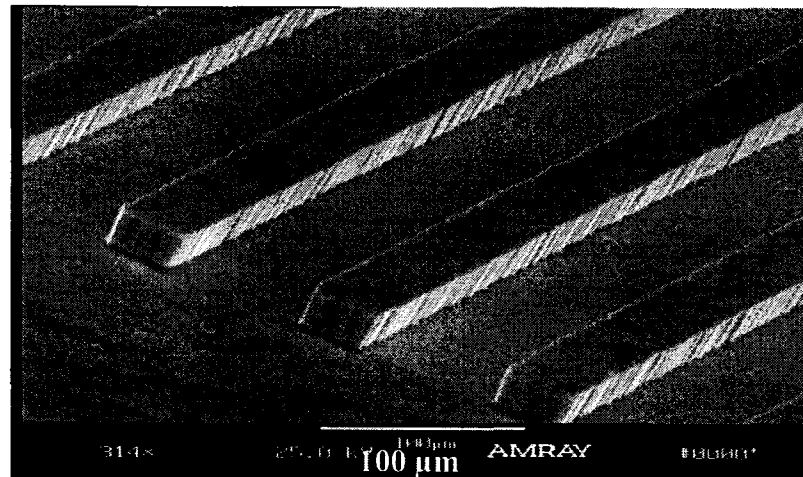


Figure 2.19 SEM image of channel walls and surface of the chip.

The depth of the microchannels was confirmed by measurement from profilometer (Stylus Profilometer - Tencor Alpha Step 500) as shown in Figure 2.20.

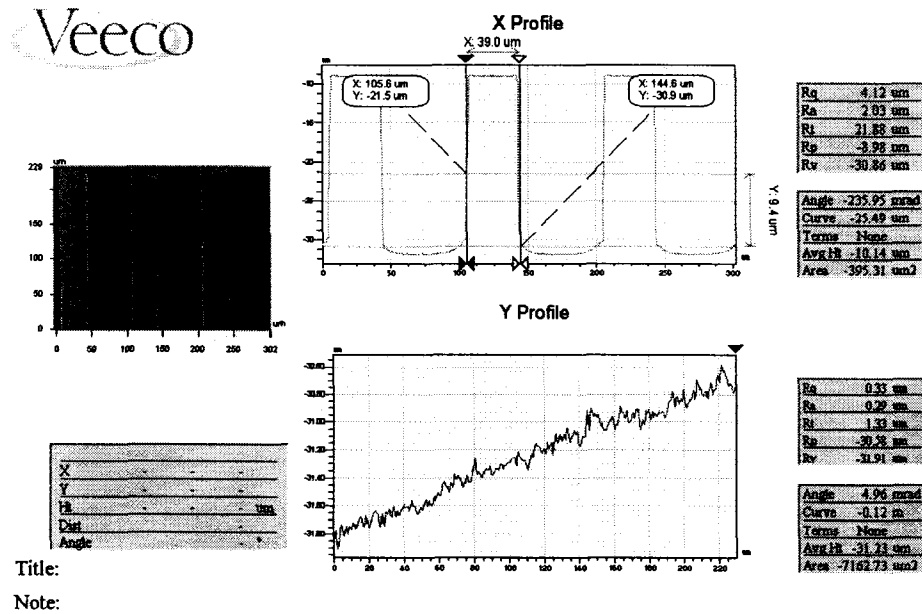


Figure 2.20 2-D image for measuring width and depth.

WYKO Roughness/Step Tester (White light Roughness-Step Tester-WYKO NT1000) was used for non-contact measurement of surface topography at high vertical and moderate lateral resolution and for sensitive measurement requirements. The standard roughness/step tester available at Institute for Micromanufacturing in Louisiana Tech University was used to measure the roughness and line width of the minimum feature size of our pattern. For all line width measurements the VSI mode was opted and the 40X magnification objective chosen. The image depicting the two dimensional analyzed result is shown in Figure 2.21. The width and depth of the channels were corroborated using a WYKO RST Profilometer and Stylus Profilometer (Tencor Alpha Step 500).

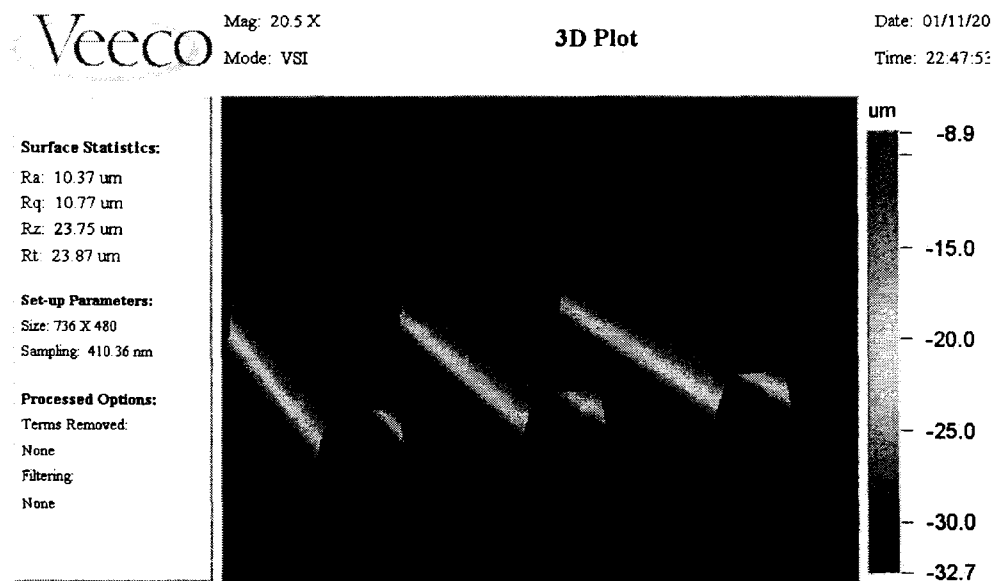


Figure 2.21 3-D image for surface smoothness testing.

2.5 Mathematical Treatment of Mass Data Obtained from Balance

During the experiments, it was necessary to measure the changes in ethanol concentration periodically. As such, a small amount of feed ethanol solution was taken out from the feed tank using a pipette between the experiments, which can be observed as mass loss or discontinuities in Figure 2.22. To account for the specific amount of mass used for concentration analysis, each sampling period was considered an individual set of data as shown in Figure 2.23. This graph represents the mass changes observed in the feed tank observed during 4 to 10 hours of that experiment. As we can see in this graph a linear regression equation provides a very good fit for the entire data. Similar linear regression equations were used for all the sampling periods through out a given experiment. These regression equations were then treated mathematically to develop a smooth curve as shown in Figure 2.24.

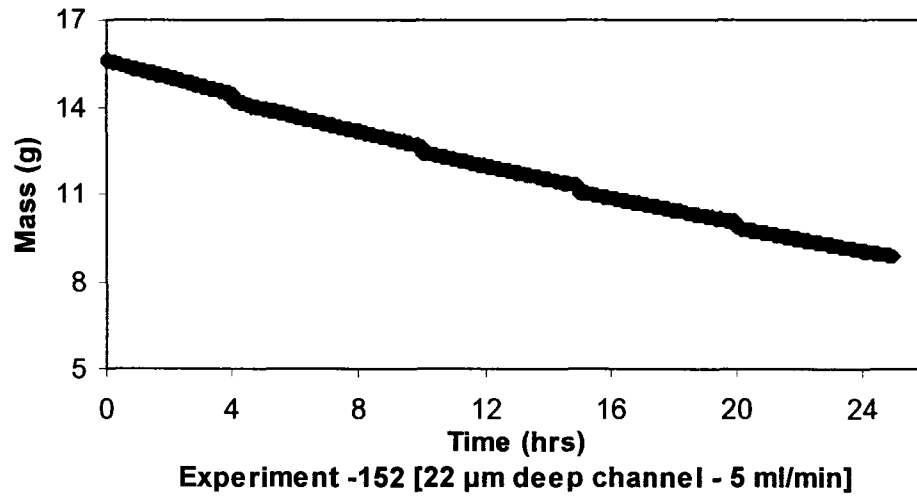


Figure 2.22 Sample representation of untreated mass data obtained from the balance.

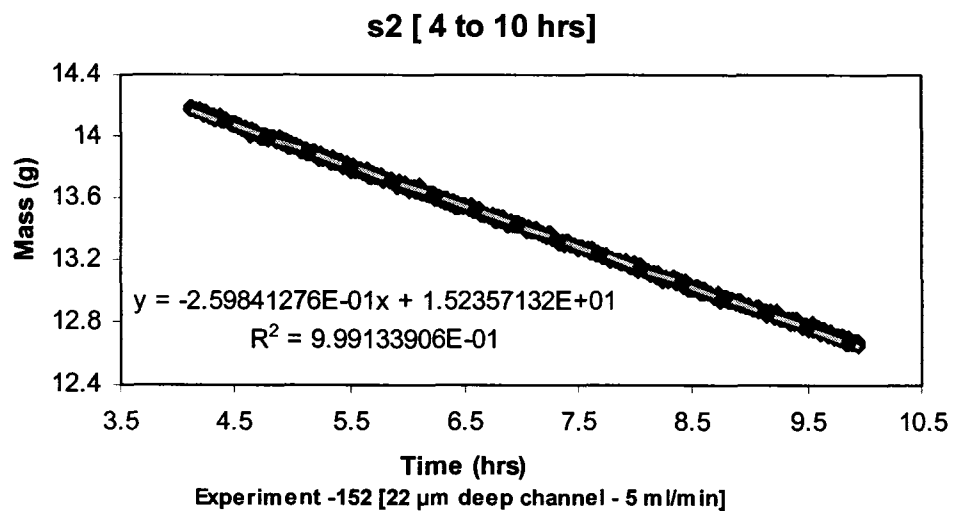


Figure 2.23 Sample representation of mass data between a sampling interval.

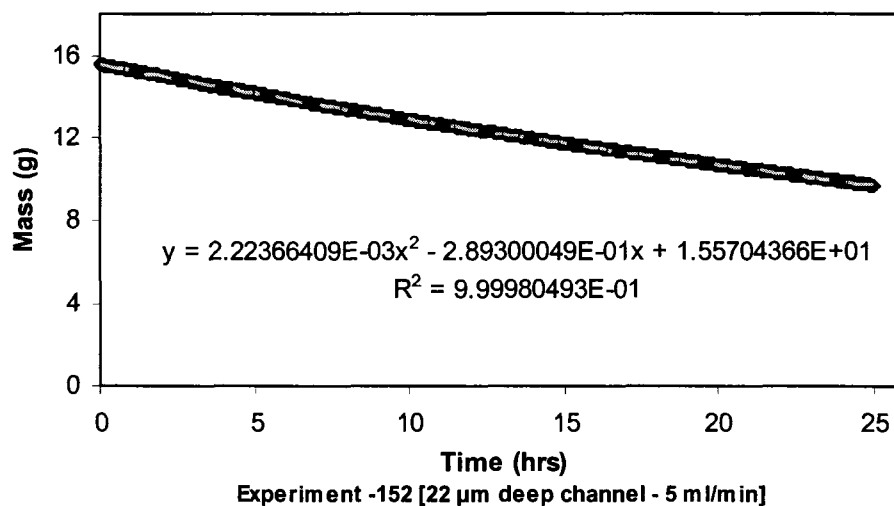


Figure 2.24 Sample representation of a treated mass data.

During the treatment of the mass data, a point was created to indicate the mass lost at the exact time of sampling, between any two sampling periods, using the regression equation of the respective sampling period. In other words, this point is the approximate estimation of the mass at that time period when the sample was taken out to analyze. The difference from the two sets of regression data obtained from the two sampling periods predicted the actual mass change occurred as a result of sampling at that specific time period. As a consequence of this mathematical manipulation, a nearly accurate method was developed to calculate the entire amount of ethanol that was used during the concentration analysis. This mass was then added back into the mass data to obtain a smooth curve as shown in Figure 2.23. These data were further regressed using a polynomial second order fit, which was eventually used in the model to predict the mass lost from the feed tank all through out the experiment.

In this graph (Figure 2.25) the ethanol concentration in the feed is plotted as a function of time. As we can observe from the graph the ethanol concentration increases

as a result of selective removal of water by the membrane. The ethanol concentration was measured periodically by a refractometer as described earlier.

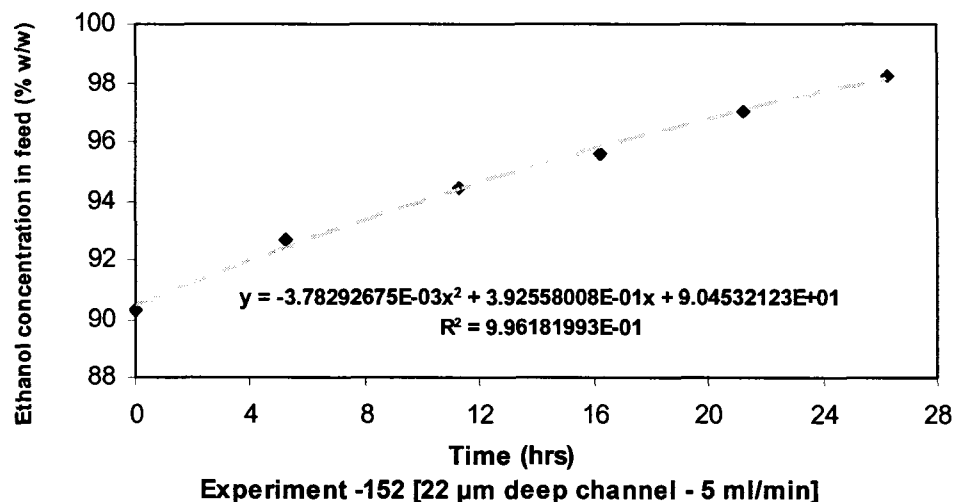


Figure 2.25 Ethanol concentration analysis by Abbe Mark II refractometer.

2.6 Mathematical Model

The objective of this model was to predict the permeate flux and selectivity using the experimental data. The mass change data acquired from the balance and the ethanol concentration measurement by refractometer analysis were used to measure the separation performance of the microscale pervaporation process. Using this mass and ethanol concentration data from the respective regression equations, the exact mass and concentration at any given time during the experiment were predicted. A spread sheet was developed with differential time units of an hour, with corresponding mass and ethanol concentration. The changes between differential mass balance of any mass data predicted the mass lost both by evaporation of ethanol and as a result of membrane pervaporation. The mass lost by evaporation has been described earlier in Section 2.5; the

regression equation obtained from the evaporation experiments was used to predict the evaporation loss occurred at any concentration in the feed tank. Deducting the evaporation loss from the total mass for every single cell predicted the actual mass lost as a result of separation by pervaporation. This mass was used to calculate the flux and the separation factor from equation as described earlier in Section 2.1. In order to calculate the average separation factor and flux, the separation factor at every hour was predicted from the model described above.

CHAPTER 3

RESULTS AND DISCUSSION

In this chapter, the results from pervaporation experiments from both the single pass and retentate recycle experimental setup described in Sections 2.2 and 2.3 will be discussed in detail. The retentate recycle pervaporation experiments will be the focus of attention. The influence of key variables such as evaporation effects, effect of feed temperature, effect of permeate pressure, effect of residence time, and effect of hydraulic diameter will be discussed. The mass transfer analysis for the separation of water from ethanol solution in a microscale pervaporation device will also be described.

3.1 Microseparator Geometry Justification

To ensure uniform flow distribution in the microchannels hydrodynamic calculations were performed. In this study, the parameters that directly relate to the uniform flow distribution in the microchannels are the inlet geometry, number of channels and the hydraulic diameter. The Hagen-Poiseuille equation was used to ensure that the pressure drop through the microchannels were an order of magnitude higher than that of the pressure drop at the inlet region. This inlet criterion for the uniform flow distribution from a manifold to a piping network was described in Perry's Chemical Engineering Handbook [94]. The graph shown below relates the pressure drop in the inlet and the microchannels to the various hydraulic diameters tested. Three flow rates 1, 25

and 50 ml/min were used in these calculations and these flow rates were within the range that was used in the experiments. The y-axis of this graph is based on the logarithmic scale to facilitate in better depiction of the difference between the two regions compared. Figure 3.1 clearly indicates that the pressure drop of the microchannels were a magnitude higher than those at the inlet region. The pressure drop in the microchannels is also within the limits of functional feasibility.

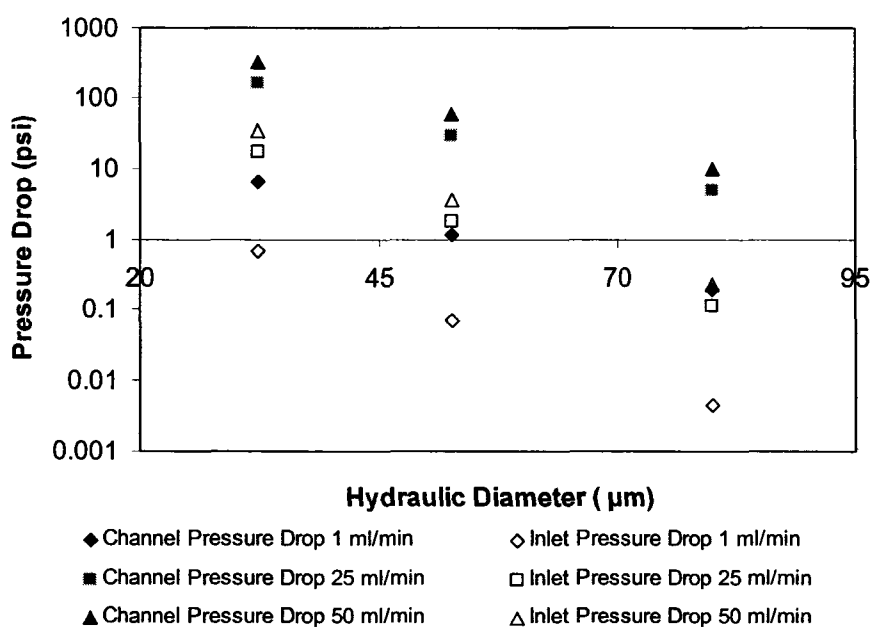


Figure 3.1 Comparison of inlet and channel pressure drop with hydraulic diameter.

3.2 Results from Single Pass Pervaporation **Experimental Setup**

This section deals with results from single pass pervaporation experimental setup as described in Section 2.2. In these experiments 22 and 120 μm deep channels were tested at flow rates varying from 0.4 to 2 ml/hr. The initial ethanol feed concentration used in these experiments was 90 % w/w and the operating temperatures tested were 40

and 60°C. The vacuum pressure was kept constant at 0.06 Torr for all the experiments. The ethanol concentration in the retentate was measured from the gas chromatograph (GC) analysis. In order to determine the statistical significance of the parameters involved, Analysis of Variance (ANOVA) was performed on each set of data.

Table 3.1 is the result from Analysis of Variance (ANOVA) for mean flux from single pass pervaporation experiments. We can infer from the F - test ($Pr > F$) in the table that the depth and the flow rate within each depth are significant, since the p values are lower than 0.05.

Table 3.1 ANOVA for mean flux from single pass pervaporation experiments.

Source	DF	Type III SS	Mean Square	F Value	Pr > F
Depth	1	0.0213	0.0213	6.40	0.0145
Temperature	1	0.0055	0.0055	1.65	0.2047
Flow rate(Depth)	6	6	6 0.034	10.20	<.0001
Depth* Temperature	1	0.0057	0.0057	1.72	0.1954
Temperature * Flow rate (Depth)	6	0.0240	0.0040	1.20	0.3210

Figure 3.2 relates the mean flux (over temperature within each depth) to the various flow rates tested in the 22 μm deep channel. Figure 3.3 relates mean flux to flow rate in the 120 μm deep channel. As it is evident from these figures, higher flow rates have exhibited higher flux. Figure 3.4 shows that the mean flux (over temperature and flow rate) increases with depth. This increase is significant as seen from the p-value ($p < 0.0145$) in Table 3.1.

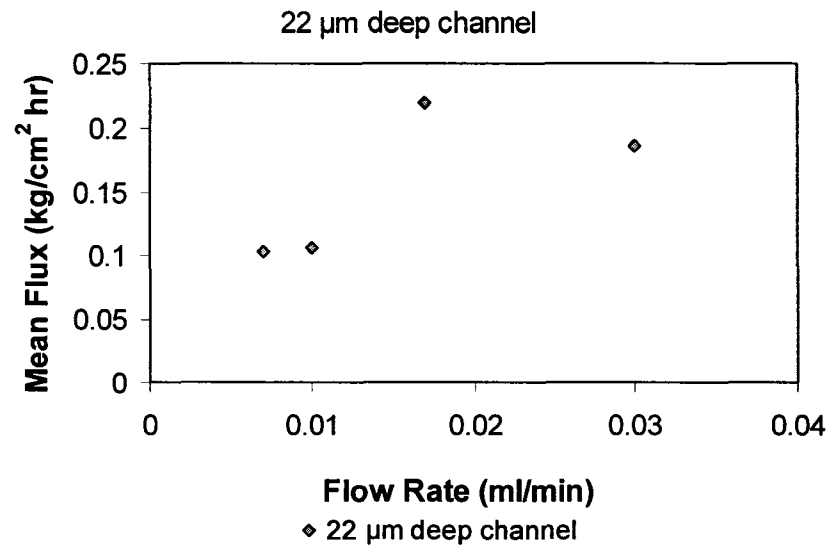


Figure 3.2 Mean flux vs. flow rate for 22 μm deep channel in single pass pervaporation experiments.

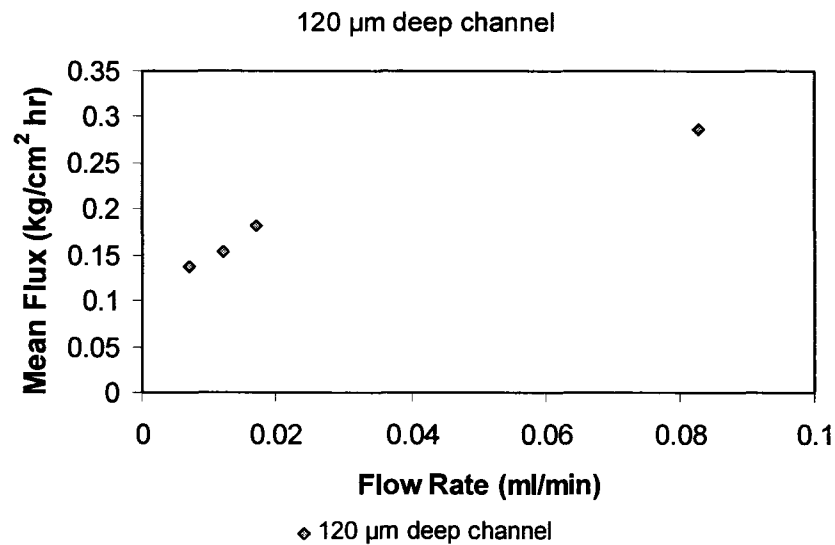


Figure 3.3 Mean flux vs. flow rate for 120 μm deep channel in single pass pervaporation experiments.

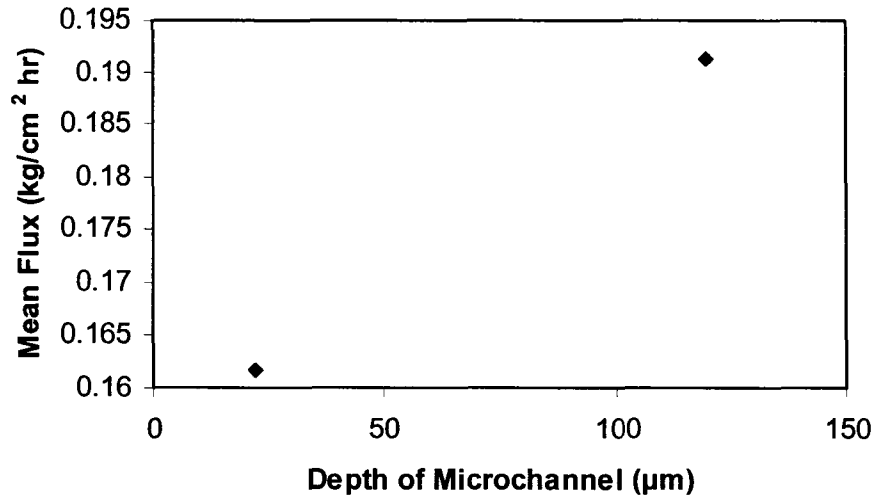


Figure 3.4 Mean flux vs. depth of microchannel in single pass pervaporation experiments.

The ANOVA for separation factor is shown in Table 3.2. The results from the F-test ($Pr > F$) in Table 3.2 have indicated that the temperature, flow rate within each depth, depth*temperature and temperature for flow rates within each depth are significant, since the p values are lower than 0.05.

Table 3.2 ANOVA for mean separation factor from single pass pervaporation experiments.

Source	DF	Type III	SS Mean Square	F Value	Pr>F
Depth	1	0.076	0.076	0.18	0.6732
Temperature	1	30.874	30.874	72.65	<.0001
Flow rate(Depth)	6	22.660	3.776	8.89	<.0001
Depth * Temperature	1	2.034	2.034	4.79	0.0337
Temperature * Flow rate(Depth)	6	13.839	2.306	5.43	0.0002

Figure 3.5 shows the trends in mean separation factor for temperature and flow rate (depth) from the statistical analysis. It can be seen from these graphs that the mean separation factor increases with temperature.

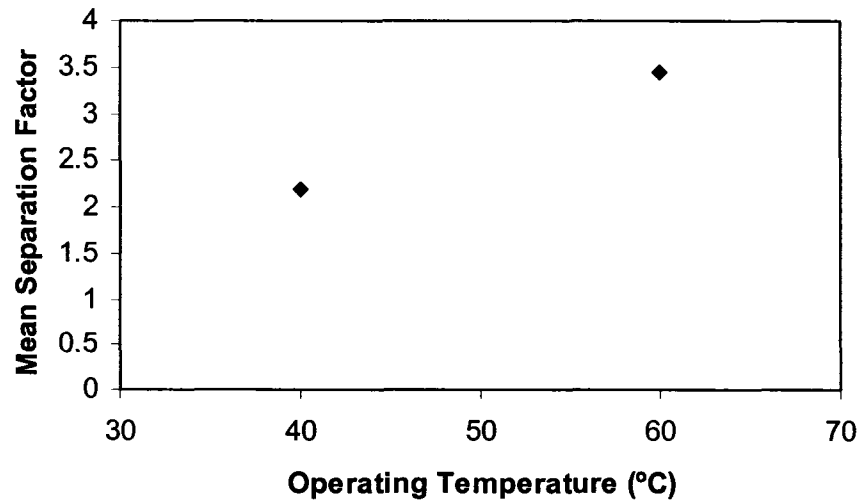


Figure 3.5 Mean separation factor vs. temperature in single pass pervaporation experiments.

Figures 3.6 and 3.7 depict the influence of flow rate within depth on mean separation factor. It can be inferred that in general there is a decrease in mean separation factor as the flow rate increases.

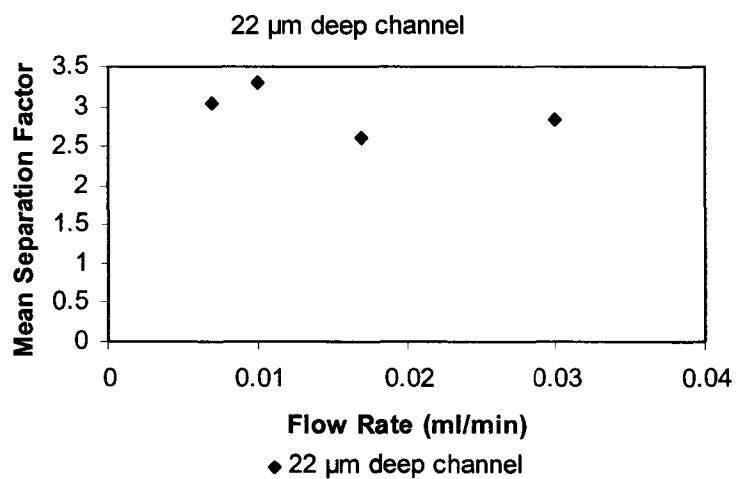


Figure 3.6 Mean separation factor vs. flow rate for 22 μm deep channel in single pass pervaporation experiments.

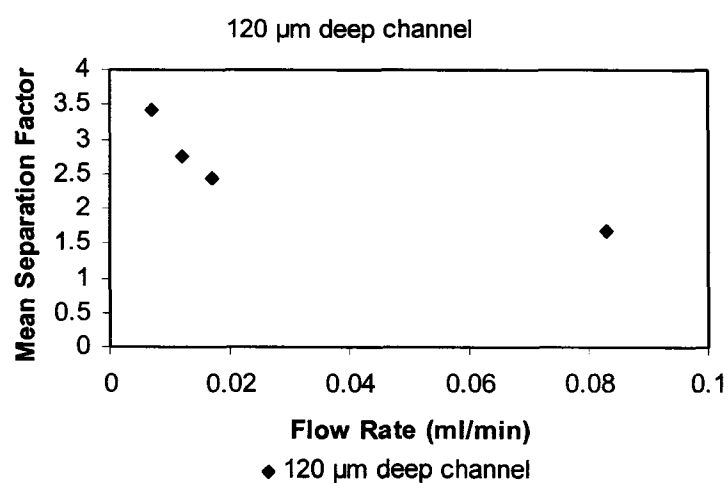


Figure 3.7 Mean separation factor vs. flow rate for 120 μm deep channel in single pass pervaporation experiments.

Figure 3.8 relates the plots for depth* temperature interaction. It can be observed from Figure 3.8 that for the highest temperature tested i.e. 60 $^{\circ}\text{C}$, both the depths tested exhibit similar mean separation factor.

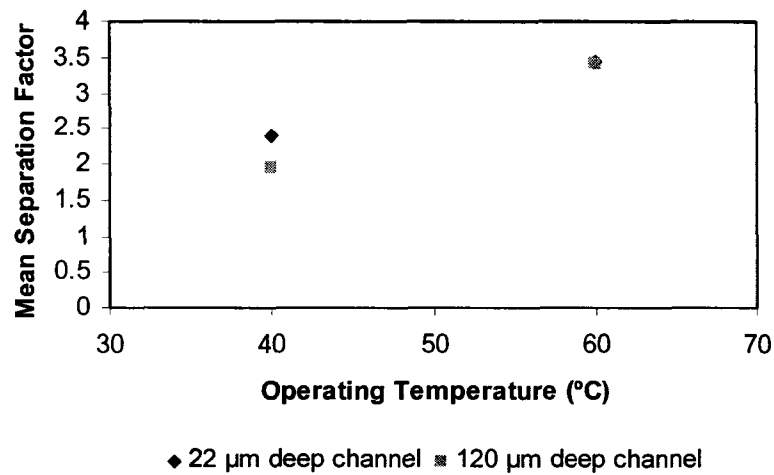


Figure 3.8 Mean separation factor vs. depth of microchannel at different operating temperatures in single pass pervaporation experiments.

Figures 3.9 and 3.10 (for the interaction between temperature and flow rate within depth) show in general that the mean separation factor is higher at the high temperature but decreases with an increase in flow rate. The interaction effect is largely manifested in Figure 3.9 for the 22 μm deep channel.

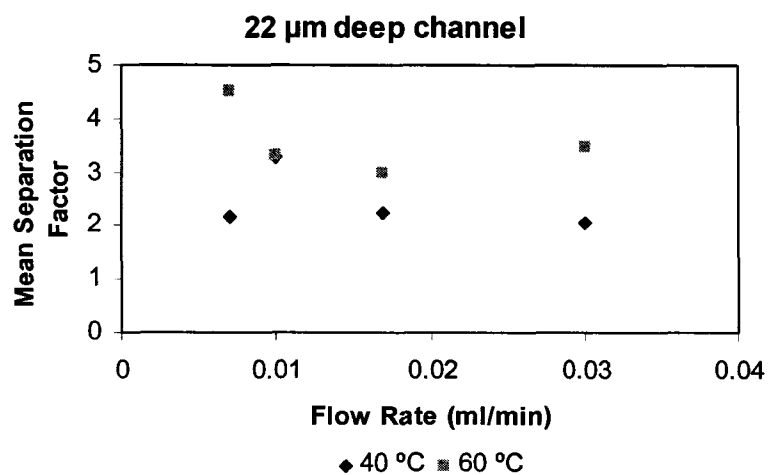


Figure 3.9 Mean separation factor vs. flow rate for 22 μm deep channel at different operating temperatures in single pass pervaporation experiments.

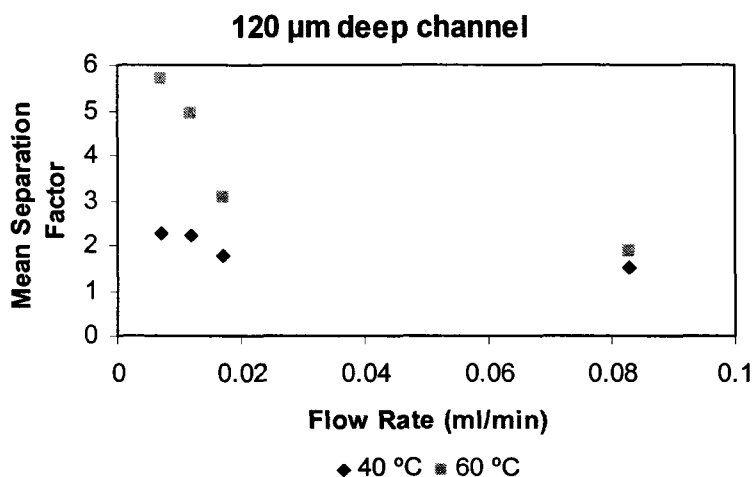


Figure 3.10 Mean separation factor vs. flow rate for 120 μm deep channel at different operating temperatures in single pass pervaporation experiments.

The ANOVA from the F- test ($Pr > F$) for ethanol concentration exhibited trends similar to that of the separation factor where all the factors and interactions were significant, with the p values lower than 0.05. It could be inferred that in general there was a decrease in mean ethanol concentration as the flow rate increased. Also, the mean ethanol concentration increased with depth and with temperature. It was concluded from the analysis that the mean ethanol concentration increased with temperature in the 120 μm deep channels, but decreased or does not change significantly in the 22 μm deep channels.

The results from these low flow rates experiments have not exhibited process intensification; further the results have indicated that higher operating temperature was required to improve the performance of the membrane. As such, it was decided to improve the experimental setup by incorporating appropriate modifications that enabled the limitations experienced in the single pass experimental setup to be overcome. The high operating temperature necessitated a cooler for the retentate lines to minimize

evaporation and also facilitate in analyzing the samples. A cooler was designed as described in Appendix E to maintain the feed solution at room temperature. While analyzing the results from the experiments with single pass retentate setup, it was also noted that the gas chromatographic analysis required a relatively large sample volume for analysis. As such, other avenues for analytical development were explored and refractometer analysis was chosen because of the advantages of a smaller sample volume and no additional sample preparation required. In addition, the experimental setup was modified to make arrangements to measure transient flux values for higher flow rate studies with the addition of an analytical balance interfaced to a computer. The results from this experimental setup will be discussed in the following sections.

3.3 Pervaporation Experimental Setup with Retentate Recycle

In this section the results obtained from experiments at high flow rates that were operated on the experimental setup with retentate recycle will be discussed. In Section 3.3.1 detailed description of permeate collection and results are discussed. Sections 3.3.2 to 3.3.9 the effects of the various operating parameters such as evaporation, operating temperature, permeate pressure, residence time, and hydraulic diameter that were studied will be discussed. This section also introduces the mass transfer analysis developed for the transport process through the membrane. In the mass transfer analysis the resistances involved in the transport process have been theoretically evaluated. The procedure required to calculate the mass transfer resistance from experimental data has also been discussed. The experimental data for this set of experiments are included in Appendix D.

3.3.1 Permeate Collection

This section describes the attempts made to collect the permeate, the challenges involved during the process and detailed analysis of experimental results associated with collecting the permeate. The foremost reason for being unable to condense all the vapors in the permeate was that only a very small amount of material permeated through the membrane at a given interval of time. Condensing this small amount of permeate was coupled with problems from significant air leaks that resulted from the use of common piping versus standard vacuum fittings. The air leaks created difficulties in the precise control of the pressure and stripped the ethanol and water from the liquid nitrogen cold traps. Results of the mass of permeate obtained varied with the other operating parameters involved in the experiment.

To overcome this problem, all components (hose tubings, pipe fittings, valves, vacuum trap and vacuum pump) in the membrane downstream were analyzed closely. The vacuum pump was tested for leaks, and periodic oil change was performed to maintain regular operation of the pump. The membrane module was also tested separately for leaks. The leak tests were performed with a thin metal plate replaced as a substitute for the microseparator. The metal plate sealed the membrane module effectively allowing a leak rate of 1.18 sccm to be measured. The swagelok fitting (union) connecting the membrane module and the tubing connecting to the vacuum lines were welded to minimize the air leaks. The leaks in the membrane module could not be improved any further due to the brittle silicon microseparator with which it housed. The membrane module was tightened to maximum possible extent without breaking the

silicon microseparator. As such, the other components in the downstream region were monitored to improve the vacuum system.

The vacuum trap design was studied and various designs of the vacuum traps were tested to observe if the retentate recovery could be improved. The U-tube vacuum trap shown in Figure 2.9 was one such design tested. This trap had a leak rate of 0.15 sccm when tested for leaks with a bypass system in the downstream region. However, this trap developed leaks around the inlet valve and resulted in collection of smaller amount of permeate.

The vacuum trap shown in Figure 2.11 was a regular vacuum trap with a common design for the flow of vapors. Two such traps were connected in series to try to collect all the permeate vapors. An experiment with 22 μm deep channel, a 10 ml/min flow rate, 60 $^{\circ}\text{C}$ operating temperature, and a vacuum pressure of 1.5 Torr was performed. This experiment resulted in an 18.75 % recovery of permeate, in comparison with the retentate mass loss acquired by the analytical balance. Therefore, no further experiments were conducted with vacuum trap in series because of its low performance.

A single trap resulted in better permeate collection than the two in series or U-tube vacuum trap. This single vacuum trap setup had a leak rate of 0.07 sccm, and although total closure of permeate was not obtained, this setup was adapted for all the experiments.

The experimental results from the 14 experiments in which the permeate was collected and analyzed are discussed below. Experiments were performed with different microchannel depths of 22 μm , 47 μm and 120 μm . These experiments were conducted at an operating temperature of 90 $^{\circ}\text{C}$ and a vacuum pressure of 2-3 Torr. The range of

residence time tested was between 25 to 250 milliseconds. At the end of each experiment the permeate condensed in the vacuum trap as shown in Figure 2.11. The total and partial flux for all the microseparator depths and residence time tested is tabulated in Table 3.3.

Table 3.3 Comparison of permeate and retentate flux.

Microseparator Channel Depth	Residence Time	Permeate Flux [$\text{g cm}^{-2} \text{hr}^{-1}$]			Retentate Flux [$\text{g cm}^{-2} \text{hr}^{-1}$]		
		Total	Water	Ethanol	Total	Water	Ethanol
μm	milliseconds						
22	235	0.036	0.028	0.007	0.064	0.023	0.041
22	117	0.039	0.030	0.009	0.051	0.025	0.026
22	47	0.040	0.033	0.007	0.045	0.027	0.018
22	23	0.034	0.029	0.005	0.050	0.024	0.025
22	23	0.040	0.035	0.006	0.058	0.026	0.031
47	100	0.052	0.042	0.010	0.072	0.035	0.037
47	100	0.041	0.029	0.011	0.054	0.027	0.027
47	50	0.054	0.041	0.013	0.052	0.022	0.031
47	20	0.043	0.041	0.002	0.065	0.036	0.029
47	20	0.039	0.036	0.004	0.063	0.037	0.026
47	10	0.052	0.041	0.011	0.073	0.038	0.035
120	250	0.062	0.053	0.009	0.078	0.052	0.027
120	51	0.037	0.033	0.003	0.055	0.028	0.027
120	51	0.033	0.025	0.008	0.046	0.023	0.023
120	25	0.037	0.034	0.003	0.046	0.019	0.027

The separation factor and flux was calculated as described earlier. The data from the collected permeate are referred to as the experimental values in the following discussion. The separation factor and flux calculated from the model as described in the Section 2.6 are referred as the retentate values in the following discussion.

The graph shown in Figure 3.11 relates the permeate mass recovered to the various residence time tested. The mass recovery is the ratio of the mass of permeate that was collected and the mass lost through the membrane based on the retentate. It can be

observed that only four experiments have crossed the 90 % recovery while for the rest of the experiments the mass recovery was dispersed between 70 to 90%. The low mass recovery clearly indicated the problems associated with attaining total closure for the permeate.

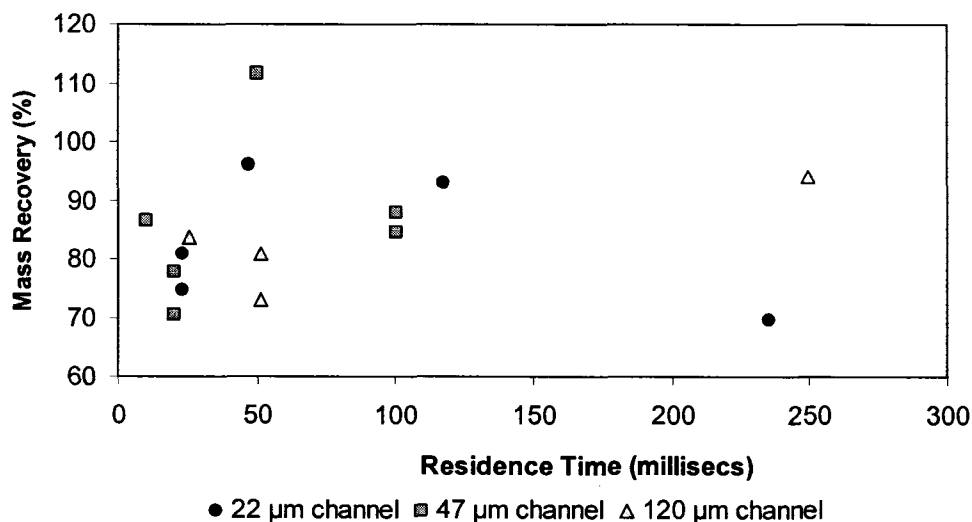


Figure 3.11 Permeate mass recovery analysis.

The graph in Figure 3.12 was plotted to understand the correlation between the total flux obtained from both the retentate and the permeate. The total flux varied linearly, indicating the effect of operating parameters such as residence time and hydraulic diameter. From the graph it is evident that the water flux was higher than the ethanol flux.

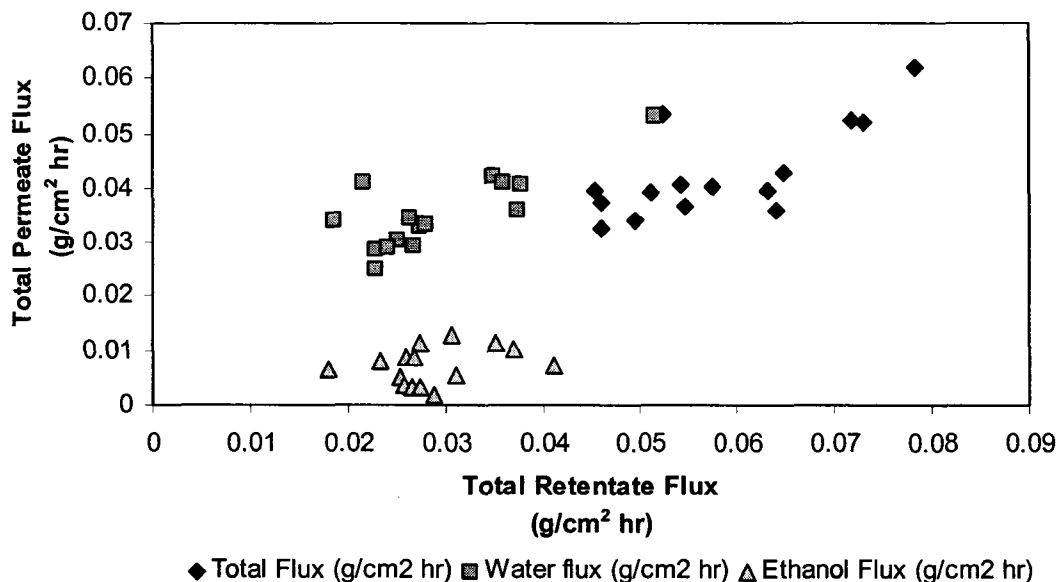


Figure 3.12 Total permeate flux vs. total retentate flux.

The graph in Figure 3.13 compares the flux values at the different residence times tested for both the retentate and the permeate fluxes. The flux data calculated from the retentate data are higher than those from the permeate data. The reason that not all permeate was collected to account for accurate flux calculations. To further understand the behavior of ethanol flux in the permeate and the retentate the graph in Figure 3.14 was plotted. In this graph the ethanol fluxes for both the retentate and the permeate are plotted as a function of residence time. The ethanol fluxes from the permeate are lower than the ones from the retentate for the residence times tested because not all of the ethanol vapors were condensed. Similar results were observed for ethanol flux when the hydraulic diameter was varied.

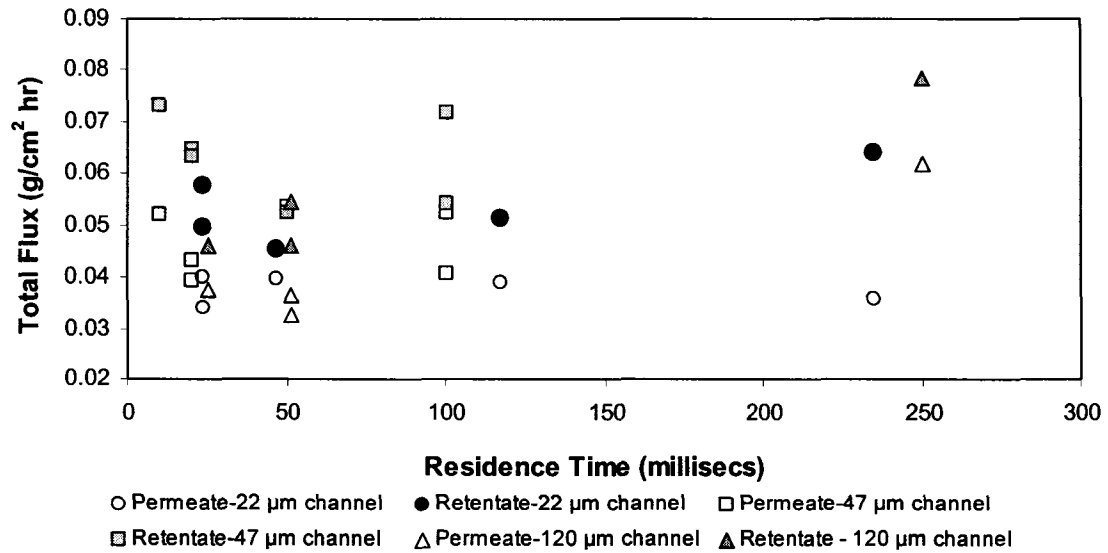


Figure 3.13 Comparison of permeate and retentate total flux with residence time.

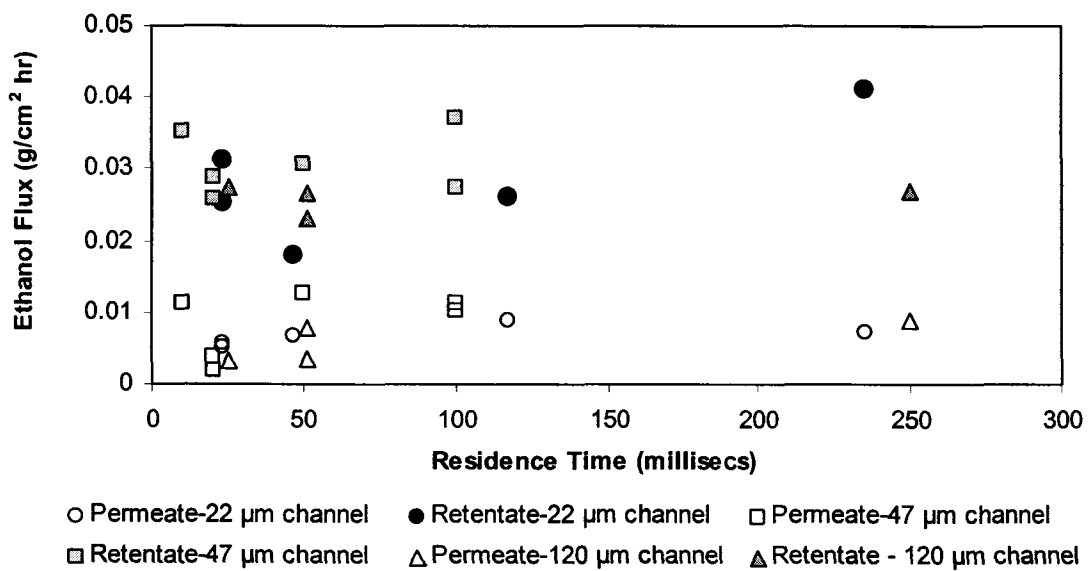


Figure 3.14 Comparison of ethanol flux from permeate and retentate with residence time.

The graph in Figure 3.15 depicts the water flux from both the retentate and the permeate plotted as a function of residence time. Here the permeate water fluxes are very

close to the values of the retentate water fluxes. Similar results were also observed for the water flux when the hydraulic diameter was varied.

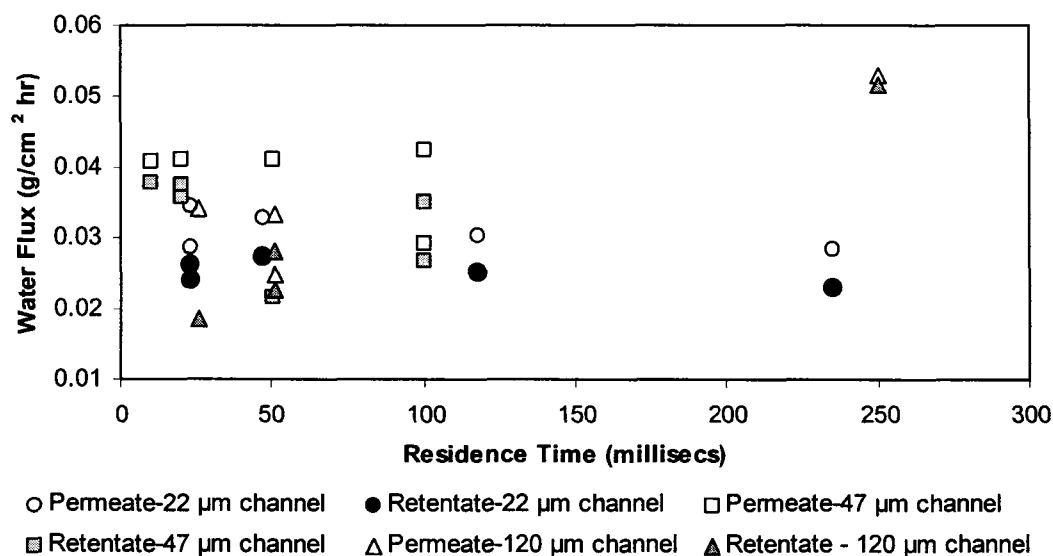


Figure 3.15 Comparison of water flux from permeate and retentate with residence time.

The moisture content in air condensed during refrigeration of vacuum traps by liquid nitrogen was calculated to observe if water flux measurement was coupled with the moisture condensed from air. The apparent water flux was calculated from the total leak rate of the system and using the lowest and the highest relative humidity conditions observed during the experiments. It can be observed from Table 3.4 that the apparent water flux values are not very significant in comparison with those reported for permeate water flux (Table 3.3), indicating the fact that the moisture condensation during refrigeration of permeate was not a contributing factor.

Table 3.4 Apparent water flux data from relative humidity calculations.

	Temperature	
	20° C	25° C
Relative Humidity	Apparent Water Flux	Apparent Water Flux
%	$\text{g cm}^{-2} \text{hr}^{-1}$	$\text{g cm}^{-2} \text{hr}^{-1}$
30	1.63×10^{-4}	1.96×10^{-4}
60	2.94×10^{-4}	3.92×10^{-4}

In the graph shown in Figure 3.16, the separation factor was compared for both the retentate and permeate at the various residence times and microchannel depths tested. The separation factor from the analysis of the collected permeate was higher than those predicted from the model using the retentate data for all the microchannel depths and residence time tested because of the problems associated while condensing the permeate vapors for extended duration (> 24 hrs) of each experiment, which was also a common feature for all the pervaporation experiments performed with the microseparator. The problem was that of the evaporation of ethanol in the permeate that led to lower ethanol content in the permeate and subsequently contributed towards a higher separation factor. It was for these reasons that values predicted from the retentate were considered for characterization of membrane performance.

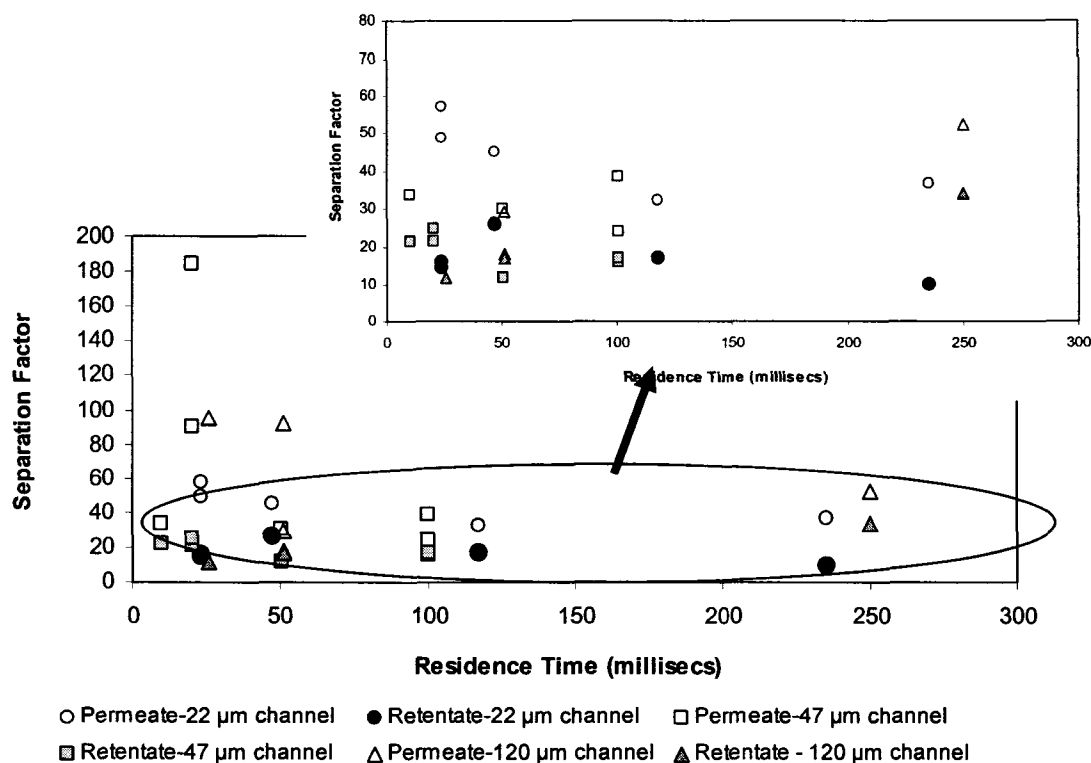


Figure 3.16 Permeate analysis of separation factor.

3.3.2 Effect of Evaporation

To account for the mass lost by evaporation from the feed tank containing ethanol-water binary mixture during a pervaporation experiment, evaporation tests were conducted as explained below. Ethanol concentration of 90, 93, and 97 % w/w were used in this experiment. All experiments were conducted at room temperature, and the indoor humidity was measured using a digital hygrometer (Thermo-Hygro). In the experiment, the prepared feed ethanol solution was introduced into a 50 ml glass beaker previously set on a balance. This ethanol feed solution was circulated through the inlet and outlet lines of the actual experimental setup as described in Section 2.3 using a peristaltic pump at two different flow rates of 5 and 50 ml/min. These flow rates were so chosen because it was in this range that most of the pervaporation experiments were conducted. The reason

to circulate through the lines was to simulate the process that occurred during a typical pervaporation experiment. The mass lost due to evaporation from the feed tank was continuously acquired by a computer; then the mass change observed during the entire duration of experiment was plotted against the experimental time as shown in Figure 3.17. In this figure, mass lost due to evaporation by 90 % w/w ethanol concentration solution was monitored for a period of 4 hours. Using a linear regression model, a curve fit was obtained to calculate the mass change observed during any given time interval. This curve fit was then used to determine evaporation rate at that specific concentration of ethanol discussed in the following sections.

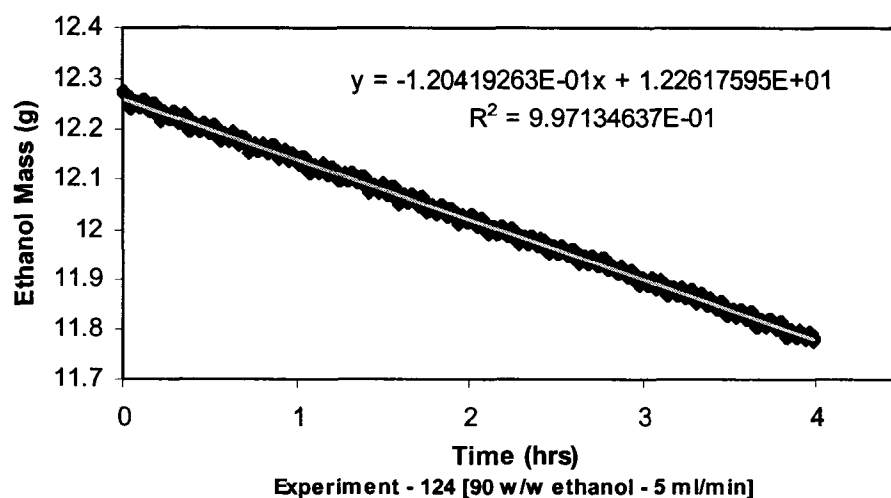


Figure 3.17 Mass loss by evaporation vs. time.

Evaporation experiments as described earlier were conducted for ethanol concentration varying from 90, 93 and 97 w/w % and at flow rates of 5 and 50 ml/min. The evaporation rate for specific ethanol concentration is plotted as shown in Figure 3.18. From this graph, we note that the mass loss due to evaporation for the varying

concentration follows a polynomial second-order relationship. Although the evaporation rate for the ethanol concentrations tested decreased with increase in ethanol concentration in the feed, the difference in evaporation rate between the 97 and 90 % w/w ethanol concentrations is not very significant. This graph exhibits the average evaporation rate of the successive runs for the two different flow rates tested. The regression equation from Figure 3.18 was used in all experiments to calculate the evaporation rate.

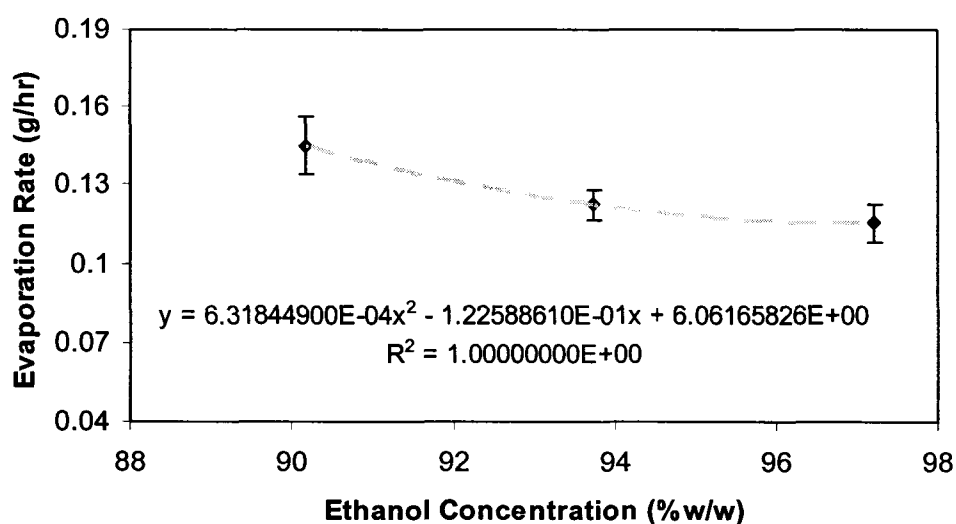


Figure 3.18 Ethanol-water evaporation effects with varying ethanol concentration.

Ethanol solutions prepared were accurately measured to determine their concentration before and after the experiment using an ABBE Mark II refractometer. Figure 3.19 relates the effect of changes in concentration in the feed ethanol mixture due to evaporation. It is clear from the graph in Figure 3.19 that the highest ethanol concentration tested exhibited the maximum change in composition of ~1.5 wt % over the duration of the evaporation experiment. This change in composition is within the confidence limit for errors in refractometer measurements. As such, it can be explained

that this change in concentration may not have been caused totally by an effect due to evaporation. The humidity conditions varied between experiments but remained relatively constant within any given run. The evaporation rate for 90 % w/w ethanol was higher than the 97 % w/w ethanol even though they have been tested within the similar humidity conditions.

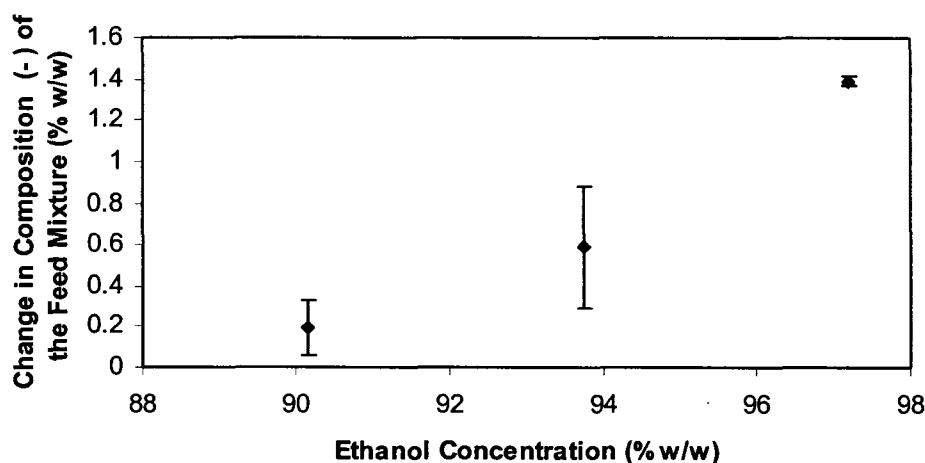


Figure 3.19 Changes in composition in ethanol feed by evaporation.

3.3.3 Effect of Separation Factor with Varying Feed Ethanol Concentration

The graph in Figure 3.20 is an example for separation factor behavior with varying ethanol concentration in feed. This experimental result was obtained from 22 μm channel depth at a feed flow rate of 5 ml/min, feed temperature of 90 $^{\circ}\text{C}$ and downstream pressure of 3 Torr. The separation factor is constant until 96 % w/w, and beyond this concentration; the separation factor tends to increase. This anomaly was analyzed by two different approaches.

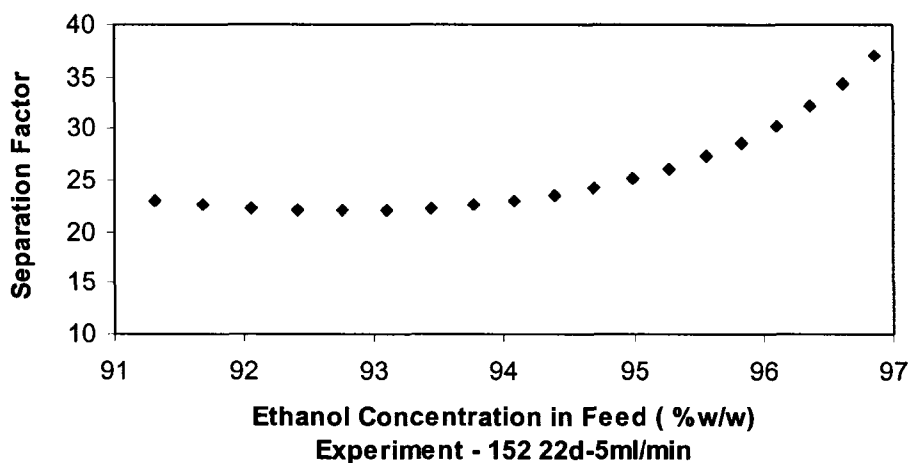


Figure 3.20 Effect of separation factor by varying ethanol concentration in feed.

In the first approach it was assumed to be an artifact from the mathematical model developed to calculate the separation factor. In the model, as the ethanol mass data decreased, the amount of water mass in the feed drastically decreased. In the formula for the separation factor, these small numbers in the denominator resulted into a big number towards the separation factor.

In the second approach, it was assumed that the reason for the anomaly was due to the low feed volume in the feed tank during the end of the experiments which caused rapid changes in concentration and consequently increased the separation factor. To verify these numbers, experiments were designed such that an initial ethanol concentration of 97% w/w with a starting volume similar to that of the experiments with 90 % w/w was conducted. The feed concentration of 97 % w/w was so chosen because it was at this concentration that the separation factor started increasing. The results from this experiment indicated no change in separation factor although the starting volume and concentration were varied. This experiment confirmed that the behavior of the separation factor towards the end was a mathematical artifact caused by the model. To be consistent

in comparison while varying residence times and hydraulic diameter, the separation factor was considered only up to 97% w/w ethanol concentration in all the experiments.

3.3.4 Effect of Total Flux with Varying Feed Ethanol Concentration

The graph in Figure 3.21 is an example for transient total flux behavior with ethanol concentration in feed.

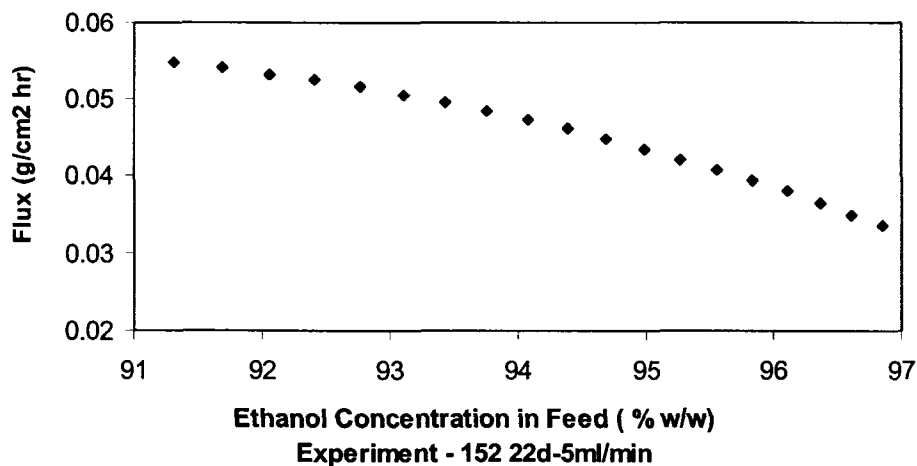


Figure 3.21 Flux variations with ethanol concentration in feed.

This experimental result was obtained from 22 μm channel depth at a feed flow rate of 5 ml/min, operating temperature of 90 $^{\circ}\text{C}$ and downstream pressure of 3 Torr. It can be clearly understood from the graph that the flux increases with water content in the feed. It was also very evident from experimental results that the total flux is a function of feed concentration and the flux varied during the entire experiment.

Procedure to calculate the overall mass transfer coefficient

To calculate the overall mass transfer coefficient for water transport from the experimental values, a graph of water flux vs. feed water concentration was plotted as

shown in Figure 3.22. The slope of the linear regression from this plot directly gives the overall mass transfer coefficient. This method was used to calculate the overall mass transfer coefficient in all the experiments.

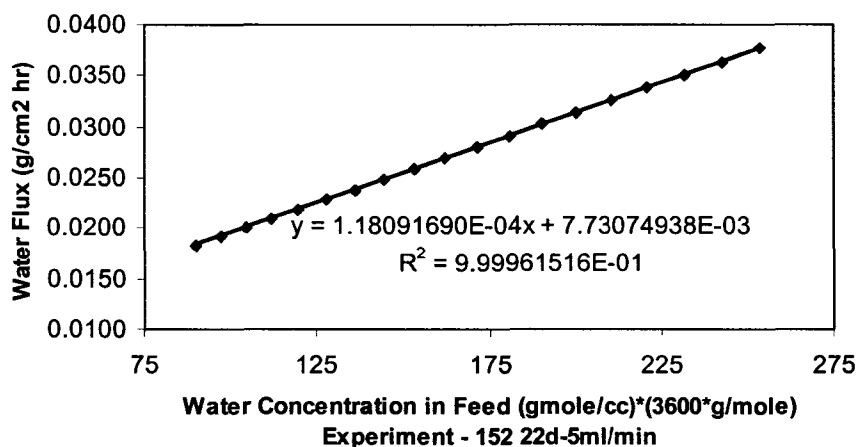


Figure 3.22 Calculation of overall mass transfer coefficient.

3.3.5 Effect of Operating Temperature

The influence of operating temperature on permeation rate and separation factor at 10 % w/w water concentration in the feed, and at a feed flow rate of 5 ml/min in the 22 μ m deep channel was evaluated. In experiments described earlier, the retentate was circulated back into the feed tank. The concentration changes observed in the feed tank was as a result of selective removal of water by the membrane, over the entire duration of the experiment. At lower temperatures the changes in concentration of ethanol was slower as a result of which the separation factor and flux was lower than those at higher temperatures. These experiments were run as long as there was enough feed left in the feed tank.

The plot for the overall mass transfer coefficient plotted against the operating temperature as shown in Figure 3.23 clearly indicates an increase in permeation when the feed temperature is increased. The experiments at higher temperatures have exhibited higher water removal. An increase in temperature from 70°C to 90°C resulted in an increase of over three times the overall mass transfer coefficient of 70°C as can be observed in Figure 3.30. The higher overall mass transfer coefficient was due to the proportionally higher selectivities observed as the temperature was increased. Therefore, the highest temperature (90°C) was chosen for the pervaporation experiments.

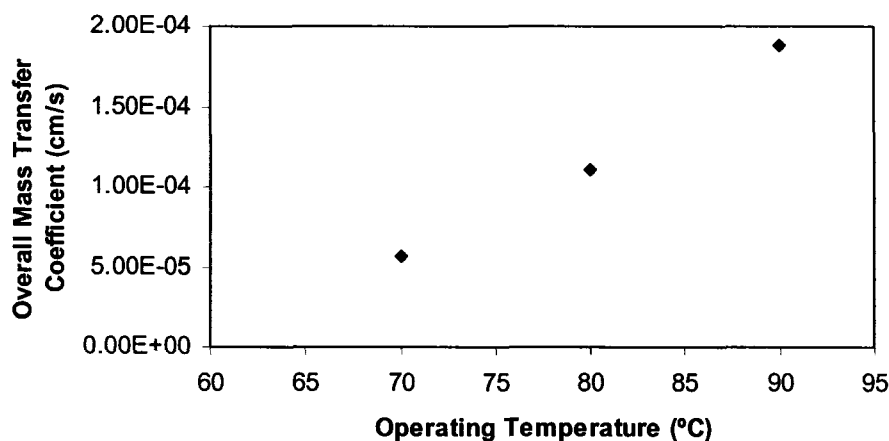


Figure 3.23 Overall mass transfer coefficients vs. operating temperature.

3.3.6 Effect of *In-situ* Heat Exchanger/ Direct Heating of Membrane

It was important to consider the enthalpy and thermal effects of the feed liquid while designing the membrane module for the microchannel pervaporation system. In the present experimental setup, the thermal mass of the module/holder was greater than the thermal mass of the fluid in the microchannels. Hence, it was imperative to choose direct

heating of the membrane, in order to maintain isothermal conditions in the membrane module. As a result, the *in-situ* heat exchanger was developed inside the membrane module/holder for the microscale pervaporation module.

The graph in Figure 3.24 is the temperature data acquired during one of the experiments.

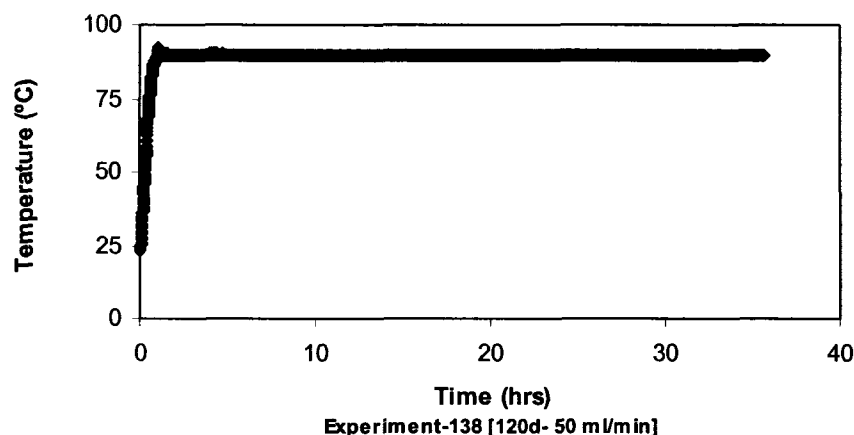


Figure 3.24 Acquired membrane module temperature data.

We can observe from the graph in Figure 3.25, which is just the enlarged version of Figure 3.24, that the time required to achieve the target temperature of 90 °C for this particular experiment was 1.5 hours. This stabilization time for the water bath varied from one experiment to another depending on factors such as room temperature and the internal fluid temperature of the water bath. As such, acquiring these temperature data provided important information related to stabilization time required for the experiment in addition to emphasize the effects of flux on instantaneous temperature changes. The graph in Figure 3.26 is an example of the temperature data from the stabilization time till the end of the experiment.

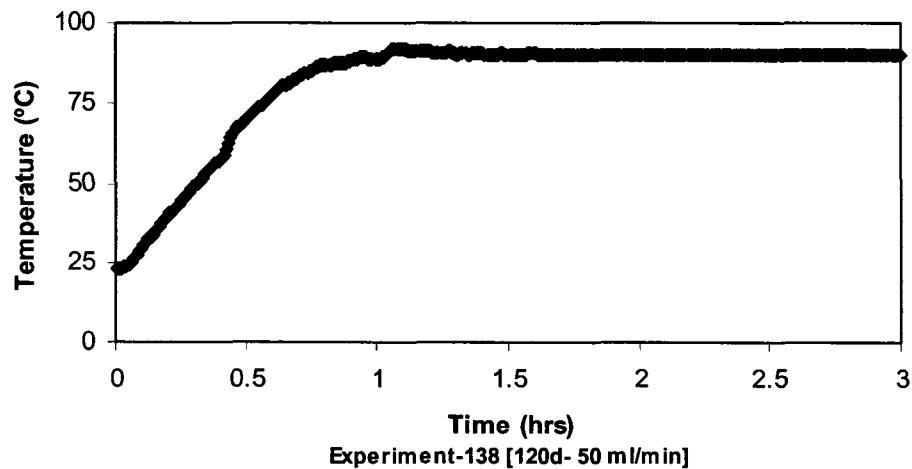


Figure 3.25 Membrane module temperature stabilization data.

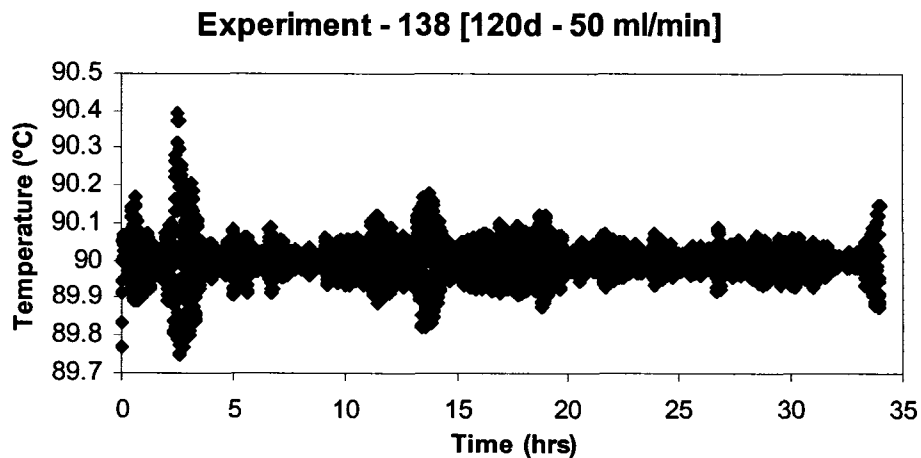


Figure 3.26 Behavior of membrane module temperature during a pervaporation experiment.

The graph in Figure 3.27 describes the standard deviation of the temperature in the membrane module observed for all the experiments as a function of residence time. The standard deviation for the feed temperature of 90°C was calculated from the

membrane module temperature data acquired by the computer during the experiments. It can be noted from the graph that most of the experiments exhibit a standard deviation of ≤ 0.05 °C from the set temperature of 90°C.

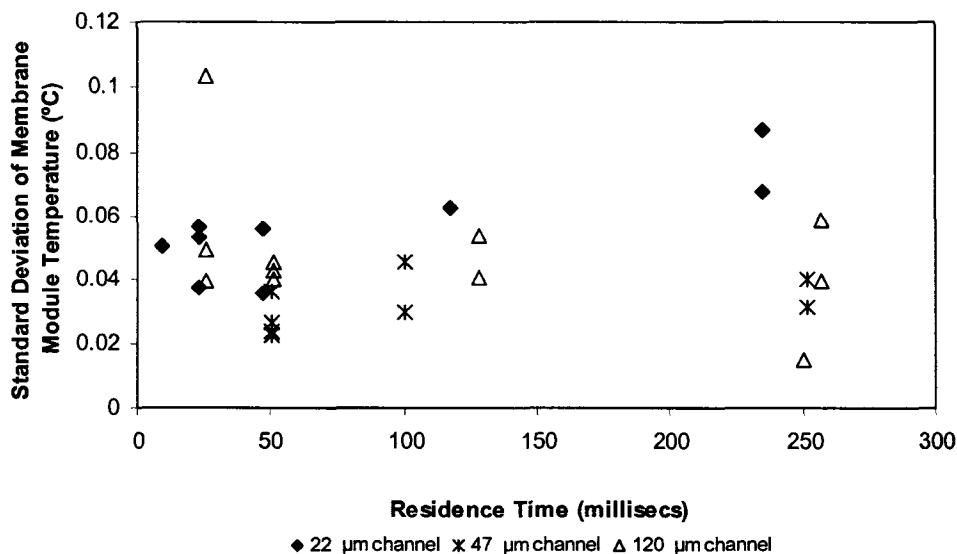


Figure 3.27 Membrane module temperature effects on residence time.

On certain occasions during the experiments the temperature in the membrane module exhibited instantaneous increase or decrease in temperature. This behavior was sporadic and was difficult to identify or predict its occurrence. The acquired temperature data indicated such behavior which can be noticed in the form of those isolated points in the standard deviation on the graph below. The reasons for this behavior, though, could be only surmised. One possible explanation is the controller on rare scenarios would lose control of the external temperature probe and allow over heating or cooling, and a stable set point could not be achieved. This resulted in small intervals of instability during experiments in the membrane module temperature management.

3.3.7 Effect of Permeate Pressure

To study the influence of vacuum pressure three experiments were carried out at 2, 3 and 5 Torr. In these experiments a 22 μm deep channel was used with a 10 % w/w water concentration in the feed as the starting concentration with a feed flow rate of 5 ml/min and operating temperature of 90°C. It has been reported in the literature [7] that the increase in permeate pressure decreases the driving force for transport through the membranes. The trend is also evident from the graph as shown in Figure 3.28 in which the overall mass transfer coefficient is plotted against the permeate (vacuum) pressures tested. As expected, the overall mass transfer coefficient was inversely proportional to the operating pressure. Therefore, all subsequent experiments were conducted at the lowest vacuum pressure achievable in this system.

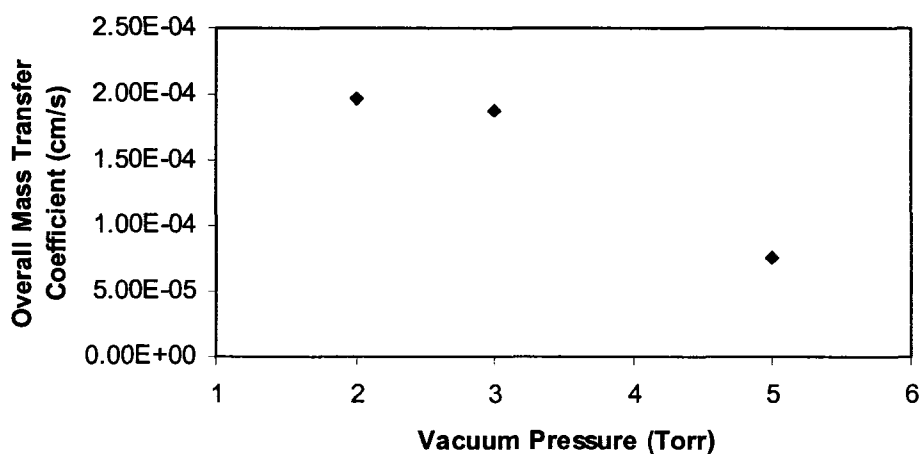


Figure 3.28 Overall mass transfer coefficients vs. permeate pressure.

3.3.8 Effect of Feed Flow Rate/ Residence Time

To evaluate the effect of changes in feed flow rate at the different depths tested, it was important to choose the optimum flow conditions. The highest possible flow rate that could be tested was 50 ml/min in the existing experimental setup. Flow rates higher than 50 ml/min resulted in problems with leaks in the lines and fittings at the membrane module. The feed pump and tubing size provided a range from 1 to 50 ml/min that could be operated without any problems related to the experimental setup. The microseparator depths tested were 22, 47 and 120 μm . Each depth corresponded to a different residence time for any given flow rate. To facilitate in comparison of performance at these different depths, the residence times were calculated and each depth of microseparator tested at residence times of 25, 50, 100 and 250 milliseconds although the flow rates tested varied for different microchannels. The flow rates and the corresponding residence times for the different microseparators are tabulated in Table 3.5.

The primary objective of the study was to decide if smaller microchannel dimensions facilitated shorter diffusion distances, resulting in a favorable impact on the overall mass transfer coefficient of the chosen system. The sensitivity of flow-rate to the overall mass transfer coefficient was also examined. The maximum velocity achievable with the current system was approximately 1.3 m/s for the three microchannels depths tested. The minimum velocity tested for each depth was an order of magnitude lower than the maximum.

Table 3.5 Index of flow rates used at varying depths of microseparator.

Depth	Hydraulic	Flow	Residence	Nre
	Diameter	Rate	Time	
[μm]	[μm]	[ml/min]	[milliseconds]	
22	32.6	1	235	7.9
22	32.6	2	117	15.8
22	32.6	5	47	39.7
22	32.6	10	23	79.4
47	52.7	2	251	12.2
47	52.7	5	100	30.6
47	52.7	10	50	61.2
47	52.7	25	20	153.0
120	80	5	250	18.1
120	80	10	128	36.3
120	80	25	51	90.8
120	80	50	25	181.7

To predict the impact that the channel dimension and velocity would have on the overall mass transfer coefficient of the system, the commonly used resistance-in-series model was employed [84]. Three resistances are noted during transport in membrane separation:

- (a) Mass transfer from the feed bulk to the feed membrane surface
- (b) Diffusion through the membrane
- (c) Desorption at the membrane permeate interface

Assuming the desorption at the membrane permeate interface is negligible; the overall mass transfer resistance is the sum of membrane resistance and the boundary layer resistance.

$$R_{ov} = R_{bl} + R_m \quad (1)$$

The mass transfer coefficients are reciprocal of the respective resistances.

$$\frac{1}{k_{ov,i}} = \frac{1}{k_{bl,i}} + \frac{1}{k_{m,i}} \quad (2)$$

The flux through the membrane can be given by the following equation.

$$J_i = k_{ov,i} C_{b,i} \quad (3)$$

Sherwood correlations

It is important to choose the appropriate semi-empirical Sherwood correlation to accurately predict the role of boundary layer resistance. Reviewing the literature, it was observed that the earliest studies were developed for convective heat transfer in laminar regime by Graetz [95] 1885, Leveque [96] 1928, and Sieder and Tate [97] 1936. In 1972 Porter [98] reported the modified mass transfer correlations to the Leveque and Graetz solutions. In 1987 Hallstrom [99] discussed in a review about using appropriate Sherwood correlations for turbulent flow particularly to membrane operations. Most of the recent researchers [81-91] who have reported the Sherwood correlations for laminar flow in membrane processes have cited Rautenbach, Huang, Hallstrom or Karlsson [100-101]. While, Hallstrom and Karlsson have adapted the Sherwood correlations developed by Porter, Huang's references for adaptation of these correlations have not been mentioned. Rautenbach has used the correlations from Sieder and Tate.

The Sherwood correlations thus far reported by different authors are shown in Eq. (4-6). The different values of coefficients a, b, and C reported by these authors is tabulated in Table 3.6.

Table 3.6 Coefficients for Sherwood correlations.

Coefficients for Sherwood correlations				
Eq.	Ref.	C	a	b
(4)	98	-	1.62	0.33
(5)	99	-	1.85	0.33
(6)	102, 103	3.66	1.61	0.33

$$Sh = C + a \left(\text{Re} Sc \left(\frac{D_h}{L} \right) \right)^b \quad (4-6)$$

Figures 3.29 and 3.30 depict the effect of the different Sherwood correlations at varying flow rates. These graphs relate the boundary layer thickness across the channel length of 3 cm for the 22 μm deep channels at the lowest and the highest flow rate tested. It can be observed from the figures that Eq. (4) and (5) are applicable in the developing region of the channel. Eq. (6) is applicable for both the developing and fully developed region. The short microchannel length and large range of flow velocities tested resulted in situations that varied between completely developed profiles for the majority of the channel to developing profiles continuing at the exit of the channel. The Sherwood number used to calculate the boundary layers and mass transfer resistances below was determined using Eq (6) at every 0.1 cm increment of the microchannel and taking an average over the entire 3 cm length.

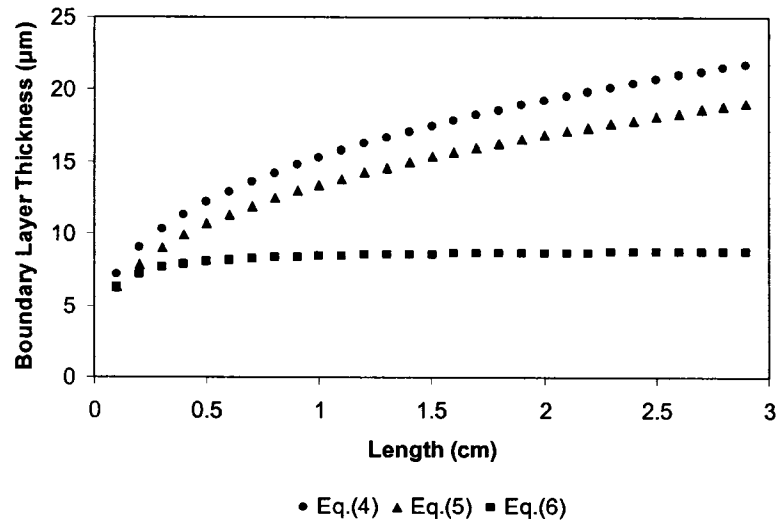


Figure 3.29 Effect of different Sherwood correlations in 22 μm deep channel at 12.7 cm/s.

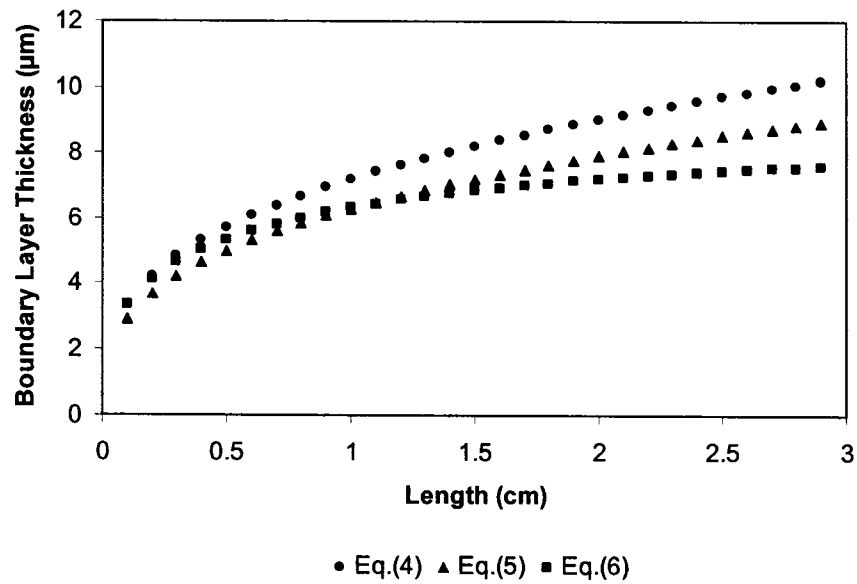


Figure 3.30 Effect of different Sherwood correlations in 22 μm deep channel at 127 cm/s.

$$\delta_i = \frac{D_h}{Sh} \quad (7)$$

δ_i = boundary layer thickness

The Reynolds number, Re , is the dimensionless parameter that describes the feed flow conditions;

$$Re = \frac{D_h v \rho}{\mu} \quad (8)$$

The Schmidt number, Sc , relates the diffusivity of momentum and the diffusivity of mass in the feed,

$$Sc = \frac{\nu}{D_i} \quad (9)$$

The boundary layer mass transfer coefficient can be calculated by simple manipulation of Eq. (7).

$$k_{bt} = \frac{D_i Sh}{D_h} \quad (10)$$

D_i = Diffusion coefficient of water in ethanol at 90°C [104].

$$D_h = \frac{2wd}{w+d} = \text{Hydraulic diameter}$$

w = width of the microchannel

d = depth of the microchannel

L = Length of the microchannel

v = Velocity of the fluid in the microchannel

ρ = Density of ethanol solution at 90°C

μ = Viscosity of ethanol solution at 90°C

From the above correlations, the dependence of velocity on boundary layer thickness can be described by Eq. (11). Eq. (12) and (13) depict the dependence of hydraulic diameter on boundary layer thickness for situations involving constant

volumetric flow-rate, constant Reynolds Number, and constant velocity with Table 3.7 providing the constants C1 and C2 for these relationships.

$$\frac{\delta_1}{\delta_2} = \left(\frac{v_2}{v_1} \right)^{\frac{1}{3}} \quad \text{Constant hydraulic diameter} \quad (11)$$

$$\frac{\delta_1}{\delta_2} = \left(\frac{D_{h1}}{D_{h2}} \right)^{C_1} \quad (12)$$

$$\frac{dP_1}{dP_2} = \left(\frac{D_{h1}}{D_{h2}} \right)^{C_2} \quad (13)$$

dP = Pressure drop

Table 3.7 Exponents relating hydraulic diameter to boundary layer thickness and pressure drop.

Eq.	C	Constant Volumetric Flow	Constant Reynolds Number	Constant Velocity
(12)	C ₁	1	2/3	1/3
(13)	C ₂	4	3	2

As evident from the above correlations, the boundary layer thickness has a higher dependence with hydraulic diameter than velocity if the Reynolds Number is maintained as a constant; however, the pressure required rises dramatically as the hydraulic diameter is reduced. The ten-fold increase in velocity tested in each microchannel resulted in 22%, 36% and 40% decrease in the predicted boundary layer thickness for the 22, 47 and 120 μm depth microchannels respectively. The 5.5 fold decrease in depth from 120 to 22 μm resulted in a 53% decrease in predicted boundary layer thickness at the lowest velocity tested but only a 39% decrease at the highest velocity tested. Therefore, reducing channel

dimensions to reduce boundary layer thickness appears to be most advantageous when low velocities are desired or required for a given application.

The overall mass transfer coefficient is plotted as a function of residence time as shown in Figure 3.31. In the range of residence time tested, the overall mass transfer coefficient has exhibited almost identical overall mass transfer coefficient clustered in the same order of magnitude for all the depths of the microseparator tested. The dispersion in the data appears to increase for shorter residence times, i.e, at higher flow rates. The highest overall mass transfer coefficient, 2.57×10^{-4} cm/s, was achieved with the smallest microchannel depth and the highest flow velocity which was predicted to achieve the lowest boundary layer. Most of the overall mass transfer coefficient data was dispersed primarily between 1.2 and 1.8×10^{-4} with an average value of approximately 1.6×10^{-4} cm/s and did not exhibit the expected trends with respect to fluid velocity or hydraulic diameter. Indeed, Figure 3.31 suggests that, on average, a higher velocity tended to result in a slightly lower overall mass transfer coefficient, which would contradict the predictions for a boundary layer dominant system. The variation is most likely due to a confluence of small deviations in temperature and pressure that occurred during testing.

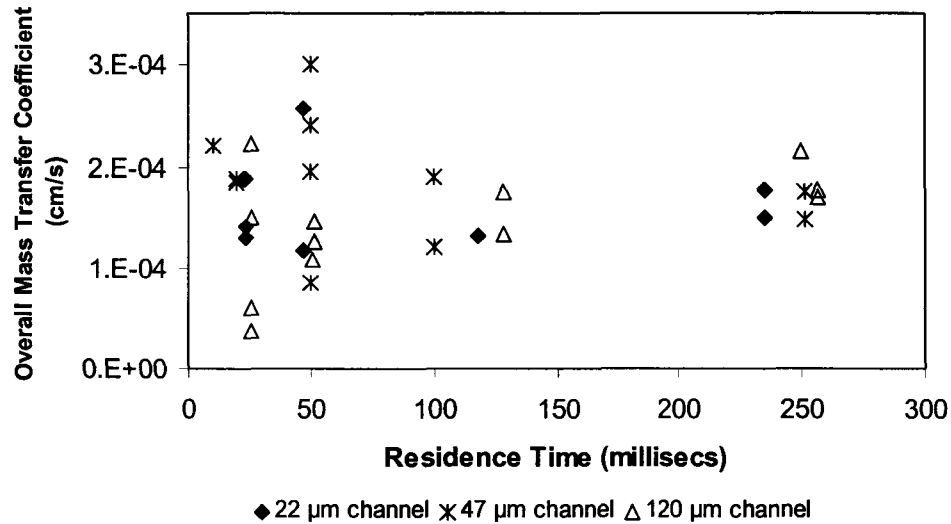


Figure 3.31 Overall mass transfer coefficients vs. residence time.

3.3.9 Effect of Varying Hydraulic Diameter on Separation Performance

For us to understand the effects of change in channel depth, the overall mass transfer coefficient is plotted as a function of hydraulic diameter as shown in Figure 3.32. From this figure, the overall mass transfer coefficient is clearly not affected by the changes in the range of channel depth and the fluid velocity tested. The strong influence of the membrane resistance shows that the mass transfer is limited by the membrane, because no effect in hydraulic diameter is observed. In the pervaporation of ethanol-water mixtures in the microchannel separator using the commercial polymer dehydration membrane, the membrane resistance contributes significantly to the overall transport resistance.

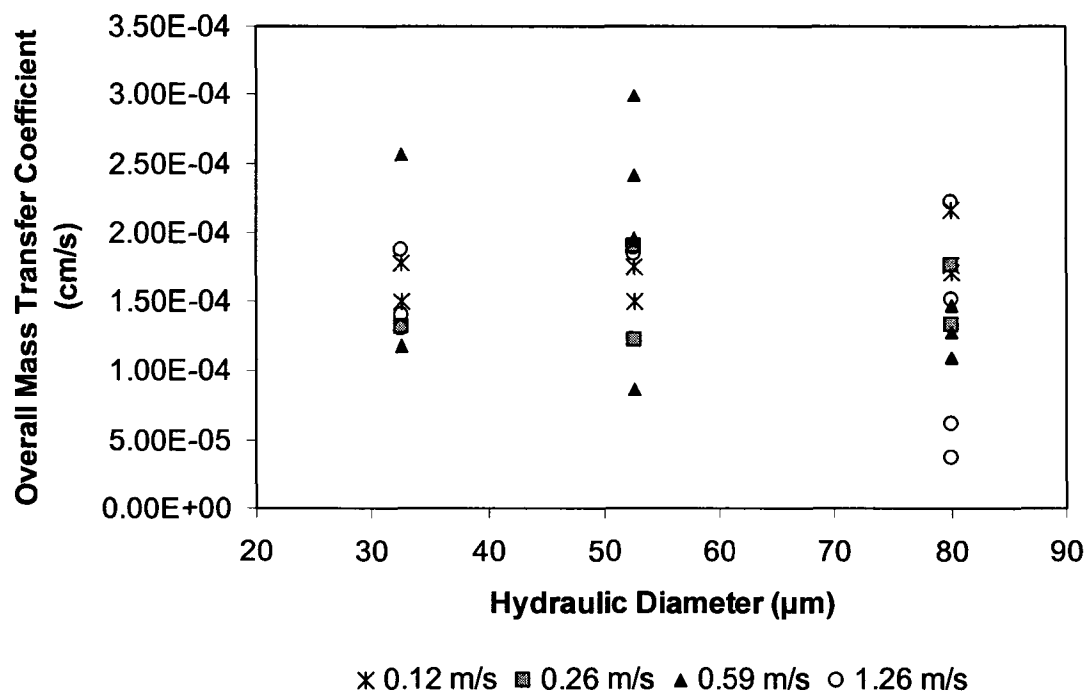


Figure 3.32 Overall mass transfer coefficients vs. hydraulic diameter.

In Table 3.8 the confidence interval at 95 and 99 % are reported for both the separation factor and the flux for all the pervaporation experiments conducted with retentate recycle. It can be noted from the table that a trend could not be observed while comparing the 95 and 99 % confidence interval for both the separation factor and flux data when the residence times and hydraulic diameter were varied. The median value from the average separation factor data for the smallest and largest hydraulic diameter at the different residence time tested differs marginally. Similar results can also be observed from the table for the flux data.

Table 3.8 Confidence interval for separation factor and flux data from retentate recycle experiments.

Hydraulic Diameter [μm]	Residence Time [milliseconds]	Separation Factor				Flux [$\text{g cm}^{-2} \text{hr}^{-1}$]			
		Average	Stdev	Confidence		Average	Stdev	Confidence	
				95%	99%			95%	99%
32.6	235	9.59	0.32	0.449	0.590	0.077	0.018	0.025	0.033
32.6	47	21.27	6.49	8.989	11.81	0.069	0.033	0.046	0.061
32.6	23	14.58	1.27	1.438	1.890	0.061	0.013	0.015	0.019
52.7	251	16.44	0.92	1.280	1.682	0.076	0.011	0.015	0.020
52.7	100	16.37	0.68	0.936	1.230	0.063	0.012	0.017	0.023
52.7	50	23.19	9.97	9.771	12.84	0.070	0.012	0.012	0.015
52.7	20	23.06	2.45	3.401	4.469	0.064	0.001	0.002	0.002
80.0	250	21.33	11.1	12.56	16.50	0.075	0.011	0.013	0.017
80.0	128	16.31	1.86	2.582	3.394	0.063	0.020	0.027	0.036
80.0	51	15.41	3.70	4.184	5.499	0.056	0.011	0.012	0.016
80.0	25	18.94	7.39	7.246	9.523	0.064	0.017	0.017	0.022

In Figure 3.33 all the mass transfer resistances studied are compared with the residence times tested. The y-axis on this graph is plotted on the logarithmic scale to emphasize the difference in the resistances evaluated. It is clear from the graph that the boundary layer mass transfer resistance is over three orders of magnitude lower than the overall mass transfer resistance. This result further corroborates the fact that the process is limited by the membrane resistance.

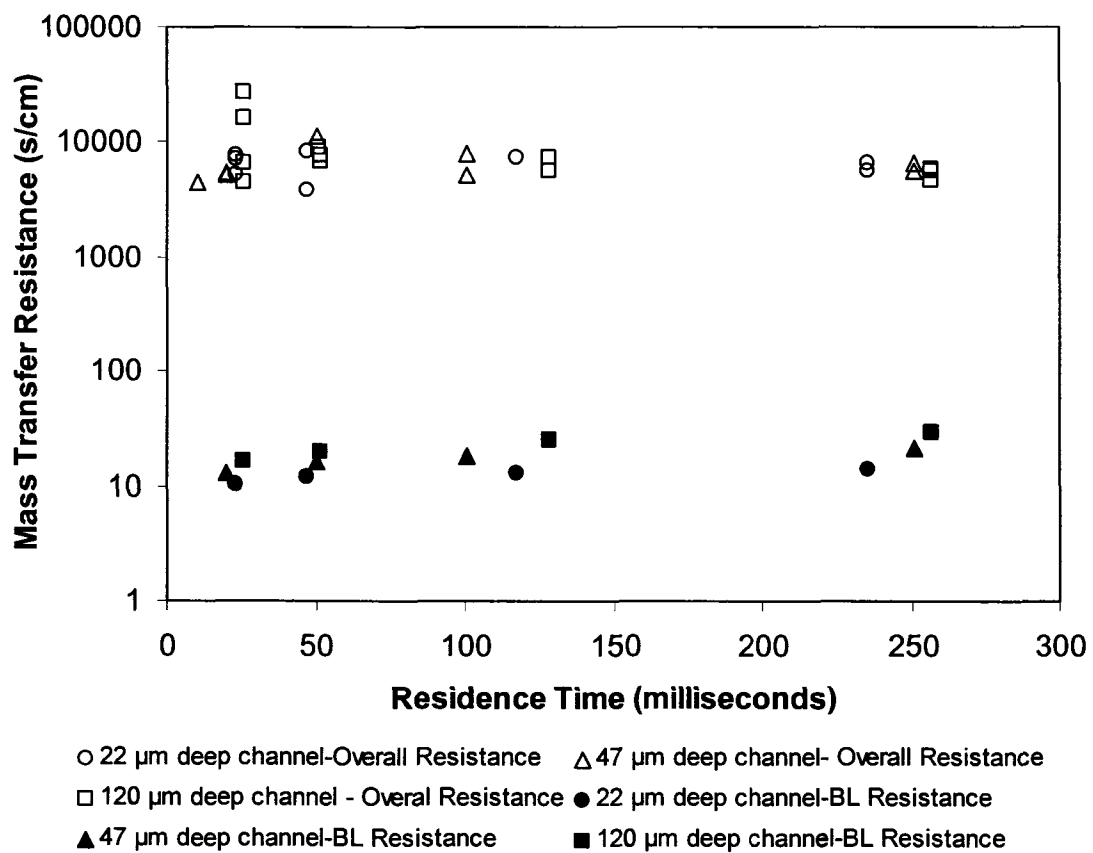


Figure 3.33 Mass transfer resistances vs. residence time.

CHAPTER 4

CONCLUSIONS AND FUTURE WORK

4.1 Conclusions

In this project, a detailed description of developing and functioning of a novel microchannel separator based on the pervaporation process has been reported to evaluate process intensification effects and the separation performance of the microchannel pervaporation module with a 3 cm² membrane area using a commercial polymer dehydration membrane was investigated. The microchannel pervaporation module also served as an *in-situ* heat exchanger for the process. The various parameters tested were hydraulic diameter, residence time, permeate pressure and operating temperature.

This study involved two different experimental setups varying in the retentate flow mode. The two modes of retentate were the single pass and the retentate recycle.

The single pass experiments were conducted at very low flow rates with Reynolds number in the range of 0.02 to 0.3 and at operating temperature $\leq 60^{\circ}\text{C}$. The results of these experiments demonstrated the need to modify the experimental setup to improve the separation performance.

The retentate recycle pervaporation experimental setup enabled operating at higher flow rates and at elevated operating temperature than the single pass experimental setup. The unique features of the retentate recycle pervaporation setup was that it facilitated in

acquiring data from online measurement of temperature variations in the membrane module and the continuous measurement of changes in mass of the feed tank. The flow rates tested in this setup corresponded to Reynolds number within the range of 8 to 181. In these experiments an operating temperature of 90°C and a low vacuum pressure of 2 to 3 Torr favored high fluxes and separation factor. In addition to the operating conditions, the evaporation effects, the temperature effects caused by the *in-situ* heat exchanger, and feed concentration influenced the separation performance.

In-depth mass transfer analysis was developed by adapting resistance-in-series model and Sherwood correlations; which indicated that the boundary layer mass transfer coefficient was over three orders of magnitudes lower than that of the overall mass transfer coefficient. It could be inferred from the experimental results that the separation factor, flux and the overall mass transfer coefficient were independent of changes in residence time and hydraulic diameter. The experimental results also indicated that under the conditions of this study for pervaporation of water from ethanol/water solution using the microseparator, the mass transfer resistance due to the membrane was dominating.

4.2 Future Work

The project so far is a first-generation prototype microfluidic device for liquid phase separation by pervaporation process. Systems that have demonstrated significant boundary layer resistances in the literature would benefit the greatest from the reduction in hydraulic diameter. For example, trichloroethylene (TCE) has a reported diffusivity that is higher in PDMS than an aqueous environment [92], and is a classic example in the literature of a pervaporation system that exhibits significant boundary layer resistance. TCE removal from water and similar systems would be appropriate choices for future

studies in micro-chemical separation, especially for applications requiring a laminar or low flow velocity.

In addition to testing with an appropriate membrane, it is also required to test the process with membranes of different thickness. The data obtained from experiments with varying membrane thickness can provide valuable information on predicting the boundary layer resistance and the membrane resistance. Also, experiments should be designed for measuring the diffusion coefficients of the selective component in the membrane in order to further validate the mass transfer analysis.

The ultimate objective of the project is to demonstrate the significance of liquid phase separation in microchannel devices, and it is important to compare the performance of this device with a conventional size pervaporation experimental setup with similar testing conditions. The results from this comparative study can then be used in drawing conclusions regarding the advantages, if any, from a microchannel based pervaporation process.

The present experimental setup has certain limitations that could be improved in the next generation experiments. A gas chromatograph directly connected to the permeate line could facilitate in on-line analysis of the permeate. The permeate data were predicted using a mathematical model in the present experiments. The direct measurement of permeate can provide experimental data to calculate separation factor and flux.

The use of an in-line analytical instrument can eliminate the need to measure the concentration of the feed mixture in the feed tank manually. It is also important to mention the fact that the results from the present experiments have indicated a very slow change in concentration in the feed tank within a short interval of time. As such, by using

a high precision in-line analytical instrument the subtle changes that occur in the feed tank can be easily measured. Also, the most significant advantage of introducing an in-line analytical instrument to monitor the changes in concentration in the feed tank is that the experiment can be operated for extended hours without disturbing the feed tank. This eliminates the treatment of the mass data and evaporation effects could also be minimized by using a different feed tank. The data from the feed tank concentration measurement and the permeate could be used to check the mass balance of the complete system with real time data. These improvements can significantly assist in developing a microchannel separator based on pervaporation process with potential applications as a pre-concentrator.

APPENDIX A

ETHANOL METHOD DEVELOPMENT IN A HP 5890 Series II GAS CHROMATOGRAPH

An internal standard method was developed to determine the ethanol content in the feed and retentate samples obtained from pervaporation experiments. The unknown ethanol concentration from these samples were diluted with n-propanol internal standard solution and injected directly into GC for analysis. In the following sections the detailed procedure for the method development and specifications of the instrumentation involved are discussed.

Preparation of standard solutions

The feed concentration and the samples were prepared on volume basis to minimize the errors caused while using small vials to prepare samples on mass basis. A 2.5 ml of n-propanol solution was dispensed into 25 ml volumetric flask and then de-ionized water was added to the 25 ml mark. The resulting solution was the 10 % (v/v) n-propanol internal standard which was maintained constant for all the analysis.

Ethanol concentrations of 72, 80, 88, 90, 96 and 100 % v/v were prepared using standard volumetric flask to develop a calibration curve. 18, 20, 22 and 24 ml of ethanol was dispensed into four separate 25 ml volumetric flasks and then de-ionized water was added to the 25 ml mark respectively. These were the 72, 80, 88, and 96 % (v/v) ethanol standard solution respectively. For 90 % (v/v) ethanol standard solution 45 ml of ethanol solution was dispensed into a 50 ml volumetric flask and then de-ionized water was added to the 50 ml mark. These high ethanol concentrations were chosen for the standard solutions since these concentration cover the range of concentration expected from our experimental results.

Calibration chart

The calibration curve was constructed by plotting the ratio of peak area of the ethanol to the peak area of the internal standard against the ratio of the concentration of the analytes to the concentration of internal standard. The peak area ratio was independent of injection volume and normally resulted in better calibration curves. Each sample was analyzed in triplicate and the RSD was less than 0.5 % for the area ratio.

Calculation of unknown analyte concentration

The ratio of the analyte area to internal standard area was calculated from the GC chromatogram data. The corresponding ratio of analyte concentration to internal standard concentration was determined from the linear regression equation ($Y = 0.6693x$) in the calibration chart as shown in Figure A.1. The concentration of internal standard in the sample was multiplied by this ratio and corresponding dilution factors. This provided the concentration of the analyte in the unknown sample.

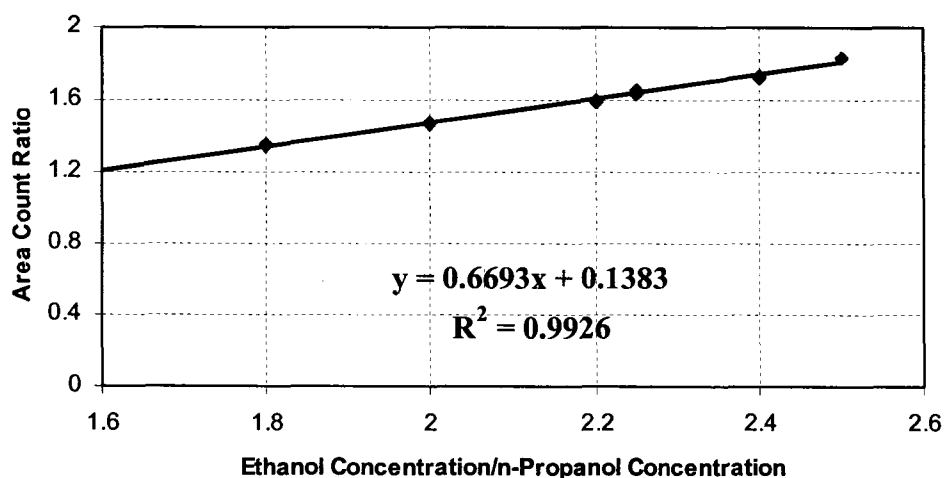


Figure A.1 Calibration chart for ethanol analysis by gas chromatography.

Preparation of sample for analysis in gas chromatograph

To a small vial containing 0.8ml of internal standard solution, 0.2 ml of analyte was added. A high-precision Eppendorf micropipette (Research® Series 2100 Adjustable-volume Pipette) was used for dispensing these volumes precisely. This pipette could be used for dispensing volumes in the range from 20 to 200 μL . The pipette had an accuracy of $\pm 0.6 - \pm 2.5$ (%). The small vial used for sample preparation was a target clear screw thread vial (National Scientific Company) and the size of the vial was 12×32 mm with a 2 ml capacity.

Analyzing the unknown sample

A 0.2 ml of unknown sample was added in to a sample vial containing 0.8 ml of the internal standard solution. This method was adapted to avoid the separate addition of another solvent such as water. The internal standard solution used was very dilute and this solution adequately diluted the unknown ethanol solution on mixing. As such good peaks without tailing could be obtained. The sample vial was mixed well and 0.5 μL was injected with a high-precision syringe into the injector maintained at 150 $^{\circ}\text{C}$. From our earlier experiments, we learned that 0.5 μL was the optimum volume for injection since water tends to expand at the inlet. It was also important to choose the syringe of appropriate capacity to maintain the reproducibility of injections as such, a syringe (Agilent-5182-9623) with removal needle and with 5 μL capacity was used to improve the accuracy of injections.

The (AUC) Area under curve for ethanol and n-propanol was obtained and the ratio was calculated.

$$\frac{\text{Area under curve for ethanol}}{\text{Area under curve for n - propanol}} = \text{Area Count Ratio (y)}$$

$$\frac{\text{Concentration of ethanol solution after dilution \% v/v}}{\text{Concentration of n - propanol solution after dilution \% v/v}} = \text{Ratio of concentration (x)}$$

The ratio of concentration for the unknown sample was calculated from the linear regression equation ($R^2 \geq 0.999$) obtained from the calibration chart.

$$y = 0.6693x + 0.1383 \quad (1)$$

The Area Count Ratio (y) of the unknown sample was directly available from the integration of data during the analysis by using the Chemstation software. On using the area count ratio in Eq.1, the ratio of concentration of ethanol and n-propanol solution (x) was obtained. The ratio was then multiplied with the concentration of n-propanol solution after dilution to arrive at the concentration of ethanol after dilution. When multiplied with appropriate dilution factors the actual concentration of the unknown sample was determined. The dilution factor is the ratio of total volume used in sample preparation (1 ml) to the volume of ethanol in sample preparation (0.2 ml)

Procedure

1. A clean and dry sample vial was taken and 0.8 ml of prepared internal standard solution was added to it.
2. A 0.2 ml of the unknown ethanol concentration sample was added into the vial containing the internal standard solution.
3. The vial containing the internal standard and the unknown sample was well mixed.
4. The gas chromatograph was maintained at the operating conditions as described earlier.
5. A 0.5 μL of sample from the vial was injected into the GC column

6. The peak area of both the internal standard and the unknown ethanol concentration was recorded.

Operating conditions of gas chromatograph

The settings in the GC were as follows:

Initial oven temperature = 50 °C

Final oven temperature = 150 °C

Initial time = 0 min

Oven ramp rate = 25 °C / min

Total time for analysis = 8 min

Injector temperature = 150 °C

Detector temperature = 240 °C

Carrier gas = He

Column head pressure = 5 Kpa

Combustion Gases = H₂ and air

Total He flow rate = 68.5 ml/min

Injection volume = 0.5 µl

Retention times:

Ethanol - 0.74 min

n -propanol - 1 min

The GC shown in Figure A.2 uses a HP-FFAP 30m × 0.53mm × 1.0mm capillary column. This Hewlett Packard 5890 series II Gas chromatograph as was interconnected with Chemstation software, Rev.A.06.03 copyright© by Hewlett Packard 1990-1998. The sample analysis was performed using gas chromatography (GC) with flame ionization detector (FID). The FID signal was set at a range = 10, and attenuation = 1.

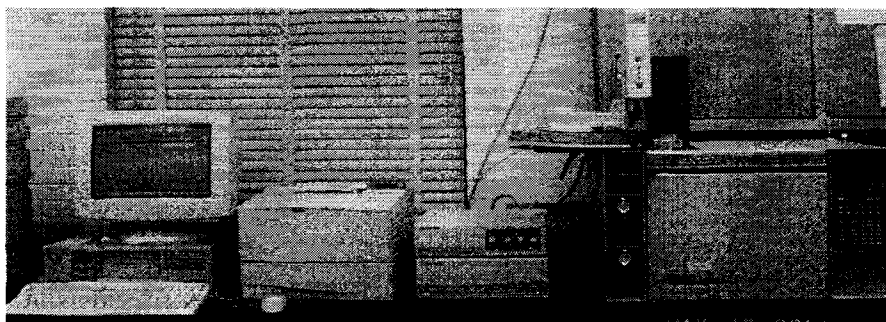


Figure A.2 Picture of Hewlett-Packard gas chromatograph 5890 series II.

To improve the reproducibility and obtain better peaks a general purpose split/split less tapered liner with deactivated glass wool was used. This liner had a small internal diameter of 4 mm which lead to a small internal volume. It is in this small volume of the liner that the phase transition of the sample from the liquid phase to the vapor phase occurs. It was vital to choose an appropriate liner so that the vapor fits in within the volume of the liner being used. The glass wool provided additional surface area for complete volatilization of the sample to minimize thermal discrimination, they also trapped non-volatile components and septum particles before they reached the column, thereby increasing reproducibility and preventing sample residue build-up at the septum [105]. Using the glass wool in the liner also resulted in a more controlled evaporation of the sample, which consequently assisted in obtaining a good peak shape. In the absence of the glass wool, the stream of water could shoot right out the bottom of the inlet, without even evaporating.

The specifications of the instrumentation in the gas chromatograph used are listed below:

Split/ Splitless Capillary

- Range to 400°C in 1°C increments
- Back-pressure design permits independent adjustment of split flow rate without affecting column flow
- Septum purge built in at 3 ml/min
- Accepts columns up to 1.2-mm O.D.
- Multimode design includes split and splitless injection
- Splitless purge time variable in 0.01-min elements

Flame Ionization Detector

- Range to 450°C
- Grounded jet and current limited design for operator safety
- Push-button flame ignition
- Sensitive:
 - > 22mCo µl/gm carbon: nitrogen carrier, 0.018-in. id capillary jet
 - > 18 mCo µl/gm carbon: helium carrier, 0.018-in. id capillary jet
- Minimum detectable: <5 pg carbon/sec, nitrogen carrier at S/N=2
- Linear dynamic range: <+/- 10% over a 10^7 range with 0.018-in. ID jet
- Conditions: column flow 50 ml/min, 45 ml/min H₂, 650 ml/min air, propane sample

Column Oven

- Operating range: 4 °C above ambient to 450 °C
- Setpoint entry: 1 °C for temperatures, 0.1 °C for program rates
- Programming: Rates 0.1 to 70 °C per min, 650 min maximum run time, three ramps with initial/final holds.

The data presented in Tables A.1 to A.3 were used in developing the ethanol calibration curve as described earlier.

Table A.1 GC ethanol method development data.

Target	Ethanol	n-Propanol	Ethanol	n-Propanol	Ratio
Concentration			Concentration	Concentration	Concentration
			after dilution	after dilution	
% v/v	ml	ml	% v/v	% v/v	
70	0.2	0.8	14.4	8	1.8
					1.8
					1.8
80	0.2	0.8	16	8	2
					2
					2
88	0.2	0.8	17.6	8	2.2
					2.2
					2.2
90	0.2	0.8	18	8	2.25
					2.25
					2.25
96	0.2	0.8	19.2	8	2.4
					2.4
					2.4
100	0.2	0.8	20	8	2.5
					2.5
					2.5

Table A.2 GC ethanol method development chromatograph details -1.

Ethanol Area	n-propanol Area	Area Ratio	Mean	Standard deviation	RSD*	
2.69E+05	1.98E+05	1.358893	1.351285	0.007666	0.567299	Area-ratio
2.63E+05	1.96E+05	1.343562	2.67E+05	3020.009	1.132937	Ethanol- Area
2.67E+05	1.97E+05	1.3514	1.97E+05	1124.27	0.569933	n- propanol- Area
2.97E+05	2.00E+05	1.483298	1.476625	0.006857	0.464399	
3.07E+05	2.08E+05	1.48E+00	3.06E+05	8228.563	2.689536	
3.14E+05	2.13E+05	1.469597	2.07E+05	6520.999	3.146993	
3.33E+05	2.08E+05	1.599424	1.60E+00	0.007806	0.488418	
3.56E+05	2.22E+05	1.605277	2.11E+05	9638.05	4.567775	
3.23E+05	2.03E+05	1.589817	2.13E+05	9281.658	4.34816	
3.62E+05	2.21E+05	1.639719	1.642211	0.006983	0.425211	
3.59E+05	2.19E+05	1.636816	3.42E+05	32048.98	9.365953	
3.05E+05	1.85E+05	1.650098	2.08E+05	20325.24	9.751825	
3.68E+05	2.14E+05	1.720458	1.729501	0.008619	0.498329	
3.60E+05	2.07E+05	1.737621	3.58E+05	11432.73	3.194426	
3.46E+05	2.00E+05	1.730425	2.07E+05	7155.626	3.457665	
3.88E+05	2.12E+05	1.833368	1.832745	0.002886	0.157482	
3.87E+05	2.11E+05	1.835269	3.86E+05	2556.624	0.661517	
3.84E+05	2.10E+05	1.829598	3.85E+05	2699.027	0.700143	

*RSD = Relative Standard Deviation

Table A.3 GC ethanol method development chromatograph details -2.

Et-OH	n- POH	Et-OH	n- POH	Ethanol	n-POH	Ethanol	n- POH	Total
Retention Time	Width		Height		Area		Area	
min	min		μV		%			
0.74	1	0.0322	0.0356	2.69E+05	1.98E+05	57.6	42.39	4.67E+05
0.719	0.982	0.0403	0.0429	9.24E+04	7.39E+04	57.3	42.67	4.59E+05
0.73	0.994	0.0405	0.0389	8.77E+04	6.61E+04	57.47	42.52	4.64E+05
0.739	1	0.0341	0.0372	1.28E+05	7.74E+04	59.73	40.26	4.97E+05
0.729	0.993	0.0406	0.0389	1.00E+05	6.90E+04	59.6	40.37	5.15E+05
0.734	0.998	0.0388	0.0427	1.36E+05	8.36E+04	59.5	40.49	5.26E+05
0.74	1.004	0.0473	0.0455	1.16E+05	7.73E+05	61.5	38.46	5.42E+05
0.742	1.004	0.036	0.0381	1.38E+05	7.81E+05	61.61	38.38	5.77E+05
0.738	0.998	0.038	0.0416	1.45E+05	8.28E+04	61.38	38.61	5.26E+05
0.737	0.998	0.036	0.0379	1.36E+05	7.60E+04	62.11	37.88	5.83E+05
0.741	1	0.037	0.0384	1.35E+05	7.66E+04	62.07	37.92	5.79E+05
0.727	0.988	0.048	0.0401	1.04E+05	6.52E+04	62.26	37.73	4.90E+05
0.737	0.996	0.0437	0.0461	1.39E+05	7.79E+04	63.24	36.75	5.82E+05
0.74	0.999	0.0386	0.0369	1.37E+05	7.33E+04	63.47	36.53	5.67E+05
0.743	1.002	0.0433	0.0429	1.24E+05	7.53E+05	62.61	37.38	5.17E+05
0.743	1.002	0.0372	0.0387	1.45E+05	7.32E+04	64.7	35.29	6.00E+05
0.747	1.005	0.0368	0.037	1.51E+05	7.46E+04	64.72	35.27	5.98E+05
0.744	1.007	0.0498	0.0457	1.29E+05	7.72E+04	64.65	35.34	5.93E+05

Et-OH = Ethanol

n- POH = n-propanol

APPENDIX B

ETHANOL METHOD DEVELOPMENT IN ABBE MARK II REFRACTOMETER

Reichert Abbe Mark II refractometer was used to analyze the composition of the ethanol/water solution. It is widely known that the temperature variations affect the measurement of the refractometer. The refractive index values decrease with increase in temperature because the density of the solution decreases with increasing temperature, consequently affecting the concentration values. The prism assembly in the refractometer was provided with ports to circulate coolant so that readings could be recorded from the refractometer at any desired constant temperature. A programmable digital circulator (Polyscience Model 9510) was used to circulate water maintained at a slightly lower temperature than 20°C. This circulator served a dual role by not only maintaining the refractometer at a constant temperature of 20°C, but also the retentate line from the experimental setup was directly immersed inside this water bath to ensure the feed ethanol inside the feed tank was always at room temperature. To optimize the reading accuracy, the refractometer was kept ON all throughout the duration of the experiment as recommended by the manufacturer.

Ethanol concentrations from 90 to 100 % w/w were prepared using a high precision analytical balance (Denver Instrument - Model: TR-104). This balance had a capacity of 110g, readability of 0.1mg, repeatability of 0.1mg, and linearity of ± 0.2 mg. These high ethanol concentrations were chosen for the standard solutions since these concentrations cover the range expected from our experimental results. The calibration curve as shown in Figure B.1 was constructed by plotting the measured refractive index of respective ethanol concentration against the actual ethanol concentration prepared.

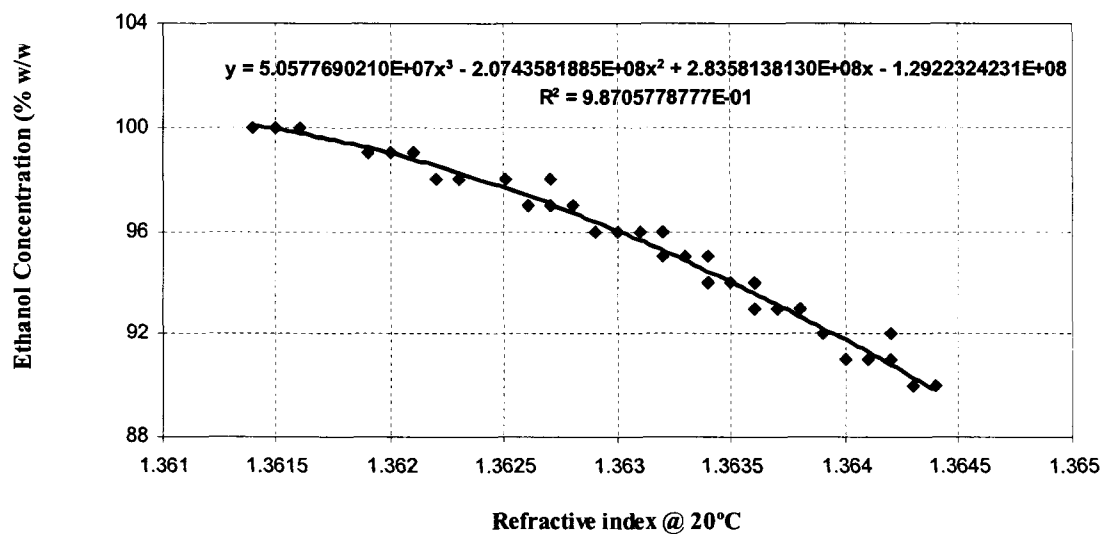


Figure B.1 Calibration chart for ethanol analysis by refractometer.

For each known concentration six refractive index values were recorded in a randomized manner. A polynomial third-order equation provided the best fit for all the points. This equation was used in all the experiments to determine the unknown ethanol concentration. The average standard deviation and 99% confidence interval for the refractive index of individual ethanol concentration was calculated. From these calculations it was observed that for the 99% confidence interval the average refractive index value was in the range of ± 0.0001 nD (nD here refers to the wavelength of monochromatic light, which is 589nm, in the sodium D line) [106]. Figure B.2 provides the error analysis and we can observe from the graph that a resolution of ± 0.0001 nD provided by the refractometer translates to $\pm 0.5\%$ ethanol concentration as predicted by the calibration chart.

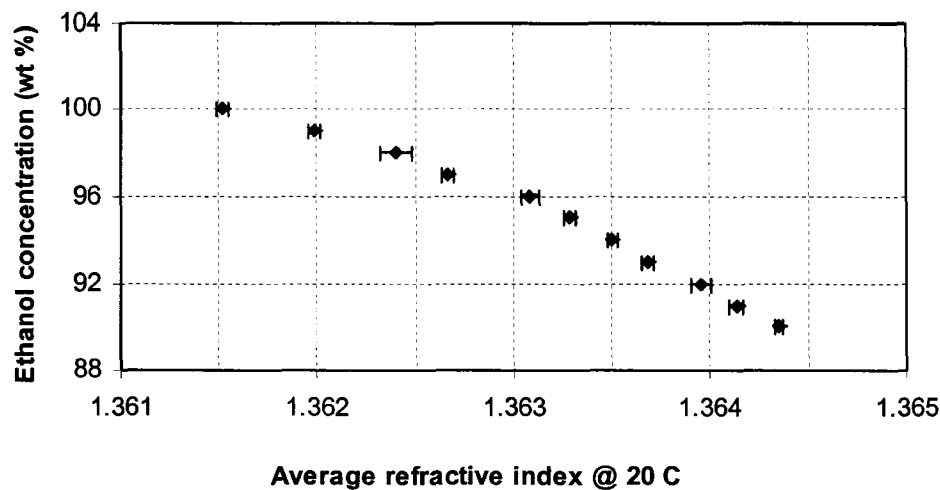


Figure B.2 X-Bar analysis for calibration chart.

Procedure

Samples in the range of 0.15 to 0.2 g were adequate to cover the entire surface of the prism. It was required to ensure that the entire surface of the prism was covered with the sample free from air bubbles. Care was also taken to maintain the prism surface clean and free from dust. The sample and the prism assembly were allowed to reach an equilibrium temperature before any measurement. All measurements are made at a constant temperature of 20°C. Measurements were made by matching a sharp shadow line (free from any green or red color near the edges) with the intersection of the cross lines as shown in the Figure B.3 (adapted from Reichert instruction manual). The refractive index and the temperature were displayed on the LCD screen of the refractometer. This simple technique required only a small amount of sample and refractive index measurements could be made quickly and precisely.

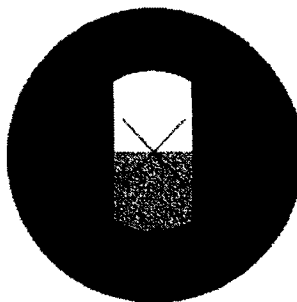


Figure B.3 Picture of shadow mark intersection with cross lines in refractometer.

The specifications of Reichert ABBE MARK II refractometer are listed below:

Display: Digital LED Display, 2"W X 0.75"H (5.0 X 1.9 cm)

Precision: $\pm 0.0001nD$

Reading Range: 1.3200 to 1.7000 (refractive index)

Temperature control method: Ports for external circulator

Temperature control range: 10 to 80 ° C

Temperature precision: 0.1 ° C

Sample types: Transparent and Translucent Liquids or Solids

Prism assembly: Glass Prism sealed with Epoxy to 416 Grade Stainless Steel Housing

User interface: Read and Temperature Buttons as well as 3-way Mode Selector Knob

The data presented in Tables B.1 and B.2 was used in developing the ethanol calibration curve with the ABBE Mark II refractometer.

Table B.1 Ethanol standard solution data for method development in refractometer.

#	Target Concentration wt%	Mass of Water g	Mass of Ethanol g	Actual Concentration wt%
1	86	1.3973	8.6063	86.0320
2	83	1.8252	8.8015	82.8244
3	90	1.0047	9.0088	89.9665
4	91	0.8963	9.1079	91.0408
5	92	0.8041	9.2030	91.9647
6	93	0.6954	9.2923	93.0374
7	94	0.5981	9.3942	94.0144
8	95	0.5043	9.4940	94.9561
9	96	0.3950	9.3484	95.9460
10	97	0.2996	9.6940	97.0021
11	98	0.1960	9.8031	98.0398
12	99	0.1090	9.9035	98.9114
13	100	0.0000	10.0000	100.0000

Table B.2 Refractive index data from ethanol method development in refractometer.

#	Target Concentration wt%	Actual Concentration wt%	nd	Temperature °C
1	90	89.9665	1.3643	20
2	90	89.9665	1.3644	20
3	90	89.9665	1.3643	20
4	90	89.9665	1.3644	20
5	90	89.9665	1.3643	20
6	90	89.9665	1.3644	20
7	91	91.0408	1.3642	20
8	91	91.0408	1.3642	20
9	91	91.0408	1.364	20
10	91	91.0408	1.3641	20
11	91	91.0408	1.3642	20
12	91	91.0408	1.3641	20
13	92	91.9647	1.3639	20
14	92	91.9647	1.3639	20
15	92	91.9647	1.3639	20
16	92	91.9647	1.3639	20
17	92	91.9647	1.3639	20
18	92	91.9647	1.3642	20
19	93	93.0374	1.3638	20
20	93	93.0374	1.3637	20

21	93	93.0374	1.3637	20
22	93	93.0374	1.3637	20
23	93	93.0374	1.3636	20
24	93	93.0374	1.3636	20
25	94	94.0144	1.3635	20
26	94	94.0144	1.3635	20
27	94	94.0144	1.3635	20
28	94	94.0144	1.3635	20
29	94	94.0144	1.3636	20
30	94	94.0144	1.3634	20
31	95	94.9561	1.3634	20
32	95	94.9561	1.3633	20
33	95	94.9561	1.3633	20
34	95	94.9561	1.3633	20
35	95	94.9561	1.3632	20
36	95	94.9561	1.3632	20
37	96	95.9460	1.3632	20
38	96	95.9460	1.3631	20
39	96	95.9460	1.3629	20
40	96	95.9460	1.3632	20
41	96	95.9460	1.3631	20
42	96	95.9460	1.363	20
43	97	97.0021	1.3627	20
44	97	97.0021	1.3628	20
45	97	97.0021	1.3626	20
46	97	97.0021	1.3626	20
47	97	97.0021	1.3627	20
48	97	97.0021	1.3626	20
49	98	98.0398	1.3627	20
50	98	98.0398	1.3625	20
51	98	98.0398	1.3623	20
52	98	98.0398	1.3622	20
53	98	98.0398	1.3625	20
54	98	98.0398	1.3622	20
55	99	98.9114	1.362	20
56	99	98.9114	1.3621	20
57	99	98.9114	1.3619	20
58	99	98.9114	1.3619	20
59	99	98.9114	1.362	20
60	99	98.9114	1.362	20
61	100	100.0000	1.3614	20
62	100	100.0000	1.3615	20
63	100	100.0000	1.3616	20
64	100	100.0000	1.3616	20
65	100	100.0000	1.3615	20
66	100	100.0000	1.3615	20

APPENDIX C

FABRICATION OF SILICON MICROSEPARATOR

This section describes the photolithography and etching techniques that were employed to fabricate the microseparators. Photolithography is the process of transferring a pattern from a photomask onto the surface of a silicon wafer or substrate. The procedure involved in fabricating the microseparator by photolithography is described below:

C.1 Emulsion Mask

The first step in the fabrication was to create a design of the microseparator to be fabricated. The microseparator design was created in AutoCAD 14. The drawing file was stored as a .dxf and then using LinkCAD software this file was converted to a postscript file. The postscript file was then viewed in Ghostview and evaluated for any changes in dimension during the conversion of the files. This file format was required due to the print settings specified by University of Illinois Urbana Chicago (UIUC), where the file was sent for printing. The mask obtained was printed on a transparency film using commercial image settings (5080 dpi) by a high resolution printer. The emulsion mask was printed negative down with the pattern light and the field dark.

C.2 Transfer of Emulsion Mask to Chrome Mask

The emulsion mask has limited life and is more susceptible for physical damage on the mask over repeated use. As such this emulsion mask was used to transfer the patterns to a chrome mask that overcomes these limitations of the emulsion mask.

The emulsion mask was initially placed on a clear glass plate of similar dimensions of that of typical chrome masks i.e. 4 x 4 ". A mark was made on the emulsion mask and then carefully the exact size of the chrome mask dimensions was cut out from the emulsion mask. The emulsion mask was then placed on contact with the

blank resist - coated chrome mask and ensuring that the printed side faces down against the mask. A clear glass mask was placed on the top of the resist-coated chrome mask and the emulsion film containing the pattern. The emulsion film and the chrome mask together were held closely to the plain glass so that that the design was transferred without distortion during exposure in the aligner. It was then exposed for 12 seconds from an UV lamp in the G-line range. The mask was developed in MF-319 developer for 30 seconds, washed with DI water and dried, followed by post bake at 150°C for 8 minutes. The pattern was finally inspected in the optical microscope. The testified mask was then immersed in the chrome etcher solution for 20 seconds and then washed with DI water and dried. After the inspection of the pattern it was then immersed in acetone for photoresist removal. Care was taken in this step as it was critical to immerse the mask in water immediately after it was taken out of acetone. The chrome mask was now ready to use. Two such chrome masks for the microseparator were generated one for the front side containing the channels and the other containing only the vias, i.e., the inlet and outlet ports for the microseparator.

C.3 Fabrication of Microseparator

The microchannels for the membrane separator were fabricated from silicon using standard lithographic processes. A <100> silicon wafer, four inches in diameter, double side polished, with a thickness of 500 μm and the oxide layer thickness of 1- 2 μm was used for the fabrication of microseparator. The wafer was cleaned by acetone, isopropanol and de-ionized water to remove any dust particles, organic and inorganic impurities present on its surface. The cleaned wafer was then blow dried by nitrogen. The dried wafer was placed on a hot plate at 250°C for a half hour to ensure that the wafer

was completely dry before photoresist was coated on to it. The wafer was then held on a vacuum chuck of the spinner (CEE Model- 100) for liquid priming by spin coating HMDS (hexamethydisiloxane) primer at 1500 rpm with 150 rpm/s for 40 seconds. The spinner had the spin controlled by PID (Proportional Integral Derivative) Microprocessor controlled to a maximum speed of 6000 rpm (+/- 5 RPM) with an acceleration of 30,000 RPM/s. This primer improved the adhesion of photoresist on to the wafer surface by removing any traces of water vapor adhered to it, consequently rendering it hydrophobic. A positive G-line photoresist Shipley 1813 was dispensed on to the center of the wafer. Two-thirds of the wafer was covered with photoresist surface and care was taken to maintain the wafer was free from dust particles after the photoresist was coated. The photoresist was coated according to the spin curve shown in Figure C.1 to obtain a thickness of 1-2 μm .

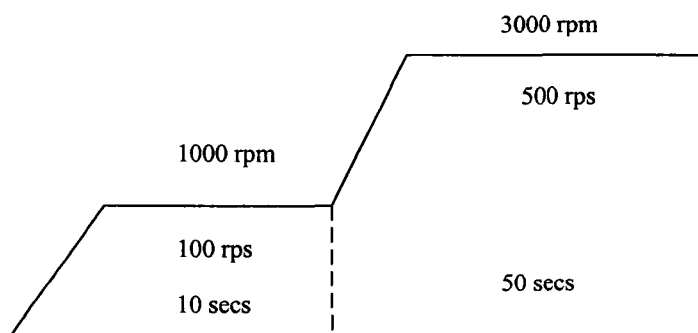


Figure C.1 Spin curve for Shipley 1813 photoresist.

The wafer was then subjected to soft baking during which the wafer was placed on a hot plate maintained at 115°C for a minute. This mild heat treatment ensured the removal of residual solvents and stress and also promoted the adhesion of the resist layers on to the wafer. The resist-coated wafer was then cooled down to room temperature. The

chrome mask previously described was now used to transfer the pattern on to the wafer. The wafer and chrome mask for the front side of the microseparator (Figure C.3.g) were placed in the mask aligner (Dual-side Mask Aligner-Electronic Vision) and were separated by a distance of 30 μm to prevent any damage that might occur to both the mask and the photoresist on contact. The mask was aligned such that the pattern to be transferred was on the center of the wafer. UV light in the g-line was exposed from a 7 W/cm^2 light source for 18 seconds.

The exposed wafer was then developed in MF 319 developer for around 30 seconds and the wafer was then washed under running water and dried using nitrogen. From experience, the actual developing time cannot be quoted but rather a decision on when to stop the development was made on visual judgment. The pattern was inspected under an optical microscope (Olympus Vanox AHM 73 Microscope) to evaluate any defects in the patterns transferred. Because the microseparator consisted of several microchannels, care was taken to ensure that all the channels were fully developed and free from any defects. If any defects were observed on the pattern the photoresist was removed and the entire sequence of steps described above were repeated. Once it was ensured that the patterns were free from defects, it was hard baked by placing the wafer on a hot plate maintained at 165°C for 1 minute. Hard baking improved selectivity during dry etching and promotes adhesion during wet etching. This baking step improved the hardness of the film, by removing residual developing solvents and annealed the film to promote interfacial adhesion of the resist weakened by developer penetration along the resist- substrate interface [107].

For wet etching, an etching bath was prepared in which a solution of hydrogen fluoride and ammonium fluoride was buffered in the ratio of 1: 6. Buffered oxide etch (BOE) was used to remove SiO_2 . BOE is a very selective etchant, meaning that it stops at the silicon and does not etch further. BOE removes the underlying sacrificial oxide layer from the microchannels on silicon wafers in addition to removing the unwanted silicon dioxide on the patterned silicon wafer. Buffered oxide etch was used instead of hydrofluoric acid etch due to the reason that the etch rate of hydrofluoric acid was very high and could not be easily controlled. The wafer was placed in the etchant with the oxide side up for one minute; it was then rinsed under running water and examined. A wafer free from oxide was rendered hydrophobic, and therefore water washes off the wafer. After rinsing the wafer from its etching solution, the wafer was dried with high pressure nitrogen. The wafer was then immersed in a bath containing acetone to remove the photoresist for 3 minutes. It was then rinsed with water and then dried quickly with nitrogen.

The wafer was then placed inside the chamber of ICP machine (Inductively Coupled Plasma Etch System -Alcatel A601 E) for deep dry etching into silicon substrate via Inductive Coupled Plasma (ICP). The ICP employs the Bosch process in which alternating amounts of SF_6 and C_4F_8 are fed to the reactor through RF plasma. In Bosch process for dry etching, the material removal reactions occur in the gas phase, a detailed description of this process can be obtained in Fundamentals of Microfabrication by Marc Madou [107]. The process conditions used are as shown in Table C.1.

Table C.1 Process parameters for Deep Reactive Ion Etching.

Process Parameters for DRIE (ICP-Bosch Process)		
Source Power	1800 W	1800 W
Pressure	20 %	20 %
Bias Power	50W	30W
SF ₆ Flow	300 sccm	300 sccm
SF ₆ Time	7 mins	7 mins
C ₄ F ₈ Flow	100 sccm	50 sccm
C ₄ F ₈ Time	2 mins	3 mins
Process Time	5 mins	90 mins
Depth	120 μm	Etched through wafer

Before ICP etching, the wafer on which the etching has to be achieved was glued with another wafer using photoresist; this was done to prevent any damage to the actual wafer being etched. During ICP a wafer was initially placed for conditioning at the required temperature and time. Then the wafer to be etched was placed and a suitable recipe was chosen depending on the depth required. The etching was stopped after one or two minutes and then the etch rate was determined by measuring the depth of the microchannels in the profilometer. The preliminary etching provided an estimate for the actual process time required for etching. The wafer was then examined for even color and also to ensure that the oxide area was clean. The silicon areas must be clear and gray color. The channels were etched with the ICP process to produce perpendicular walls and through vias for inlet and outlet.

The processing of the via patterns to the back side of the wafer are as explained below. The wafer was cleaned with acetone, isopropanol and water, dried with nitrogen. The backside of the wafer was prebaked at 115°C for 5 minutes. AZ 9260 a thick photoresist was used since this provided the required thickness to sustain during the through hole etching of the vias. This resist coated wafer was then soft baked at 110°C for 80 seconds. By using the spin curve shown in Figure C.2, a uniform coating of 10 μm was obtained. Using the same spin curve again an additional 10 μm of photoresist was coated and soft baked again at 110°C for 160 seconds. The edge bead of the photoresist on the wafer was removed by using EBR solvent. This removal prevented any potential damage that might occur due to attachment of the resist coated- wafer to the mask during alignment in the mask aligner.

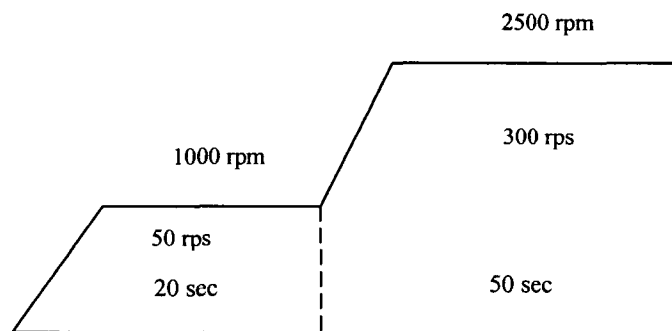


Figure C.2 Spin curve for AZ9260 photoresist.

The wafer and chrome mask for the back side of the microseparator were placed in the mask aligner and were separated by a distance of 150 μm . The mask was appropriately positioned with respect to the alignment mark on the front side of the wafer. UV light in the g-line was exposed from a 7 w/cm² light source for 135 seconds.

The exposed wafer was then developed AZ 400 K developer (1: 4:: AZ 400K :Water) and the wafer was then washed under running water for at least two minutes to strip any of the remaining thick photoresist, and it was then blow dried by nitrogen. The pattern was inspected under an optical microscope to evaluate for any defects in the vias of the microseparator. It was then hard baked at 125°C for 15 minutes. Table C.2 and Figure C.3 is a schematic representation of the photolithography process.

Table C.2 Description of sequence in photolithography for silicon microseparator.

a)	Double side oxide coated silicon wafer
b)	Silicon wafer coated with HMDS primer
c)	Silicon wafer coated with HMDS primer and photoresist
d)	Photoresist coated wafer containing microchannels exposed to UV light
e)	Development
f)	Oxide removal by BOE
g)	Dry Etch by DRIE of microchannels
h)	Photoresist coated wafer containing vias exposed to UV light
i)	Development
j)	Dry Etch by DRIE of vias (through hole etching)

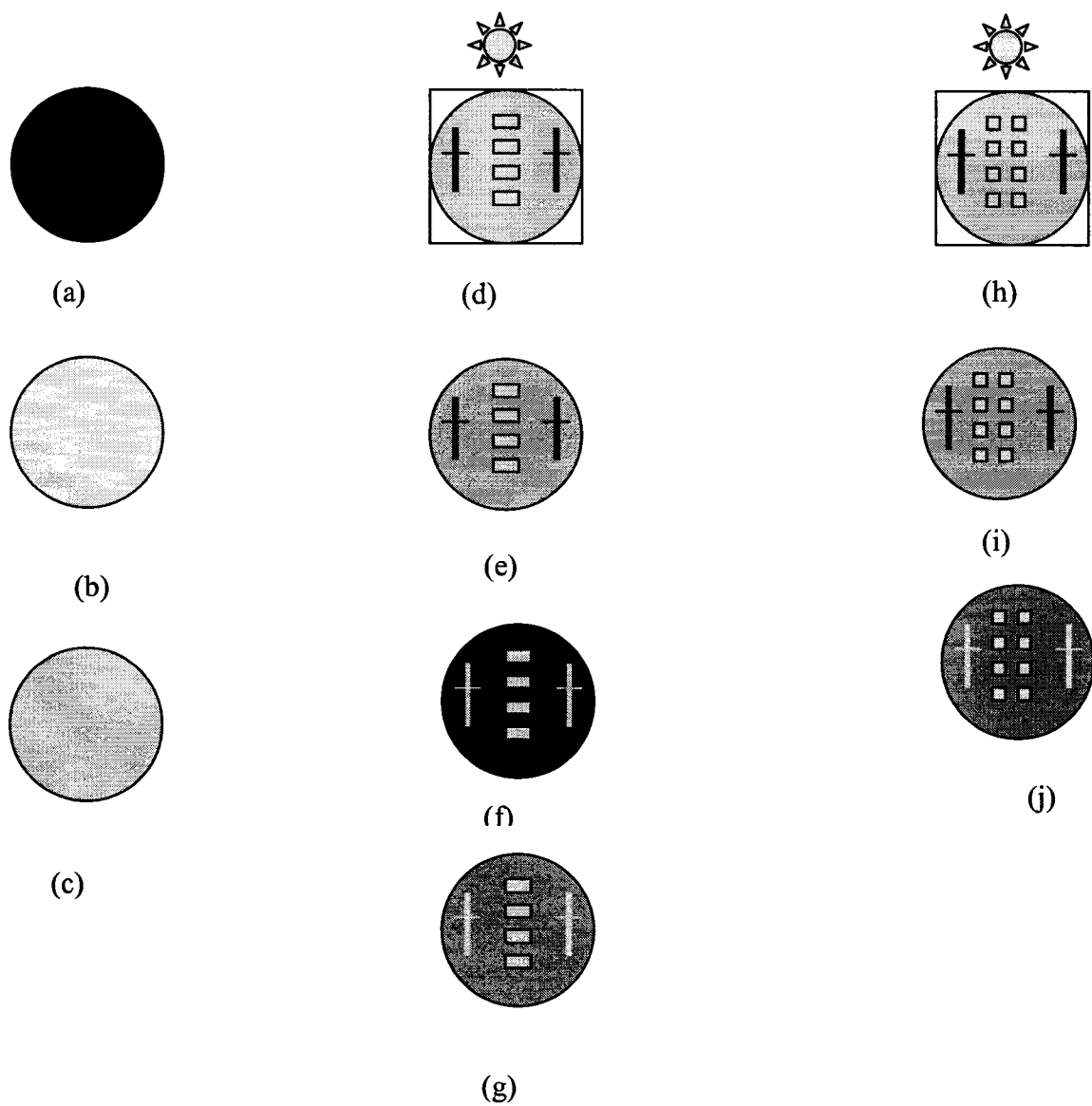


Figure C.3 Schematic of photolithography process for silicon microseparator.

APPENDIX D

EXPERIMENTAL DATA OF PERVAPORATION EXPERIMENTS WITH RETENTATE RECYCLE

All tables and figures in this section are from pervaporation experiments with retentate recycle. Tables exhibit the operating parameters and the recorded data during each experiment. Figures exhibit data from the balance and the temperature of the membrane module that was acquired during each experiment.

Table D.1 Experiment-152 Operating parameters for 22 μm deep channel, 47 milliseconds, 2/19/06 to 2/20/06.

	Date	Day	Time	
Start	2/19/06	Sun	9:15	
End	2/20/06	Mon	10:15	
Experiment #	152			
Experimental Time	25	hrs		
Depth of microchannel	22	μm	0.0022	cm
Length of microchannel	30000	μm	3	cm
Width of microchannel	60	μm	0.006	cm
Number of channels	99			
Volume of fluid in reactor	0.0039204	cm^3		
Residence Time	47.0448	millisec		
Average temperature in feed tank	23.2624917	$^{\circ}\text{C}$		
Membrane area	0.0003	m^2		
Membrane	2216			
Target Temperature	90	$^{\circ}\text{C}$		
Pump head	7016			
RPM	6.1			
Feed flow rate	5	ml/min		
Initial Feed ethanol	27.5	g		
Stabilization time	1.25	hrs		
Membrane History	Expt # used	Exptl	Flow	
Date of 1st use		Time	rate	
		hrs	ml/min	
	2/15/06	condition	26	5
	2/16/06	151	30	1
Permeate	2.9702	g		
Refractive Index	1.3447			

Table D.2 Experiment-152 Recorded data for 22 μm deep channel, 47 milliseconds, 2/19/06 to 2/20/06.

#	Date	Time hrs	Sampling Time	Temperature		R.H %	Pressure		Refractometer	
				Chiller	Internal		Upstream	vacuum	temp	nd
				$^{\circ}\text{C}$	$^{\circ}\text{C}$		psi	Torr	$^{\circ}\text{C}$	
	2/19	0	9:15	21	100.6	22	6 to 9	3	20	1.3643
1	2/19	4	13:19	21.2	100.59	22	7 to 9	3	20	1.3638
2	2/19	10	19:15	21.2	100.53	22	9 to 13	3	20	1.3634
3	2/20	15	0:15	21.2	100.6	24	9 to 13	3	20	1.3631
4	2/20	20	5:15	21.2	100.45	25	9 to 13	3	20	1.3627
5	2/20	25	10:15	21.2	100.34	26	10 to 14	3	20	1.3623

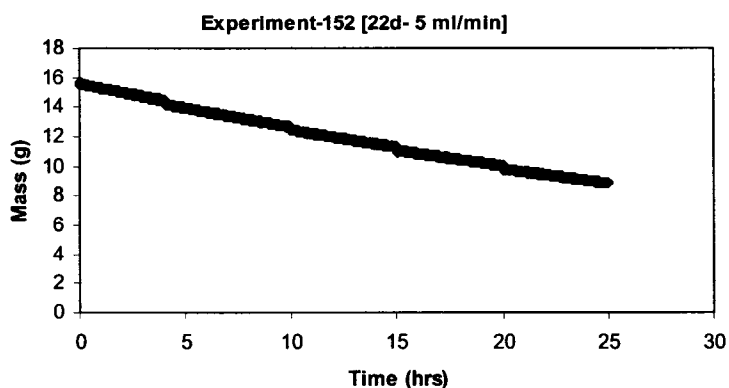


Figure D.1 Experiment - 152 Untreated mass data for 22 μm deep channel, 47 milliseconds, 2/19/06 to 2/20/06.

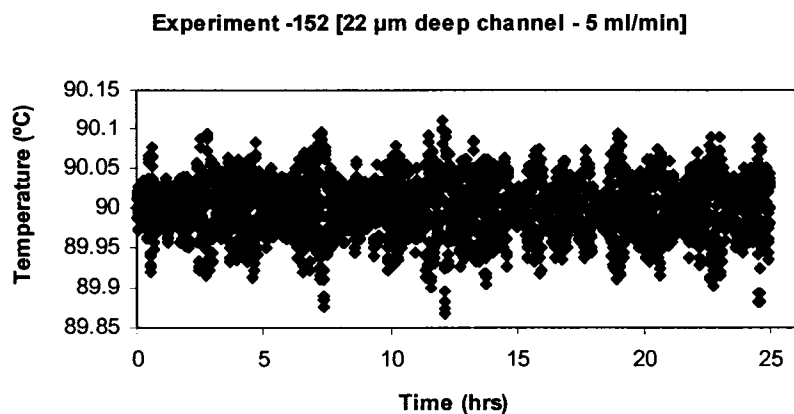


Figure D.2 Experiment - 152 Membrane module temperature profile for 22 μm deep channel, 47 milliseconds, 2/19/06 to 2/20/06.

Table D.3 Experiment - 153 Operating parameters for 22 μm deep channel, 117 milliseconds, 2/20/06 to 2/21/06.

	Date	Day	Time	
Start	2/20/06	Mon	12:45	
End	2/21/06	Tues	18:45	
Experiment #	153			
Experimental Time	30	hrs		
Depth of microchannel	22	μm	0.0022	cm
Length of microchannel	30000	μm	3	cm
Width of microchannel	60	μm	0.006	cm
Number of channels	99			
Volume of fluid in reactor	0.0039204	cm^3		
Residence Time	117.612	millisec		
Average temperature in feed tank	23.0283176	$^{\circ}\text{C}$		
Membrane area	0.0003	m^2		
Membrane	2216			
Target Temperature	90	$^{\circ}\text{C}$		
Pump head	7016			
RPM	2.5			
Feed flow rate	2	ml/min		
Initial Feed ethanol	27.5	g		
Stabilization time	1.25	hrs		
Membrane	Expt # used	Exptl	Flow	
Date of 1st use		Time	rate	
		hrs	ml/min	
	2/15/06	condition	26	5
	2/16/06	151	30	1
	2/19/06	152	25	5
Permeate	3.5182	g		
Refractive Index	1.3485			

Table D.4 Experiment - 153 Recorded data for 22 μm deep channel, 117 milliseconds, 2/20/06 to 2/21/06.

#	Date	Time hrs	Sampling Time	Temperature		R.H %	Pressure		Refractometer	
				Chiller $^{\circ}\text{C}$	Internal $^{\circ}\text{C}$		Upstream psi	Vacuum Torr	Temp $^{\circ}\text{C}$	nd
	2/20	0	12:45	21.2	99.6	26	3	3	20	1.3643
1	2/20	5.25	16:50	20.9	99.737	29	3	3	20	1.3639
2	2/20	11.25	22:45	20.9	99.754	30	3 to 4	3	20	1.3635
3	2/21	16.25	3:45	20.9	100.02	30	3 to 4	3	20	1.3631
4	2/21	21.25	8:53	20.9	99.87	30	3 to 4	3	20	1.3628
5	2/21	26.25	13:50	20.9	99.605	35	3 to 4	2.5	20	1.3626
6	2/21	31.25	18:45	20.7	99.227	37	3 to 4	2.2	20	1.3622

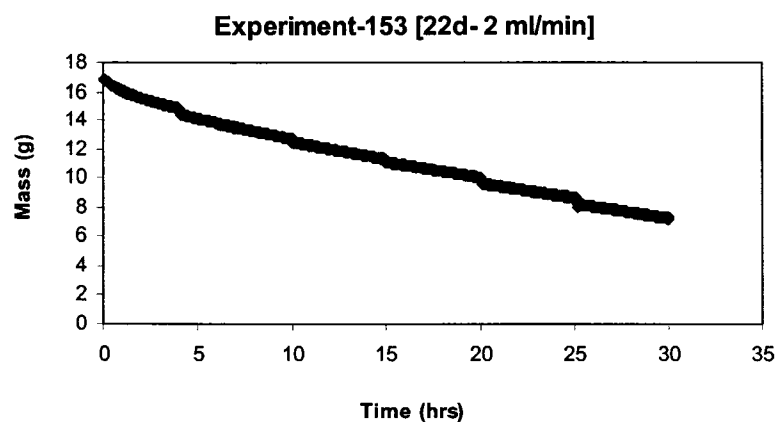


Figure D.3 Experiment - 153 Untreated mass data for 22 μm deep channel, 117 milliseconds, 2/20/06 to 2/21/06.

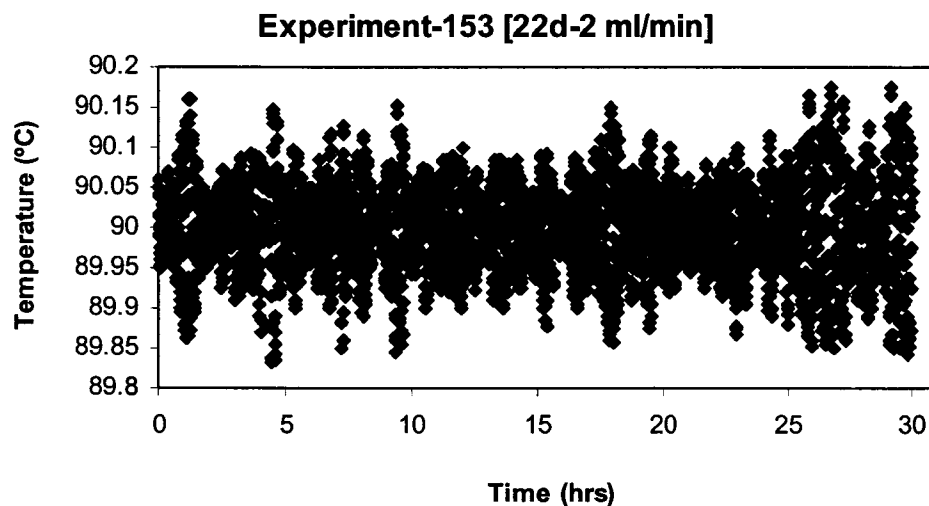


Figure D.4 Experiment - 153 Membrane module temperature profile for 22 μm deep channel, 117 milliseconds, 2/20/06 to 2/21/06.

Table D.5 Experiment - 156 Operating parameters 22 μm deep channel, 23 milliseconds, 2/23/06 to 2/24/06.

	Date	Day	Time	
Start	2/23/06	Thurs	1:00	
End	2/24/06	Fri	7:00	
Experiment #	156			
Experimental Time	30	hrs		
Depth of microchannel	22	μm	0.0022	cm
Length of microchannel	30000	μm	3	cm
Width of microchannel	60	μm	0.006	cm
Number of channels	99			
Volume of fluid in reactor	0.0039204	cm^3		
Residence Time	23.5224	millisec		
Average temperature in feed tank	23.0416435	$^{\circ}\text{C}$		
Membrane area	0.0003	m^2		
Membrane	2216			
Target Temperature	90	$^{\circ}\text{C}$		
Pump head	7016			
RPM	12.1			
Feed flow rate	10	ml/min		
Initial Feed ethanol	27.5	g		
Stabilization time	1.5	hrs		
Membrane History	Expt # used	Exptl	Flow	
Date of 1st use		Time	rate	
		hrs	ml/min	
	2/15/06	condition	26	5
	2/16/06	151	30	1
	2/19/06	152	25	5
	2/20/06	153	30	2
	2/21/06	154	1	25
	2/21/06	154	6	25
	2/22/06	155	9	25
Permeate	3.612	g		
Refractive Index	1.3425			

Table D.6 Experiment - 156 Recorded data for 22 μm deep channel, 23 milliseconds, 2/23/06 to 2/24/06.

#	Date	Time hrs	Sampling Time	Temperature		R.H %	Pressure		Refractometer	
				Chiller	Internal		Upstream	Vacuum	Temp	nd
				$^{\circ}\text{C}$	$^{\circ}\text{C}$		psi	Torr	$^{\circ}\text{C}$	
	2/23	0	1:00	20.3	100.18	39	11 to 20	3	20	1.3643
1	2/23	6.5	5:59	20.3	100.22	36	11 to 24	3	20	1.3638
2	2/23	11.5	10:59	20.3	99.684	35	11 to 24	3	20	1.3634
3	2/23	16.5	15:59	19.9	99.438	31	11 to 24	2	20	1.3631
4	2/23	21.5	20:59	19.9	99.439	30	11 to 24	2	20	1.3628
5	2/24	26.5	1:59	19.9	99.664	30	11 to 24	2	20	1.3626
6	2/24	31.5	6:59	19.9	100.35	30	11 to 24	2	20	1.3622

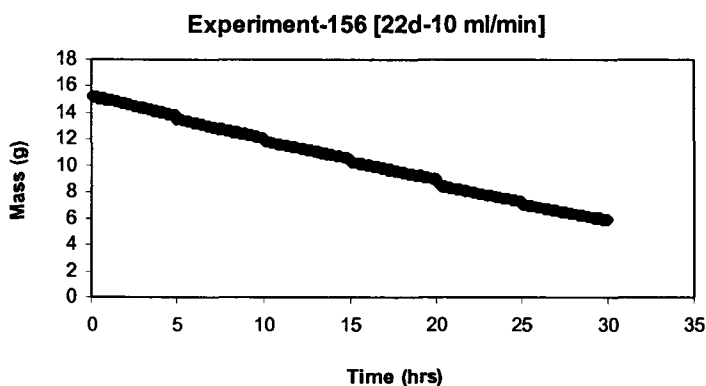


Figure D.5 Experiment - 156 Untreated mass data for 22 μm deep channel, 23 milliseconds, 2/23/06 to 2/24/06.

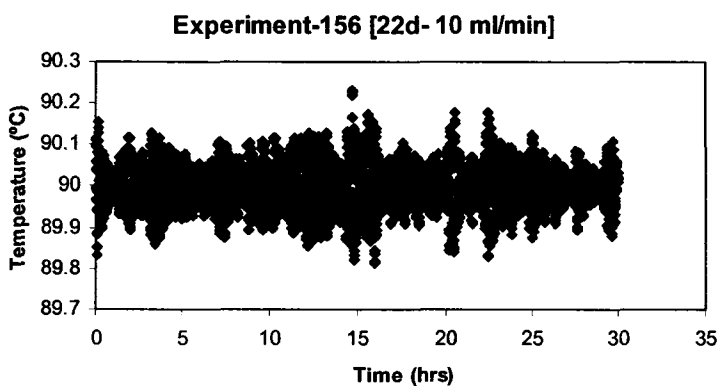


Figure D.6 Experiment - 156 Membrane module temperature profile for 22 μm deep channel, 23 milliseconds, 2/23/06 to 2/24/06.

Table D.7 Experiment - 157 Operating parameters for 22 μm deep channel, 235 milliseconds, 2/24/06 to 2/25/06.

	Date	Day	Time
Start	2/24/06	Fri	10:00
End	2/25/06	Sat	22:00
Experiment #	157		
Experimental Time	36	hrs	
Depth of microchannel	22	μm	
Length of microchannel	30000	μm	
Width of microchannel	60	μm	
Number of channels	99		
Volume of fluid in reactor	0.0039204	cm^3	
Residence Time	235.224	millisec	
average temperature in feed tank	23.0101805	$^{\circ}\text{C}$	
Membrane area	0.0003	m^2	
Membrane	2216		
Target Temperature	90	$^{\circ}\text{C}$	
Pump head	7016		
RPM	1.6		
Feed flow rate	1	ml/min	
Initial Feed ethanol	27.5	g	
Stabilization time	75	mins	
Membrane history	Expt # used	Exptl	Flow
Date of 1st use		Time	rate
		hrs	ml/min
	2/15/06	condition	26 5
	2/16/06	151	30 1
	2/19/06	152	25 5
	2/20/06	153	30 2
	2/21/06	154	1 25
	2/21/06	154	6 25
	2/22/06	155	9 25
	2/23/06	156	30 10
Permeate	3.8614	g	
Refractive Index	1.347		

Table D.8 Experiment - 157 Recorded data for 22 μm deep channel, 235 milliseconds, 2/24/06 to 2/25/06.

#	Date	Time hrs	Sampling Time	Temperature		R.H %	Pressure		Refractometer	
				Chiller	Internal		Upstream	Vacuum	Temp	nd
				$^{\circ}\text{C}$	$^{\circ}\text{C}$		psi	Torr	$^{\circ}\text{C}$	
	2/24	0	10:00	19.9	98.762	30	2.5	3	20	1.3643
1	2/24	5	15:00	19.9	98.39	30	2.5	3	20	1.3639
2	2/24	10	20:00	19.9	98.652	30	2.5	3	20	1.3636
3	2/25	15	1:00	19.9	98.743	34	2.5	3	20	1.3633
4	2/25	20	6:00	19.9	99.011	39	2.5	3	20	1.363
5	2/25	25	11:00	19.9	99.101	41	2.5	3	20	1.3627
6	2/25	31	17:00	19.9	98.795	41	2.5	3	20	1.3625
7	2/25	36	22:00	19.9	98.885	41	2.5	3	20	1.3623

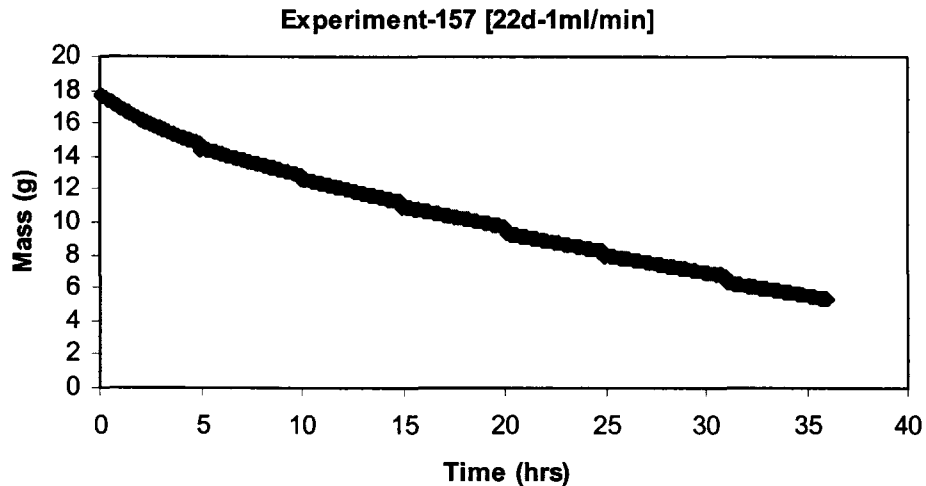


Figure D.7 Experiment - 157 Untreated mass data for 22 μm deep channel, 235 milliseconds, 2/24/06 to 2/25/06.

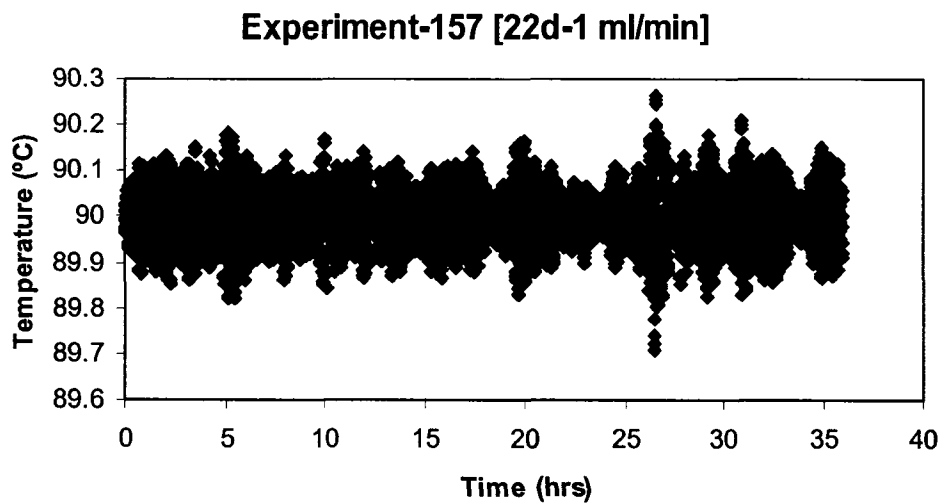


Figure D.8 Experiment - 157 Membrane module temperature profile for 22 μm deep channel, 235 milliseconds, 2/24/06 to 2/25/06.

Table D.9 Experiment - 158 Operating parameters for 22 μm deep channel, 23 milliseconds, 2/26/06 to 2/27/06.

	Date	Day	Time	
Start	2/26/06	Sun	1:00	
End	2/27/06	Mon	13:00	
Experiment #	158			
Experimental Time	36	hrs		
Depth of microchannel	22	μm	0.0022	cm
Length of microchannel	30000	μm	3	cm
Width of microchannel	60	μm	0.006	cm
Number of channels	99			
Volume of fluid in reactor	0.0039204	cm^3		
Residence Time	23.5224	millisec		
Average temperature in feed tank	23.1079467	$^{\circ}\text{C}$		
Membrane area	0.0003	m^2		
Membrane	2216			
Target Temperature	90	$^{\circ}\text{C}$		
Pump head	7016			
RPM	12.1			
Feed flow rate	10	ml/min		
Initial Feed ethanol	27.5	g		
Stabilization time	75	mins		
Membrane	Expt # used	Exptl	Flow	
Date of 1st use		Time	rate	
		hrs	ml/min	
	2/15/06	condition	26	5
	2/16/06	151	30	1
	2/19/06	152	25	5
	2/20/06	153	30	2
	2/21/06	154	1	25
	2/21/06	154	6	25
	2/22/06	155	9	25
	2/23/06	156	30	10
	2/24/06	157	36	1
Permeate	3.677	g		
Refractive Index	1.3434			

Table D.10 Experiment - 158 Recorded data for 22 μm deep channel, 23 milliseconds, 2/26/06 to 2/27/06.

#	Date	Time hrs	Sampling Time	Temperature		R.H %	Pressure		Refractometer	
				Chiller $^{\circ}\text{C}$	Internal $^{\circ}\text{C}$		Upstream psi	Vacuum Torr	Temp $^{\circ}\text{C}$	nd
	2/26	0	1:00	19.9	99.898	35	11 to 25	3	20	1.3644
1	2/26	6.8333	6:30	20.8	99.964	30	11 to 25	3	20	1.3637
2	2/26	11.333	11:00	20.8	100.04	30	11 to 25	3	20	1.3634
3	2/26	16.333	16:00	20.2	99.754	27	11 to 25	2.5	20	1.3632
4	2/26	21.333	21:00	20.2	99.645	27	11 to 25	2.5	20	1.363
5	2/27	26.333	2:00	20.2	99.877	27	11 to 25	2.8	20	1.3628
6	2/27	31.333	7:00	20.5	99.877	27	11 to 25	2.8	20	1.3625
7	2/27	37.333	13:00	20.5	99.688	30	12 to 25	3.8	20	1.362

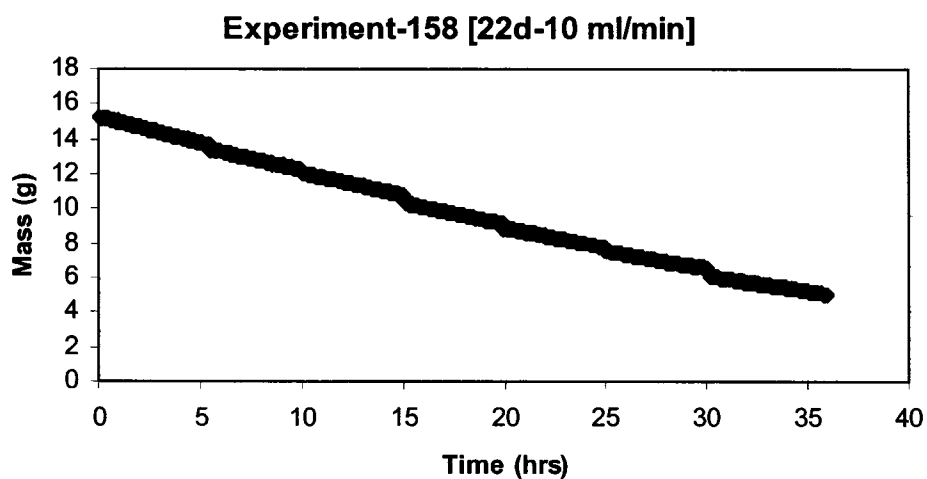


Figure D.9 Experiment - 158 Untreated mass data for 22 μm deep channel, 23 milliseconds, 2/26/06 to 2/27/06.

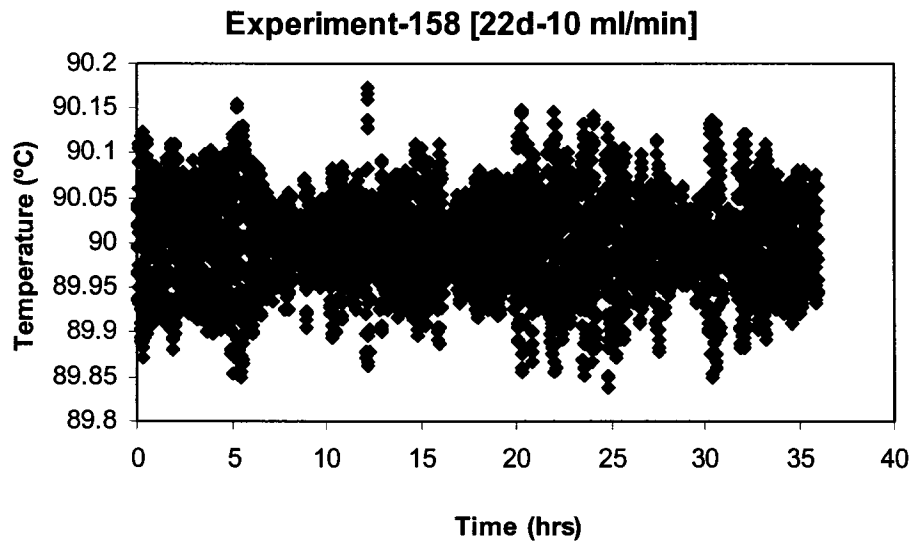


Figure D.10 Experiment - 158 Membrane module temperature profile for 22 μm deep channel, 23 milliseconds, 2/26/06 to 2/27/06.

Table D.11 Experiment - 176 Operating parameters for 22 μm deep channel, 23 milliseconds, 3/29/06 to 3/30/06.

	Date	Day	Time	
Start	3/29/06	Wed	14:45	
End	3/30/06	Thurs	14:45	
Experiment #	176			
Experimental Time	24	hrs		
Depth of microchannel	22	μm	0.0022	cm
Length of microchannel	30000	μm	3	cm
Width of microchannel	60	μm	0.006	cm
Number of channels	99			
Volume of fluid in reactor	0.0039204	cm^3		
Residence Time	23.5224	millisec		
Average temperature in feed tank	21.9395833	$^{\circ}\text{C}$		
Membrane area	0.0003	m^2		
Membrane	2216			
Target Temperature	90	$^{\circ}\text{C}$		
Pump head	7016			
RPM	12.1			
Feed flow rate	10	ml/min		
Initial Feed Ethanol	27.5	g		
Stabilization time	2	hrs		
Membrane History	Expt # used	Exptl	Flow	
Date of 1st use		Time	rate	
		hrs	ml/min	
	3/28/06	condition	15	5 rpm

Table D.12 Experiment - 176 Recorded data for 22 μm deep channel, 23 milliseconds, 3/29/06 to 3/30/06.

#	Date	Time	Sampling	Temperature		R.H	Pressure		Refractometer	
				Chiller	Internal		Upstream	Vacuum	Temp	nd
		hrs	Time	$^{\circ}\text{C}$	$^{\circ}\text{C}$	%	psi	Torr	$^{\circ}\text{C}$	
	3/29	0		19.8	100.24	41	9 to 11	3	20	1.3644
1	3/29	6	18:45	19.3	99.927	42	9 to 11	3	20	1.3637
2	3/29	10	22:45	19.3	100.12	42	9 to 11	3	20	1.3634
3	3/30	14	2:45	19.3	100.21	42	9 to 11	3	20	1.3631
4	3/30	20	8:45	19.3	100.14	42	9 to 11	3	20	1.3627
5	3/30	26	14:45	19.3	99.727	42	9 to 11	3	20	1.3622

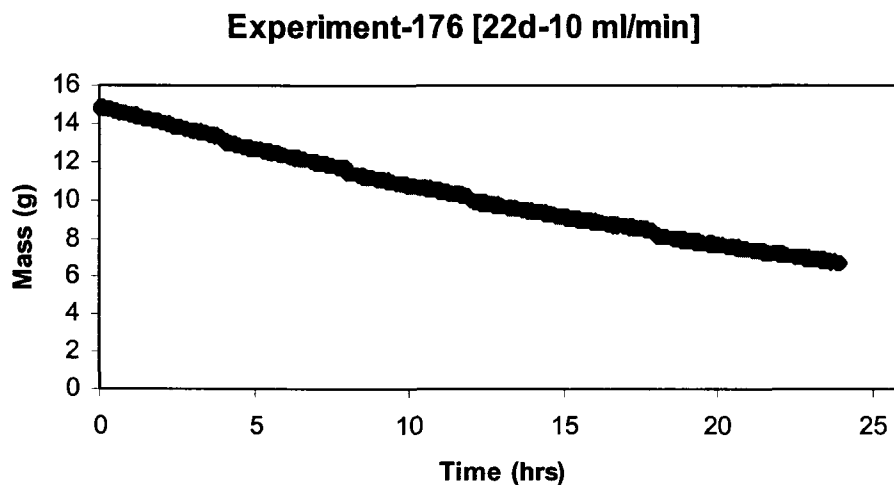


Figure D.11 Experiment - 176 Untreated mass data for 22 μm deep channel, 23 milliseconds, 3/29/06 to 3/30/06.

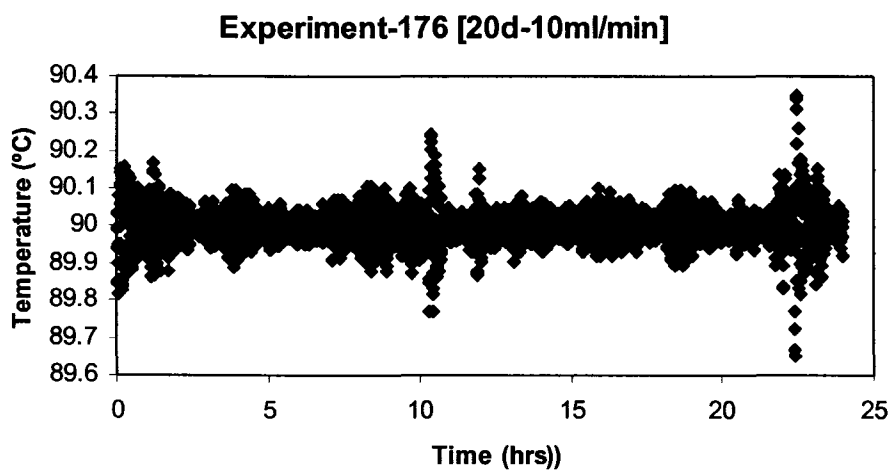


Figure D.12 Experiment - 176 Membrane module temperature profile for 22 μm deep channel, 23 milliseconds, 3/29/06 to 3/30/06.

Table D.13 Experiment -177 Operating parameters for 22 μm deep channel, 235 milliseconds, 3/30/06 to 3/31/06.

	Date	Day	Time	
Start	3/30/06	Thurs	18:30	
End	3/31/06	Fri	18:30	
Experiment #	177			
Experimental Time	24	hrs		
Depth of microchannel	22	μm	0.0022	cm
Length of microchannel	30000	μm	3	cm
Width of microchannel	60	μm	0.006	cm
Number of channels	99			
Volume of fluid in reactor	0.0039204	cm^3		
Residence Time	235.224	millisec		
Average temperature in feed tank	23.1236111	$^{\circ}\text{C}$		
Membrane area	0.0003	m^2		
Membrane	2216			
Target Temperature	90	$^{\circ}\text{C}$		
Pump head	7016			
RPM	1.6			
Feed flow rate	1	ml/min		
Feed ethanol	27.5	g		
Stabilization time	1.25	hrs		
Membrane History	Expt # used	Exptl	Flow	
Date of 1st use		Time	rate	
		hrs	ml/min	
	3/28/06	condition	15	
	3/29/06	176	24+1	10

Table D.14 Experiment -177 Recorded data for 22 μm deep channel, 235 milliseconds, 3/30/06 to 3/31/06.

#	Date	Time hrs	Sampling Time	Temperature		R.H %	Pressure		Refractometer	
				Chiller $^{\circ}\text{C}$	Internal $^{\circ}\text{C}$		Upstream psi	Vacuum Torr	Temp $^{\circ}\text{C}$	nd
										1.3644
	3/30	0		19.3	98.585	42	2	3	20	1.3643
1	3/30	5.25	22:30	19.3	99.039	42	2	3	20	1.3638
2	3/31	9.25	2:36	19.3		42	2	3	20	1.3635
3	3/31	13.25	6:30	19.3	98.918	46	2	3	20	1.3632
4	3/31	17.25	10:30	19.3	98.701	47	2	3	20	1.3629
5	3/31	21.25	14:30	19.3	98.271	47	2	3	20	1.3625
6	3/31	25.25	18:30	19.3	98.475	47	2	3	20	1.3623

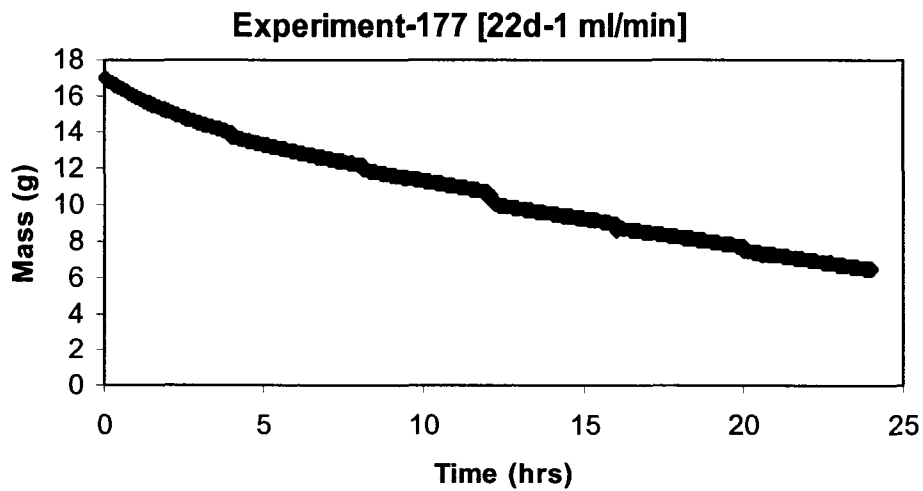


Figure D.13 Experiment - 177 Untreated mass data for 22 μm deep channel, 235 milliseconds, 3/30/06 to 3/31/06.

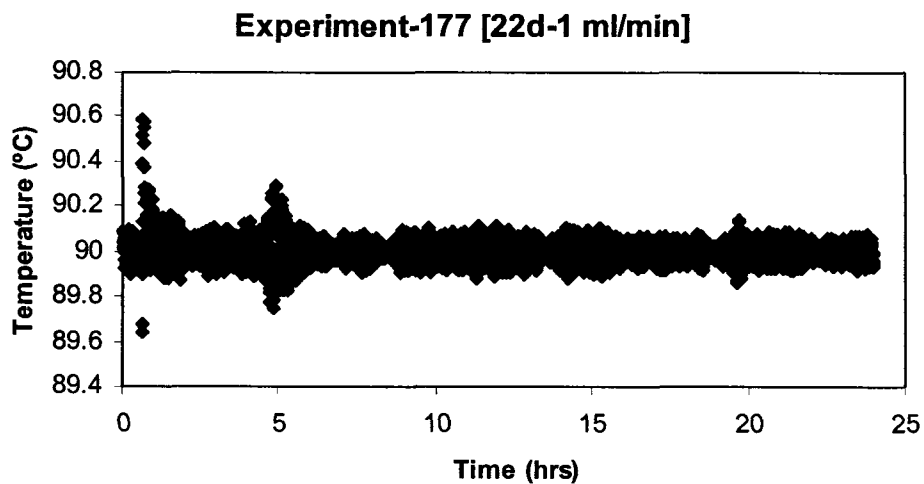


Figure D.14 Experiment - 177 Membrane module temperature profile for 22 μm deep channel, 235 milliseconds, 3/30/06 to 3/31/06.

Table D.15 Experiment - 180 Operating parameters for 22 μm deep channel, 47 milliseconds, 4/3/06 to 4/4/06.

	Date	Day	Time	
Start	4/3/06	Mon	20:45	
End	4/4/06	Tues	16:45	
Experiment #	180			
Experimental Time	20	hrs		
Depth of microchannel	22	μm	0.0022	cm
Length of microchannel	30000	μm	3	cm
Width of microchannel	60	μm	0.006	cm
Number of channels	99			
Volume of fluid in reactor	0.0039204	cm^3		
Residence Time	47.0448	millisec		
Average temperature in feed tank	22.9108333	$^{\circ}\text{C}$		
Membrane area	0.0003	m^2		
Membrane	2216			
Target Temperature	90	$^{\circ}\text{C}$		
Pump head	7016			
RPM	6.1			
Feed flow rate	5	ml/min		
Feed ethanol	27.5			
Stabilization time	1.08333333	hrs		
Membrane History	Expt # used	Exptl	Flow	
Date of 1st use		Time	rate	
		hrs	ml/min	
	3/28/06	condition	15	
	3/29/06	176	24+1	10
	3/30/06	177	24	1
	3/31/06	178	35	5
	4/2/06	179	30	5

Table D.16 Experiment -180 Recorded data for 22 μm deep channel, 47 milliseconds, 4/3/06 to 4/4/06.

#	Date	Time	Sampling	Temperature		R.H	Pressure		Refractometer	
				Chiller	Internal		Upstream	Vacuum	Temp	nd
		hrs	Time	$^{\circ}\text{C}$	$^{\circ}\text{C}$	%	psi	Torr	$^{\circ}\text{C}$	
	4/3	0		19	99.656	30	5	3	20	1.3645
1	4/3	5.0833	0:45	19	99.877	30	5	3	20	1.3638
2	4/4	9.0833	4:45	19	100.1	31	5	3	20	1.3634
3	4/4	13.333	9:00	19.5	100.29	31	5	3	20	1.3629
4	4/4	17.083	12:45	19.5	89.958	31	5	3	20	1.3626
5	4/4	21.083	16:45	19.5	89.985	31	5	3	20	1.3622

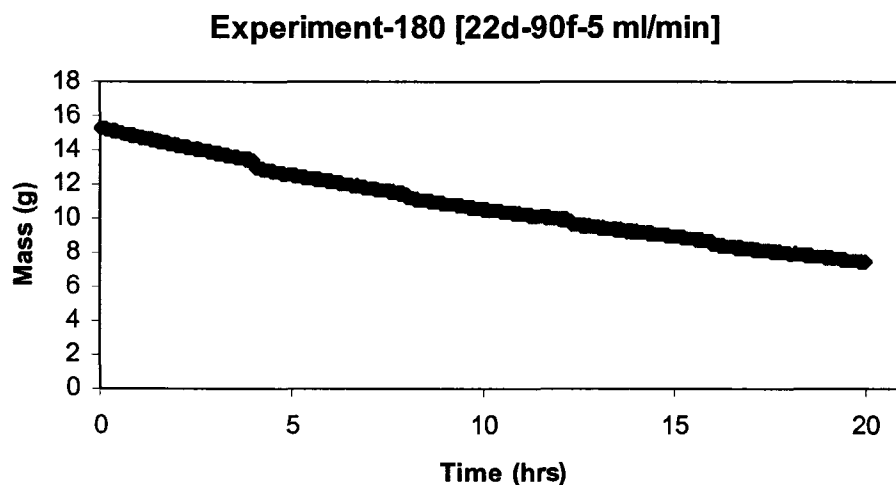


Figure D.15 Experiment - 180 Untreated mass data for 22 μm deep channel, 47 milliseconds, 4/3/06 to 4/4/06.

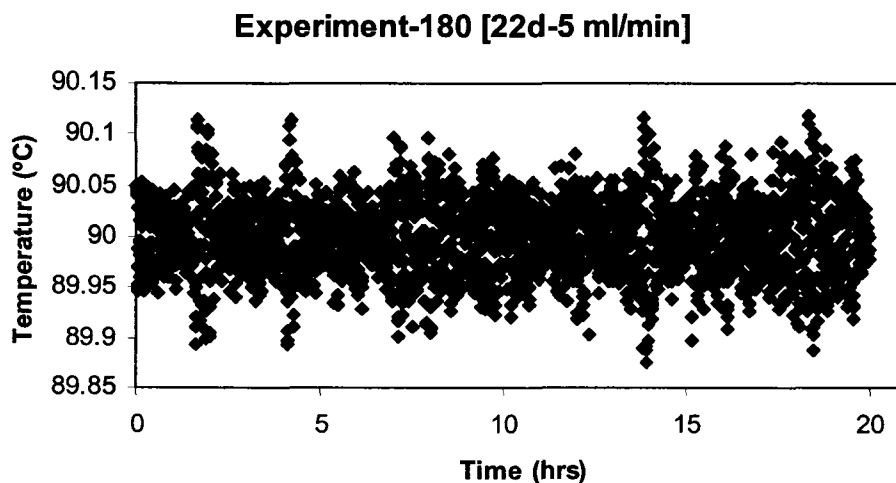


Figure D.16 Experiment - 180 Membrane module temperature profile for 22 μm deep channel, 47 milliseconds, 4/3/06 to 4/4/06.

Table D.17 Experiment - 181 Operating parameters for 22 μm deep channel, 47 milliseconds, 4/4/06 to 4/6/06.

	Date	Day	Time	
Start	4/4/06	Tues	20:00	
End	4/6/06	Thurs	8:00	
Experiment #	181			
Experimental Time	36	hrs		
Depth of microchannel	22	μm	0.0022	cm
Length of microchannel	30000	μm	3	cm
Width of microchannel	60	μm	0.006	cm
Number of channels	99			
Volume of fluid in reactor	0.0039204	cm^3		
Residence Time	47.0448	millisec		
Average temperature in feed tank	22.9717723	$^{\circ}\text{C}$		
Membrane area	0.0003	m^2		
Membrane	2216			
Target Temperature	90	$^{\circ}\text{C}$		
Pump head	7016			
RPM	6.1			
Feed flow rate	5	ml/min		
Initial Feed ethanol	27.5	g		
Stabilization time	1.5	hrs		
Membrane	Expt # used	Exptl	Flow	
Date of 1st use		Time	rate	
		hrs	ml/min	
	3/28/06	condition	15	
	3/29/06	176	24+1	10
	3/30/06	177	24	1
	3/31/06	178	35	5
	4/2/06	179	30	5
	4/3/06	180	20	5

Table D.18 Experiment - 181 Recorded data for 22 μm deep channel, 47 milliseconds, 4/4/06 to 4/6/06.

#	Date	Time	Sampling	Temperature		R.H	Pressure		Refractometer	
				Chiller	Internal		Upstream	Vacuum	Temp	nd
		hrs	Time	$^{\circ}\text{C}$	$^{\circ}\text{C}$	%	psi	Torr	$^{\circ}\text{C}$	
	4/4	0		19.3	77.189	31	4 to 5	3	20	1.3644
1	4/5	7.5	2:00	19.3	77.558	31	4 to 5	3	20	1.3642
2	4/5	16.5	11:00	19.7	77.607	32	4 to 6	3	20	1.3639
3	4/5	22.5	17:00	19.3	77.096	40	4 to 6	3	20	1.3637
4	4/6	29.5	0:00	19.3	77.057	42	4 to 6	3	20	1.3635
5	4/6	37.5	8:00	19.4	77.21	44	5 to 8	3	20	1.3632

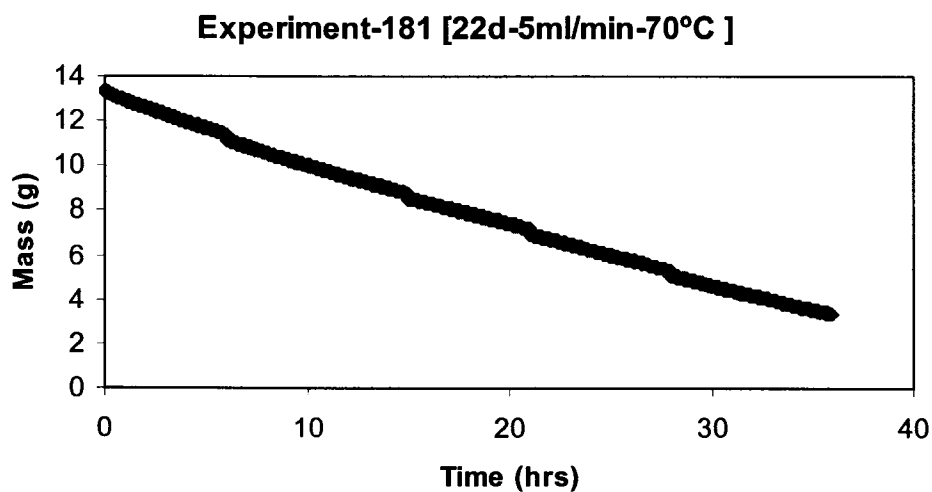


Figure D.17 Experiment - 181 Untreated mass data for 22 μm deep channel, 47 milliseconds, 4/4/06 to 4/6/06.

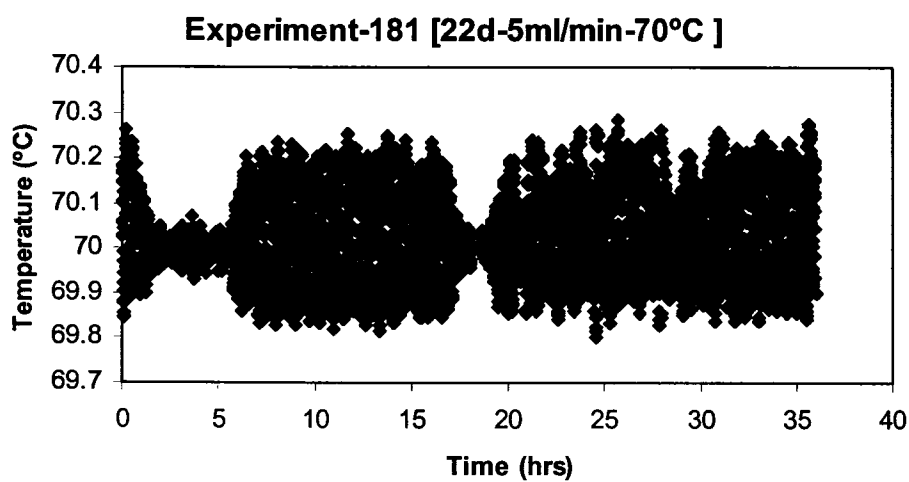


Figure D.18 Experiment - 181 Membrane module temperature profile for 22 μm deep channel, 47 milliseconds, 4/4/06 to 4/6/06.

Table D.19 Experiment - 182 Operating parameters for 22 μm deep channel, 47 milliseconds, 4/6/06 to 4/7/06.

	Date	Day	Time	
Start	4/6/06	Thurs	11:00	
End	4/7/06	Fri	19:00	
Experiment #	182			
Experimental Time	32	hrs		
Depth of microchannel	22	μm	0.0022	cm
Length of microchannel	30000	μm	3	cm
Width of microchannel	60	μm	0.006	cm
Number of channels	99			
Volume of fluid in reactor	0.0039204	cm^3		
Residence Time	47.0448	millisec		
Membrane area	0.0003	m^2		
Membrane	2216			
Target Temperature	90	$^{\circ}\text{C}$		
Pump head	7016			
RPM	6.1			
Feed flow rate	5	ml/min		
Feed ethanol	27.5			
Stabilization time	1.16666667	hrs		
Membrane	Expt # used	Exptl	Flow	
Date of 1st use		Time	rate	
		hrs	ml/min	
	3/28/06	condition	15	
	3/29/06	176	24+1	10
	3/30/06	177	24	1
	3/31/06	178	35	5
	4/2/06	179	30	5
	4/3/06	180	20	5
	4/4/06	181	36	5

Table D.20 Experiment - 182 Recorded data for 22 μm deep channel, 47 milliseconds, 4/6/06 to 4/7/06.

#	Date	Time	Sampling	Temperature		R.H	Pressure		Refractometer	
				Chiller	Internal		Upstream	Vacuum	Temp	nd
		hrs	Time	$^{\circ}\text{C}$	$^{\circ}\text{C}$	%	psi	Torr	$^{\circ}\text{C}$	
	4/6	0		19.4	88,506	44	5	3	20	1.3643
1	4/6	6.1667	16:00	19.3	88,027	44	5	3	20	1.3639
2	4/6	13.167	23:00	19.3	88,126	44	5	3	20	1.3636
3	4/7	21.167	7:00	19.3	88,425	47	5	3	20	1.3631
4	4/7	29.167	15:00	19.3	88,171	41	5	3	20	1.3626
5	4/7	33.167	19:00						20	1.3625

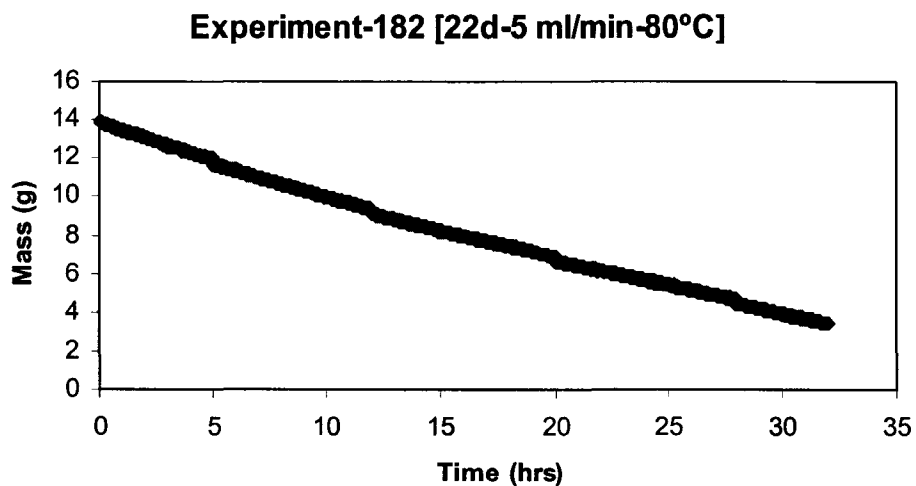


Figure D.19 Experiment - 182 Untreated mass data for 22 μm deep channel, 47 milliseconds, 4/6/06 to 4/7/06.

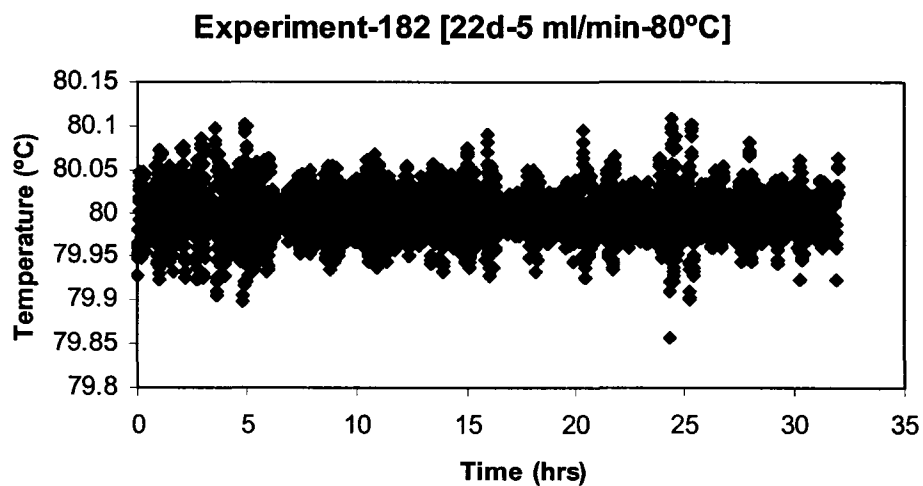


Figure D.20 Experiment - 182 Membrane module temperature profile for 22 μm deep channel, 47 milliseconds, 4/6/06 to 4/7/06.

Table D.21 Experiment - 183 Operating parameters for 22 μm deep channel, 47 milliseconds, 4/7/06 to 4/8/06.

	Date	Day	Time	
Start	4/7/06	Fri	22:00	
End	4/8/06	Sat	22:00	
Experiment #	183			
Experimental Time	24	hrs		
Depth of microchannel	22	μm	0.0022	cm
Length of microchannel	30000	μm	3	cm
Width of microchannel	60	μm	0.006	cm
Number of channels	99			
Volume of fluid in reactor	0.0039204	cm^3		
Residence Time	47.0448	millisec		
Average temperature in feed tank	22.9465649	$^{\circ}\text{C}$		
Membrane area	0.0003	m^2		
Membrane	2216			
Target Temperature	90	$^{\circ}\text{C}$		
Pump head	7016			
RPM	6.1			
Feed flow rate	5	ml/min		
Initial Feed ethanol	27.5	g		
Stabilization time	1.4	hrs		
Membrane History	Expt # used	Exptl	Flow	
Date of 1st use		Time	rate	
		hrs	ml/min	
	3/28/06	condition	15	
	3/29/06	176	24+1	10
	3/30/06	177	24	1
	3/31/06	178	35	5
	4/2/06	179	30	5
	4/3/06	180	20	5
	4/4/06	181	36	5
	4/6/06	182	32	5

Table D.22 Experiment - 183 Recorded data for 22 μm deep channel, 47 milliseconds, 4/7/06 to 4/8/06.

#	Date	Time hrs	Sampling Time	Temperature		R.H %	Pressure		Refractometer	
				Chiller	Internal		Upstream	Vacuum	Temp	nd
				$^{\circ}\text{C}$	$^{\circ}\text{C}$		psi	Torr	$^{\circ}\text{C}$	
	4/7	0		19.2		47	9	2	20	1.3643
1	4/8	6.4	3:00	19.6	100.119	35	7 to 11	2	20	1.3637
2	4/8	11.4	8:00	19.6		34	7 to 11	2	20	1.3632
3	4/8	16.4	13:00	19.6	100.248	37	7 to 11	2	20	1.3629
4	4/8	21.4	18:00	19.6	99.997	35	7 to 11	2	20	1.3625
5	4/8	25.4	22:00	19.6	100.76	33	7 to 11	2	20	1.3623

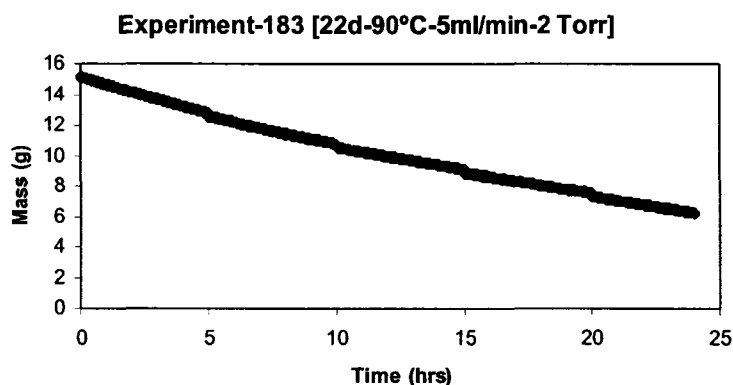


Figure D.21 Experiment - 183 Untreated mass data for 22 μm deep channel, 47 milliseconds, 4/7/06 to 4/8/06.

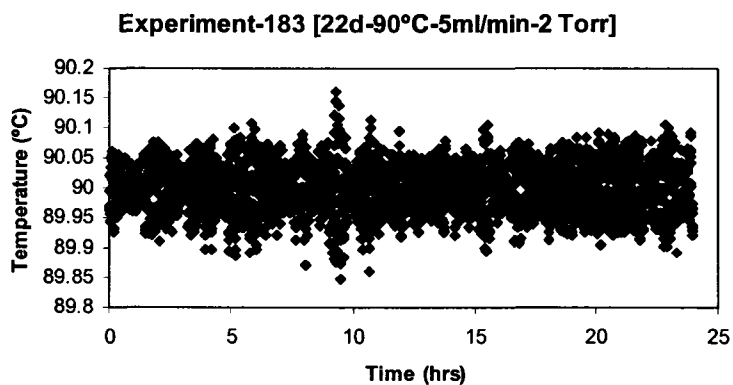


Figure D.22 Experiment - 183 Membrane module temperature profile for 22 μm deep channel, 47 milliseconds, 4/7/06 to 4/8/06.

Table D.23 Experiment - 184 Operating parameters for 22 μm deep channel, 47 milliseconds, 4/9/06 to 4/10/06.

	Date	Day	Time	
Start	4/9/06	Sun	1:00	
End	4/10/06	Mon	1:00	
Experiment #	184			
Experimental Time	24	hrs		
Depth of microchannel	22	μm	0.0022	cm
Length of microchannel	30000	μm	3	cm
Width of microchannel	60	μm	0.006	cm
Number of channels	99			
Volume of fluid in reactor	0.0039204	cm^3		
Residence Time	47.0448	millisec		
Average temperature in feed tank	23.0395833	$^{\circ}\text{C}$		
Membrane area	0.0003	m^2		
Membrane	2216			
Target Temperature	90	$^{\circ}\text{C}$		
Pump head	7016			
RPM	6.1			
Feed flow rate	5	ml/min		
Initial Feed ethanol	27.5	g		
Stabilization time	1.5	hrs		
Membrane History	Expt # used	Exptl	Flow	
Date of 1st use		Time	rate	
		hrs	ml/min	
	3/28/06	condition	15	
	3/29/06	176	24+1	10
	3/30/06	177	24	1
	3/31/06	178	35	5
	4/2/06	179	30	5
	4/3/06	180	20	5
	4/4/06	181	36	5
	4/6/06	182	32	5
	4/7/06	183	24	5

Table D.24 Experiment - 184 Recorded data for 22 μm deep channel, 47 milliseconds, 4/9/06 to 4/10/06.

#	Date	Time	Sampling	Temperature		R.H	Pressure		Refractometer	
	hrs	Time		Chiller	Internal		Upstream	Vacuum	Temp	nd
				$^{\circ}\text{C}$	$^{\circ}\text{C}$	%	psi	Torr	$^{\circ}\text{C}$	
	4/9	0		19.6		32	7 to 11	5	20	1.3643
1	4/9	6.5	6:00	19.9	101.1	30	7 to 9	5	20	1.3638
2	4/9	12	11:30	19.9	100.93	29	7 to 9	5	20	1.3634
3	4/9	16.5	16:00	19.9	100.46	26	7 to 9	5	20	1.3628
4	4/9	21.5	21:00	19.9	100.53	27	7 to 9	5	20	1.3625
5	4/10	25.5	1:00	19.9	100.51	29	7 to 9	5	20	1.3622

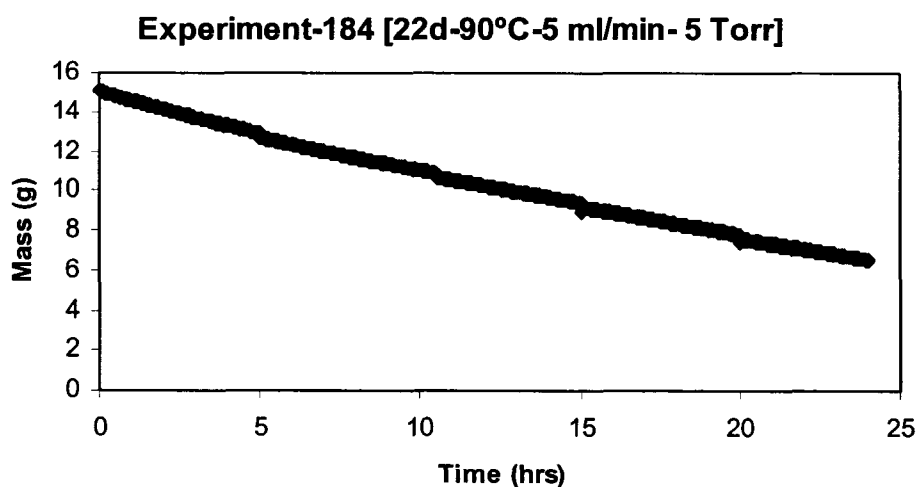


Figure D.23 Experiment - 184 Untreated mass data for 22 μm deep channel, 47 milliseconds, 4/9/06 to 4/10/06.

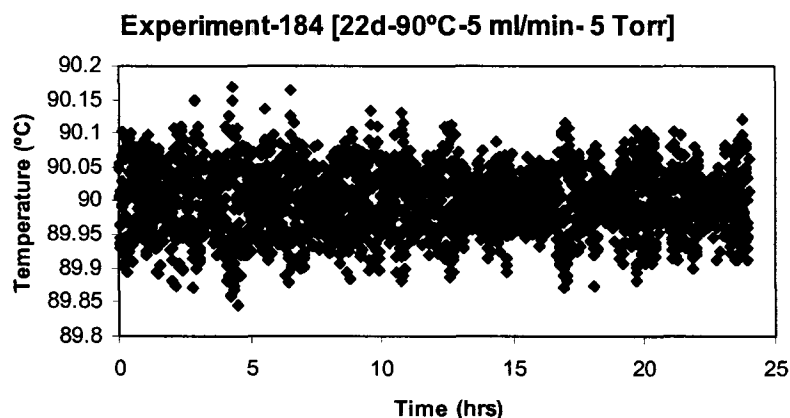


Figure D.24 Experiment - 184 Membrane module temperature profile for 22 μm deep channel, 47 milliseconds, 4/9/06 to 4/10/06.

Table D.25 Experiment - 101 Operating parameters for 47 μm deep channel, 20 milliseconds, 12/17/05 to 12/18/05.

	Date	Day	Time	
Start	12/17/05	Sat	19:45	
End	12/18/05	Sun	19:45	
Experiment #	101			
Experimental Time	24	hrs		
Depth of microchannel	47	μm	0.0047	cm
Length of microchannel	30000	μm	3	cm
Width of microchannel	60	μm	0.006	cm
Number of channels	99			
Residence Time	20.10096	millisec		
Average temperature in feed tank	22.9465649	$^{\circ}\text{C}$		
Membrane area	0.0003	m^2		
Membrane	2216			
Target Temperature	90	$^{\circ}\text{C}$		
Pump head	7016			
RPM	30.3			
Feed flow rate	25	ml/min		
Initial Feed ethanol	27.5	g		
Stabilization time	0.75	hrs		
Membrane	Expt # used	Exptl	Flow	
Date of 1st use		Time	rate	
		hrs	ml/min	
	12/17/05	condition	12	10
Permeate	3.1	g		
Refractive Index	1.3358			

Table D.26 Experiment - 101 Recorded data for 47 μm deep channel, 20 milliseconds, 12/17/05 to 12/18/05.

#	Date	Time	Samp- ling Time	Temperature			Pressure		Refractometer	
		hrs		Chiller °C	Heater °C	Internal °C	Upstream psi	Vacuum Torr	Temp °C	nd
	12/17	0		19.51	89.567	100.6	16 to 20	4	20	1.3644
1	12/18	5.75	0:40	19.51	90	101	16 to 20	3.8	20	1.3636
2	12/18	12.75	7:51	19.51	90	100	16 to 20	3.8	20	1.3631
3	12/18	18.75	13:43	19.35	89.8	100.6	16 to 20	3	20	1.3626
4	12/18	24.75		19.15	90.07	100.8	14 to 20	3	20	1.3621

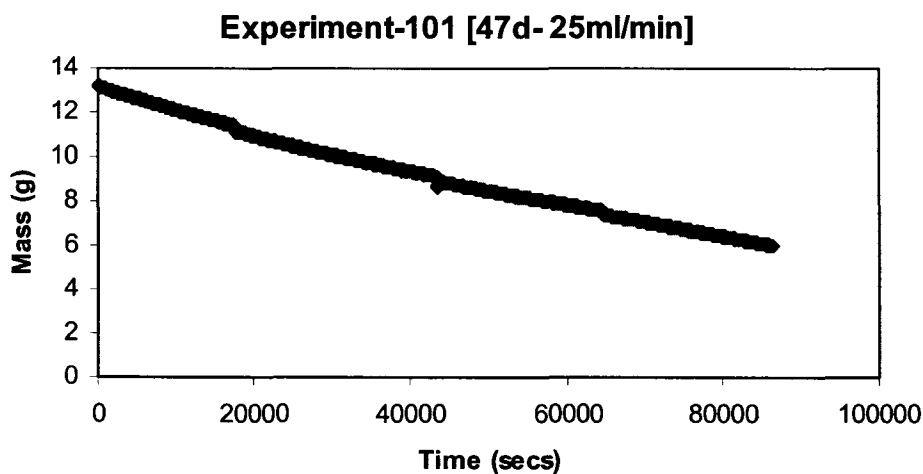


Figure D.25 Experiment - 101 Untreated mass data for 47 μm deep channel, 20 milliseconds, 12/17/05 to 12/18/05.

Table D.27 Experiment - 109 Operating parameters for 47 μm deep channel, 20 milliseconds, 12/31/05 to 1/1/06.

	Date	Day	Time	
Start	12/31/05	Sat	9:30	
End	1/1/06	Sun	9:30	
Experiment #	109			
Experimental Time	24	hrs		
Depth of microchannel	47	μm	0.0047	cm
Length of microchannel	30000	μm	3	cm
Width of microchannel	60	μm	0.006	cm
Number of channels	99			
Volume of fluid in reactor	0.0083754	cm^3		
Residence Time	20.10096	millisec		
Average temperature in feed tank	19.9270358	$^{\circ}\text{C}$		
Membrane area	0.0003	m^2		
Membrane	2216			
Target Temperature	90	$^{\circ}\text{C}$		
Pump head	7016			
RPM	30.3			
Feed flow rate	25	ml/min		
Feed ethanol	26.0721			
Tss	0.41666667	hrs		
Membrane	Expt # used	Exptl	Flow	
Date of 1st use		Time	rate	
	12/30/05	conditioning	15 hrs	25
Permeate	2.838	g		
Refractive Index	1.3392			

Table D.28 Experiment - 109 Recorded data for 47 μm deep channel, 20 milliseconds, 12/31/05 to 1/1/06.

#	Date	Time	Sampling Time	Temperature			Pressure		Refractometer	
				Chiller $^{\circ}\text{C}$	Heater $^{\circ}\text{C}$	Internal $^{\circ}\text{C}$	Upstream psi	Vacuum torr	Temp $^{\circ}\text{C}$	nd
	12/31	0		19.6	90.25	101.3	15 to 20	4	20	1.3643
1	12/31	5.4167	14:29	19	89.861	100.4	15 to 20	3.5	20	1.3639
2	12/31	10.417	19:29	19	90.121	100.3	15 to 20	3.25	20	1.3632
3	1/1	15.417	0:25	19	89.899	100.5	15 to 20	3	20	1.3627
4	1/1	20.417	5:28	19	90.188	100.7	15 to 20	3	20	1.3624
5	1/1	24.417	9:30						20	1.3622

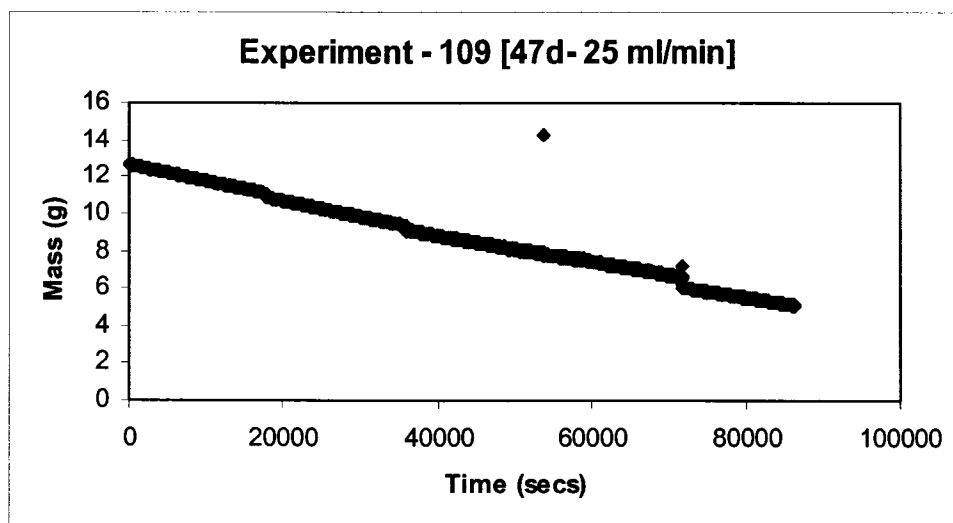


Figure D.26 Experiment - 109 Untreated mass data for 47 μm deep channel, 20 milliseconds, 12/31/05 to 1/1/06.

Table D.29 Experiment - 129 Operating parameters for 47 μm deep channel, 10 milliseconds, 1/17/06 to 1/18/06.

	Date	Day	Time	
Start	1/17/06	Tues	13:15	
End	1/18/06	Wed	13:15	
Experiment #	129			
Experimental Time	24	hrs		
Depth of microchannel	47	μm	0.0047	cm
Length of microchannel	30000	μm	3	cm
Width of microchannel	60	μm	0.006	cm
Number of channels	99			
Volume of fluid in reactor	0.0083754	cm^3		
Residence Time	10.05048	millisec		
Average temperature in feed tank	22.4355152	$^{\circ}\text{C}$		
Membrane area	0.0003	m^2		
Membrane	2216			
Target Temperature	90	$^{\circ}\text{C}$		
Pump head	7026			
RPM	60.5			
Feed flow rate	50	ml/min		
Feed ethanol	26			
Tss	0.75	hrs		
Membrane History	Expt # used	Exptl	Flow	
Date of 1st use		Time	rate	
		hrs	ml/min	
12/30/05	conditioning	16	25	
12/31/05	109	24	25	
1/1/06	110	15	50	
1/2/06	111	28	50	
1/16/06	conditioning	14	50	
Permeate	3.7369	g		
Refractive Index	1.348			

Table D.30 Experiment - 129 Recorded data for 47 μm deep channel, 10 milliseconds, 1/17/06 to 1/18/06.

#	Date	Time hrs	Time	Temperature			R.H %	Pressure		Refractometer	
				Chiller $^{\circ}\text{C}$	Heater $^{\circ}\text{C}$	Internal $^{\circ}\text{C}$		Up- stream psi	vacuum Torr	Temp $^{\circ}\text{C}$	nd
	1/17	0		19.25	89	99	42	max	4	20	1.3643
1	1/17	5.75	18:15	19.05	89.982	99.64	32	20 to max	3.5	20	1.3635
2	1/17	10.75	23:14	19.05	90.065	99.42	31	20 to max	3.5	20	1.363
3	1/18	15.75	4:14	19.2	89.91	99.58	30	20 to max	3.5	20	1.3626
4	1/18	20.75	9:14	19.2	90.076	99.9	30	20 to max	3.5	20	1.3622
5	1/18	24.75		19.2	89.72	99.6	30	20 to max	3.5	20	1.3619

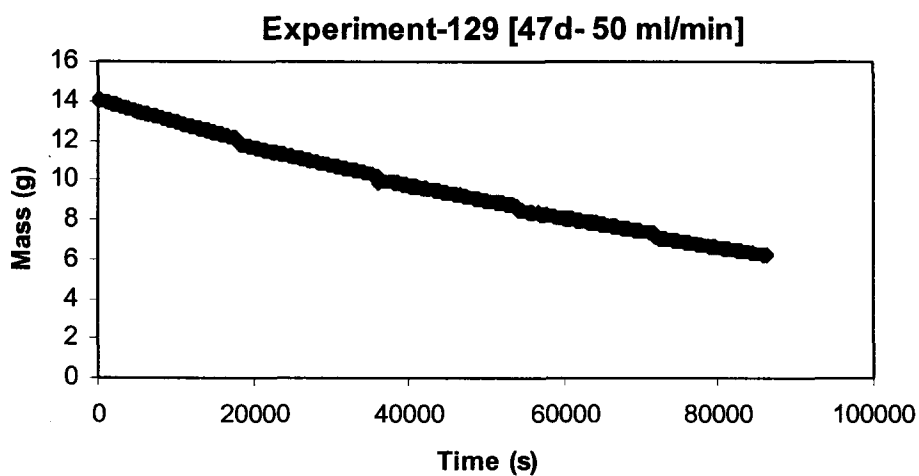


Figure D.27 Experiment - 129 Untreated mass data for 47 μm deep channel, 10 milliseconds, 1/17/06 to 1/18/06.

Table D.31 Experiment - 131 Operating parameters for 47 μm deep channel, 100 milliseconds, 1/19/06 to 1/20/06.

	Date	Day	Time	
Start	1/19/06	Thurs	15:15	
End	1/20/06	Fri	15:15	
Experiment #	131			
Experimental Time	24	hrs		
Depth of microchannel	47	μm	0.0047	cm
Length of microchannel	30000	μm	3	cm
Width of microchannel	60	μm	0.006	cm
Number of channels	99			
Volume of fluid in reactor	0.0083754	cm^3		
Residence Time	100.5048	millisec		
Average temperature in feed tank	22.9914586	$^{\circ}\text{C}$		
Membrane area	0.0003	m^2		
Membrane	2216			
Target Temperature	90	$^{\circ}\text{C}$		
Pump head	7016			
RPM	6.1			
Feed flow rate	5	ml/min		
Feed ethanol	26	g		
stabilization time	0.75	hrs		
Membrane History	Expt # used	Exptl	Flow	
Date of 1st use		Time	rate	
		hrs	ml/min	
	12/30/05	condition	16	25
	12/31/05	109	24	25
	1/1/06	110	15	50
	1/2/06	111	28	50
	1/16/06	condition	14	50
	1/17/06	129	24	50
	1/18/06	130	<5	5
Permeate	3.778+0.2	g		
Refractive Index	1.3464			

Table D.32 Experiment - 131 Recorded data for 47 μm deep channel, 100 milliseconds, 1/19/06 to 1/20/06.

#	Date	Time	Sampling	Temperature		R.H	Pressure		Refractometer	
		hrs	Time	Chiller	Internal		Upstream	Vacuum	Temp	nd
				$^{\circ}\text{C}$	$^{\circ}\text{C}$	%	psi	Torr	$^{\circ}\text{C}$	
	1/19	0	15:15	19.8	99	38	4 to 5	3.5	20	1.3643
1	1/19	5.75	20:14	19.8	99.59	34	4 to 5	3	20	1.3637
2	1/20	10.75	1:14	19.8	99.74	35	4 to 5	3	20	1.3631
3	1/20	15.75	6:30	19.8	99.88	38	4 to 5	3	20	1.3628
4	1/20	20.75	11:14	19.8	99.77	36	4 to 5	3	20	1.3625
5	1/20	24.75		19.8	99.59	36	4 to 5	3	20	1.3621

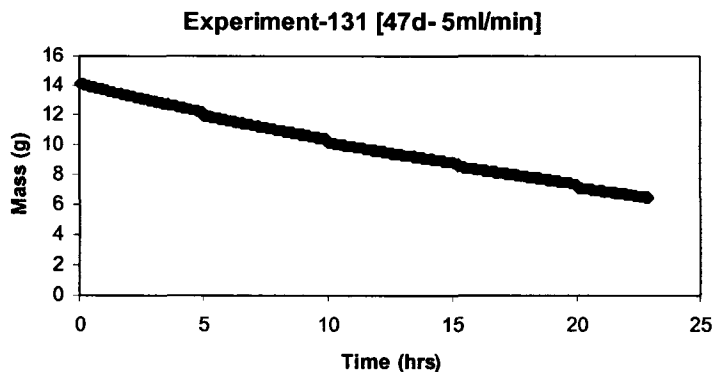


Figure D.28 Experiment - 131 Untreated mass data for 47 μm deep channel, 100 milliseconds, 1/19/06 to 1/20/06.

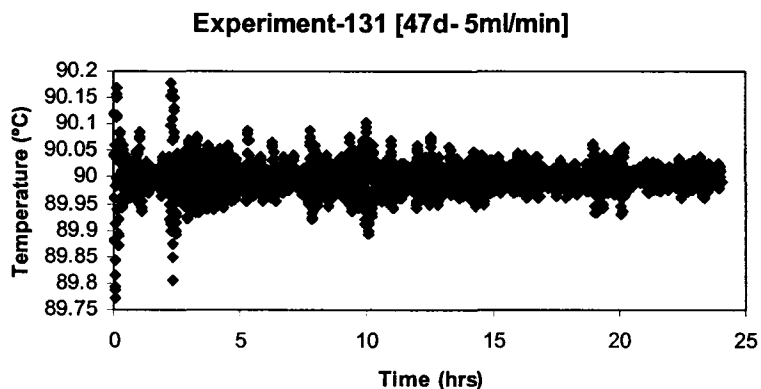


Figure D.29 Experiment - 131 Membrane module temperature profile for 47 μm deep channel, 100 milliseconds, 1/19/06 to 1/20/06.

Table D.33 Experiment - 132 Operating parameters for 47 μm deep channel, 502 milliseconds, 1/20/06 to 1/22/06.

	Date	Day	Time	
Start	1/20/06	Fri	19:45	
End	1/22/06	Sun	0:02	
Experiment #	132			
Experimental Time	30	hrs		
Depth of microchannel	47	μm	0.0047	cm
Length of microchannel	30000	μm	3	cm
Width of microchannel	60	μm	0.006	cm
Number of channels	99			
Volume of fluid in reactor	0.0083754	cm^3		
Residence Time	502.524	millisec		
Average temperature in feed tank	23.0566352	$^{\circ}\text{C}$		
Membrane area	0.0003	m^2		
Membrane	2216			
Target Temperature	90	$^{\circ}\text{C}$		
Pump head	7016			
RPM	1.6			
Feed flow rate	1	ml/min		
Feed ethanol	26.081			
Tsz	1	hr		
Membrane	Expt # used	Exptl	Flow	
Date of 1st use		Time	rate	
		hrs	ml/min	
	12/30/05	conditioning	16	25
	12/31/05	109	24	25
	1/1/06	110	15	50
	1/2/06	111	28	50
	1/16/06	conditioning	14	50
	1/17/06	129	24	50
	1/18/06	130	<5	5
	1/19/06	131	24	5
Permeate	4.5925 +0.3	g		
Refractive Index	1.3531			

Table D.34 Experiment - 132 Recorded data for 47 μm deep channel, 502 milliseconds, 1/20/06 to 1/22/06.

#	Date	Time hrs	Sampling Time	Temperature		R.H %	Pressure		Refractometer	
				Chiller	Internal		Upstream	Vacuum	Temp	nd
				$^{\circ}\text{C}$	$^{\circ}\text{C}$		psi	Torr	$^{\circ}\text{C}$	
	1/20	0	19:45	19.8	97.77	38	2	3.5	20	1.3643
1	1/21	6		19.8	98.353	41	2	3	20	1.3639
2	1/21	11.5	6:16	19.8	98.541	31	2	3	20	1.3633
3	1/21	16	10:44	19.8	99.233	30	2	3	20	1.363
4	1/21	20	14:44	19.8	98.872	30	2	3	20	1.3627
5	1/21	25		19.8	99.249	30	2	3	20	1.3625
6	1/22	31				30	2	3	20	1.3622

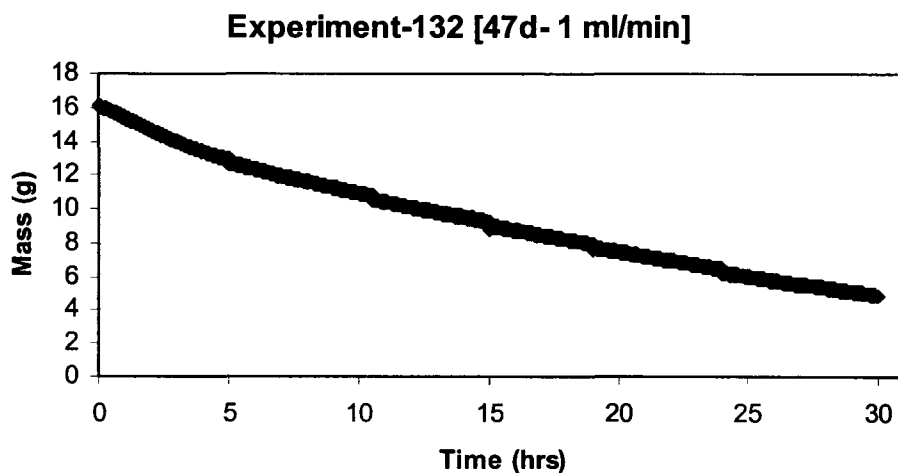


Figure D.30 Experiment - 132 Untreated mass data for 47 μm deep channel, 502 milliseconds, 1/20/06 to 1/22/06.

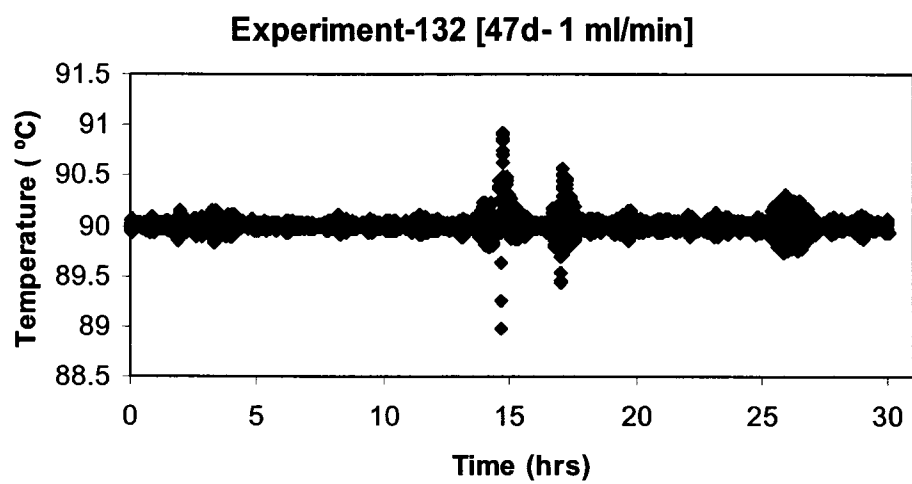


Figure D.31 Experiment - 132 Membrane module temperature profile for 47 μm deep channel, 502 milliseconds, 1/20/06 to 1/22/06.

Table D.35 Experiment - 135 Operating parameters for 47 μm deep channel, 50 milliseconds, 1/24/06 to 1/25/06.

	Date	Day	Time	
Start	1/24/06	Tues	0:30	
End	1/25/06	Wed	10:30	
Experiment #	135			
Experimental Time	34	hrs		
Depth of microchannel	47	μm	0.0047	cm
Length of microchannel	30000	μm	3	cm
Width of microchannel	60	μm	0.006	cm
Number of channels	99			
Volume of fluid in reactor	0.0083754	cm^3		
Residence Time	50.2524	millisec		
Average temperature in feed tank	22.1033048	$^{\circ}\text{C}$		
Membrane area	0.0003	m^2		
Membrane	2216			
Target Temperature	90	$^{\circ}\text{C}$		
Pump head	7016			
RPM	12.1			
Feed flow rate	10	ml/min		
Feed ethanol	26	g		
Tss	1.25	hrs		
Membrane	Expt # used	Exptl	Flow	
Date of 1st use		Time	rate	
		hrs	ml/min	
12/30/05	condition	16	25	
12/31/05	109	24	25	
1/1/06	110	15	50	
1/2/06	111	28	50	
1/16/06	condition	14	50	
1/17/06	129	24	50	
1/18/06	130	<5	5	
1/19/06	131	24	5	
1/20/06	131	30	1	
1/22/06	132		10	
1/23/06	133		10	
Permeate	5.4645	g		
Refractive Index	1.3494			

Table D.36 Experiment - 135 Recorded data for 47 μm deep channel, 50 milliseconds, 1/24/06 to 1/25/06.

#	Date	Time hrs	Sampling Time	Temperature		R.H %	Pressure		Refractometer	
				Chiller	Internal		Upstream	Vacuum	Temp	nd
				$^{\circ}\text{C}$	$^{\circ}\text{C}$		psi	Torr	$^{\circ}\text{C}$	
	1/23	0		20.5	100	32	5 to 6	3.5	20	1.3643
1	1/24	6.25		20.5	100	34	5 to 6	3.5	20	1.3639
2	1/24	11.25	10:29	20.5	99.908	31	5 to 6	3.5	20	1.3636
3	1/24	16.25	15:28	19.8	99.312	31	5 to 6	3	20	1.3634
4	1/24	21.25	20:29	19.8	99.557	30	5 to 6	3	20	1.363
5	1/25	25.25	0:29	19.8	99.666	29	5 to 6	3	20	1.3628
6	1/25	31.25	6:29	20.3	100.11	28	5 to 6	3	20	1.3624
7	1/25	35.25	10:30	20.3	99.942	27	5 to 6	3	20	1.3621

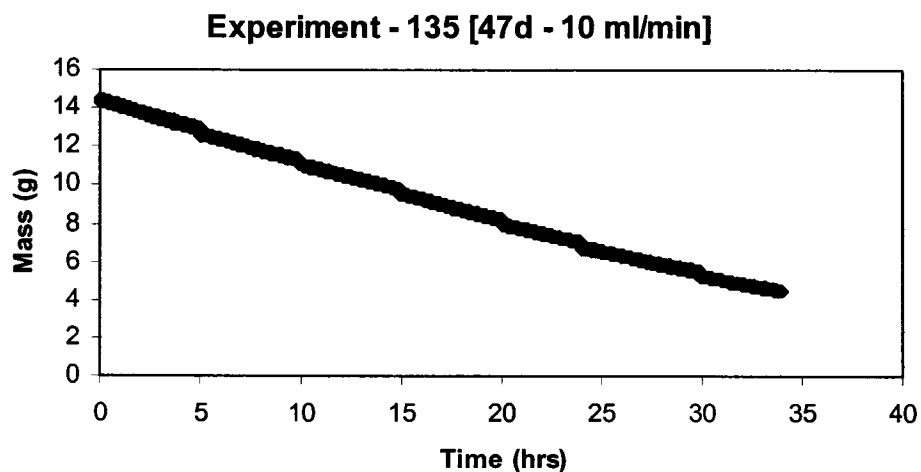


Figure D.32 Experiment - 135 Untreated mass data for 47 μm deep channel, 50 milliseconds, 1/24/06 to 1/25/06.

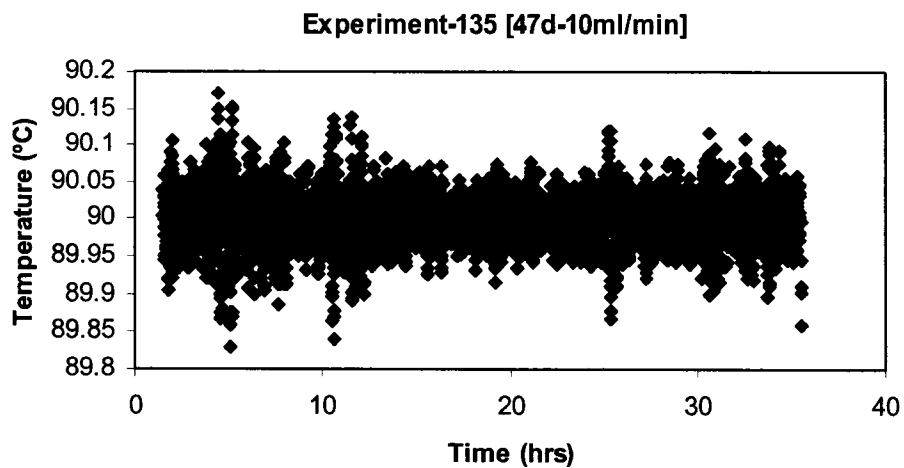


Figure D.33 Experiment - 135 Membrane module temperature profile for 47 μm deep channel, 50 milliseconds, 1/24/06 to 1/25/06.

Table D.37 Experiment - 136 Operating parameters for 47 μm deep channel, 100 milliseconds, 1/25/06 to 1/26/06.

	Date	Day	Time	
Start	1/25/06	Wed	14:00	
End	1/26/06	Thurs	18:00	
Experiment #	136			
Experimental Time	28	hrs		
Depth of microchannel	47	μm	0.0047	cm
Length of microchannel	30000	μm	3	cm
Width of microchannel	60	μm	0.006	cm
Number of channels	99			
Volume of fluid in reactor	0.0083754	cm^3		
Residence Time	100.5048	millisec		
Average temperature in feed tank	23.0910173	$^{\circ}\text{C}$		
Membrane area	0.0003	m^2		
Membrane	2216			
Target Temperature	90	$^{\circ}\text{C}$		
Pump head	7016			
RPM	6.1			
Feed flow rate	5	ml/min		
Feed ethanol	26	g		
Tsz	0.66666667	hrs		
Membrane	Expt # used	Exptl	Flow	
Date of 1st use		Time	rate	
		hrs	ml/min	
	12/30/05	condition	16	25
	12/31/05	109	24	25
	1/1/06	110	15	50
	1/2/06	111	28	50
	1/16/06	condition	14	50
	1/17/06	129	24	50
	1/18/06	130	<5	5
	1/19/06	131	24	5
	1/20/06	131	30	1
	1/22/06	132		10
	1/23/06	133		10
	1/24/06	135	36	10
Permeate	3.4149+0.2	g		
Refractive Index	1.3524			

Table D.38 Experiment - 136 Recorded data for 47 μm deep channel, 100 milliseconds, 1/25/06 to 1/26/06.

#	Date	Time hrs	Sampling Time	Temperature		R.H %	Pressure		Refractometer	
				Chiller	Internal		Upstream	Vacuum	Temp	nd
				$^{\circ}\text{C}$	$^{\circ}\text{C}$		psi	Torr	$^{\circ}\text{C}$	
	1/25	0		20.4	99	26	4 to 5	3	20	1.3643
1	1/25	6.6667		19.9	99.965	24	4 to 5	3	20	1.3638
2	1/25	10.667	23:59	19.9	100.09	22	4 to 5	2.8	20	1.3635
3	1/26	15.667	4:59	20.5	100.37	23	4 to 5	3	20	1.3631
4	1/26	20.667	9:59	20.5	100.39	23	4 to 5	3	20	1.3627
5	1/26	24.667	13:59	20.3	100.14	22	4 to 5	3	20	1.3624
6	1/26	28.667	18:00	20.3	100.9	22	4 to 5	2.5	20	1.3622

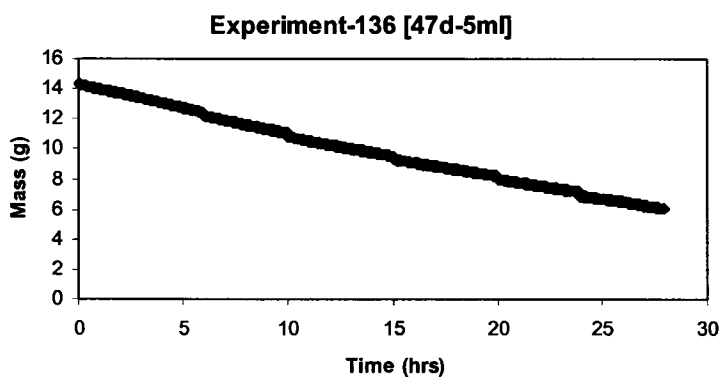


Figure D.34 Experiment -136 Untreated mass data for 47 μm deep channel, 100 milliseconds, 1/25/06 to 1/26/06.

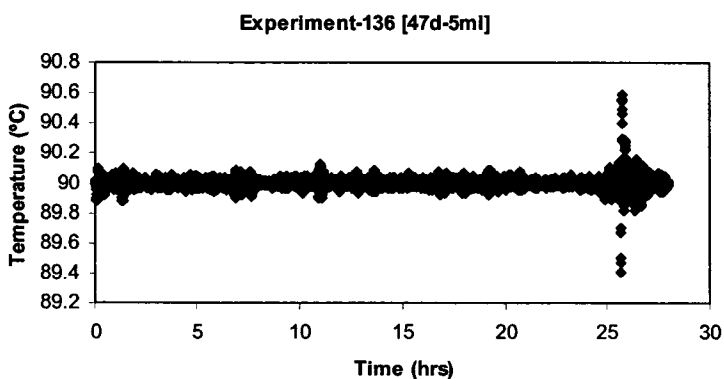


Figure D.35 Experiment - 136 Membrane module temperature profile for 47 μm deep channel, 100 milliseconds, 1/25/06 to 1/26/06.

Table D.39 Experiment - 163 Operating parameters for 47 μm deep channel, 251 milliseconds, 3/9/06 to 3/10/06.

	Date	Day	Time	
Start	3/9/06	Thurs	21:30	
End	3/10/06	Fri	17:30	
Experiment #	163			
Experimental Time	20	hrs		
Depth of microchannel	47	μm	0.0047	cm
Length of microchannel	30000	μm	3	cm
Width of microchannel	60	μm	0.006	cm
Number of channels	99			
Volume of fluid in reactor	0.0083754	cm^3		
Residence Time	251.262	millisec		
Average temperature in feed tank	23.2358333	$^{\circ}\text{C}$		
Membrane area	0.0003	m^2		
Membrane	2216			
Target Temperature	90	$^{\circ}\text{C}$		
Pump head	7016			
RPM	2.5			
Feed flow rate	2	ml/min		
Feed ethanol	27.5			
Stabilization time	2.25	hrs		
Membrane	Expt # used	Exptl	Flow	
Date of 1st use		Time	rate	
		hrs	ml/min	
	3/8/06	condition	25	5

Table D.40 Experiment - 163 Recorded data for 47 μm deep channel, 251 milliseconds, 3/9/06 to 3/10/06.

#	Date	Time hrs	Sampling Time	Temperature		R.H %	Pressure		Refractometer	
				Chiller $^{\circ}\text{C}$	Internal $^{\circ}\text{C}$		Upstream psi	Vacuum Torr	Temp $^{\circ}\text{C}$	nd
	3/9	0	21:30	19.6	99.467	30	11 to 16	3	20	1.3644
1	3/10	7.25	2:30	19.6	99.199	30	11 to 16	3	20	1.3637
2	3/10	12.25	7:30	19.8	99.594	30	11 to 16	3	20	1.3633
3	3/10	17.25	12:30	19.7	99.312	30	11 to 16	3	20	1.3628
4	3/10	22.25	17:30	19.7	99.199	34	11 to 16	3	20	1.3624

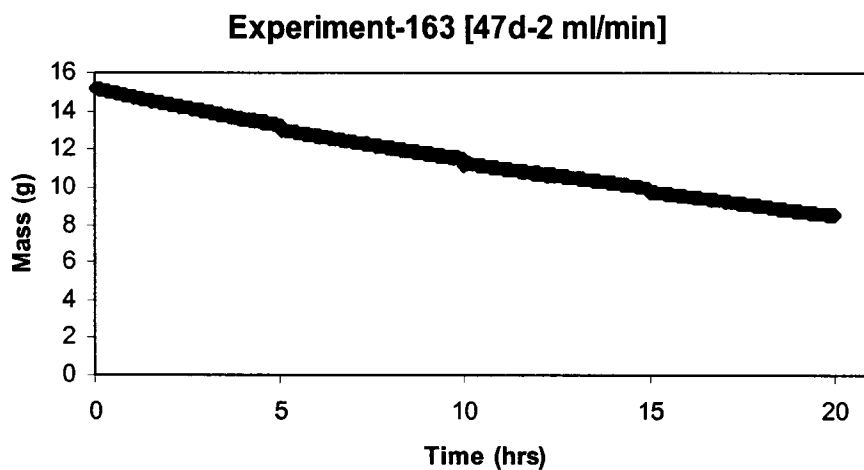


Figure D.36 Experiment - 163 Untreated mass data for 47 μm deep channel, 251 milliseconds, 3/9/06 to 3/10/06.

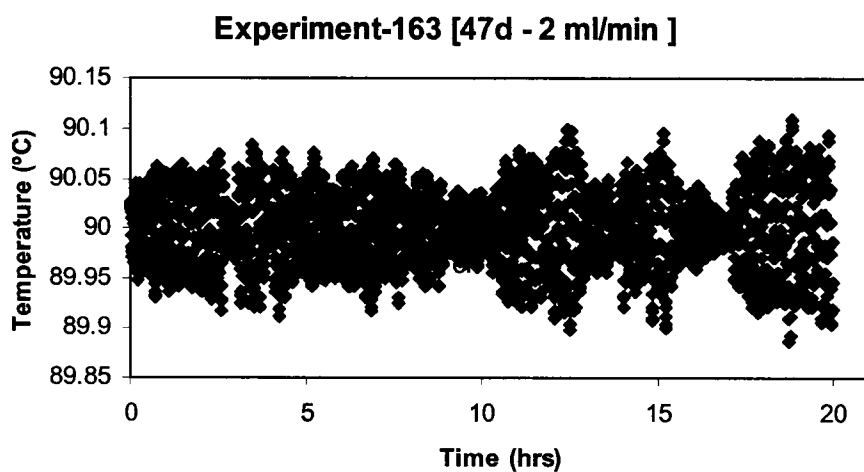


Figure D.37 Experiment - 163 Membrane module temperature profile for 47 μm deep channel, 251 milliseconds, 3/9/06 to 3/10/06.

Table D.41 Experiment - 169 Operating parameters for 47 μm deep channel, 251 milliseconds, 3/20/06 to 3/21/06.

	Date	Day	Time	
Start	3/20/06	Mon	16:00	
End	3/21/06	Tues	12:00	
Experiment #	169			
Experimental Time	20	hrs		
Depth of microchannel	47	μm	0.0047	cm
Length of microchannel	30000	μm	3	cm
Width of microchannel	60	μm	0.006	cm
Number of channels	99			
Volume of fluid in reactor	0.0083754	cm^3		
Residence Time	251.262	millisec		
Average temperature in feed tank	23.0524563	$^{\circ}\text{C}$		
Membrane area	0.0003	m^2		
Membrane	2216			
Target Temperature	90	$^{\circ}\text{C}$		
Pump head	7016			
RPM	2.5			
Feed flow rate	2	ml/min		
Initial Feed ethanol	27.5	g		
Stabilization time	1.16666667	hrs		
Membrane	Expt # used	Exptl	Flow	
Date of 1st use		Time	rate	
		hrs	ml/min	
	3/19/06	condition	24	2

Table D.42 Experiment - 169 Recorded data for 47 μm deep channel, 251 milliseconds, 3/20/06 to 3/21/06.

#	Date	Time	Sampling	Temperature		R.H	Pressure		Refractometer	
				Chiller	Internal		Upstream	Vacuum	Temp	nd
		hrs	Time	$^{\circ}\text{C}$	$^{\circ}\text{C}$	%	psi	Torr	$^{\circ}\text{C}$	
	3/20	0		20.4	99.493	49	3 to 5	3	20	1.3644
1	3/20	5.1667	20:00	20.4	99.522	47	3 to 5	3	20	1.3638
2	3/21	9.1667	12:00	20.4	99.4	47	3 to 5	3	20	1.3634
3	3/21	13.167	4:05	20.4	99.021	33	3 to 5	3	20	1.363
4	3/21	17.167	8:00	20.4	99.81	31	3 to 5	3	20	1.3625
5	3/21	21.167	12:00	20.4	99.506	31	3 to 5	3	20	1.3621

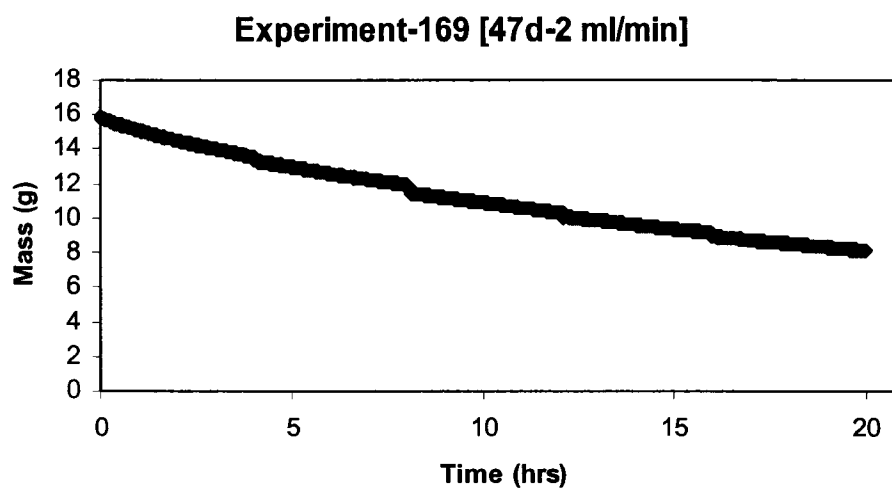


Figure D.38 Experiment - 169 Untreated mass data for 47 μm deep channel, 251 milliseconds, 3/20/06 to 3/21/06.

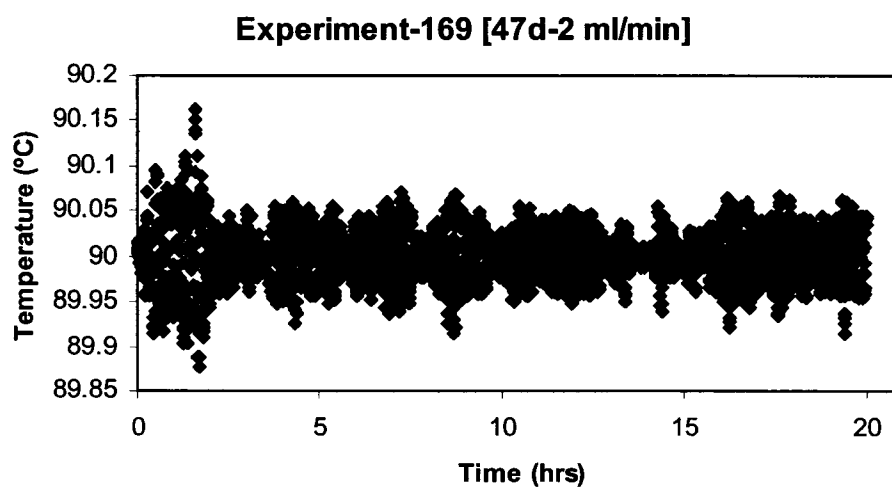


Figure D.39 Experiment - 169 Membrane module temperature profile for 47 μm deep channel, 251 milliseconds, 3/20/06 to 3/21/06.

Table D.43 Experiment - 170 Operating parameters for 47 μm deep channel, 50 milliseconds, 3/21/06 to 3/22/06.

	Date	Day	Time	
Start	3/21/06	Tues	15:00	
End	3/22/06	Wed	6:00	
Experiment #	170			
Experimental Time	15	hrs		
Depth of microchannel	47	μm	0.0047	cm
Length of microchannel	30000	μm	3	cm
Width of microchannel	60	μm	0.006	cm
Number of channels	99			
Volume of fluid in reactor	0.0083754	cm^3		
Residence Time	50.2524	millisec		
Average temperature in feed tank	23.0044395	$^{\circ}\text{C}$		
Membrane area	0.0003	m^2		
Membrane	2216			
Target Temperature	90	$^{\circ}\text{C}$		
Pump head	7016			
RPM	12.1			
Feed flow rate	10	ml/min		
Feed ethanol	27.5			
Stabilization time	1.25	hrs		
Membrane	Expt # used	Exptl	Flow	
Date of 1st use		Time	rate	
		hrs	ml/min	
	3/19/06	condition	24	2
	3/20/06	169	20+1	2

Table D.44 Experiment - 170 Recorded data for 47 μm deep channel, 50 milliseconds, 3/21/06 to 3/22/06.

#	Date	Time	Sampling	Temperature		R.H	Pressure		Refractometer	
				Chiller	Internal		Upstream	Vacuum	Temp	nd
		hrs	Time	$^{\circ}\text{C}$	$^{\circ}\text{C}$	%	psi	Torr	$^{\circ}\text{C}$	
	3/21	0		20.4	99.815	31	14 to 20	3	20	1.3644
1	3/21	6.25	20:00	20.4	100.05	30	10 to 20	3	20	1.3636
2	3/22	11.25	1:00	20.4	100.08	30	10 to 20	3	20	1.363
3	3/22	16.25	6:00	20.4	100.15	30	10 to 20	3	20	1.3624

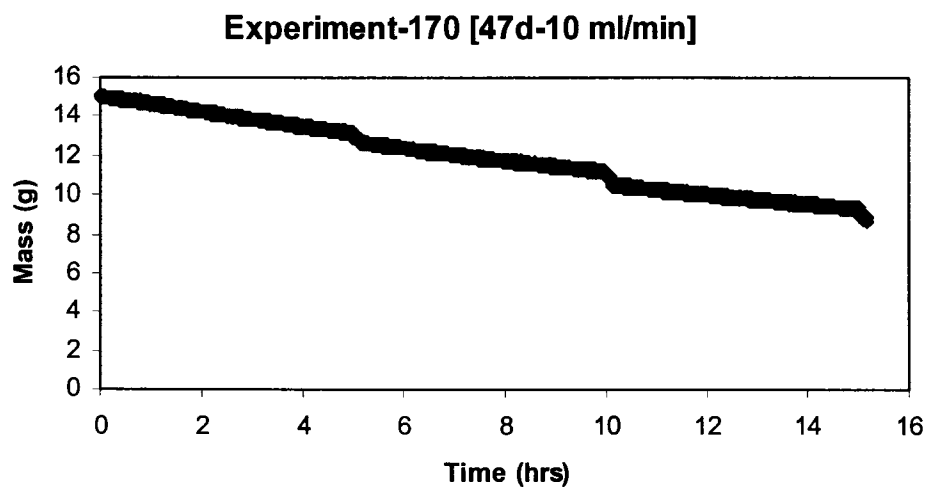


Figure D.40 Experiment - 170 Untreated mass data for 47 μm deep channel, 50 milliseconds, 3/21/06 to 3/22/06.

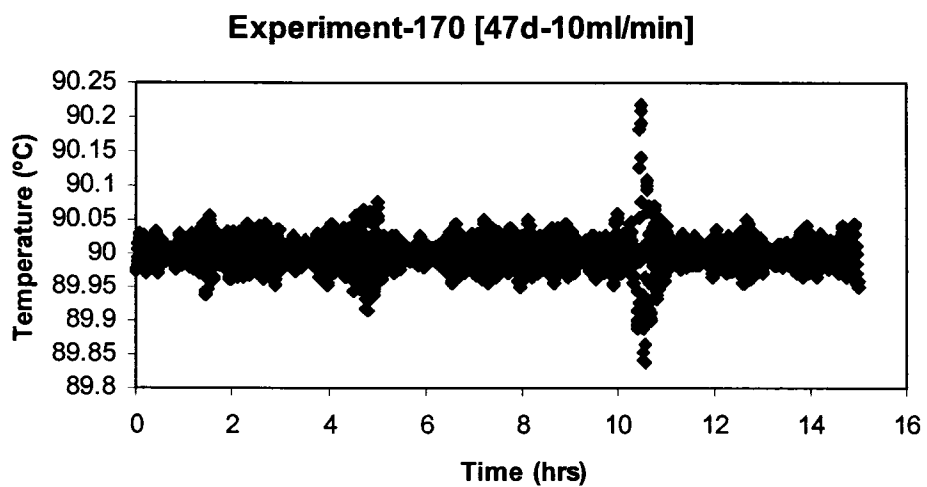


Figure D.41 Experiment - 170 Membrane module temperature profile for 47 μm deep channel, 50 milliseconds, 3/21/06 to 3/22/06.

Table D.45 Experiment - 171 Operating parameters for 47 μm deep channel, 50 milliseconds, 3/22/06 to 3/23/06.

	Date	Day	Time	
Start	3/22/06	Wed	9:15	
End	3/23/06	Thurs	1:15	
Experiment #	171			
Experimental Time	16	hrs		
Depth of microchannel	47	μm	0.0047	cm
Length of microchannel	30000	μm	3	cm
Width of microchannel	60	μm	0.006	cm
Number of channels	99			
Volume of fluid in reactor	0.0083754	cm^3		
Residence Time	50.2524	millisec		
Membrane area	0.0003	m^2		
Membrane	2216			
Target Temperature	90	$^{\circ}\text{C}$		
Pump head	7016			
RPM	12.1			
Feed flow rate	10	ml/min		
Feed ethanol	27.5			
Stabilization time	1.25	hrs		
Membrane	Expt # used	Exptl Time	Flow rate	
Date of 1st use		hrs	ml/min	
3/19/06	condition	24	2	
3/20/06	169	20+1	2	
3/21/06	170	15	10	

Table D.46 Experiment - 171 Recorded data for 47 μm deep channel, 50 milliseconds, 3/22/06 to 3/23/06.

#	Date	Time hrs	Sampling Time	Temperature		R.H %	Pressure		Refractometer	
				Chiller $^{\circ}\text{C}$	Internal $^{\circ}\text{C}$		Upstream psi	Vacuum Torr	Temp $^{\circ}\text{C}$	nd
	3/22	0		20.4	100.25	30	20 to max	3	20	1.3643
1	3/22	5.25	13:15	20.3	100.24	28	26 to max	3	20	1.3636
2	3/22	9.25	17:15	20.3	100.09	27	26 to max	3	20	1.363
3	3/22	13.25	21:15	20.3	100.19	27	26 to max	3	20	1.3627
4	3/23	17.25	1:15	20.5	100.29	27	24 to max	3	20	1.3624

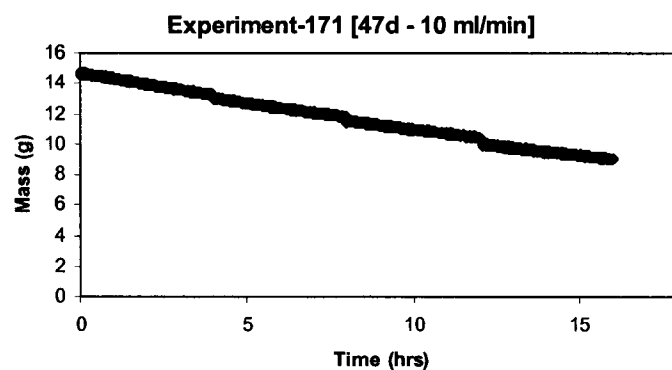


Figure D.42 Experiment - 171 Untreated mass data for 47 μm deep channel, 50 milliseconds, 3/22/06 to 3/23/06.

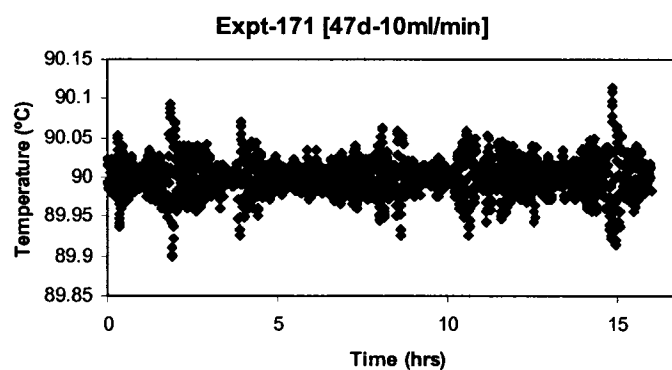


Figure D.43 Experiment - 171 Membrane module temperature profile for 47 μm deep channel, 50 milliseconds, 3/22/06 to 3/23/06.

Table D.47 Experiment - 172a Operating parameters for 47 μm deep channel, 50 milliseconds, 3/23/06 to 3/24/06.

	Date	Day	Time	
Start	3/23/06	Thurs	11:30	
End	3/24/06	Fri	7:30	
Experiment #	172-a			
Experimental Time	20	hrs		
Depth of microchannel	47	μm	0.0047	cm
Length of microchannel	30000	μm	3	cm
Width of microchannel	60	μm	0.006	cm
Number of channels	99			
Volume of fluid in reactor	0.0083754	cm^3		
Residence Time	50.2524	millisec		
Average temperature in feed tank	22.6777685	$^{\circ}\text{C}$		
Membrane area	0.0003	m^2		
Membrane	2216			
Target Temperature	90	$^{\circ}\text{C}$		
Pump head	7016			
RPM	12.1			
Feed flow rate	10	ml/min		
Initial Feed ethanol	27.5	g		
Stabilization time	1.16666667	hrs		
Membrane	Expt # used	Exptl	Flow	
Date of 1st use		Time	rate	
		hrs	ml/min	
	3/19/06	condition	24	2
	3/20/06	169	20+1	2
	3/21/06	170	15	10
	3/22/06	171	16	10
	3/23/06	172	4.75	10

Table D.48 Experiment - 172a Recorded data for 47 μm deep channel, 50 milliseconds, 3/23/06 to 3/24/06.

#	Date	Time	Sampling	Temperature		R.H	Pressure		Refractometer	
				Chiller	Internal		Upstream	Vacuum	Temp	nd
		hrs	Time	$^{\circ}\text{C}$	$^{\circ}\text{C}$	%	psi	Torr	$^{\circ}\text{C}$	
		0		20.7	100.35	32	8 to 11	3	20	1.3643
1	3/23	5.1667	15:30	20.4	100.12	32	10 to 13	3	20	1.3638
2	3/23	9.1667	19:30	20.4	100.27	32	10 to 16	3	20	1.3633
3	3/23	13.167	23:30	20.4	100.45	31	10 to 16	3	20	1.3628
4	3/24	17.167	3:43	20.6	100.58	30	12 to 19	3	20	1.3626
5	3/24	21.167	7:30	20.6	100.56	30	14 to 19	3	20	1.3624

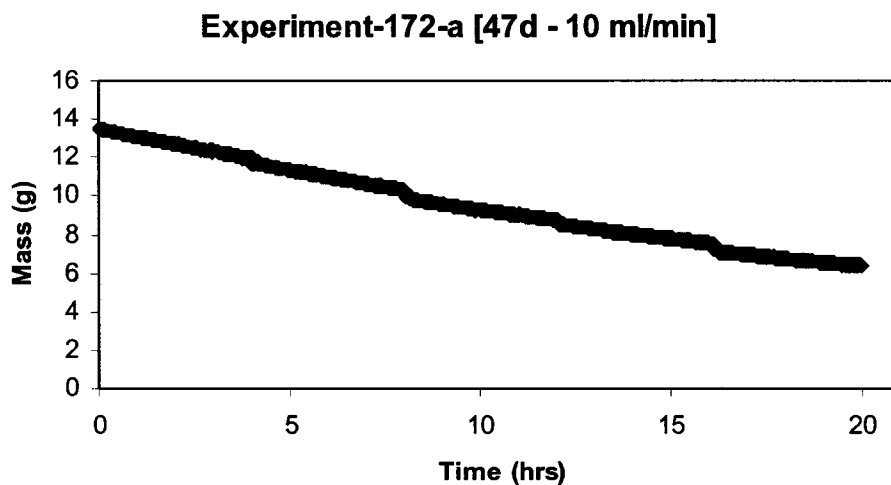


Figure D.44 Experiment - 172a Untreated mass data for 47 μm deep channel, 50 milliseconds, 3/23/06 to 3/24/06.

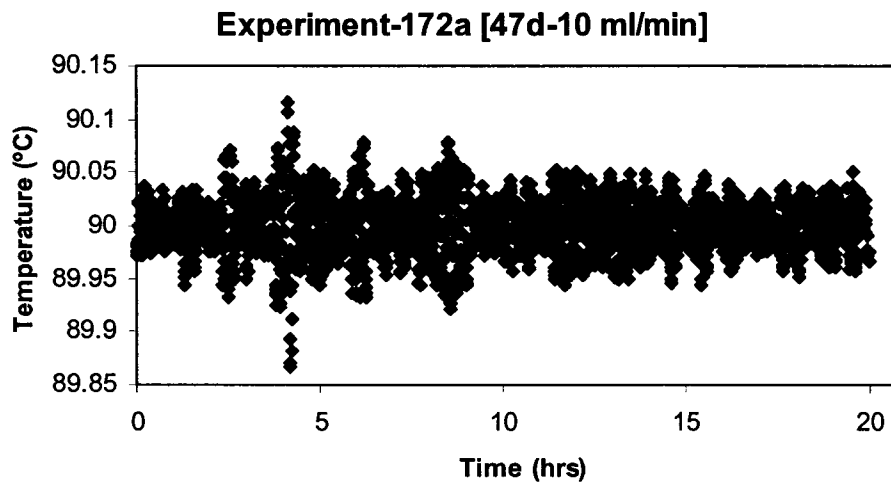


Figure D.45 Experiment - 172a Membrane module temperature profile for 47 μm deep channel, 50 milliseconds, 3/23/06 to 3/24/06.

Table D.49 Experiment - 138 Operating parameters for 120 μm deep channel, 25 milliseconds, 1/28/06 to 1/29/06.

	Date	Day	Time	
Start	1/28/06	Sat	11:45	
End	1/29/06	Sun	21:45	
Experiment #	138			
Experimental Time	34	hrs		
Depth of microchannel	120	μm	0.012	cm
Length of microchannel	30000	μm	3	cm
Width of microchannel	60	μm	0.006	cm
Number of channels	99			
Volume of fluid in reactor	0.021384	cm^3		
Residence Time	25.6608	millisec		
avg temp feed tank	21.0171485	$^{\circ}\text{C}$		
Membrane area	0.0003	m^2		
Membrane	2216			
Target Temperature	90	$^{\circ}\text{C}$		
Pump head	7016			
RPM	60.5			
Feed flow rate	50	ml/min		
Feed ethanol	26			
stabilization time	0.66666667	hrs		
Membrane History	Expt # used	Exptl	Flow	
Date of 1st use		Time	rate	
		hrs	ml/min	
	condition			
	1/27/06	pre-138	18	25
Permeate	3.8245	g		
Refractive Index	1.3389			

Table D.50 Experiment - 138 Recorded data for 120 μm deep channel, 25 milliseconds, 1/28/06 to 1/29/06.

#	Date	Time	Sampling	Temperature		R.H	Pressure		Refractometer	
	hrs		Time	Chiller	Internal		Upstream	Vacuum	Temp	nd
				$^{\circ}\text{C}$	$^{\circ}\text{C}$	%	psi	Torr	$^{\circ}\text{C}$	
	1/28	0	11:45	20.3	101.4	38	24 to 27	3	20	1.3643
1	1/28	5.6667	16:44	19.9	102.21	40	25 to 30	3	20	1.3641
2	1/28	12.667	23:44	19.9	102.1	40	25 to 30	3	20	1.3637
3	1/29	18.667	5:44	19.9	102.47	37	25 to 30	3	20	1.3635
4	1/29	24.667	11:44	19.9	102.09	33	25 to 30	2.5	20	1.3631
5	1/29	30.667	17:46	19.9	101.71	29	20 to 30	2	20	1.3627
6	1/29	34.667	21:45	19.9		28	21 to 30	2	20	1.3624

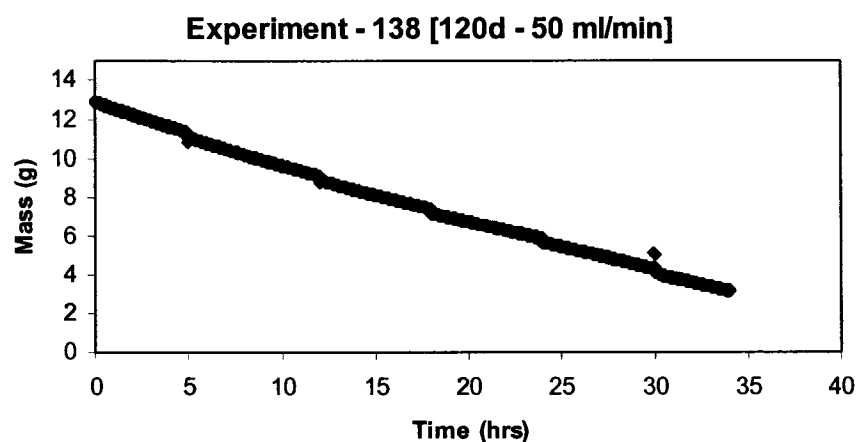


Figure D.46 Experiment - 138 Untreated mass data for 120 μm deep channel, 25 milliseconds, 1/28/06 to 1/29/06.

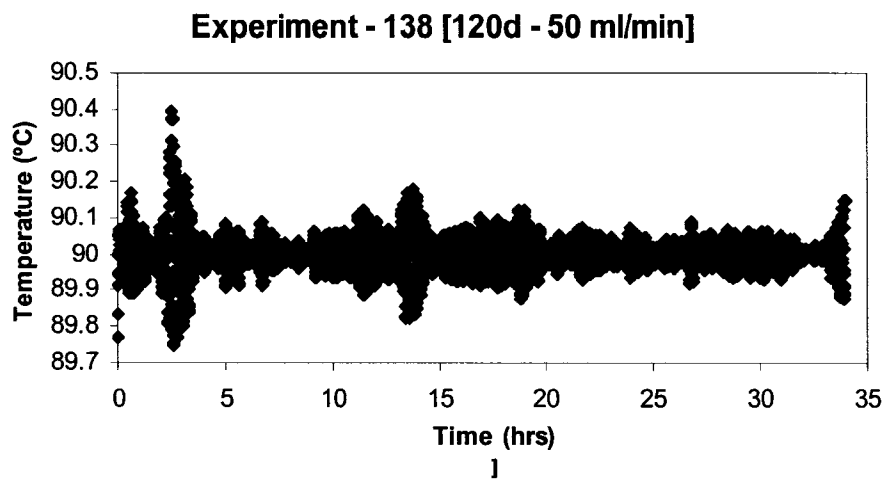


Figure D.47 Experiment - 138 Membrane module temperature profile for 120 μm deep channel, 25 milliseconds, 1/28/06 to 1/29/06.

Table D.51 Experiment - 140 Operating parameters for 120 μm deep channel, 51 milliseconds, 1/30/06 to 2/1//06.

	Date	Day	Time	
Start	1/30/06	Mon	22:00	
End	2/1/06	Wed	2:00	
Experiment #	140			
Experimental Time	28	hrs		
Depth of microchannel	120	μm	0.012	cm
Length of microchannel	30000	μm	3	cm
Width of microchannel	60	μm	0.006	cm
Number of channels	99			
Volume of fluid in reactor	0.021384	cm^3		
Residence Time	51.3216	millisec		
avg temp feed tank		$^{\circ}\text{C}$		
Membrane area	0.0003	m^2		
Membrane	2216			
Target Temperature	90	$^{\circ}\text{C}$		
Pump head	7016			
RPM	30.3			
Feed flow rate	25	ml/min		
Feed ethanol	26			
Tss	0.66666667	hrs		
Membrane	Expt # used	Exptl	Flow	
Date of 1st use		Time	rate	
		hrs	ml/min	
	condition			
	1/27/06	pre-138	18	25
	1/28/06	138	34	50
	1/29/06	139	20	12.5
Permeate	3.0754	g		
Refractive Index	1.3391			

Table D.52 Experiment - 140 Recorded data for 120 μm deep channel, 51 milliseconds, 1/30/06 to 2/1/06.

#	Date	Time hrs	Sampling Time	Temperature		R.H %	Pressure		Refractometer	
				Chiller	Internal		Upstream	Vacuum	Temp	nd
				$^{\circ}\text{C}$	$^{\circ}\text{C}$		psi	Torr	$^{\circ}\text{C}$	
	1/31	0	22:00	19.8	99.406	23	16 to 20	3	20	1.3643
1	1/31	6.667	3:59	19.8	99.936	22	16 to 20	3	20	1.3639
2	1/31	14.667	11:59	19.8	100.02	23	16 to 20	3	20	1.3631
3	1/31	19.667	16:59	19.8	99.537	22	16 to 20	2	20	1.3627
4	1/31	24.667	21:59	19.8	99.661	22	16 to 20	2	20	1.3625
5	2/1	28.667		19.8	99.798	23	16 to 20	2	20	1.3623

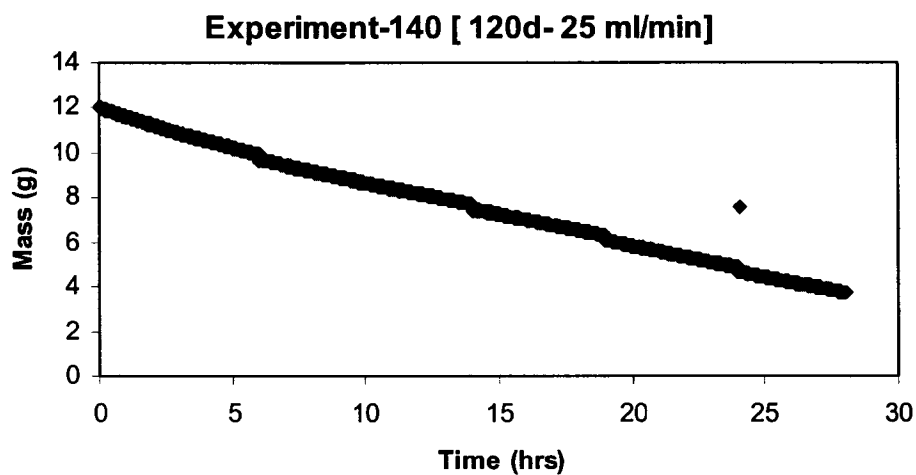


Figure D.48 Experiment - 140 Untreated mass data for 120 μm deep channel, 51 milliseconds, 1/30/06 to 2/1/06.

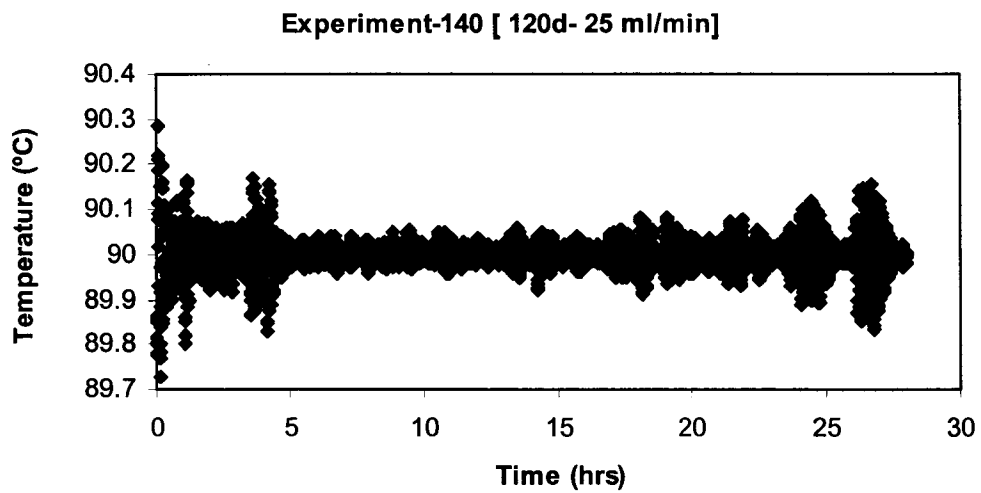


Figure D.49 Experiment - 140 Membrane module temperature profile for 120 μm deep channel, 51 milliseconds, 1/30/06 to 2/1/06.

Table D.53 Experiment - 143 Operating parameters for 120 μm deep channel, 51 milliseconds, 2/6/06 to 2/7/06.

	Date	Day	Time	
Start	2/6/06	Mon	9:30	
End	2/7/06	Tues	19:30	
Experiment #	143			
Experimental Time	34	hrs		
Depth of microchannel	120	μm	0.012	cm
Length of microchannel	30000	μm	3	cm
Width of microchannel	60	μm	0.006	cm
Number of channels	99			
Volume of fluid in reactor	0.021384	cm^3		
Residence Time	51.3216	millisec		
avg temp feed tank	21.9167075	$^{\circ}\text{C}$		
Membrane area	0.0003	m^2		
Membrane	2216			
Target Temperature	90	$^{\circ}\text{C}$		
Pump head	7016			
RPM	30.3			
Feed flow rate	25	ml/min		
Feed ethanol	27.5			
Tss	1	hr		
Membrane History	Expt # used	Exptl	Flow	
Date of 1st use		Time	rate	
		hrs	ml/min	
	condition	18	5	
2/5/06	142	20	5	
Permeate	3.3872+0.25	g		
Refractive Index	1.3497			

Table D.54 Experiment - 143 Recorded data for 120 μm deep channel, 51 milliseconds, 2/6/06 to 2/7/06.

#	Date	Time hrs	Sampling Time	Temperature		R.H %	Pressure		Refractometer	
				Chiller	Internal		Upstream	Vacuum	Temp	nd
				$^{\circ}\text{C}$	$^{\circ}\text{C}$		psi	Torr	$^{\circ}\text{C}$	
	2/6	0		20.2	101.01	34	18 to 23	3	20	1.3643
1	2/6	7	14:29	20.2	101.14	36	20 to 25	2.5	20	1.3639
2	2/6	12	19:29	20.2	101.7	32	20 to 25	2.5	20	1.3635
3	2/7	17	0:29	20.2	102.68	31	20 to 25	2.5	20	1.3633
4	2/7	22	5:29	20.4	102.76	30	20 to 25	3	20	1.363
5	2/7	26	9:29	20.4	102.64	30	20 to 25	3	20	1.3627
6	2/7	32	15:30	20	101.83	26	19 to 24	2	20	1.3624
7	2/7	36	19:30	20	101.77	25	19 to 22	2	20	1.3622

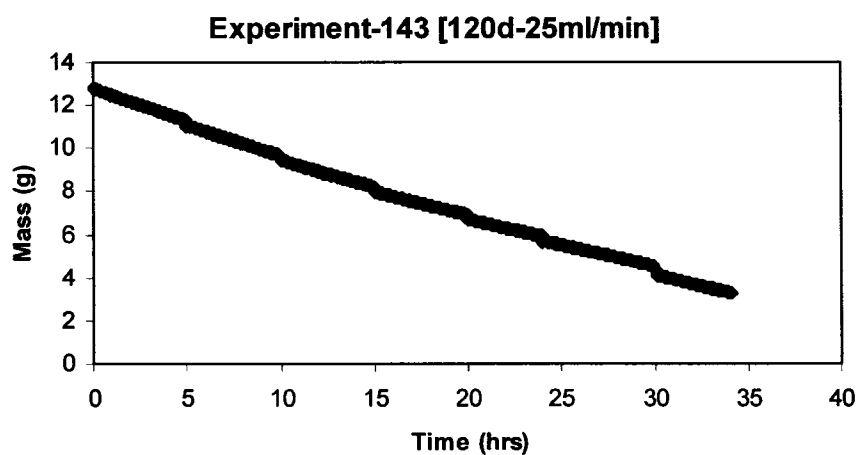


Figure D.50 Experiment - 143 Untreated mass data for 120 μm deep channel, 51 milliseconds, 2/6/06 to 2/7/06.

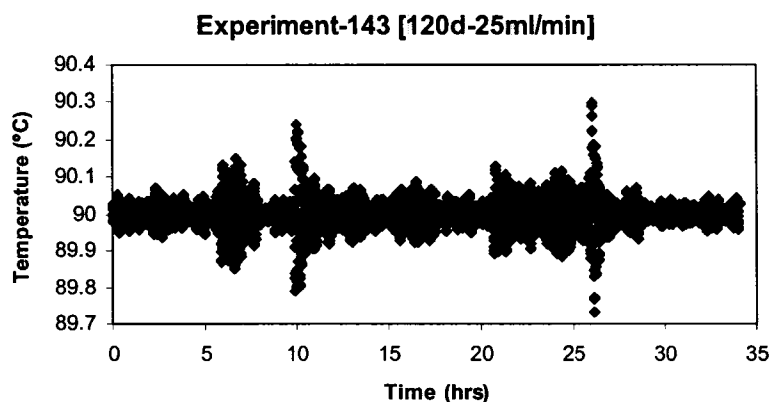


Figure D.51 Experiment - 143 Membrane module temperature profile for 120 μm deep channel, 51 milliseconds, 2/6/06 to 2/7/06.

Table D.55 Experiment - 144 Operating parameters for 120 μm deep channel, 256 milliseconds, 2/7/06 to 2/8/06.

	Date	Day	Time	
Start	2/7/06	Tues	21:30	
End	2/8/06	Wed	13:30	
Experiment #	144			
Experimental Time	16	hrs		
Depth of microchannel	120	μm	0.012	cm
Length of microchannel	30000	μm	3	cm
Width of microchannel	60	μm	0.006	cm
Number of channels	99			
Volume of fluid in reactor	0.021384	cm^3		
Residence Time	256.608	millisec		
avg temp feed tank	23.0478668	$^{\circ}\text{C}$		
Membrane	2216			
Target Temperature	90	$^{\circ}\text{C}$		
Pump head	7016			
RPM	6.1			
Feed flow rate	5	ml/min		
Feed ethanol	27.5			
Tss	1	hr		
Membrane	Expt # used	Exptl	Flow	
Date of 1st use		Time	rate	
		hrs	ml/min	
	condition	18	5	
	2/5/06	142	20	5
	2/6/06	143	34	25
Permeate	2.9742	g		
Refractive Index	1.3428			

Table D.56 Experiment - 144 Recorded data for 120 μm deep channel, 256 milliseconds, 2/7/06 to 2/8/06.

#	Date	Time hrs	Sampling Time	Temperature		R.H %	Pressure		Refractometer	
				Chiller $^{\circ}\text{C}$	Internal $^{\circ}\text{C}$		Upstream psi	Vacuum Torr	Temp $^{\circ}\text{C}$	nd
							9			
	2/7	0	21:30	20.1	99.616	26	7 to 12	3	20	1.3644
1	2/8	5	1:29	20.1	99.82	25	7 to 12	3	20	1.3637
2	2/8	9	5:29	20.4	100.06	26	6 to 9	3	20	1.3631
3	2/8	13	9:29	20.4	99.953	26	6 to 9	3	20	1.3626
4	2/8	17	13:30	20.3	99.644	27	6 to 9	3	20	1.3621

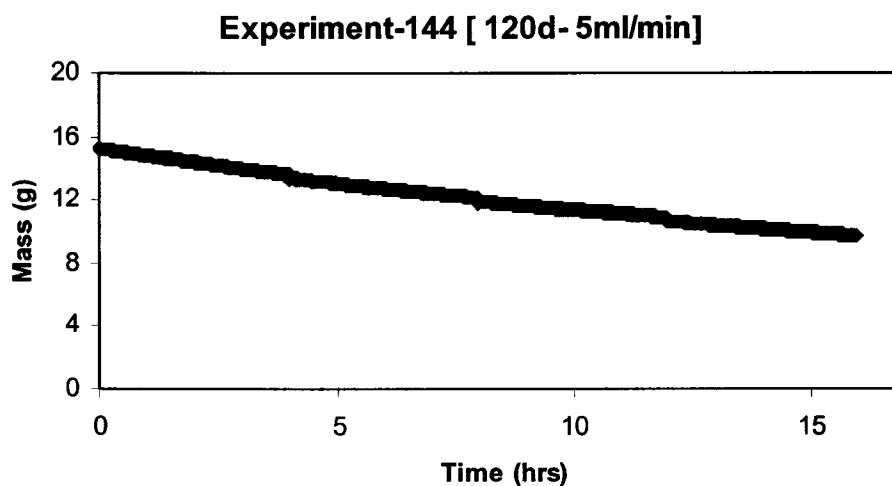


Figure D.52 Experiment - 144 Untreated mass data for 120 μm deep channel, 256 milliseconds, 2/7/06 to 2/8/06.

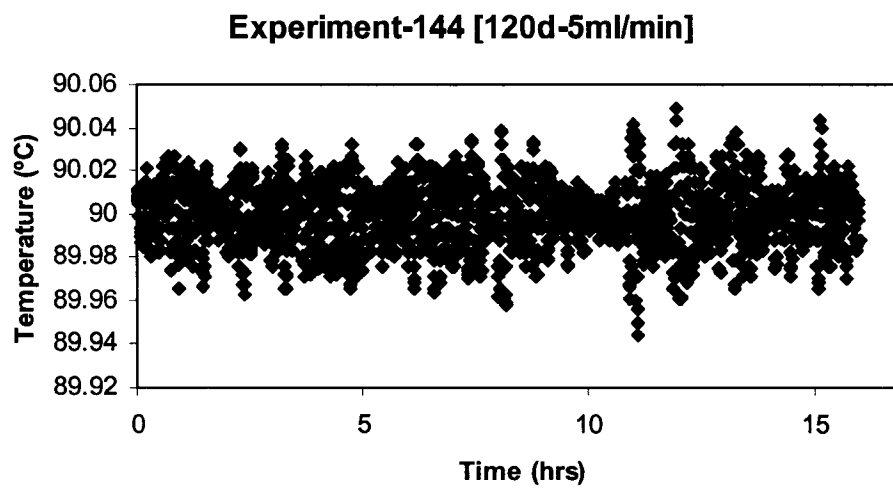


Figure D.53 Experiment - 144 Membrane module temperature profile for 120 μm deep channel, 256 milliseconds, 2/7/06 to 2/8/06.

Table D.57 Experiment - 145 Operating parameters for 120 μm deep channel, 25 milliseconds, 2/8/06 to 2/9/06.

	Date	Day	Time	
Start	2/8/06	Wed	16:00	
End	2/9/06	Thurs	23:00	
Experiment #	145			
Experimental Time	31	hrs		
Depth of microchannel	120	μm	0.012	cm
Length of microchannel	30000	μm	3	cm
Width of microchannel	60	μm	0.006	cm
Number of channels	99			
Volume of fluid in reactor	0.021384	cm^3		
Residence Time	25.6608	millisec		
avg temp feed tank		$^{\circ}\text{C}$		
Membrane area	0.0003	m^2		
Membrane	2216			
Target Temperature	90	$^{\circ}\text{C}$		
Pump head	7016			
RPM	60.5			
Feed flow rate	50	ml/min		
Feed ethanol	27.5			
stabilization time	1.25	hrs		
	Expt #	Exptl	Flow	
Membrane	used	Time	rate	
Date of 1st use		hrs	ml/min	
	condition	18	5	
	2/5/06	142	20	5
	2/6/06	143	34	25
	2/7/06	144	16	5

Table D.58 Experiment - 145 Recorded data for 120 μm deep channel, 25 milliseconds, 2/8/06 to 2/9/06.

#	Date	Time	Sampling	Temperature		R.H	Pressure		Refractometer	
				Chiller	Internal		Upstream	Vacuum	Temp	nd
		hrs	Time	$^{\circ}\text{C}$	$^{\circ}\text{C}$	%	psi	Torr	$^{\circ}\text{C}$	
	2/8	0		20.4	102.78	27	25 to 30	2.5	20	1.3644
1	2/8	6.25	20:59	20	102.06	27	25 to 30	2.5	20	1.3642
2	2/9	13.25	3:59	20	102.02	25	25 to 30	2.5	20	1.3637
3	2/9	19.25	9:59	20.4	102.16	24	25 to 30	3	20	1.3634
4	2/9	25.25	15:59	20	101.85	23	25 to 30	2	20	1.363
5	2/9	32.25	23:00	20.1	102.1	22	25 to 30	2	20	1.3625

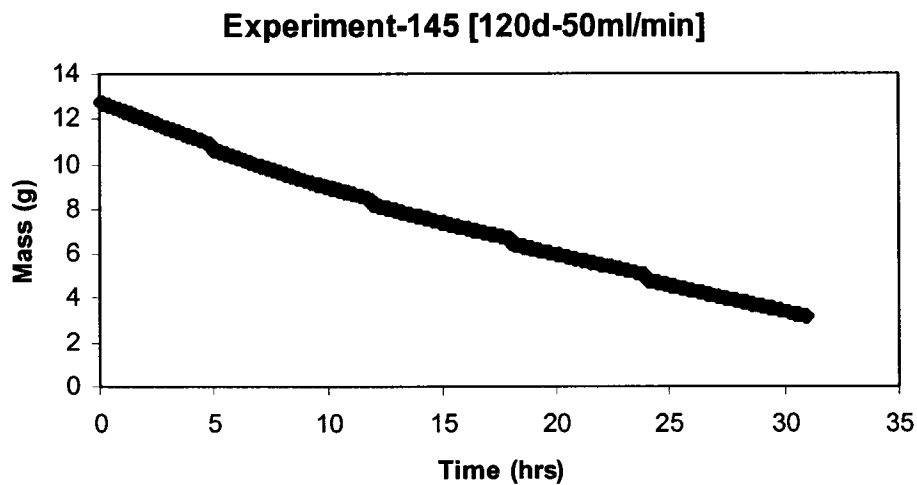


Figure D.54 Experiment - 145 Untreated mass data for 120 μm deep channel, 25 milliseconds, 2/8/06 to 2/9/06.

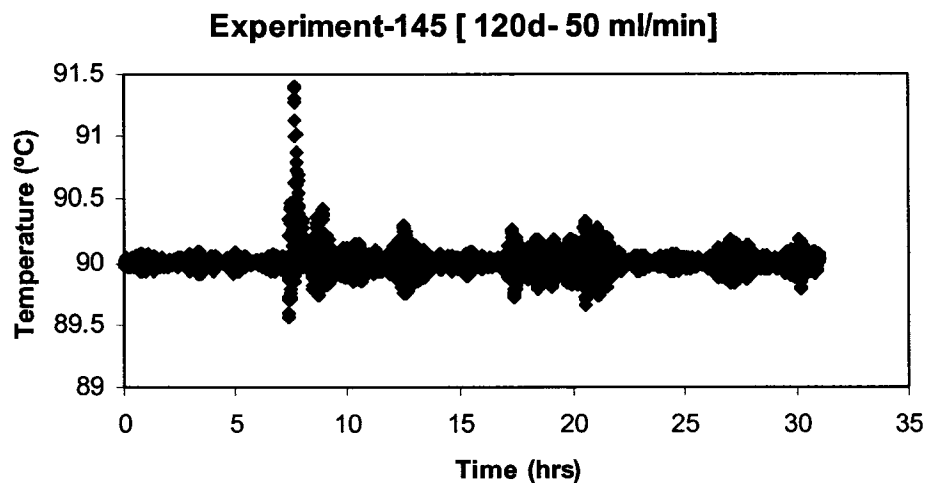


Figure D.55 Experiment - 145 Membrane module temperature profile for 120 μm deep channel, 25 milliseconds, 2/8/06 to 2/9/06.

Table D.59 Experiment - 159 Operating parameters for 120 μm deep channel, 128 milliseconds, 3/3/06 to 3/5/06.

	Date	Day	Time	
Start	3/3/06	Fri	22:30	
End	3/5/06	Sun	4:30	
Experiment #	159			
Experimental Time	30	hrs		
Depth of microchannel	120	μm	0.012	cm
Length of microchannel	30000	μm	3	cm
Width of microchannel	60	μm	0.006	cm
Number of channels	99			
Volume of fluid in reactor	0.021384	cm^3		
Residence Time	128.304	millisec		
avg temp feed tank	21.8528595	$^{\circ}\text{C}$		
Membrane area	0.0003	m^2		
Membrane	2216			
Target Temperature	90	$^{\circ}\text{C}$		
Pump head	7016			
RPM	12.1			
Feed flow rate	10	ml/min		
Feed ethanol	27.5			
Stabilization time	2.5	hrs		
Membrane	Expt # used	Exptl	Flow	
Date of 1st use		Time	rate	
		hrs	ml/min	
	3/1/06	condition	20	10
		30 hrs no contact		

Table D.60 Experiment -159 Recorded data for 120 μm deep channel, 128 milliseconds, 3/3/06 to 3/5/06.

#	Date	Time hrs	Sampling Time	Temperature		R.H %	Pressure		Refractometer	
				Chiller $^{\circ}\text{C}$	Internal $^{\circ}\text{C}$		Upstream psi	Vacuum Torr	Temp $^{\circ}\text{C}$	nd
		0	22:30	19.6	101.15	25	7 to 13	2	20	1.3643
1	3/4	7.5	3:30	19.9	101.21	24	11 to 14	3	20	1.3639
2	3/4	12.5	8:30	20.3	101.62	24	11 to 16	3	20	1.3635
3	3/4	17.5	13:30	20.1	101.48	25	11 to 16	3	20	1.3631
4	3/4	22.5	18:30	19.9	102.76	24	11 to 16	2	20	1.3628
5	3/4	27.5	21:30	19.9	102.68	23	12 to 19	2.5	20	1.3626
6	3/5	32.5	4:30	19:19	102.04	23	14 to 19	2.5	20	1.3624

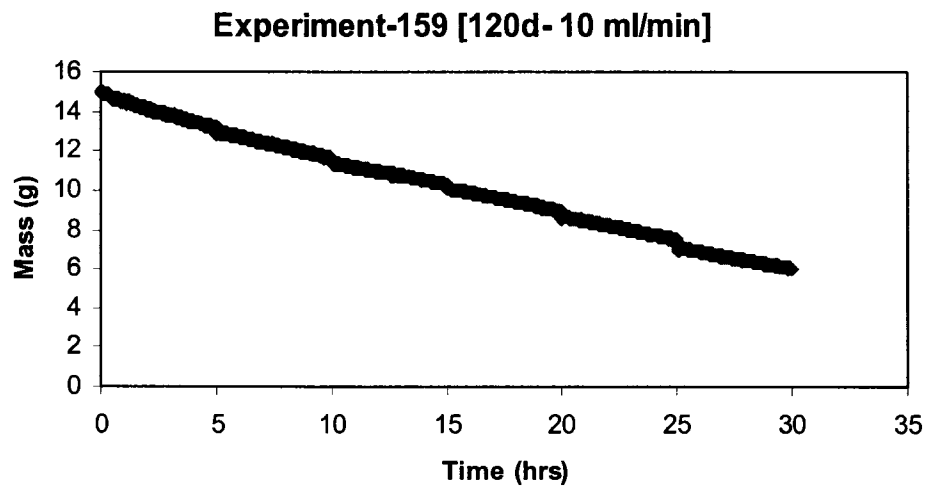


Figure D.56 Experiment - 159 Untreated mass data for 120 μm deep channel, 128 milliseconds, 3/3/06 to 3/5/06.

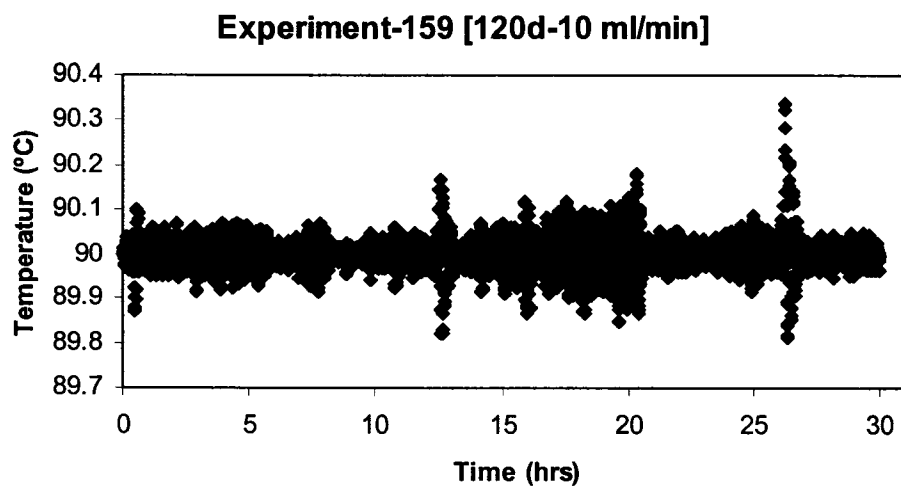


Figure D.57 Experiment - 159 Membrane module temperature profile for 120 μm deep channel, 128 milliseconds, 3/3/06 to 3/5/06.

Table D.61 Experiment - 160 Operating parameters for 120 μm deep channel, 256 milliseconds, 3/5/06 to 3/6/06.

	Date	Day	Time	
Start	3/5/06	Sun	7:00	
End	3/6/06	Mon	8:00	
Experiment #	160			
Experimental Time	25	hrs		
Depth of microchannel	120	μm	0.012	cm
Length of microchannel	30000	μm	3	cm
Width of microchannel	60	μm	0.006	cm
Number of channels	99			
Volume of fluid in reactor	0.021384	cm^3		
Residence Time	256.608	millisec		
avg temp feed tank	22.9686667	$^{\circ}\text{C}$		
Membrane area	0.0003	m^2		
Membrane	2216			
Target Temperature	90	$^{\circ}\text{C}$		
Pump head	7016			
RPM	6.1			
Feed flow rate	5	ml/min		
Feed ethanol				
Stabilization time	1.66666667	hrs		
Membrane	Expt # used	Exptl	Flow	
Date of 1st use		Time	rate	
		hrs	ml/min	
	3/1/06	condition	20	10
		30 hrs no contact		
	3/3/06	159	30	10

Table D.62 Experiment - 160 Recorded data for 120 μm deep channel, 256 milliseconds, 3/5/06 to 3/6/06.

#	Date	Time hrs	Sampling Time	Temperature		R.H %	Pressure		Temp $^{\circ}\text{C}$	nd
				Chiller $^{\circ}\text{C}$	Internal $^{\circ}\text{C}$		Upstream psi	Vacuum Torr		
	3/5	0	5:00	19.9	102.47	23	5	3	20	1.3644
1	3/5	6.667	12:00	19.9	101.88	27	5	3	20	1.364
2	3/5	11.67	17:00	19.8	101.97	27	5	3	20	1.3633
3	3/5	16.67	22:00	19.8	101.67	32	5	3	20	1.3628
4	3/6	21.67	3:00	19.8	101.83	37	5	3	20	1.3626
5	3/6	26.67	8:00	19.8	101.71	38	5	3	20	1.3624

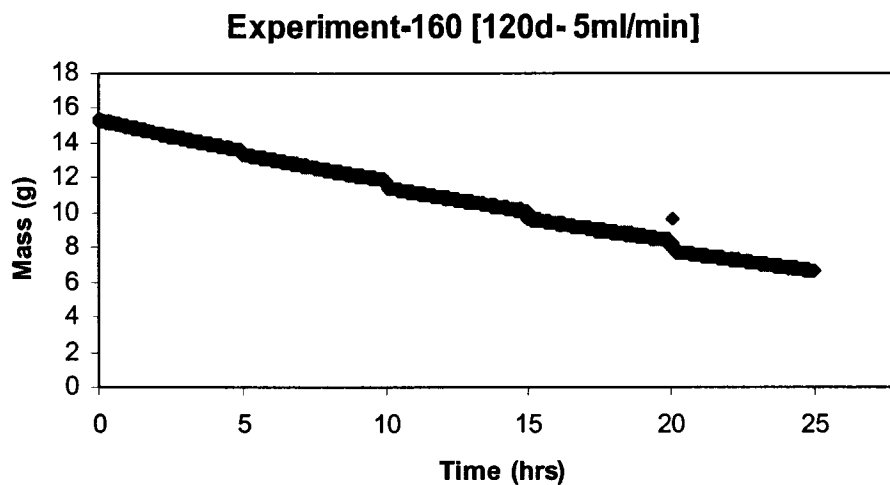


Figure D.58 Experiment - 160 Untreated mass data for 120 μm deep channel, 256 milliseconds, 3/5/06 to 3/6/06.

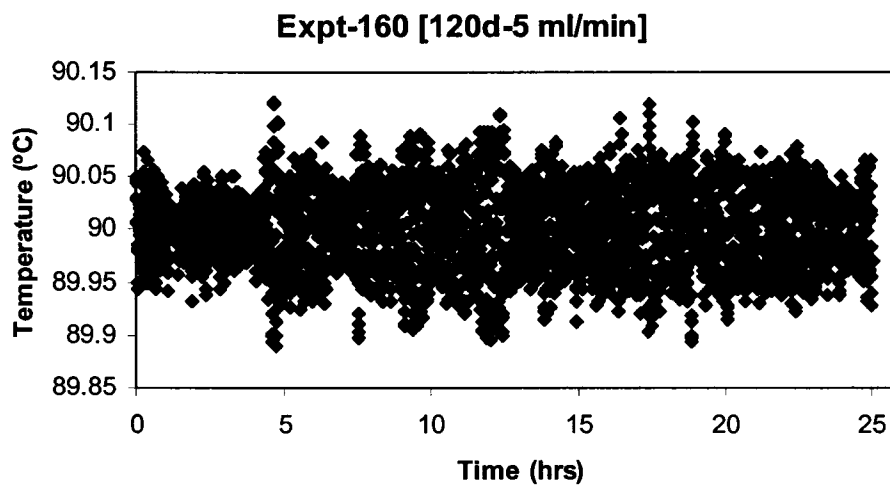


Figure D.59 Experiment - 160 Membrane module temperature profile for 120 μm deep channel, 256 milliseconds, 3/5/06 to 3/6/06.

Table D.63 Experiment - 162 Operating parameters for 120 μm deep channel, 51 milliseconds, 3/6/06 to 3/8/06.

	Date	Day	Time	
Start	3/6/06	Mon	22:00	
End	3/8/06	Wed	4:00	
Experiment #	162			
Experimental Time	30	hrs		
Depth of microchannel	120	μm	0.012	cm
Length of microchannel	30000	μm	3	cm
Width of microchannel	60	μm	0.006	cm
Number of channels	99			
Volume of fluid in reactor	0.021384	cm^3		
Residence Time	51.3216	millisec		
avg temp feed tank	23.0421988	$^{\circ}\text{C}$		
Membrane area	0.0003	m^2		
Membrane	2216			
Target Temperature	90	$^{\circ}\text{C}$		
Pump head	7016			
RPM	30.3			
Feed flow rate	25	ml/min		
Feed ethanol	27.5			
Stabilization time	1.5	hrs		
Membrane	Expt # used	Exptl	Flow	
Date of 1st use		Time	rate	
		hrs	ml/min	
	3/1/06	condition	20	10
		30 hrs no contact		
	3/3/06	159	30	10
	3/5/06	160	25	5
	3/6/06	161	50	9

Table D.64 Experiment - 162 Recorded data for 120 μm deep channel, 51 milliseconds, 3/6/06 to 3/8/06.

#	Date	Time	Sampling	Temperature		R.H	Pressure		Refractometer	
		hrs	Time	Chiller	Internal	%	Upstream	Vacuum	Temp	nd
				$^{\circ}\text{C}$	$^{\circ}\text{C}$		psi	Torr	$^{\circ}\text{C}$	
	3/6	0	22:00	19.3	99.961	30	max	3	20	1.3644
1	3/7	6.5	2:50	19.3	99.839	29	19 to 30	3	20	1.3639
2	3/7	11.5	8:00	19.6	100.38	28	19 to 30	3	20	1.3636
3	3/7	16.5	13:00	19.6	100.44	27	19 to 30	3	20	1.3632
4	3/7	21.5	18:00	19.4	100.2	34	19 to 30	3	20	1.3629
5	3/7	26.5	23:00	19.4	99.899	31	14 to 30	3	20	1.3626
6	3/8	31.5	4:00	19.4	100.42	32	14 to 30	3	20	1.3622

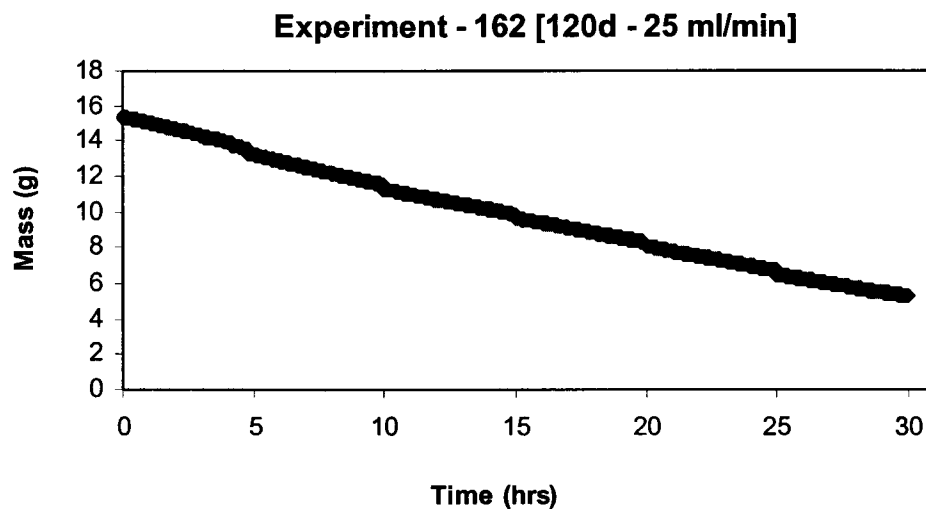


Figure D.60 Experiment - 162 Untreated mass data for 120 μm deep channel, 51 milliseconds, 3/6/06 to 3/8/06.

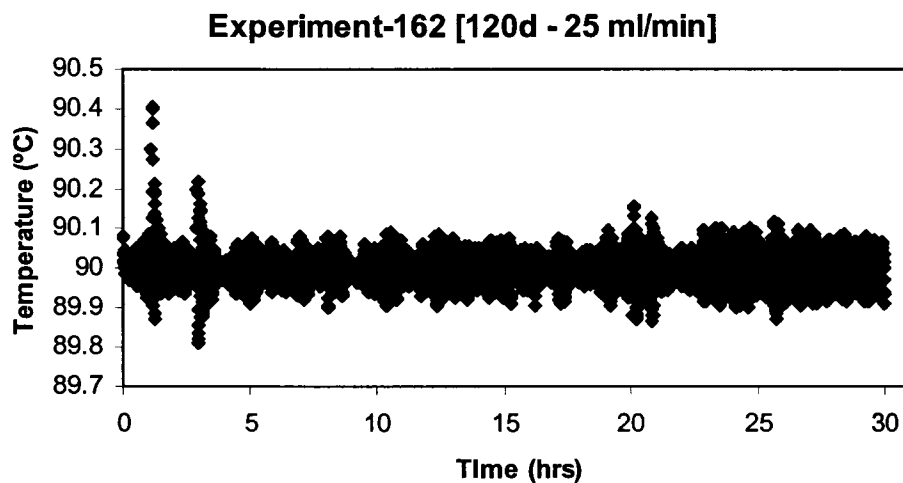


Figure D.61 Experiment - 162 Membrane module temperature profile for 120 μm deep channel, 51 milliseconds, 3/6/06 to 3/8/06.

Table D.65 Experiment - 173 Operating parameters for 120 μm deep channel, 25 milliseconds, 3/25/06 to 3/26/06.

	Date	Day	Time	
Start	3/25/06	Sat	15:00	
End	3/26/06	Sun	11:00	
Experiment #	173			
Experimental Time	173	hrs		
Depth of microchannel	120	μm	0.012	cm
Length of microchannel	30000	μm	3	cm
Width of microchannel	60	μm	0.006	cm
Number of channels	99			
Volume of fluid in reactor	0.021384	cm^3		
Residence Time	25.6608	millisec		
avg temp feed tank	23.0016653	$^{\circ}\text{C}$		
Membrane area	0.0003	m^2		
Membrane	2216			
Target Temperature	90	$^{\circ}\text{C}$		
Pump head	7016			
RPM	60.5			
Feed flow rate	50	ml/min		
Feed ethanol	27.5			
Stabilization time	1.5	hrs		
Membrane	Expt # used	Exptl Time	Flow rate	
Date of 1st use		hrs	ml/min	
	3/24/06	condition	18	2

Table D.66 Experiment - 173 Recorded data for 120 μm deep channel, 25 milliseconds, 3/25/06 to 3/26/06.

#	Date	Time hrs	Sampling Time	Temperature		R.H %	Pressure		Refractometer	
				Chiller $^{\circ}\text{C}$	Internal $^{\circ}\text{C}$		Upstream psi	Vacuum Torr	Temp	nd
	3/25	0		20.4	101.52	24	20 to 30	3	20	1.3643
1	3/25	6.5	20:00	20.2	101.67	24	20 to 30	3	20	1.3635
2	3/26	11.5	1:00	20.2	101.79	25	20 to 30	3	20	1.363
3	3/26	16.5	6:06	20.4	102.08	26	20 to 30	3	20	1.3625
4	3/26	21.5	11:00	20.4	101.91	25	20 to 30	3	20	1.3621

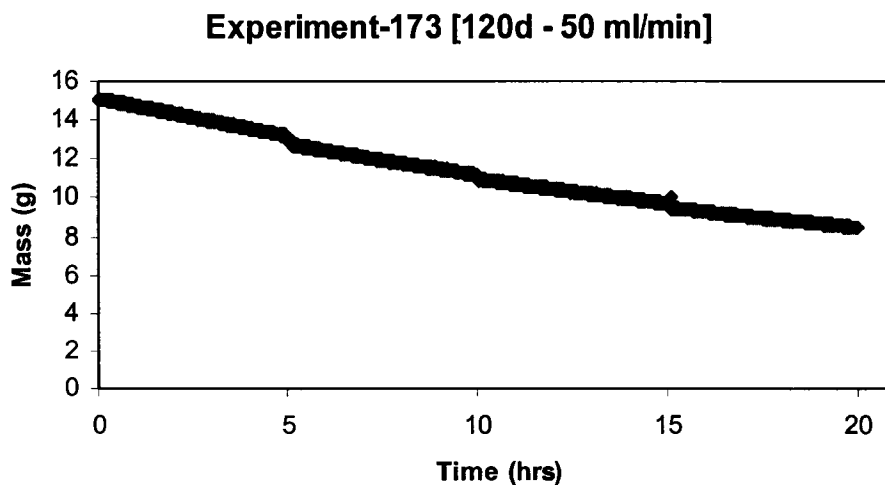


Figure D.62 Experiment - 173 Untreated mass data for 120 μ m deep channel, 25 milliseconds, 3/25/06 to 3/26/06.

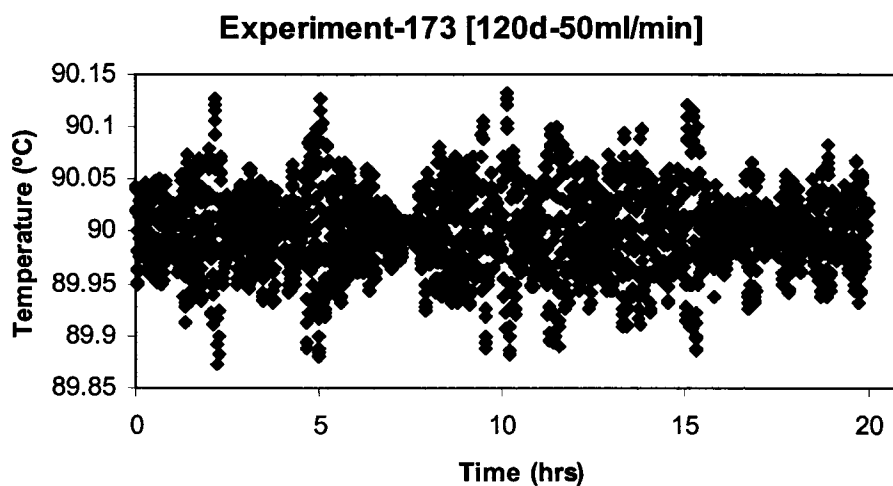


Figure D.63 Experiment - 173 Membrane module temperature profile for 120 μ m deep channel, 25 milliseconds, 3/25/06 to 3/26/06.

Table D.67 Experiment - 174 Operating parameters for 120 μm deep channel, 25 milliseconds, 3/26/06 to 3/27/06.

	Date	Day	Time	
Start	3/26/06	Sun	15:00	
End	3/27/06	Mon	7:00	
Experiment #	174			
Experimental Time	16	hrs		
Depth of microchannel	120	μm	0.012	cm
Length of microchannel	30000	μm	3	cm
Width of microchannel	60	μm	0.006	cm
Number of channels	99			
Volume of fluid in reactor	0.021384	cm^3		
Residence Time	25.6608	millisec		
avg temp feed tank	22.9823101	$^{\circ}\text{C}$		
Membrane area	0.0003	m^2		
Membrane	2216			
Target Temperature	90	$^{\circ}\text{C}$		
Pump head	7016			
RPM	60.5			
Feed flow rate	50	ml/min		
Feed ethanol	27.5			
Stabilization time	2	hrs		
Membrane	Expt # used	Exptl	Flow	
Date of 1st use		Time	rate	
		hrs	ml/min	
	3/24/06	condition		
	3/25/06	173	20	50

Table D.68 Experiment - 174 Recorded data for 120 μm deep channel, 25 milliseconds, 3/26/06 to 3/27/06.

#	Date	Time	Sampling	Temperature		R.H	Pressure		Refractometer	
				Chiller	Internal		Upstream	Vacuum	Temp	nd
		hrs	Time	$^{\circ}\text{C}$	$^{\circ}\text{C}$	%	psi	Torr	$^{\circ}\text{C}$	
	3/26	0	15:00	20.4	100.65	25	18 to 25	3	20	1.3642
1	3/26	6	19:00	20.1	100.77	25	18 to 27	3	20	1.3637
2	3/26	10	21:00	20.1	101.6	25	18 to 28	3	20	1.3631
3	3/27	14	3:06	20.1	101.92	25	18 to 28	3	20	1.3627
4	3/27	18	7:00	20.1	101.96	29	18 to 28	3	20	1.3623

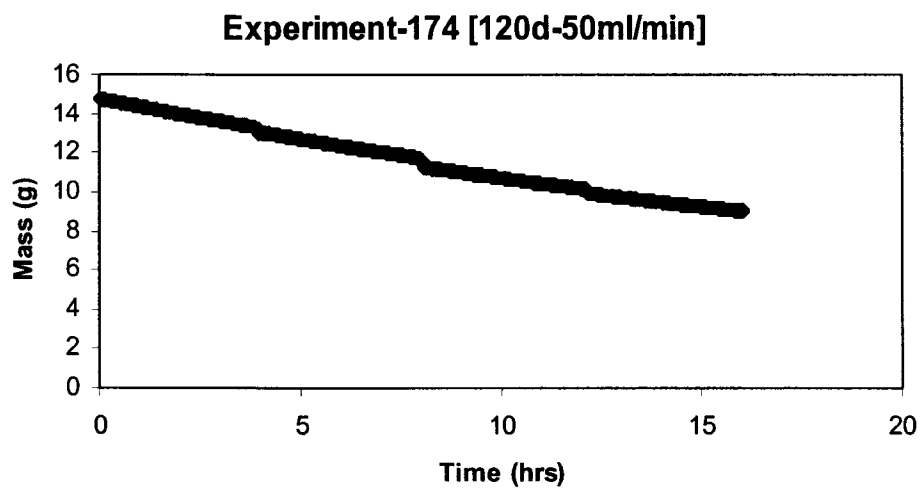


Figure D.64 Experiment - 174 Untreated mass data for 120 μm deep channel, 25 milliseconds, 3/26/06 to 3/27/06.

APPENDIX E

COOLER LENGTH CALCULATIONS

Pervaporation experiments were conducted at an elevated feed temperature of 90°C to achieve better selectivity and flux. It was necessary to maintain the feed ethanol solution inside the feed tank at room temperature to minimize evaporation. As such it was required to design a cooler so that the outlet tube with the retentate was circulated through a condensing system such that the temperature of the feed was maintained at room temperature in the feed tank.

The superior heat conduction properties of copper facilitated as the preferred choice for the outlet tubing from the membrane module. The heat transfer area calculations below indicated the approximate length of copper tubing to be used. This length of copper tubing was immersed inside a water bath maintained below room temperature, which provided sufficient heat transfer since the feed ethanol temperature measured by a temperature probe inside the feed tank always indicated a temperature between 22 to 24 °C.

Specific heat of ethanol = 2439.766 J/Kg K

Density of ethanol = 801.4652 Kg/m³

Overall heat transfer coefficient = 1250 W/m²K

Diameter of Copper tubing = D = 0.0625 inches

Feed flow rate = V = 50 ml/min

Final temperature = T_h = 90 ° C

Initial feed temperature = T_f = 22 ° C

Hot fluid inlet temperature = T_{h1} = 90 ° C

Hot fluid outlet temperature = T_{h2} = 22 ° C

Cold fluid inlet temperature = T_{c1} = 18.5 ° C

Cold fluid outlet temperature = $T_{c2} = 18.5 \text{ }^\circ\text{C}$

$$\Delta T_1 = T_{h1} - T_{c2} = 90 - 18.5$$

$$\Delta T_2 = T_{h2} - T_{c1} = 22 - 18.5$$

$$LMTD = \frac{(\Delta T_1 - \Delta T_2)}{\ln(\Delta T_1 / \Delta T_2)}$$

$$\text{Mass flow rate} = m = V * \rho$$

$$\text{Rate of heat flow} = Q = m * C_{p_c} * (T_h - T_f)$$

$$\text{Heat transfer area} = \frac{Q}{U_o * \Delta T_{LMTD}} = A$$

$$\text{Length of copper tubing} = \frac{A}{D}$$

APPENDIX F

VITON TUBING CALIBRATION FOR FEED PUMP

Choosing the appropriate tubing material and calibrating it is important before using a masterflex pump. The masterflex pump head (Model No: 7016 -20) used contains three roller rotors that provided the peristaltic action to propel fluids through the tubing. A calibration chart as shown in Figure F.1 was developed to predict the flow rate at a specific rpm.

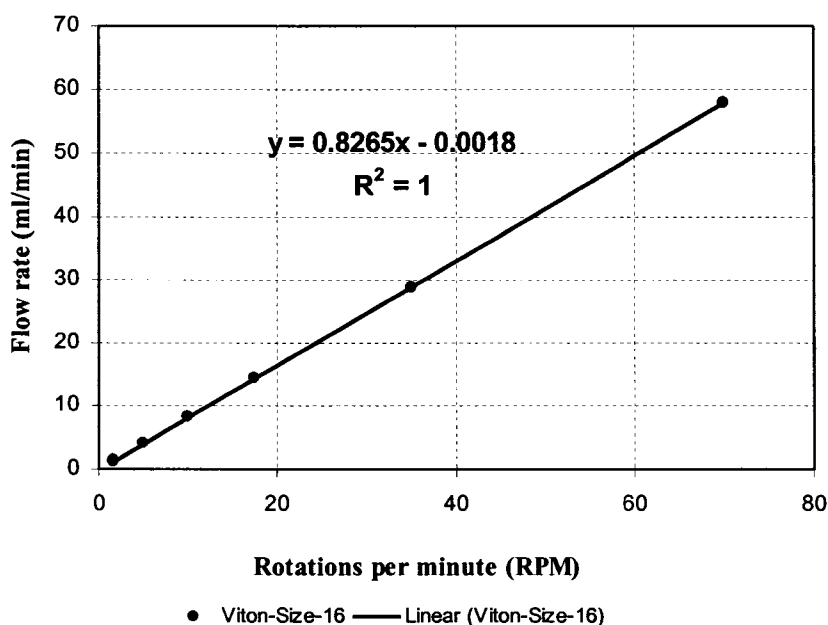


Figure F.1 Masterflex tubing calibration chart.

The feed ethanol solution used in the experiments was 90 % w/w, and the same concentration was used as the test solution for the calibration of the flow rates to maintain consistency. The tubing was tested at a specific rpm for a fixed time interval and the feed ethanol solution collected at the end of the known time interval was weighed. The density of 90 w/w % ethanol is known. This was used to calculate the volume and subsequently the flow rate was also calculated. The calculations used are as shown below:

$$Volume = \frac{\text{Mass of ethanol solution collected at a fixed interval of time}}{\text{Density of 90\% w/w ethanol solution}}$$

$$\text{Flow rate} = \frac{\text{Volume (ml)}}{\text{Time (min)}}$$

REFERENCES

1. Schubert, K., Bier, W., Brandner, J., Fichtner, M., Franz, C., Linder, G., "Realization and Testing of Microstructure Reactors, Micro Heat Exchangers and Micromixers for Industrial Applications in Chemical Engineering," in Ehrfeld, W., Rinard, I.H., Wegeng, R.S. (Eds.) *Process Miniaturization: 2nd International Conference on Microreaction Technology, IMRET 2; Topical Conference Preprints*, (1999), AIChE New Orleans, USA, 88-95.
2. Ehrfeld, W., Hessel, V., Haverkamp, V., "Microreactors," *Ullmann's Encyclopedia of Industrial Chemistry*, Wiley-VCH, Weinheim, (1999).
3. Mazanec, T., Perry, S., Tonkovich, L., Wang, Y., "Microchannel Gas-To-Liquids Conversion-Thinking Big By Thinking Small," *Studies in Surface Science and Catalysis* (2004): 169-174.
4. Lowe, H., Hessel, V., and Mueller, A., "Microreactors. Prospects Already Achieved and Possible Misuse," *Pure Applied Chemistry* 74, 12, (2002): 2271-2276.
5. Wegeng, R.S., Drost, M.K., Brenchley, D.L., "Process Intensification through Miniaturization or Micro Thermal and Chemical Systems in the 21st Century," 3rd International Conference on Microreaction Technology, Frankfurt, Germany. (April 18-21, 1999).
6. Zhang, L., Wang, E.N., Goodson, K.E., Kenny, T.W., "Phase Change Phenomena in Silicon Microchannels," *International Journal of Heat and Mass Transfer* 48, (2005):1572-1582.
7. Kandilkar, S.G., "Heat Transfer Mechanisms During Flow Boiling in Microchannels," *Journal of Heat Transfer* 126, (2004): 8-16.
8. Huang, R.Y.M., *Pervaporation Membrane Separation Process* (Amsterdam: Elsevier Science Publishers B.V., 1991), Chapter-3:193.
9. Wankat, P.C., *Separations in Chemical Engineering, Equilibrium Staged Operations* (Englewood Cliffs, NJ: Prentice Hall, 1988).
10. Sirkar, K.K., "Membrane Separation Technologies: Current Developments," *Chemical Engineering Communications* 157, (1996): 145-184.

11. Baker, R. W., Cussler, E.L., Eykamp, W., Koros, W.J., Riley, R.L., Strathmann, H., *Membrane Separation Systems: Recent Developments and Future Directions* (New Jersey: Noyes Data Corporation, 1991).
12. Tuwiner, S.B., *Diffusion and Membrane Technology* (New York: Reinhold Publishing Corporation, 1962).
13. Mulder, M., *Basic Principles of Membrane Technology* (The Netherlands: Kluwer Academic Publishers, 2nd Edition, 1998).
14. Loeb, S., "Preparation and Performance of High Flux Cellulose Acetate Desalination Membranes," In "Desalination by Reverse Osmosis." M.I.T. Press, Cambridge., U.S.A., 1966. Chap.3, 55 in *Pervaporation Membrane Separation Process*, Huang, R.Y.M, Elsevier Science Publishers B.V., Amsterdam, 1991.
15. Strathmann, H., "Membrane Separation Processes: Current Relevance and Future Opportunities," *AIChE Journal* 47, (5, May, 2001): 1077-1087.
16. Noyes, R., *Unit Operations in Environmental Engineering* (New Jersey: Noyes Data Corporation, 1994).
17. Rousseau, R.W., *Handbook of Separation Process Technology* (New York: John Wiley & Sons- IEEE, 1987).
18. Strathmann, H., "Electrodialysis and Its Application in the Chemical Process Industry," *Separation and Purification Methods* 14, n 1, (1985):41-66.
19. Kober, P.A., "Pervaporation, Perstillation, and Percrystallization," *Journal of American Chemical Society* 39, (1917):944 in *Membrane Technology and Applications*, Baker, R.W., Wiley 2nd edition.
20. Huang, R.Y.M., *Pervaporation Membrane Separation Process* (Amsterdam: Elsevier Science Publishers B.V., 1991)
21. Rautenbach, R., Albrecht, R., "The Separation Ppotential of Ppervaporation Part 1.Discussion of Transport Equations and Comparison with Reverse Osmosis," *Journal of Membrane Science* 25, (1985):1-23.
22. Gupta, B.D., Mukherjee, A.K., "Separation of Liquid Mixtures by Pervaporation," *Polymer-Plastics Technology and Engineering* 29, 4, (1990): 299-337.
23. Guerreri, G., "Membrane Alcohol Separation Process-Integrated Pervaporation and Fractional Distillation," *Chemical Engineering Research & Design* 70, Part A, (1992):501-508.

24. Karlsson, H.O.E., Tragardh, G., "Heat Transfer in Pervaporation," *Journal of Membrane Science* 119, n 2, (Oct 16, 1996): 295-306.
25. Wnuk, R., Chmiel, H., "Direct Heating of Composite Membranes in Pervaporation and Gas Separation Processes," *Journal of Membrane Science* 68, (1992): 293-300.
26. Changluo, Z., Moe, L., Wei, X., "Separation of Ethanol-Water Mixtures by Pervaporation-Membrane Separation Process," *Desalination* 62, (1987):299-313.
27. Martin, N., "Flexible and Efficient," Reprint from *Process, Europe* 1(2000), Vogel Verlag and Druck GmbH & Co. KG. Membrane Systems: Pervaporation and Vapor Permeation, Sulzer Chemtech brochure.
28. Ikegami, T., "Highly Concentrated Aqueous Ethanol Solutions by Pervaporation using Silicalite Membrane- Improvement of Ethanol Selectivity by addition of Sugars to Ethanol Solution," *Biotechnology Letters* 21, (1999):1037-1041.
29. Jiraatananon, R., Chanachai, A., Huang, R.Y.M., Uttapap, D., "Pervaporation Dehydration of Ethanol-Water Mixtures with Chitosan/Hydroxyethylcellulose (CS/HEC) Composite Membranes I. Effect of Operating Conditions," *Journal of Membrane Science* 195, (2002): 143-151.
30. Nguyen, T.Q., "The Influence of Operating Parameters on the Performance of Pervaporation Processes," 1985 Spring National Meeting and Petro Expo '85 - American Institute of Chemical Engineers., Houston, TX, USA, No.248, Vol 82, (1985):20.
31. Wijmans, J.G., Baker, R.W., "The Solution-Diffusion Model: A Review," *Journal of Membrane Science* 107, (1995):1-21.
32. Neel, J., Aptel, P., Clement, R., "Basic Aspects of Pervaporation," *Desalination* 53, (1985): 297-326.
33. Feng, X., Huang, R.Y.M., "Liquid Separation by Membrane Pervaporation: A Review," *Industrial Engineering Chemistry Research* 36, (1997):1048-1066.
34. Rafik, M., Mas, A., Guimon, M-F., Guimon, C., Elharfi, A., Schue, F., "Plasma-Modified Poly (vinyl alcohol) Membranes for the Dehydration of Ethanol," *Polymer International* 52, (2003):1222-1229.
35. Takehiko, K., Toshinori, T., Shin-ichi, N., Shoji, K., "Membrane Transport Properties of Pervaporation and Vapor Permeation in Ethanol-Water System using Polyacrylonitrile and Cellulose Acetate Membranes," *Journal of Chemical Engineering of Japan* 24, (3rd June 1991): 334-339.

36. Nagase, Y., Kazuhiko, I., Kiyohide, M., "Chemical Modification of Poly (substituted-acetylene): II. Pervaporation of Ethanol/Water Mixture through Poly (1-trimethylsilyl-1-propyne)/Poly(dimethylsiloxane) Graft Copolymer Membrane," *Journal of Polymer Science: Part B: Polymer Physics* 28, (1990): 377-386.
37. Tusel, G.F., Brusckke. H.E.A., "Use of Pervaporation in the Chemical Industry," *Desalination* 53, (1985):327-38. In *Pervaporation Membrane Separation Process*, Huang. R.Y.M, Elsevier Science Publishers B.V., Amsterdam, 1991.
38. Kashiwagi, T., Okabe, K., Okita, K., "Separation of Ethanol from Ethanol/Water Mixtures by Plasma-Polymerized Membranes from Silicone Compounds," *Journal of Membrane Science* 36, (1988):353. In *Pervaporation Membrane Separation Process*, Huang. R.Y.M, Elsevier Science Publishers B.V., Amsterdam, 1991.
39. NiemoÈller, A., Scholz, H., GoÈtz, B., Ellinghorst, G., "Radiation grafted Membranes for Pervaporation of Ethanol/Water Mixtures," *Journal of Membrane Science* 36, (1988):124. In *Pervaporation Membrane Separation Process*, Huang. R.Y.M, Elsevier Science Publishers B.V., Amsterdam, 1991.
40. Redman, J., "Pervaporation Heading for a New Horizon," *Chem. Eng. London*, 669, (1990):46. In *Pervaporation Membrane Separation Process*, Huang. R.Y.M., Elsevier Science Publishers B.V., Amsterdam, 1991.
41. Wesslein, M., Heintz, A., Lichtenthaler, R.N., "Pervaporation of Liquid Mixtures through Poly (vinyl alcohol) (PVP) membranes. II. the Binary Systems Methanol/1-propanol and Methanol/dioxane and the Ternary System Water/Methanol/1- propanol," *Journal of Membrane Science* 51, (1990):181. In *Pervaporation Membrane Separation Process*, Huang. R.Y.M, Elsevier Science Publishers B.V., Amsterdam, 1991.
42. Wesslein, M., Hwintz, A., Lichtenthaler, R.N., "Pervaporation of Liquid Mixtures through Poly (vinyl alcohol) (PVA) Membranes I. Study of Water containing Binary Systems with Complete and Partial Miscibility," *Journal of Membrane Science* 51, (1990):169. In *Pervaporation Membrane Separation Process*, Huang. R.Y.M., Elsevier Science Publishers B.V., Amsterdam, 1991.
43. Fleming, H.L., "Consider Membrane Pervaporation," *Chemical Engineering Progress* 88, (1992), 46. In *Pervaporation Membrane Separation Process*, Huang. R.Y.M, Elsevier Science Publishers B.V., Amsterdam, 1991.
44. Lai, J.Y., Li, S., Lee, K., "Permeabilities of Polysiloxaneimide Membrane for Aqueous Ethanol Mixture in Pervaporation," *Journal of Membrane Science* 93, (1994):273. In *Pervaporation Membrane Separation Process*, Huang. R.Y.M, Elsevier Science Publishers B.V., Amsterdam, 1991.

45. Sano, T., Yanagishita, H., Kiyozumi, Y., Mizukami, F., Haraya, K., "Separation of Ethanol/Water Mixture by Silicalite Membrane on Pervaporation," *Journal of Membrane Science* 95, (1994):221. In Pervaporation Membrane Separation Process, Huang. R.Y.M, Elsevier Science Publishers B.V., Amsterdam, 1991.
46. Song, K.M., Hong. W.H., "Dehydration of Ethanol and Isopropanol Using Tubular Type Cellulose Acetate Membrane with Ceramic Support in Pervaporation Process, *Journal of Membrane Science* 123, (1997):27-33. In Pervaporation Dehydration of Ethanol-Water Mixtures with Chitosan/Hydroxyethylcellulose (CS/HEC) Composite Membranes I. Effect of Operating Conditions, Jiraatananon, R., Chanachai, A., Huang, R.Y.M., Uttapap, D., *Journal of Membrane Science*, 195, 2002, 143-151
47. Zhu, C.L., Yuang, C.W., Fried. J.R., Greenberg, D.B., "Pervaporation Membranes - A Novel Separation Technique for Trace Organics, *Environmental. Progress* 2, (1983):132. In Pervaporation Membrane Separation Process, Huang. R.Y.M., Elsevier Science Publishers B.V., Amsterdam, 1991.
48. Brun, J.P., Larchet, C., Bulvestre, G., Auclair, B., "Sorption and Pervaporation of Dilute Aqueous Solutions of Organic Compounds through Polymer Membranes," *Journal of Membrane Science* 25, (1985):55. In Pervaporation Membrane Separation Process, Huang. R.Y.M, Elsevier Science Publishers B.V., Amsterdam, 1991.
49. Nguyen, T.Q., Nobe, K., "Extraction of Organic Contaminants in Aqueous Solutions by Pervaporation," *Journal of Membrane Science* 30, (1987):11. In Pervaporation Membrane Separation Process, Huang. R.Y.M, Elsevier Science Publishers B.V., Amsterdam, 1991.
50. Raghunath, B., Hwang, .S-T., "General Treatment of Liquid-Phase Boundary Layer Resistance in the Pervaporation of Dilute Aqueous Organics through Tubular Membranes," *Journal of Membrane Science* 75, (1992):29. In Liquid separation by Membrane Pervaporation: A Review, Feng, X., *Industrial Engineering Chemistry Research*, 36, 1997, 1048-1066.
51. Yamaguchi, T., Yamahara, S., Nakao, S., Kimura, S., "Preparation of Pervaporation Membranes for Removal of Dissolved Organics from Water by Plasma-Graft filling Polymerization," *Journal of Membrane Science* 95, (1994):39. In Liquid separation by Membrane Pervaporation: A Review, Feng, X. et al. *Industrial Engineering Chemistry Research*, 36, 1997, 1048-1066.
52. Wijmans, J.G., Athayde, A.L., Daniels R., Ly J.H., Le, M., Kamaruddin, H.D., Pinnau, I., "The Role of Boundary Layers in the Removal of Volatile Organic Compounds from Water by Pervaporation," *Journal of Membrane Science* 109, (1996):135.

53. Aptel, P., Challard, N., Cuny, J., Neel, J., "Application of the Pervaporation Process to Separate Azeotropic Mixtures," *Journal of Membrane Science* 1, (1976): 271. In *Membrane Technology and Applications*, Baker, R.W., Wiley 2nd edition.
54. Chen, M.S.K., Markiewicz, G.S., Venugopal, K.G., "Development of Membrane trimTM Process for Methanol Recovery from CH₃OH/MTBE/C₄ Mixtures," *Membrane Separations in Chemical Industries*, AIChE Symp, 85, 272, (1989):82. In *Membrane Technology and Applications*, Baker R.W., Wiley 2nd edition.
55. Farnand, B.A., "Pervaporation as an alternative process for the Separation of Methanol from C₄ Hydrocarbons in the production of MTBE and TAME," *Membrane Separations in Chemical Industries*, AIChE Symp, 85, 272, (1989):89.
56. Habib, S., "Removal of Water from Aroma Aqueous Mixtures using Pervaporation Processes," *Separations Technology* 6, 1, (Feb 1996):69-75.
57. Feng, X., Huang, R.Y.M., "Concentration Polarization in Pervaporation Separation Processes," *Journal of Membrane Science* 92, (1994): 201-208.
58. Stankiewicz, A.I., Moulijn, J.A., "Process Intensification: Transforming Chemical Engineering," *Chemical Engineering Progress* 96, 1, (2000):22-34.
59. Charpentier, J.-C., "Process Intensification by Miniaturization," *Chemical Engineering and Technology* 28, n 3, (March, 2005):255-258.
60. Ramshaw, C., Arkley, K., "Process Intensification by Miniature Mass Transfer," *Process Engineering* 64, n 1, (Jan, 1983):29-31.
61. Ramshaw, C., "'Higee' Distillation - An Example of Process Intensification," *Chemical Engineer* 389, (Feb, 1983): 13-14.
62. Stankiewicz, A.I., "Re-Engineering Chemical Process Plant: Process Intensification," (New York: M. Dekker, 2004).
63. Ducry, L., Bieler, N., Cretton, P., Zimmermann, B., Roberge, D.M., "Microreactor Technology: A Revolution for the Fine Chemical and Pharmaceutical Industries?" *Chemical Engineering and Technology* 28, n 3, (March, 2005):318-323.
64. Zhang, X., Stefanick, S., Villani, F.J., "Application of Microreactor Technology in Process Development," *Organic Process Research & Development* 8, (2004):455-460.
65. Thayer, A.M., "Harnessing Mmicroreactions," *Chemical and Engineering News* 83, 22, (May 30, 2005): 43-52.

66. Jensen, K.F., "The Impact of MEMS on the Chemical and Pharmaceutical Industries, Solid - State Sensor and Actuator Workshop, Hilton Head Island, South Carolina, (June 4-8, 2000).
67. Ehrfeld, W., Hessel, V., Lowe, H., "Microreactors: New Technology for Modern Chemistry," Wiley-VCH, 2000.
68. Lowe, H., Hessel, V., Mueller, A., "Microreactors, Prospects already achieved and possible misuse," *Pure Applied Chemistry* 74, n12, (2002): 2271-2276.
69. Schwalbe, T., Autze, V., Wille, G., "Chemical Synthesis in Microreactors," *CHIMIA* 56, (2002):636-646.
70. Kusakabe, K., Morooka, S., Maeda, H., "Development of a Catalytic Reactor System," *Korean Journal of Chemical Engineering* 18, 3, (2001): 271-276.
71. Martin, P.M., Matson, D.W., Bennet, W.D., "Microfabrication Methods for Microchannel Reactors and Separation Systems," *Chemical Engineering Communications* 173, (1999):245-254.
72. Tonkovich, A.Y., Perry, S., Wang, Y.D., LaPlante, T., Rogers, W.A., "Microchannel Process Technology for Compact Methane Steam Reforming," *Chemical Engineering Science* 59, (2004):4819-4824.
73. Zheng, A., Jones, F., Fang, J., "Dehydrogenation of Cyclohexane to Benzene in a Membrane Microreactor," Annual Conference on Microreaction Technology, AIChE, Spring National Meeting, Atlanta, GA, (March 5-9).
74. Franz, A.J., Jensen, K.F., Schmidt, M.A., "Palladium Membrane Micro Reactors," Proceedings of the 3rd International conference on micro reaction technology, (1999):267-276.
75. Schiewe, B., Vuin, A., Gunther, N., Gebauer, K., Richter, Th., Wegner, G., "Polymer Membranes for Product Enrichment in Microreactor Technology," Proceedings of the 3rd International conference on micro reaction technology, (1999):550-555.
76. Schiewe, B., Vuin, A., Gunther, N., Gebauer, K., Richter, Th., Wegner, G., "Membrane-Based Gas Separation of Ethylene/ Ethylene Oxide mixtures for Product Enrichment in Microreactor Technology," *Chemphyschem* 2, (2001): 211-218.
77. Jong, J.D., Lammertink, R.G.H., Wessling, M., "Membranes and Microfluidics: A Review," *Lab Chip*, 6, (2006):1125-1139.

78. Zhang, X., Lai, S.M., Ng, C.P., Aranda, R. M., Yeung, K.L., "An Investigation of Knoevenagel Condensation Reaction in Microreactors using a New Zeolite Catalyst," *Applied Catalysis A: General* 261, (2004):109-118.
79. Lai, S.M., Ng, C.P., Aranda, R. M., Yeung, K.L., "Knoevenagel Condensation Reaction in Zeolite Membrane Microreactor," *Microporous and Mesoporous* 66, (2003): 239-252.
80. Eijkel, J.C.T., Bomer, J. G., Van Den Berg, A., "Osmosis and Pervaporation in Polyimide Submicron Microfluidic Channel Structures," *Applied Physics Letters* 87, n 11, (Sep 12, 2005):103 -114.
81. Psaue, R., Aptel, Ph., Aurelle, Y., Mora, J.C., Bersillon, J.L., "Pervaporation: Importance of Concentration Polarization in the Extraction of Trace Organics from Water," *Journal of Membrane Science* 36, (1988):373-384. Raghunath, B., Hwang, S-T., "General Treatment of Liquid-Phase Boundary Layer Resistance in the Pervaporation of Dilute Aqueous Organics through Tubular Membranes," *Journal of Membrane Science* 75, (1992):29-46.
82. Raghunath, B., Hwang, S-T., "Effect of Boundary Layer Mass Transfer Resistance in the Pervaporation of Dilute Organics," *Journal of Membrane Science* 75, (1992): 147-161.
83. Feng, X., Huang. R.Y.M., "Concentration Polarization in Pervaporation Separation Processes," *Journal of Membrane Science* 92, (1994): 201-208.
84. Rautenbach, R., Helmus, F.P., "Some Consideration on Mass-Transfer Resistances in Solution-Diffusion Type Membrane Processes," *Journal of Membrane Science* 87, (1994):171-181.
85. Dotremont, C., Van den Ende, S., Vandommele, H., Vandecasteele, C., "Concentration Polarization and Other Boundary Layer Effects in the Pervaporation of Chlorinated Hydrocarbons," *Desalination* 95, (1994):91-113.
86. Wijmans, J.G., Athayde, A.L., Daniels R., Ly J.H., Le, M., Kamaruddin, H.D., Pinnau, I., "The Role of Boundary Layers in the Removal of Volatile Organic Compounds from Water by Pervaporation," *Journal of Membrane Science* 109, (1996):135.
87. Jiang, J-S., Vane, L.M., Sikdar, S.K., "Recovery of VOC's from Surfactant Solutions by Pervaporation," *Journal of Membrane Science* 136, (1997): 233-247.
88. Bhattacharya, S., Hwang, S-T., "Concentration Polarization, Separation Factor, and Peclet Number in Membrane Processes," *Journal of Membrane Science* 132, (1997):73-90.

89. Baker, R.W., Wijmans J.G., Athayde A.L., Daniels R., Ly J.H., Le M., "The Effect of Concentration Polarization on the Separation of Volatile Organic Compounds from Water by Pervaporation," *Journal of Membrane Science* 137, (1997):159-172.
90. Jou, J-D., Yoshida, W., Cohen, Y., "A Novel Ceramic-Supported Polymer Membrane for Pervaporation of Dilute Volatile Organic Compounds," *Journal of Membrane Science* 162, (1999): 269-284.
91. Liang, L., Dickson, J.M., Jiang, J., Brook, M.A., "Effect of Low Flow Rate on Pervaporation of 1, 2-Dichloroethane with Novel Polydimethylsiloxane Composite Membranes," *Journal of Membrane Science* 231, (2004):71-79.
92. Vane, L.M., Alvarez, F.R., Grioux, E.L., "Reduction Of Concentration Polarization in Pervaporation Using Vibrating Membrane Module," *Journal of Membrane Science* 153, (1999):233-241.
93. Matthiasson, E., Sivik, B., "Concentration Polarization and Fouling," *Desalination* 35, (1980):59-103.
94. Perry, J.H. and Green D.W., "Chemical Engineers Handbook", 6th edition, McGraw Hill International Editions, Chapter-5.
95. Graetz, L., "Veber die Wärmeleitungsfähigkeit von Flüssigkeiten," *Annalen der Physik und Chemie*. 25, (1883):337-357
96. Leveque, M.A., *Annales.de.Mines*, (1928)
97. Sieder, E.N., Tate, G.E., "Heat Transfer and Pressure Drop of Liquids in Tubes," *Industrial and Engineering Chemistry* 23, 12, (1936):1429-1435.
98. Porter, M.C., "Concentration Polarization with Membrane Ultrafiltration," *Industrial Engineering Chemistry Product Research Develop* 11, 3, (1972): 234-248.
99. Gekas, V., Hallstrom, B., "Mass Transfer in the Membrane Concentration Polarization Layer Under Turbulent Cross Flow I. Critical Literature Review and Adaptation of Existing Sherwood Correlations to Membrane Operations," *Journal of Membrane Science* 30, (1987):153-170.
100. Karlsson, H.O.E., Tragardh, G., "Aroma Compound Recovery with Pervaporation – Feed Flow Effects," *Journal of Membrane Science* 81, (1993):163-171.
101. Karlsson, H.O.E., Tragardh, G., "Heat Transfer in Pervaporation," *Journal of Membrane Science* 119, (1996):295-306.

102. Huang, R.Y.M., *Pervaporation Membrane Separation Process* (Amsterdam B.V: Elsevier Science Publishers, 1991), Chapter-3,193.
103. Rautenbach, R., Helmus, F.P., "Some Consideration on Mass-Transfer Resistances in Solution-Diffusion-Type Membrane Processes," *Journal of Membrane Science* 87, (1994):171-181.
104. Reid, R.C.; Prausnitz, J.M.; Poling, B.E., *The Properties of Gases & Liquids* (New York: McGraw-Hill, 4th edition., 1987), 616.
105. <http://www.chem.agilent.com/Scripts/Generic.ASP?lPage=18299&indcol=N&prodcol=Y> (last accessed: August 4, 2006).
106. <http://www2.ups.edu/faculty/hanson/labtechniques/refractometry/theory.htm> (last accessed: August 4, 2006).
107. Madou, M. J., "Fundamentals of Microfabrication," CRC-Press; 1st edition (February 1, 1998), ISBN: 0849394511.